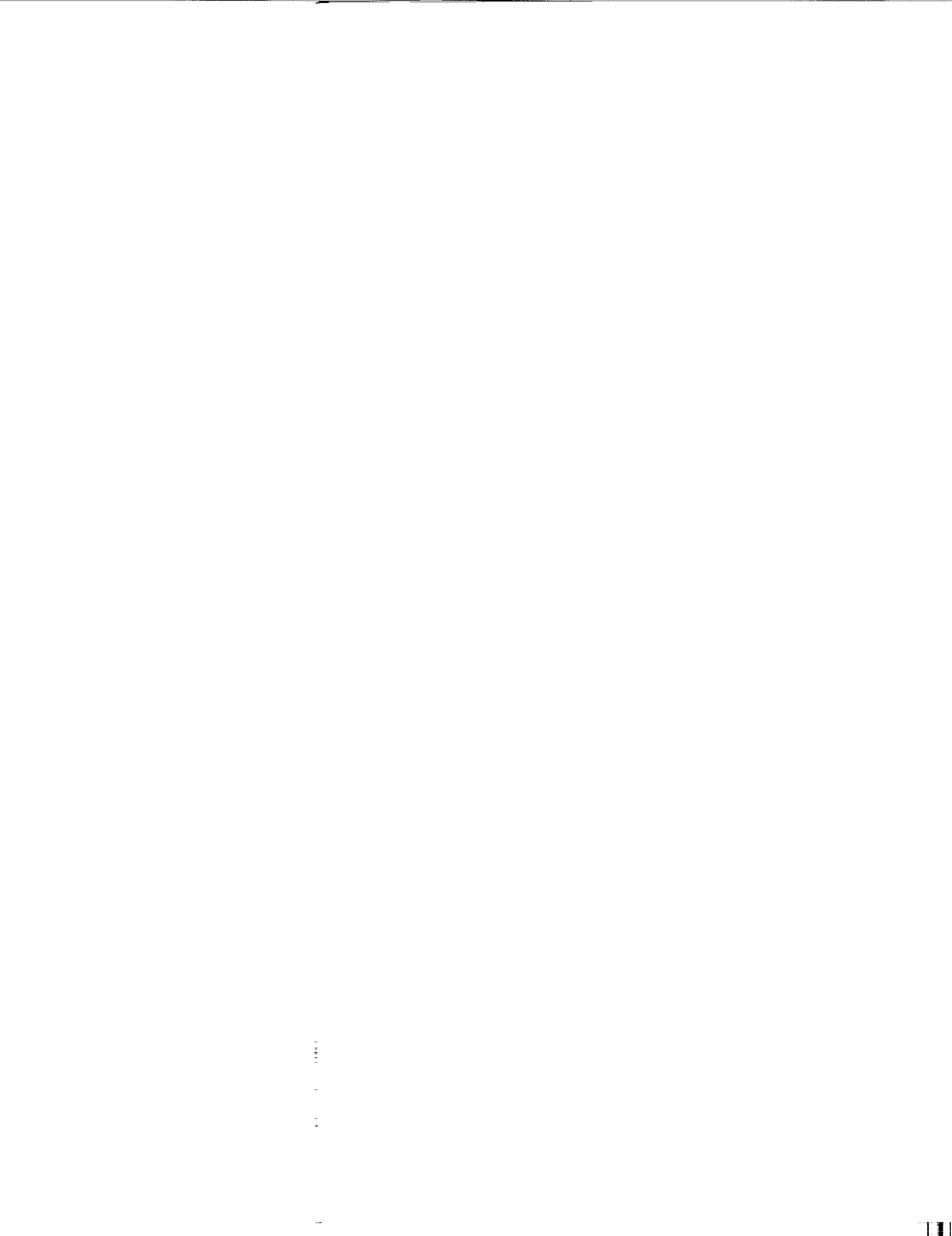# DELTA METHOD, AN EMPIRICAL
DRAG BUILDUP TECHNIQUE

R. C. Feagin, et al

Lockheed - California Company
Burbank, California

December 1978

DELTA METHOD, AN EMPIRICAL DRAG BUILDUP TECHNIQUE

Richard C. Feagin and William D. Morrison, Jr.

LOCKHEED-CALIFORNIA COMPANY
BURBANK, CALIFORNIA 91520

NASA

National Aeronautics and
Space Administration

Ames Research Center
Moffett Field, CA 94035

DELTA METHOD, AN EMPIRICAL DRAG BUILDUP TECHNIQUE

Richard C. Feagin and William D. Morrison, Jr.

LOCKHEED-CALIFORNIA COMPANY
BURBANK, CALIFORNIA 91520

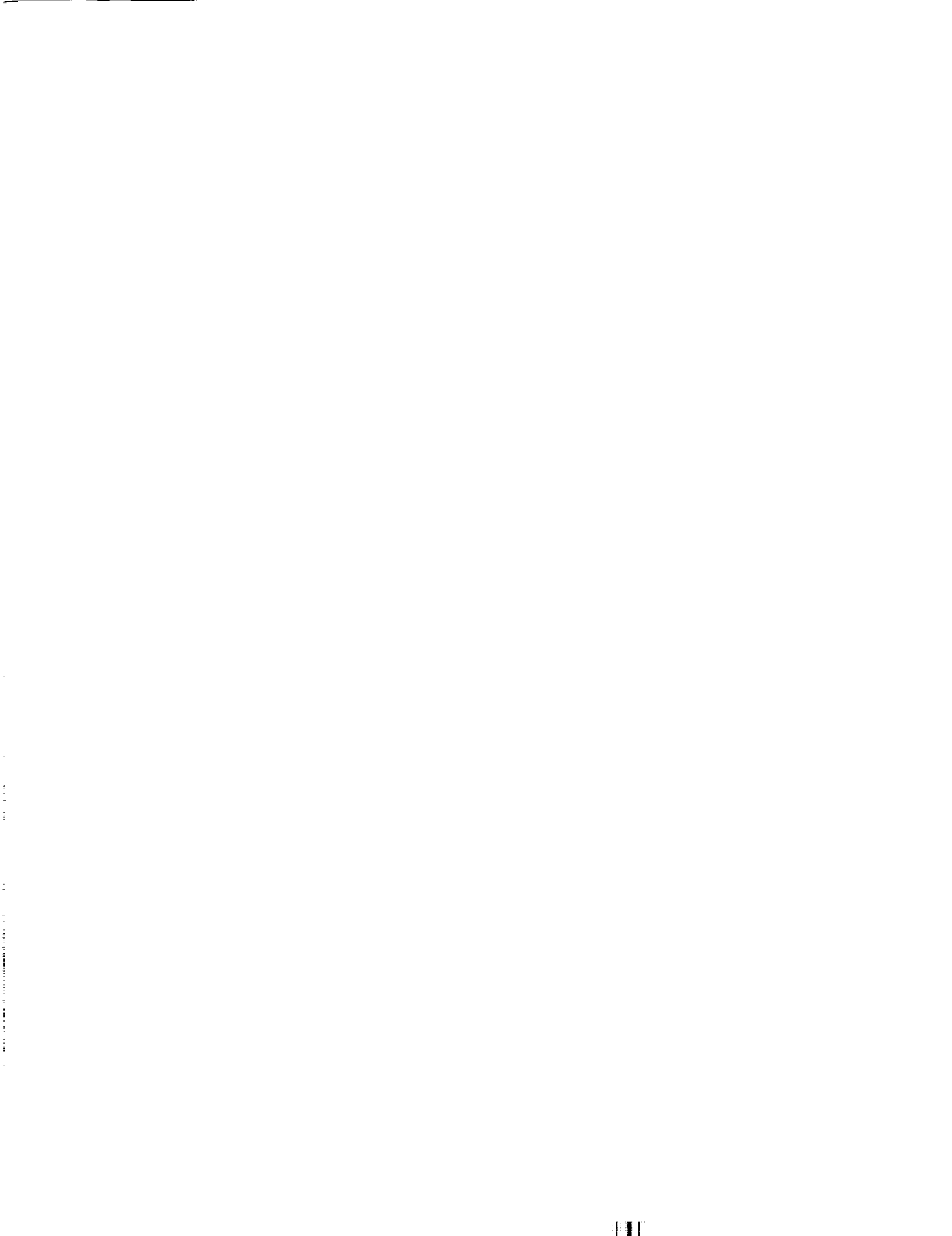| 1. REPORT NO. NASA CR 151971	2. GOVERNMENT ACCESSION NO.	3. RECIPIENT'S CATALOG NO.
4. TITLE AND SUBTITLE DELTA METHOD, AN EMPIRICAL DRAG BUILDUP TECHNIQUE		5. REPORT DATE Dec. 1978
		6. PERFORMING ORG CODE
7. AUTHOR(S) Richard C. Feagin & W.D. Morrison, Jr.		8. PERFORMING ORG REPORT NO. LR 27975 Vol I
9. PERFORMING ORGANIZATION NAME AND ADDRESS LOCKHEED-CALIFORNIA COMPANY P.O. BOX 551 BURBANK, CALIFORNIA 91520		10. WORK UNIT NO.
		11. CONTRACT OR GRANT NO. NAS2-8612, Mod. 6
12. SPONSORING AGENCY NAME AND ADDRESS Nasa Ames Research Center Moffett Field, CA. 94035		13. TYPE OF REPORT AND PERIOD COVERED Contractor Report 3/1/78 – 12/31/78
		14. SPONSORING AGENCY CODE

15. SUPPLEMENTARY NOTES

Ames Technical Monitor: Gary C. Hill

Final Report

16. ABSTRACT

An emprical drag correlation technique was developed from analysis of 19 subsonic and supersonic military aircraft and 15 advanced or super-critical airfoil configurations which can be applied in conceptual and advanced aircraft design activities. The "Delta Method", as presented in this report, may be used for estimating the clean wing drag polar for cruise and maneuver conditions up to buffet onset, and to approximately Mach 2.0. This technique incorporates a unique capability of predicting the off-design performance of advanced or supercritical airfoil sections. The buffet onset limit may also be estimated. The method is applicable to wind tunnel models as well as to full scale configurations. This technique has been converted into a computer code for use on the IBM 360 and CDC 7600 computer facilities at NASA AMES. The program, "Empirical Drag Estimation Technique (EDET)", is presented in Reference (2). Results obtained using this method to predict know aircraft characteristics are good and agreement can be obtained within a degree of accuracy judged to be sufficient for the initial processes of preliminary design.

17. KEY WORDS (SUGGESTED BY AUTHOR(S)) Empirical Drag Estimation Conventional and Supercritical Sections Preliminary Design	18. DISTRIBUTION STATEMENT		
19. SECURITY CLASSIF. (OF THIS REPORT) Unclassified	20. SECURITY CLASSIF. (OF THIS PAGE) Unclassified	21. NO. OF PAGES	22. PRICE*

TABLE OF CONTENTS

LIST OF FIGURES

LIST OF FIGURES (Continued)

LIST OF TABLES

DELTA METHOD, AN EMPIRICAL
DRAG BUILDUP TECHNIQUE

Richard C. Feagin and William D. Morrison Jr.

Lockheed-California Company
Burbank, California 91520

SUMMARY

The Lockheed-California Company, under NASA Ames Contract No. NAS2-8612, Mod 6, has applied empirical drag correlation techniques to 19 subsonic and supersonic military aircraft and 15 advanced or supercritical airfoil concepts to develop an empirical drag estimation technique which can be applied in future design activities. The resulting method is presented in this report. The use of the technique provides a capability of estimating the total configuration drag polar near the cruise lift coefficient (Design $C_L \pm 0.30$) and a speed range from Mach 0.40 to approximately Mach 2.0. Included also is the capability of predicting the subsonic off-design performance of advanced or supercritical airfoil sections. Buffet onset may also be estimated. The method can be applied to wind tunnel models as well as to full scale configurations. The technique has been converted into a computer code which is compatible with the NASA Ames computer facilities. The program, "Empirical Drag Technique (EDET)", is presented in reference 2. Results obtained using this method to predict known aircraft characteristics are good and agreement can be obtained within a degree of accuracy judged to be sufficient for the initial processes of preliminary design.

INTRODUCTION

In a conceptual and preliminary design atmosphere, it is desirable
to employ quick methods of configuration evaluation in the first step
towards configuration selection, and necessary when there are numerous
configurations under consideration. The emperical approach of analysis
is to use information already known about existing aircraft to predict
the characteristics of future designs. Such an approach is adopted for
this study.

The Lockheed-California Company, under NASA Ames Contract No. NAS2-8612,
Mod 6, has applied the empirical total drag technique of reference 1 on
19 supersonic and subsonic military aircraft and 15 advanced or super-
critical airfoil concepts to develop an empirical drag estimation technique
which can be applied in future preliminary design activities. Correlated
estimations of design lift coefficient and Mach number, compressibility and
pressure drag, and buffet onset were generated, and the resulting method
is presented in this report.

This method can be used to estimate the total configuration drag polar
within a C_L range of 0.0 to 0.60 or buffet onset and a speed range of
$0.20 < M < 2.0$. Included also is the capability of predicting the subsonic
off-design performance of advanced or supercritical airfoil sections. Buffet
onset may also be estimated. The method may be applied to wind tunnel
models as well as to full scale configurations.

The technique is presented in an easily followed format, and example
calculations are presented. Results obtained using this method to predict
known aircraft characteristics are good and agreement can be obtained within
a degree of accuracy sufficient for establishing trends and for the initial
processes of preliminary design.

This drag prediction technique, has been programmed into a computer
code for use on the NASA Ames IBM 360 and CDC 7600 computer facilities.
The program, "Empirical Drag Estimation Technique (EDET)", is presented
in reference 2.

To provide the basic data for this study, lift and drag data, buffet boundary, and geometric configuration information was supplied by NASA Ames on 18 subject aircraft. These aircraft were the T-2B, T-37B, KA-3B, A-4F, TA-4F, RA-5C, A-6A, A-7A, F-4E, F-5A, F-8C, F-11F, F-100, F-101, F-104G, F-105B, F-106A, and XB-70. Data for the S-3A and 15 advanced concepts was supplied by Lockheed.

The data on the subject aircraft included:

● Wing geometry (aspect ratio, sweep, thickness, and airfoil section)

● Cross-sectional area distribution (area progression curves)

● Drag coefficient variation with lift coefficient and Mach number (polars)

● Lift coefficient buffet limits versus Mach number

Items correlated for each aircraft include:

● Design lift coefficient

● Design Mach number

● Drag divergence Mach number

● Compressibility drag versus Mach number

● Pressure drag versus Mach number

● Lift coefficient for buffet onset versus Mach number

The drag prediction technique resulting from the above correlated items is discussed in Section 1 and the correlations themselves are presented in Section 3. Examples of the use of this technique for drag prediction and data sensitivity are given in Section 4. Basic data for individual aircraft are given by references 3 through 22 and the resulting data packages from which the correlations were obtained are collected in reference 33.

LIST OF SYMBOLS

AR	Wing aspect ratio	b^2/S_{REF}
b	Wing span	ft (m)
c	Total wing chord	ft (m)
$\bar{c}$	Mean aerodynamic chord	ft (m)
C_D	Total aircraft drag coefficient	$D/q\ S_{REF}$
ΔC_D	Incremental drag coefficient	
ΔC_{D_C}	Total compressibility drag coefficient increment	
ΔC_{D_C} FUS	Fuselage compressibility drag coefficient increment	
ΔC_{D_C} INT	Interference drag coefficient increment	
ΔC_{D_C} WING	Wing compressibility drag coefficient increment	
C_{D_F}	Friction drag coefficient	
C_{D_L}	Total drag-due-to-lift coefficient	
$C_{D_{MIN}}$	Minimum drag coefficient	
ΔC_{D_P}	Wing pressure drag coefficient	
$C_{D_{P_{MIN}}}$	Minimum pressure drag coefficient	C_F (F.F.) $\dfrac{S_{WET}}{S_{REF}}$
C_{D_π}	Drag coefficient based on maximum frontal area	
C_F	Skin friction coefficient	
$C_{F_{INC}}$	Incompressible friction drag coefficient	
C_L	Total aircraft lift coefficient	$L/q\ S_{REF}$
ΔC_L	$C_L - C_{L_{DES}}$	
$C_{L_{B.O.}}$	Lift coefficient for buffet onset	
$C_{L_{DES}}$	Design lift coefficient	C_L @ .99M $\left(\dfrac{L}{D}\right)_{MAX}$

4

Symbol	Definition	Units/Expression
D	Drag	lb (N)
d	Fuselage diameter	ft (m)
e	Oswald's wing efficiency factor	
F.F.	Form factor	
h/c	Wing camber @ .7 y/(b/2)	$\left(\dfrac{z_{upper} - z_{lower}}{2c}\right) 100$
L	Lift	lb (N)
L/D	Lift to drag ratio	
ℓ	Reference length	ft (m)
ℓ/d	Fineness ratio	
M or M_∞	Freestream Mach number	
ΔM	$M_\infty - M_{DES}$	
ΔM_{AR}	Mach correction for aspect ratio	
$\Delta M_{\Lambda_{c/4}}$	Mach correction for sweep	
M_{DES}	Design Mach number	M @ .99M $\left(L/D\right)_{max}$
M_{D2-D}	Two Dimensional drag divergence Mach number	$\dfrac{dC_D}{dM} = 0.10$
RN	Reynolds Number	
q	Freestream dynamic pressure	lb/ft^2 (N/m^2)
S_b	Fuselage base area	ft^2 (m^2)
S_{REF}	Reference wing area	ft^2 (m^2)
S_{WET}	Wetted area	ft^2 (m^2)
S_π	Maximum frontal area	ft^2 (m^2)
TOT	Subscript denoting total aircraft	
$(t/c)_{EFF}$	Effective thickness ratio. Wing frontal area divided by plan area to wing/body intersection, includes gloves.	
x, y, z	Wing coordinate system	
λ	Wing taper ratio	

$\Lambda_{c/4}$	Sweep of wing quarter chord	deg (rad)
$\Lambda_{L.E.}$	Sweep of wing leading edge	deg (rad)
η	Number of configuration component parts	
$(\ )'$	Interim calculation	

6

1. DRAG PREDICTION PROCEDURE

The Delta Method, drag correlation technique can be used to predict drag "polars" for subsonic and supersonic aircraft configurations from the limited geometric parameters known during the advanced stages of design work. This method is uniquely capable of predicting the design and off-design performance of advanced airfoil sections and supercritical wings. It is most applicable near the cruise condition and is not appropriate for analysis of turning capabilities or performance near maximum lift coefficients. The technique can be applied equally well for total aircraft configurations or analysis of wind tunnel data.

The technique is to be used in a preliminary design atmosphere where design details are minimal and where it is usually desirable to investigate the trade-off of such design parameters as sweep, aspect ratio, thickness, or body geometry on performance. All that is needed to provide input to this procedure is a three-view drawing or sketch of the basic configuration and a rough estimation of the proposed fuselage area distribution. With these data for input, a matrix on configurations can easily be analyzed and design trends noted in a time span considerably shorter than that required of most conventional methods.

As with most empirically derived procedures, the range of applicability of this method is most accurate within the range of data from which it was derived. Where such limitations exist, they are pointed out in the following discussion so that caution can be exercised if the user wishes to analyze configurations outside this range. The computer program of reference 2 is also structured so that these limits cannot be passed thereby eliminating the inadvertent calculation of data outside the region of applicability.

It should be noted that the drag correlations to follow do not include the effects of maneuvering devices such as flaps, slats, or boundary layer control and is representative of a clean wing configuration only. The effects of high lift devices if desired, will have to be added to the final results of this method by the individual concerned using conventional estimation procedures.

The flight test drag polars for all subject aircraft were broken down into their individual components by the method discussed in Section 2. These incremental values, along with the buffet onset information, were exercised in an extensive correlation study using known aircraft geometric properties and variations on the transonic simularity rules wherever these rules were deemed applicable. The additional information on current advanced or super-critical airfoil configurations included in the correlation reflects the latest levels of technology.

Total aircraft drag is considered as being composed of two major parts, that which is independent of lift ($C_{D_{MIN}}$), and drag due to lift or induced drag (C_{D_L}).

$$C_D = C_{D_{MIN}} + C_{D_L} \tag{1}$$

The minimum drag level occurs when drag due to lift is zero and is the result of friction, compressibility, and miscellaneous items such as external stores.

$$C_{D_{MIN}} = C_{D_F} + \Delta C_{D_C} + \Delta C_D \tag{2}$$

Drag-due-to-lift is assumed to be composed of the incremental value of wing pressure drag and the theoretical level of induced drag.

$$C_{D_L} = \Delta C_{D_P} + C_L^2/\pi AR \tag{3}$$

The terms ΔC_{D_C} and ΔC_{D_P} represent a departure from most classical drag buildup techniques and will now be defined in order to forgo any confusion regarding the above equation. The compressibility drag increment due to volume (ΔC_{D_C}) is assumed to be composed of form drag which is a function of shape and volume effects upon viscous pressure levels due to increases in local Mach numbers, and compressibility effects as local flows become sonic and shock waves form. In the supersonic speed range, form compressibility, and zero lift wave drag are assumed synonymous.

8

The wing pressure term (ΔC_{D_p}) is the induced drag increment above that produced by the theoretical level resulting from $C_L^2/\pi AR$. It primarily is a function of the wing and includes a combination of many effects (separation, lift dependent compressibility drag, span-wise flow, body effects, etc.) none of which are easily computed with the limited aircraft data available. The division of induced drag into two parts, theoretical and an incremental wing pressure term, provides the user an easy way of treating induced drag since the above lift dependent drag items are not usually known in a preliminary design environment.

This section presents the final correlated values resulting from this emperical drag correlation technique, called the "Delta Method". These parameters also make up the aircraft drag prediction computer program (EDET) detailed in reference 2. Included in this section is a discussion as to the use of these curves and their range of applicability. The actual data correlations are presented in Section 3.

1.1 Design Lift Coefficient and Mach Number

The design lift coefficient $(C_{L_{DES}})$ of a configuration can be obtained from the curves of figure 1 as a function of wing sweep, aspect ratio, effective thickness and camber. The presentation of $(C_{L_{DES}})$ versus $AR \left(\frac{t}{c}\right)^{1/3}$ was derived from configurations with wing effective thickness ratio less than 0.065. The curve at the top of the page is primarily for subsonic/transonic configurations where (t/c) is greater than 0.065 including current supercritical and advanced technology wings. The data correlation which produced these curves is presented in Section 3, figures 30 and 31. The lift coefficient upon which the majority of the following drag computations are based is defined as the increment from this design lift coefficient, given by the relationship

$$\Delta C_L = C_L - C_{L_{DESIGN}} \tag{4}$$

After the design lift coefficient is determined by the above method, the two-dimensional drag divergence Mach numbers is next obtained from figures 2

9

and 3 at the design lift coefficient. Figure 2 is to be used for supersonic configurations and figure 3 differenciates between conventional and the effects of the current supercritical and advanced wing technology for subsonic configurations. The data correlated to produce these relationships is presented in figures 32 and 33 of section 3.

The two-dimensional drag divergence Mach number, is corrected to a three-dimensional value by making the corrections for sweep and aspect ratio effects as presented in figure 4 to derive the configuration's design Mach number. The values are the same as given by reference 33 and are applicable to supersonic, conventional, and advanced sections.

The design Mach number (M_{DES}) is then determined by the relationship

$$M_{DES} = M_{D_{2-D}} + \Delta M_{AR} + \Delta \bar{M}_{\Lambda_{c/4}} \qquad (5)$$

and the incremental Mach number upon which the majority of the following drag computation is based is determined by

$$\Delta M = M_\infty - M_{DES} \qquad (6)$$

1.2 Turbulent Skin Friction (C_{D_F})

After the determination of the configuration's design C_L and Mach number is completed, the next step is the computation of those component drag levels which are independent of lift. The first of these is the determination of skin friction.

Using a three-view or sketch of the configuration in question and estimated area progression curve, the wetted areas and reference lengths of the fuselage, wing, and tail surfaces are determined. The reference length for the fuselage is its overall length. This dimension for the wing and tail surfaces is their individual exposed mean aerodynamic chords. The inlet capture

10

area should be retained in the subject area progression to assure a correct physical presentation for the calculation of wetted area and fuselage fineness ratio. The reference altitude for drag estimation or Reynolds number per foot together with the desired Mach number is selected by the user in computing C_F. This option is also offered in the computer code (EDET) in order that the program may be used either to compute aircraft drag or to verify (or check) wind tunned results.

The configuration component Reynolds number based on individual reference lengths is then computed and the total configuration skin friction drag estimated by the expression

$$C_{D_F} = \Sigma_0^{\eta} \; C_F \; \left(\frac{S_{WET}}{S_{REF}}\right) \; F.F. \; \left(\frac{C_F}{C_{F_{INC}}}\right) \qquad (7)$$

where η is the total number of configuration component parts.

C_F, flatplate friction coefficient, is determined from figure 5 which is extracted from references 34 and 38. C_F is presented as a function of component Reynolds number and transition location (x/ℓ). The zero transition location is assumed for aircraft drag estimation, but a value of (x/ℓ) must be specified with work concerning wind tunnel models where grit is generally applied to assure a specified transition location.

F.F., Form factor, is taken from figures 6 and 7 which are extracted from reference 34. Body form factor is presented in figure 6 as a function of fineness ratio (ℓ/d). Care must be taken for the case of internally mounted engines that inlet capture area be included to obtain the correct value of ℓ/d. Wing and tail form factors are given by figure 7 as a function of effective thickness ratio. A distinction is also made between conventional and advanced airfoil section. The reader is referred to Appendix A for the derivation of the information presented in these two figures.

Since the value of C_F obtained from figure 5 is based on zero Mach number, it must be corrected for Mach effects. This is accomplished by the inclusion of the term $(C_F/C_{F_{INC}})$ which is the ratio of compressible to

11

incompressible friction drag obtained from figure 8 at the desired Mach number. These data are extracted from information as contained in reference 35.

For most fighter configurations there is an additional level of miscellaneous drag associated with items such as gun ports, gutters, antennas, blisters, and conopy shape. These items are included in the flight test polars for each configuration presented in references 3 through 22. A drag buildup of these appendages could be made if a complete and detailed description of them were available, however this is not usually the case during preliminary design. A realistic overall drag level can successfully be estimated by a percentage increase in the level of computed friction drag. Figure 9 presents a correction factor by which the miscellaneous drag estimation may be made. It is a result of the correlation of the computed friction drag of a representative sampling of the subject aircraft versus their recorded subsonic minimum drag levels. This correlation is presented in figure 34, Section 3 and the derivation of the correction factor is presented below.

The value of average skin friction coefficient was computed from the relationship

$$AVG.C_F(\text{computed}) = C_{D_F}\left(\frac{S_{REF}}{S_{WET_{TOT}}}\right) \tag{8}$$

where C_{D_F} was computed from equation (7), and $S_{WET_{TOT}}$ is the total configuration wetted area. The value of an actual average $\overline{C}_F$ for the configuration was then obtained directly from figure 9 and this value used to predict the actual subsonic friction drag level by the relationship

$$C_{D_F}(\text{actual}) = C_{D_F}(\text{computed})\left(\frac{AVG.\ C_F\ \text{actual}}{AVG.\ C_F\ \text{computed}}\right)$$

$$= 1.284\ C_{D_F}(\text{computed}) \tag{9}$$

where 1.284 is the slope of the curve as presented in figures 9 and 34. For the case of wind tunnel models, or when the level of configuration friction drag is already known, the above correction procedure is not necessary.

12

1.3 Compressibility Drag (ΔC_{D_C})

Configuration zero lift compressibility drag (Wave) is assumed to be composed of three components - that due to wing, the fuselage, and wing/body interference effects.

$$\Delta C_{D_C} = \Delta C_{D_C}\text{WING} + \Delta C_{D_C}\text{FUS} + \Delta C_{D_C}\text{INT} \qquad (10)$$

Correlations for component compressibility drag are presented in the following discussion.

1.3.1 __Wing compressibility drag $(\Delta C_{D_C}$ WING)__. - Subsonic wing compressibility drag is presented in figure 10 as a function of effective thickness, camber, and ΔM. These curves are used for both conventional and supercritical and advanced technology airfoils. The data correlations to produce these relationships is given by figure 35.

Figure 11 presents supersonic wing compressibility drag as a function of thickness, camber, aspect ratio, sweep, and ΔM. These curves are restricted to wings of effective thickness ratio less than 0.065 and aspect ratios less than five (5) as these were the outer bounds of the data from which the correlation was derived. The reader should note the change in correlation parameter between subsonic and supersonic configurations. The data correlation for figure 11 is given by figure 36 of Section 2.

1.3.2 __Fuselage compressibility drag $(\Delta C_{D_C}$FUS)__. - To estimate properly the compressibility drag of a fuselage, the user of this technique begins with a preliminary estimation of the area distribution. Here, in contrast to the friction calculation, it is extremely important that this distribution __not__ include the inlet capture area. The cross-sectional areas of horizontal and vertical tail surfaces should be included, however, in order to remain consistent with the methods used in developing the following data. The contribution of the empennage to the overall compressibility drag is usually small when compared to the whole but still should not be overlooked.

13

From the area distribution the user estimates the total length (ℓ), maximum cross-sectional area (S_π), and base area (S_b). These parameters are configuration oriented and large variations can be expected from aircraft to aircraft. A consistent method of determining their values is, therefore, necessary to make this drag estimation procedure meaningful. Figure 12 presents the method used in this study for fuselage geometry estimation. This method should be followed as closely as possible to maintain consistency throughout the drag computation. Area progression curves for the majority of the study aircraft are presented in reference 33.

Subsonic fuselage compressibility drag is presented in figure 13 as a function of the geometry parameters and Mach number. It should be noted that fuselage and interference drag computations are based on the free stream Mach number, while all other drag items are based on the design Mach and are correlated against ΔM. The value of C_{D_π} obtained from figure 13 is based on maximum fuselage area (S_π) and is converted to the reference wing area by the relationship.

$$\Delta C_{D_C} \text{FUS} = C_{D_\pi} \left(\frac{S_\pi}{S_{REF}} \right) \qquad (11)$$

Figure 14 gives supersonic fuselage compressibility drag as a function of body fineness ratio, base to maximum area ratio, and Mach number. Equation (11) must be used to convert the value of C_{D_π} obtained from this figure to the correct area relationship also. The data correlations which produced figures 13 and 14 are presented in Section 3, figures 37 and 38.

1.3.3 <u>Interference drag (ΔC_{D_C}INT)</u>. - Wing/fuselage interference drag, as derived for this method, is presented in figure 15 as a function of body diameter to wing span ratio, taper ratio, and wing sweep. The assumption is made that interference drag is zero below Mach number equal to 1.0. The correlation of data which produced this relationship is shown on figure 39.

1.3.4 <u>Total compressibility drag (ΔC_{D_C})</u>. - The values of ΔC_{D_C}WING, ΔC_{D_C}FUS, and ΔC_{D_C}INT are now combined to produce the total configuration compressibility drag by use of Equation (5). The resulting values, when added to the previously

14

computed level of friction drag, will produce a configuration drag level which is independent of lift throughout the desired Mach range.

1.4 Miscellaneous Drag (ΔC_D)

Allowance is made within the coding of this procedure for the addition of a miscellaneous drag level (ΔC_D) so that the effects of a configuration change or an external store may be included. Such drag levels are computed external to this procedure and input as a function of Mach number. The present coding of EDET allows for a total of 10 separate miscellaneous drag items.

1.5 Induced Drag

Lift dependent drag is predicted as the sum of the theoretical induced drag ($C_L^2/\pi AR$) and a derived term called wing pressure drag (ΔC_{D_P}). The theoretical value is used to define the primary variation of induced drag with lift coefficient and assumes an Oswald's efficiency factor (e) equal to unity. The wing pressure term is, therefore, composed of all lift dependent drag items over and above that of theory. This division provides the user with an easy method for treating induced drag in a preliminary design atmosphere where not much is usually known concerning a configuration's drag characteristics with variations in angle of attack.

1.6 Wing Pressure Drag (ΔC_{D_P})

The remaining lift dependent drag, is included by this technique in the wing pressure drag term, ΔC_{D_P}. Figures 16 through 20 present the subsonic pressure drag as a function of aspect ratio, thickness, camber, ΔM, and ΔC_L. The curves are entered at the desired value of M and interpolated between at the required value of AR $(t/c)^{1/3}$ for the range of ΔC_L under consideration. These data apply to current supercritical and advanced technology wing design

as well as that of conventional subsonic sections. The correlation of data
for these curves is presented in Section 3, figures 40 through 48.

Figures 21 through 27 presents a similar correlation of wing pressure
drag for supersonic airfoils as a function of the same variables as the sub-
sonic data. Interpolation between curves is handled in the same manner.
These curves, however, are restricted to an effective wing thickness of 0.065
and values of AR $(t/c)^{1/3}$ less than 2.0 which are the outer bounds of the
basic data from which they were generated. Data correlation for these curves
is presented in figures 49 through 57.

1.7 Total Aircraft Drag (C_D)

The drag items computed under Sections 1.2 through 1.6 are now combined
with the theoretical induced drag levels by the relationship

$$C_D = C_{D_F} + \Delta C_{D_C} + \Delta C_D + \Delta C_{D_P} + C_L^2/\pi AR \qquad (12)$$

The resulting values, then, represent the estimated total configuration
flaps up drag at the Mach number and lift coefficient selected by the user.

1.8 Buffet Onset ($C_{L_{B.O.}}$)

The drag estimation technique described in the preceeding sections may
also be used for predicting the lift coefficient for buffet onset ($C_{L_{B.O.}}$).
To this end the buffet onset information for the subject aircraft were
evaluated in much the same manner as was the component drag levels. Figure 28
is used for predicting $C_{L_{B.O.}}$ as a function of thickness, aspect ratio, camber,
sweep, $C_{L_{DES}}$, and M_{DES}.

16

It can be seen that buffet onset is relatively independent of wing thickness at low speeds but, as the design Mach is approached, it begins to show an ever increasing variation. The end result of this correlation indicates that, once the design Mach number is passed, the thicker wings tend to enter into buffet at values of lift lower than $C_{L_{DES}}$ while the thinner wings common to present day fighter configurations exhibit an increasing margin in load factor from the design lift within the Mach number range of the basic data.

It should be pointed out that this correlation does not include the effects of maneuvering devices such as flaps or slats but is representative of the clean wing only. The data correlation that resulted in this relationship is presented in figure 58, Section 3.
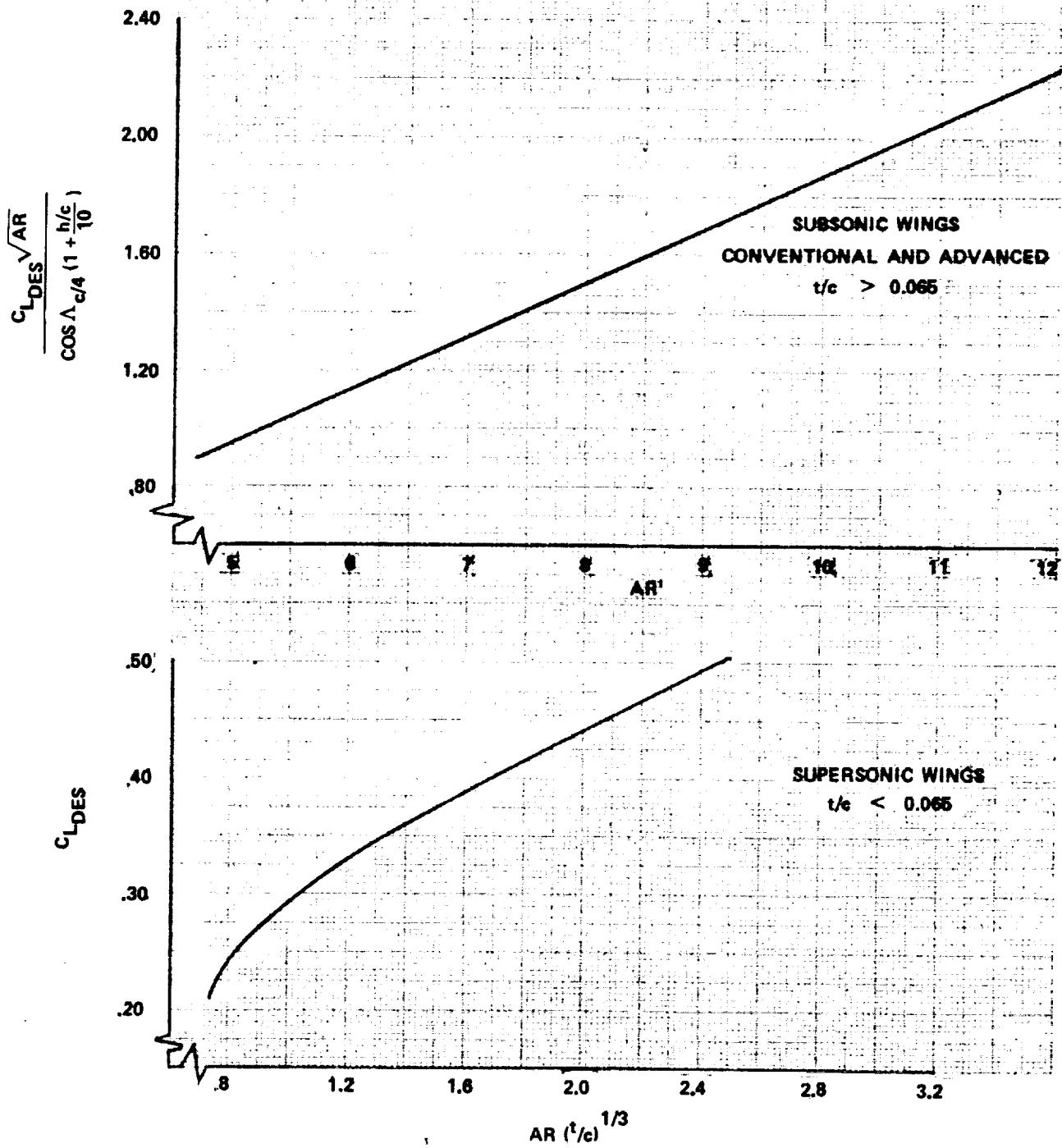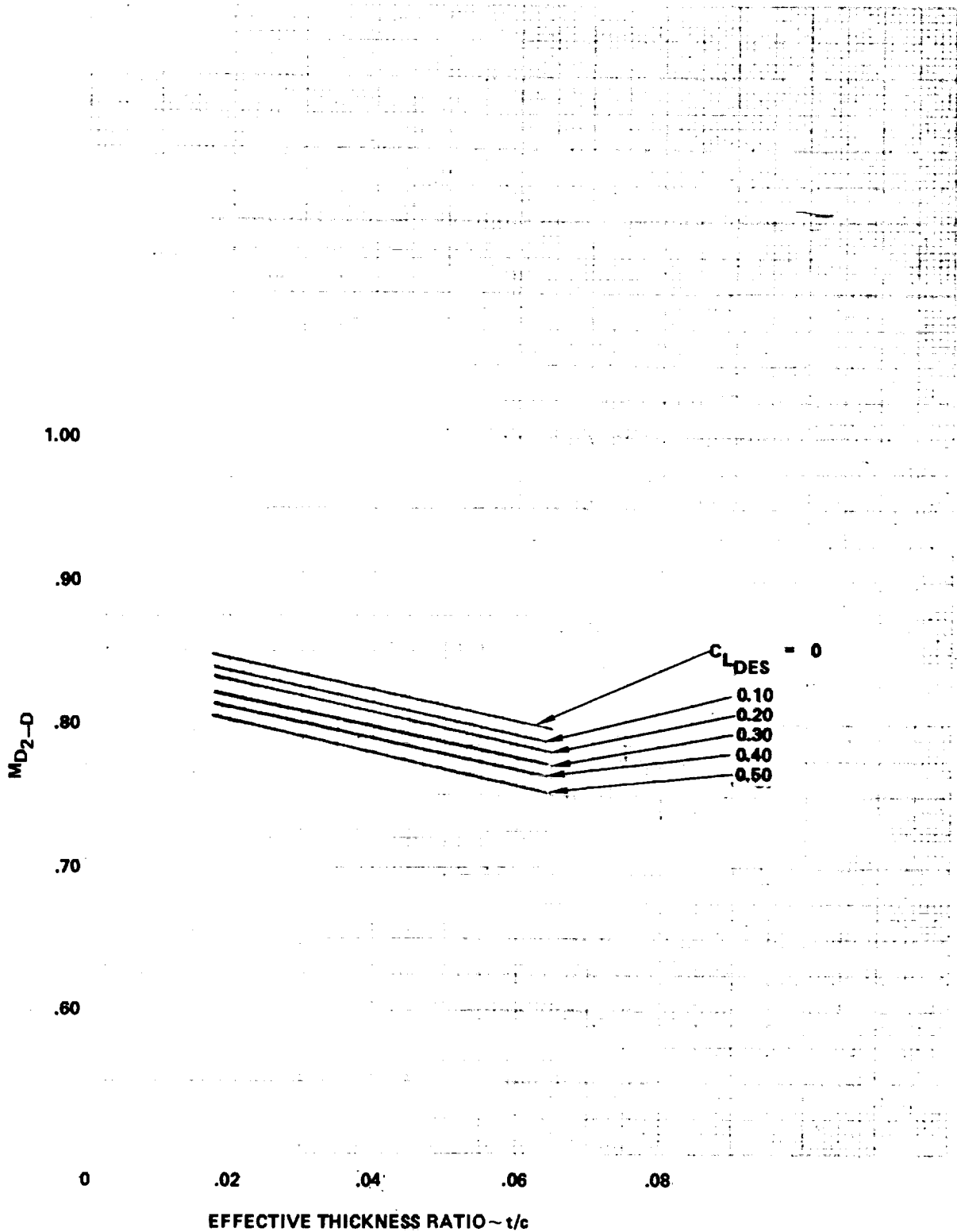
Figure 1. - Design lift coefficient.

Figure 2. - Two-dimensional drag divergence Mach number,
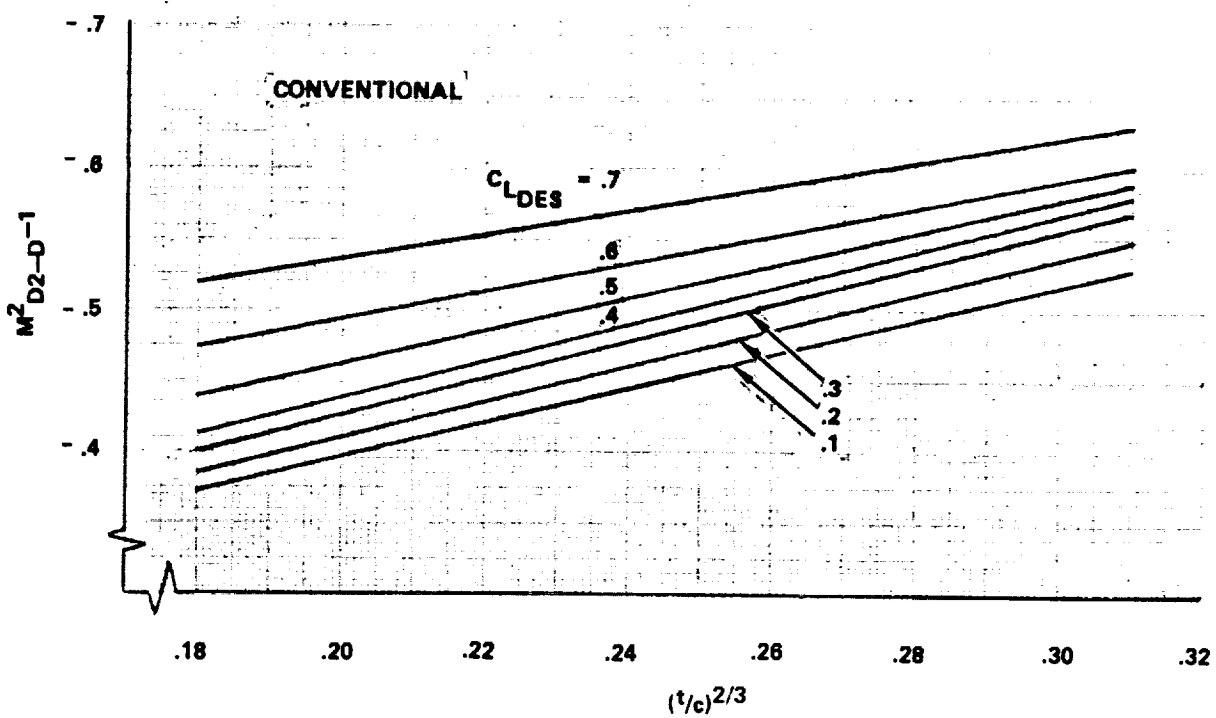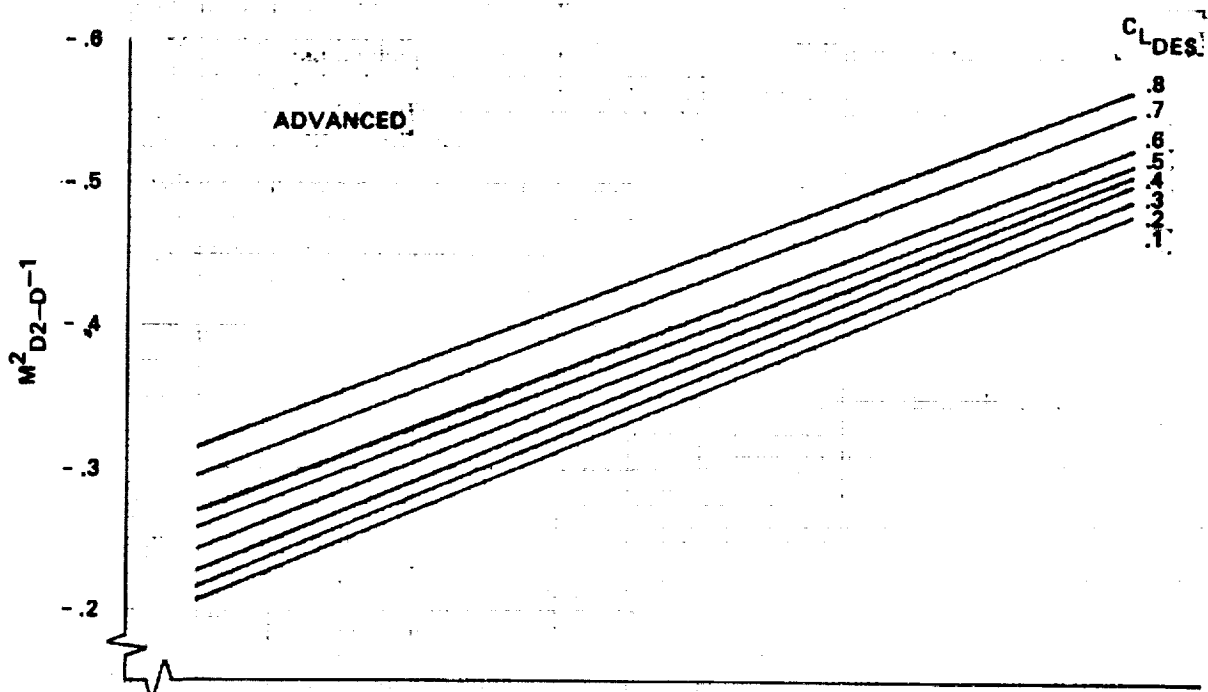supersonic airfoil sections.

19

Figure 3. – Drag divergent Mach number, subsonic airfoil sections.
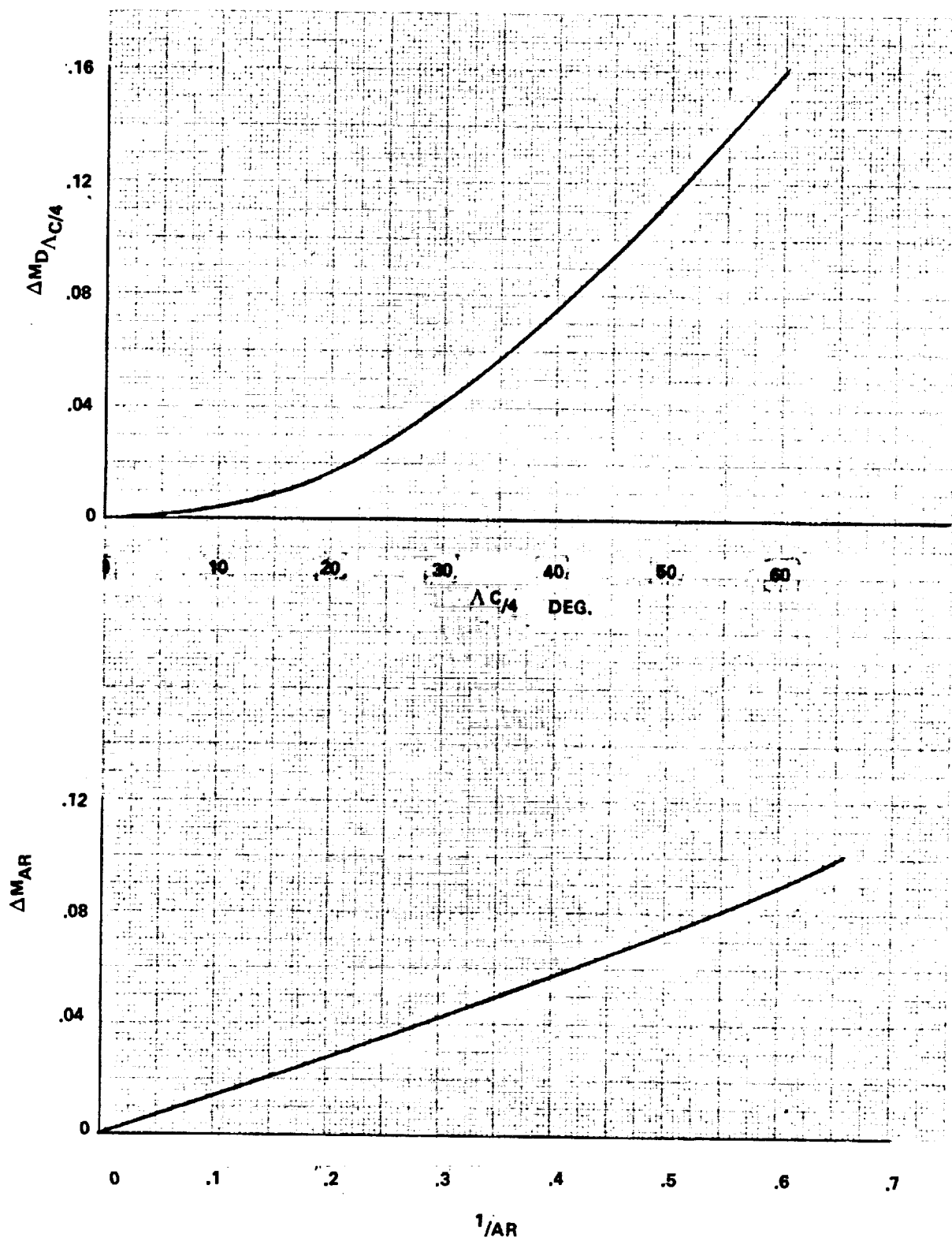
Figure 4. - $M_{D_{2-D}}$ correction parameters.
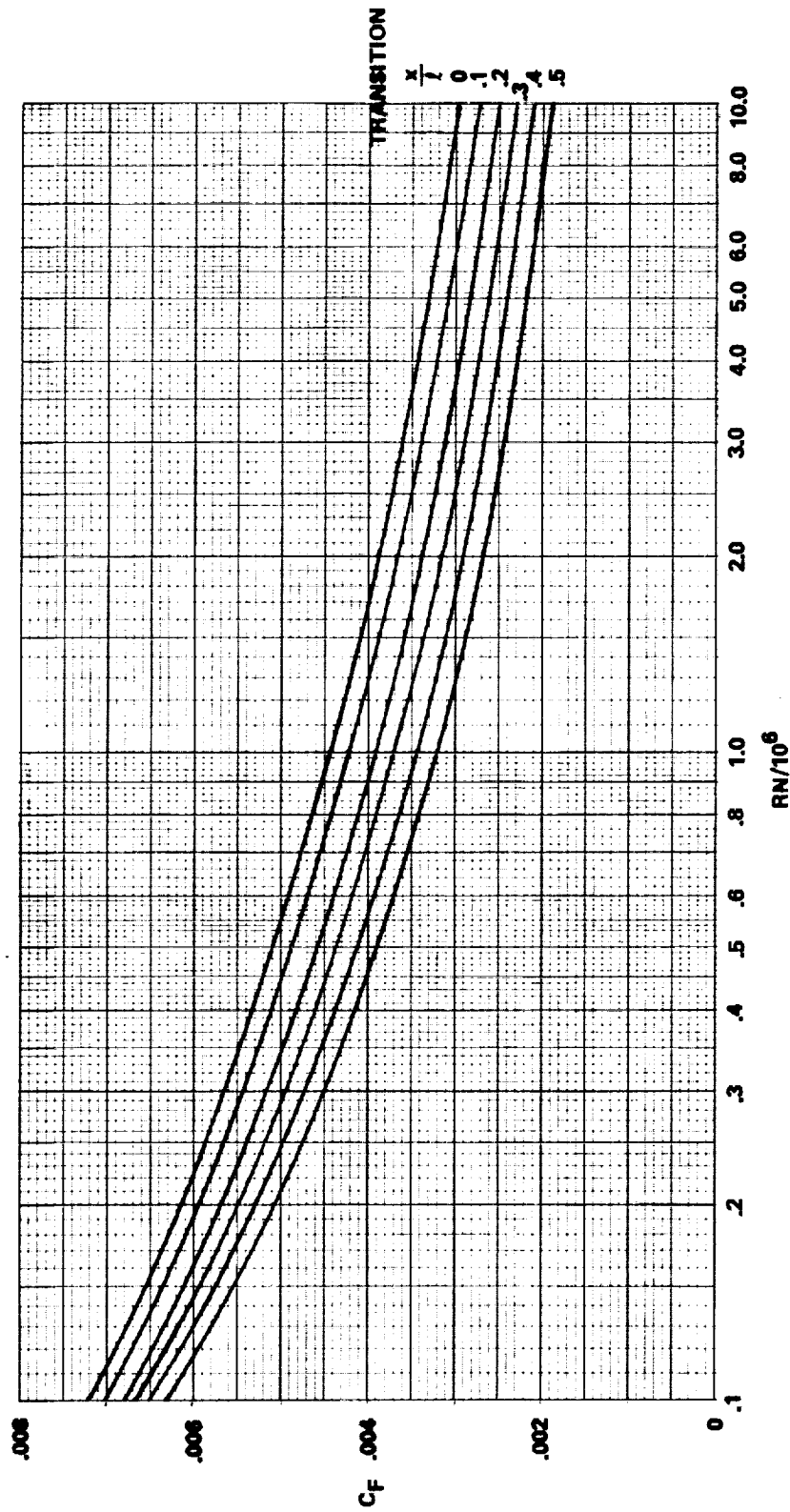
Figure 5. – Variation of flat plate incompressible turbulent skin friction coefficient with Reynolds number.

22
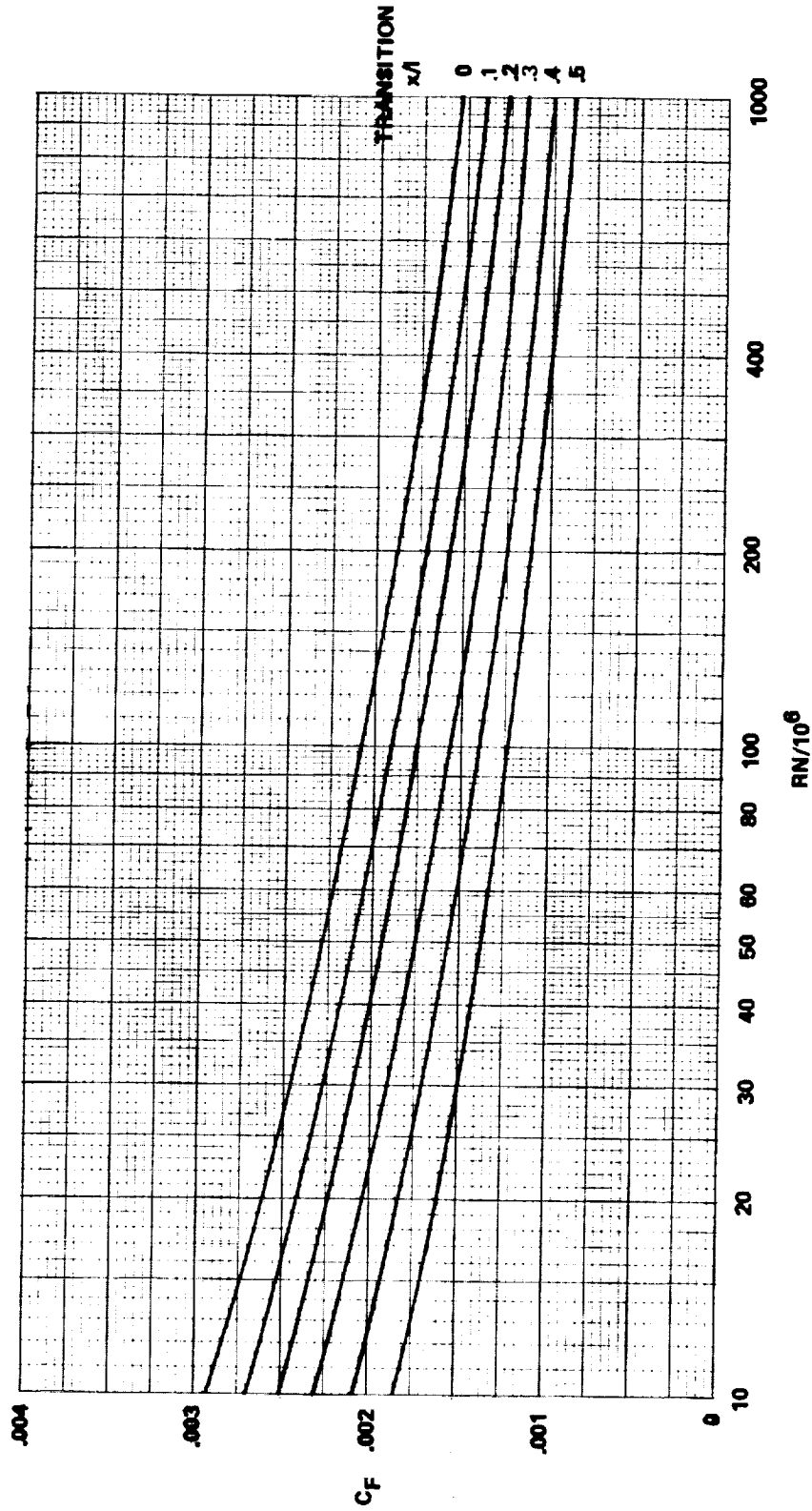
Figure 5. – Concluded.

23

BODY FINENESS RATIO ~ $\frac{\ell}{d}$

BODY FORM FACTOR ~ FF = $\frac{C_D \text{ BODY}}{C_F \text{ FLAT PLATE}}$
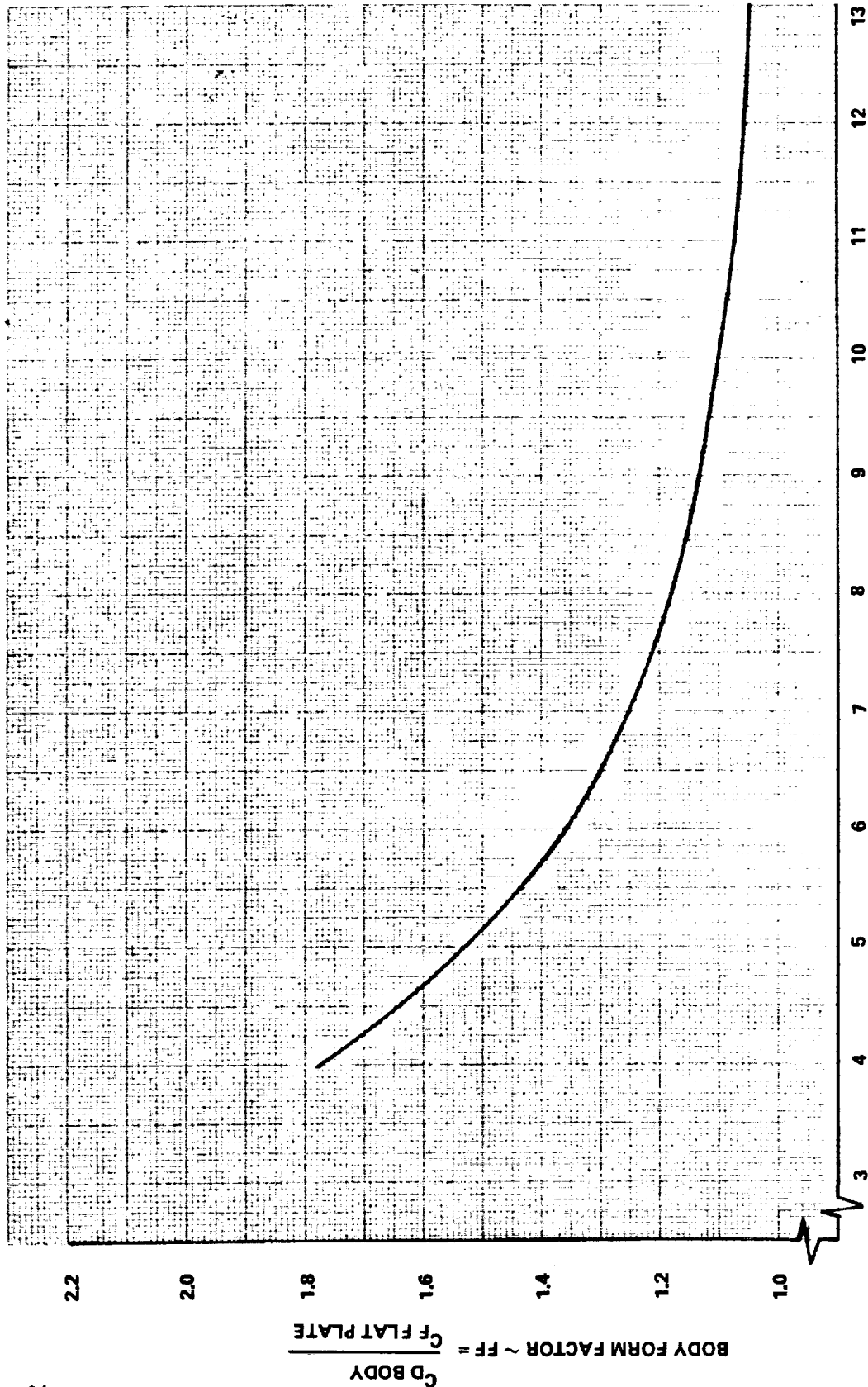
Figure 6. – Body form factor.

24
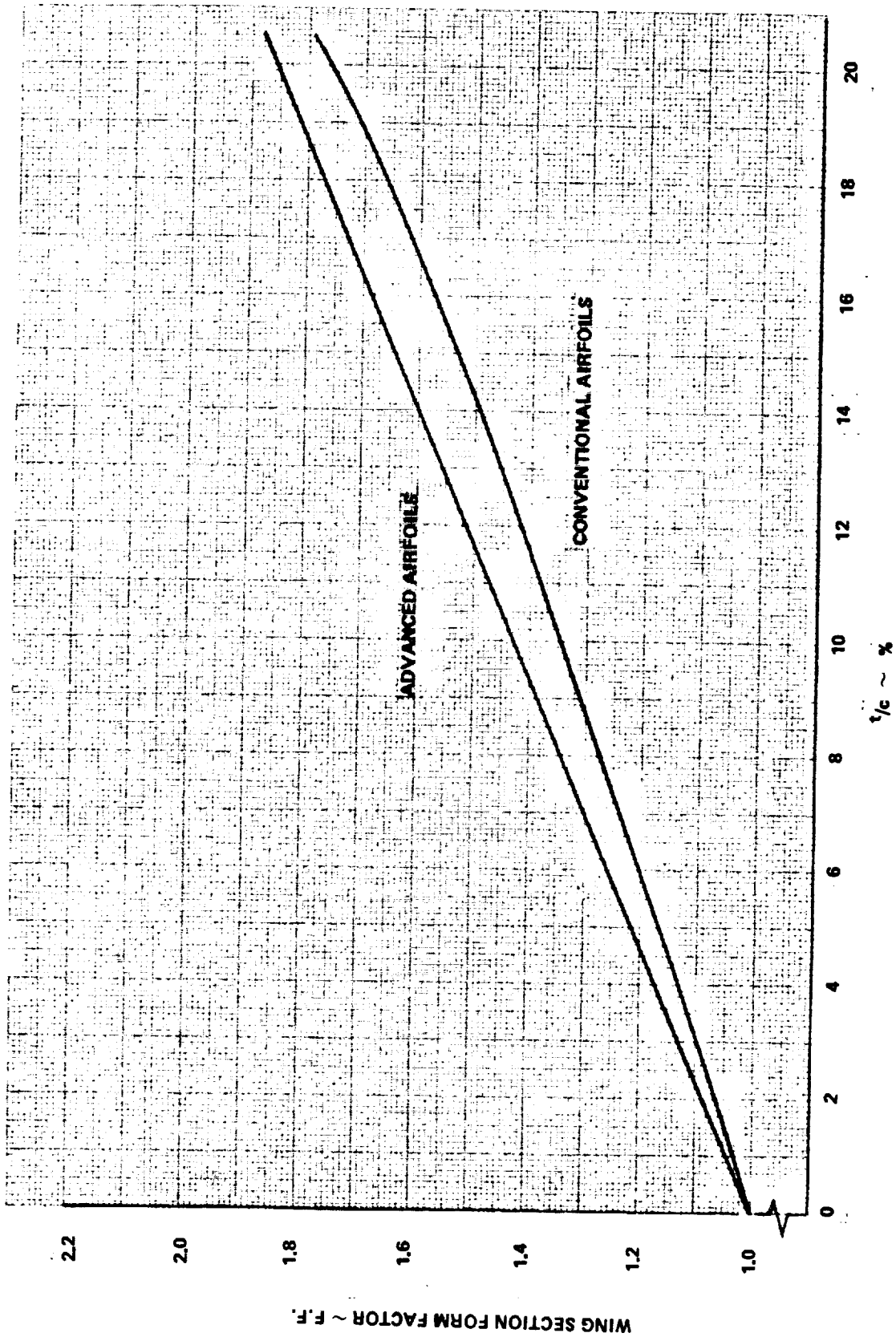
Figure 7. – Wing section form factors.
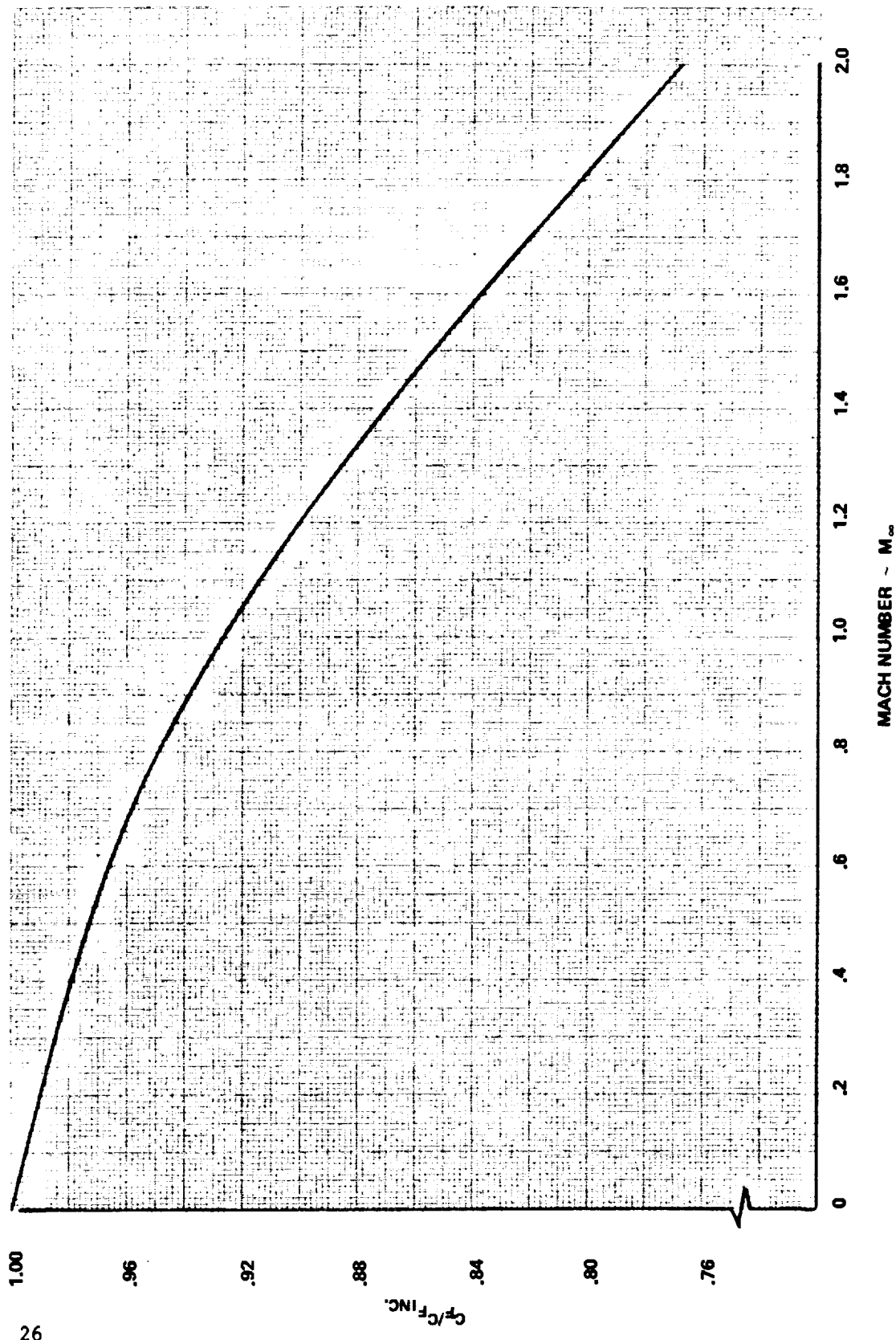
Figure 8. – Compressibility correction to skin friction coefficient.

$$C_F \text{ (COMPUTED)} = C_{D_F} \left(\frac{S_{REF}}{S_{WET}} \right)$$

AVG. C_F (ACTUAL)

AVG. C_F (COMPUTED)
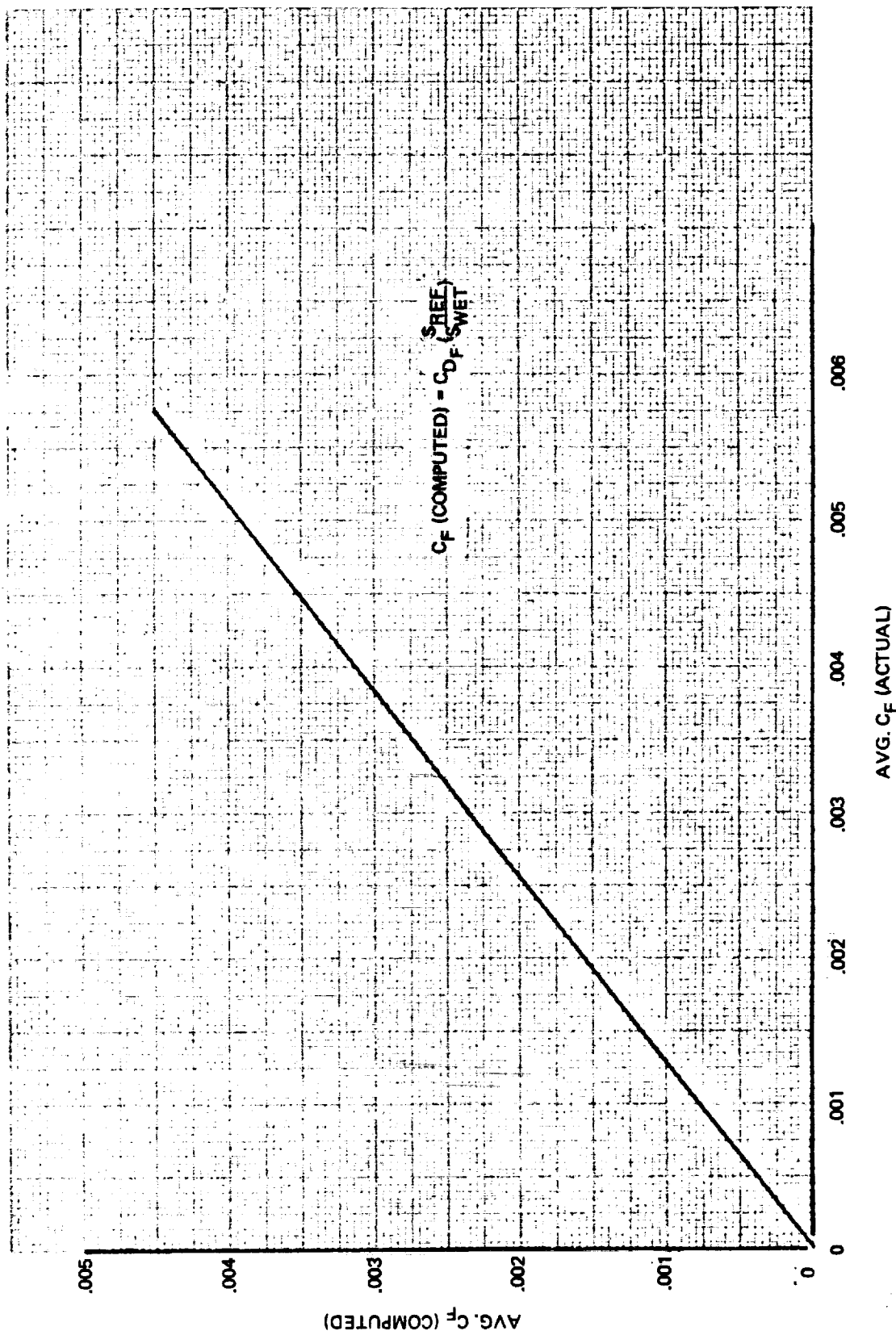
Figure 9. - Friction drag correction parameter.
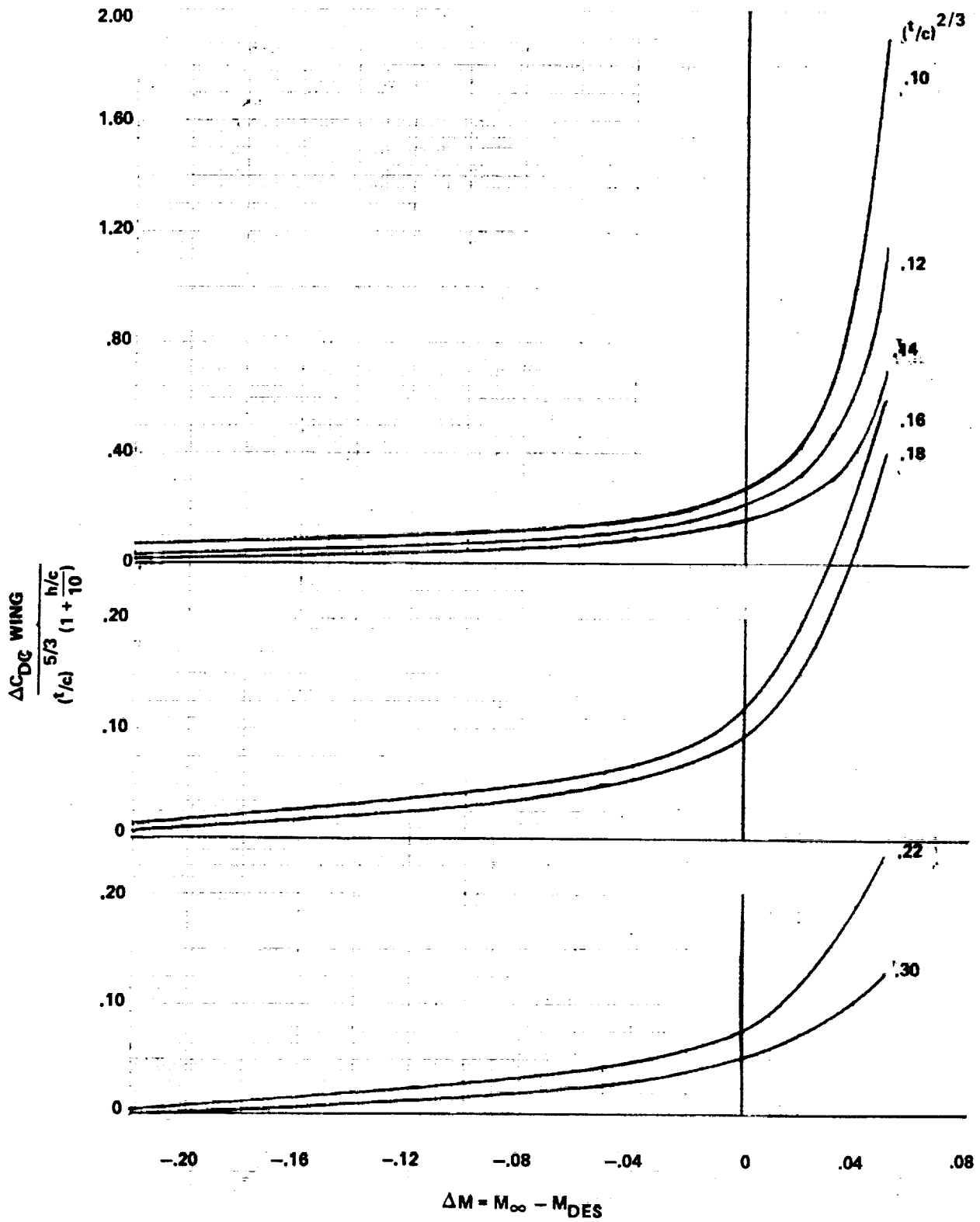
Figure 10. – Subsonic wing compressibility drag.
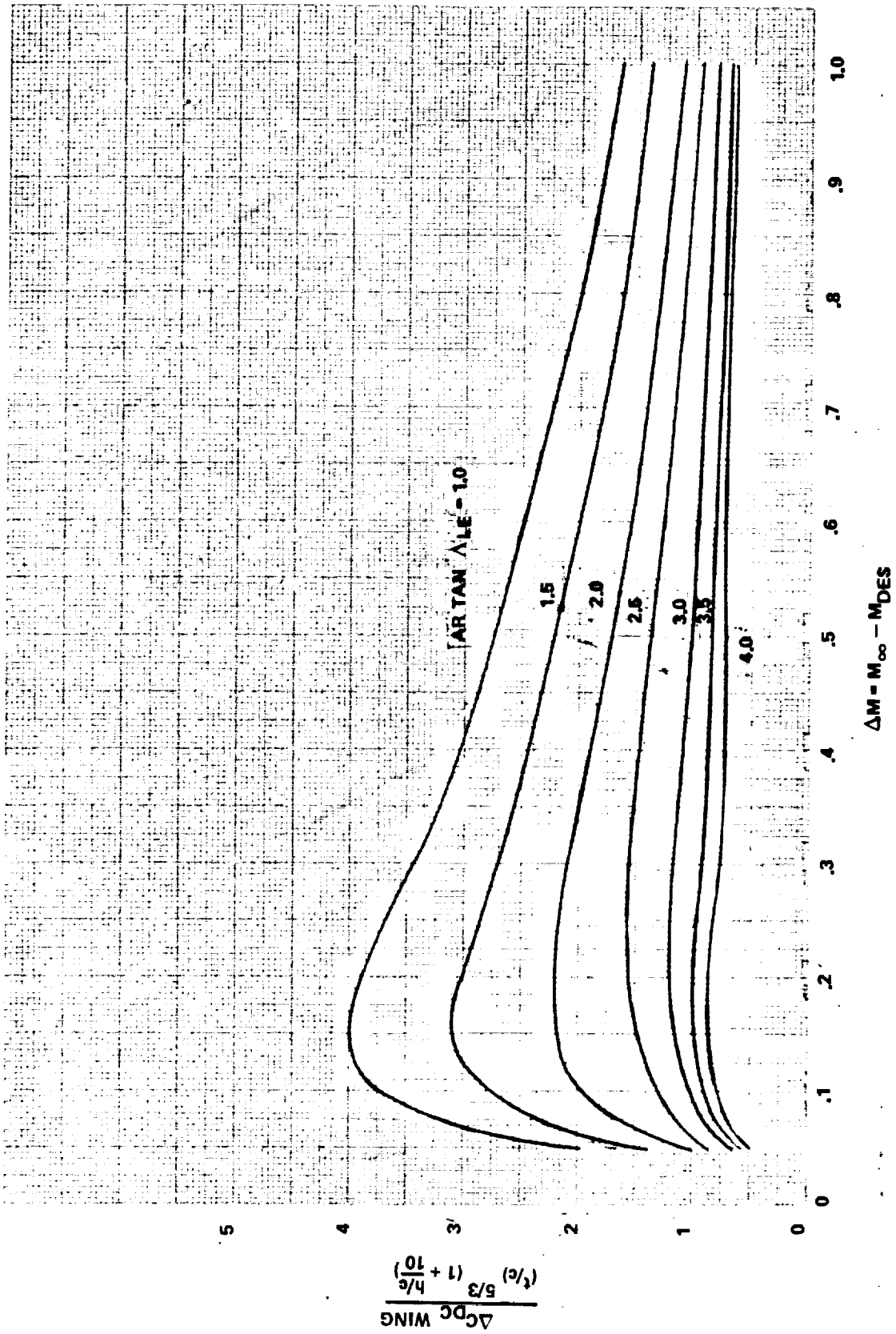
Figure 11. - Supersonic wing compressibility drag.
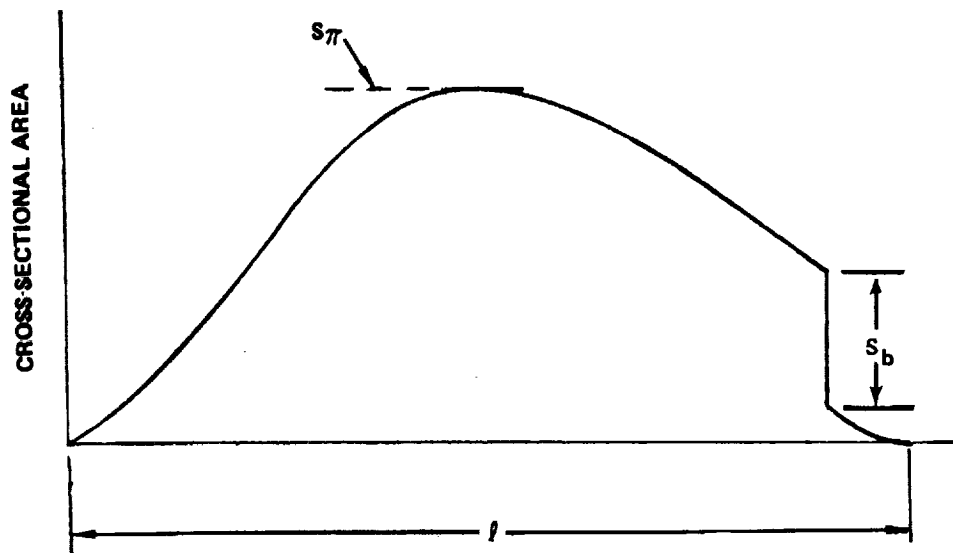
NOTES: HORIZONTAL AND VERTICAL TAIL AREAS ARE INCLUDED.
          WINGS ARE NOT INCLUDED.
          INLET CAPTURE AREAS ARE REMOVED FOR INTERNAL
          MOUNTED ENGINES.
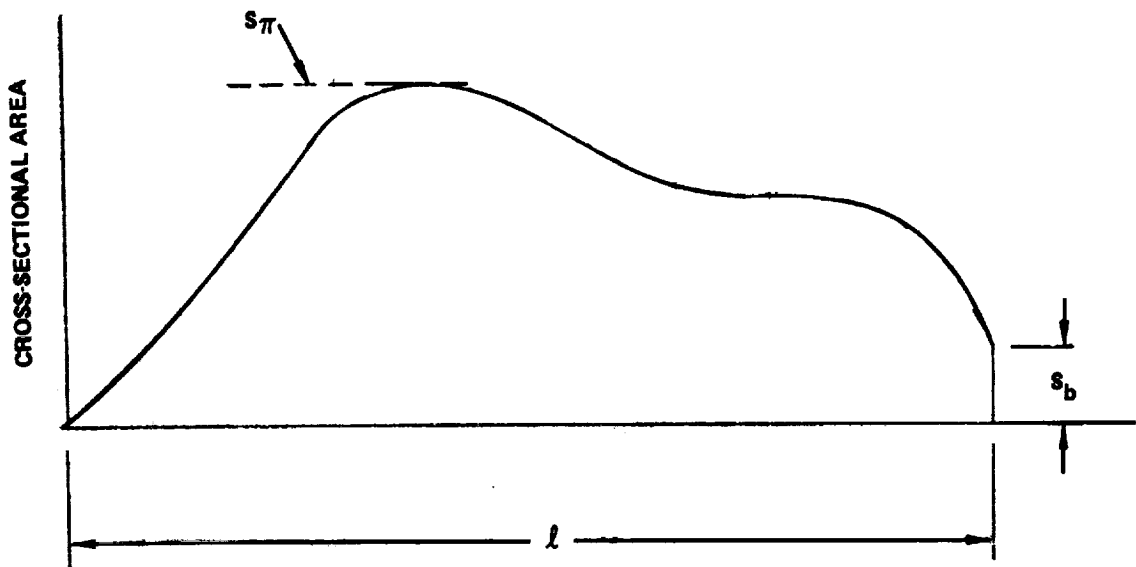
Figure 12. – Suggested method of fuselage geometry parameter selection.

30
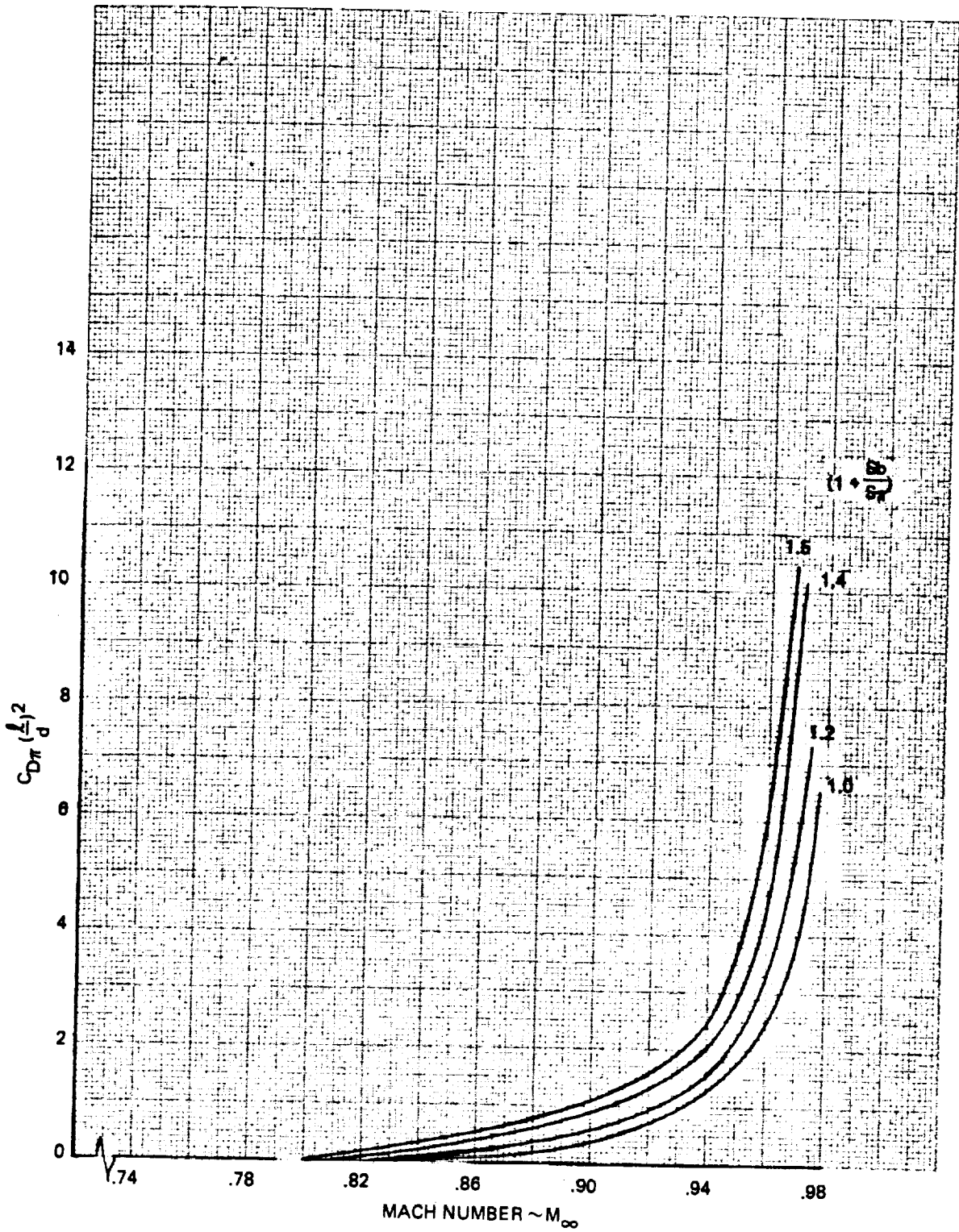
Figure 13. – Subsonic fuselage compressibility drag.
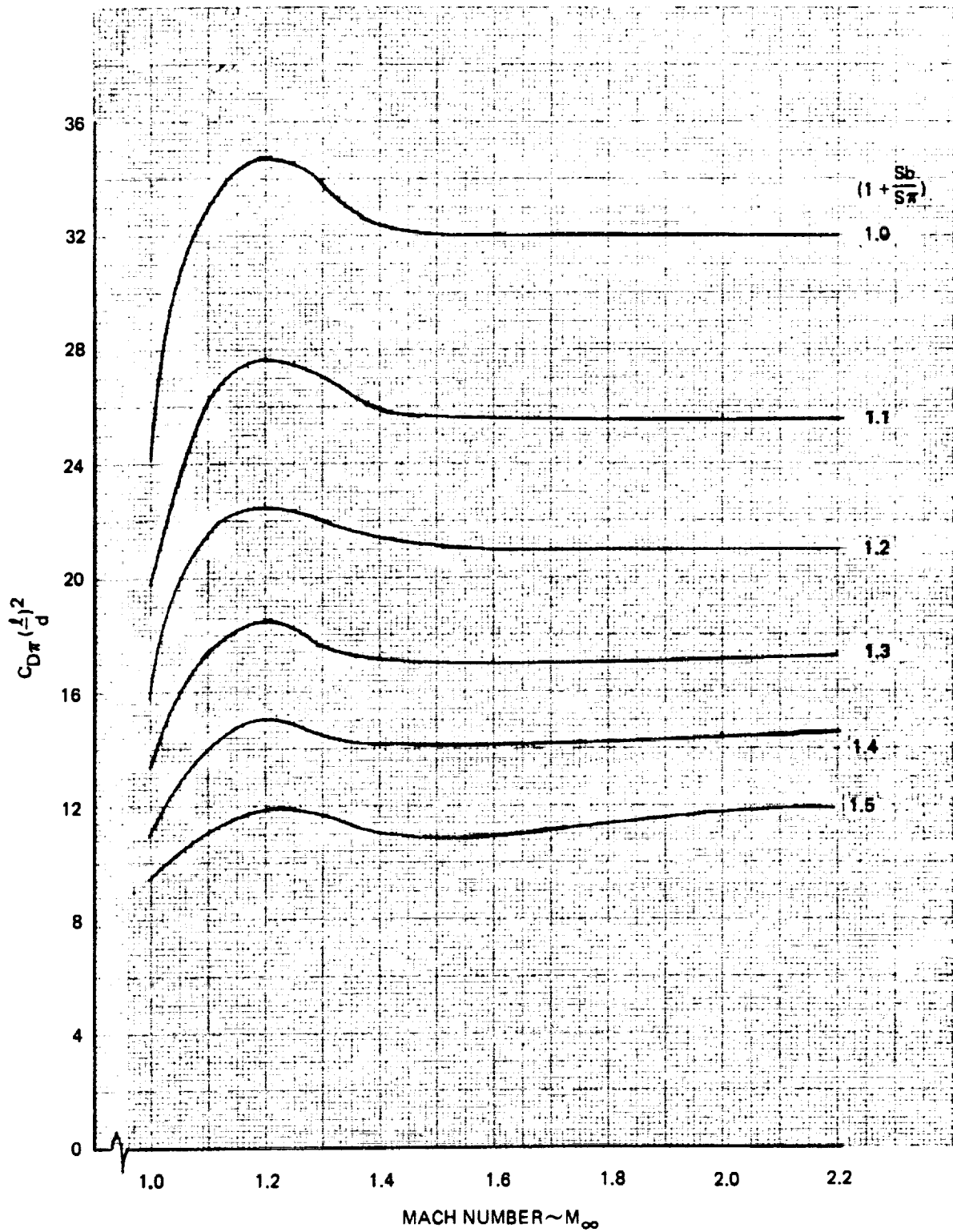
Figure 14. - Supersonic fuselage compressibility drag.
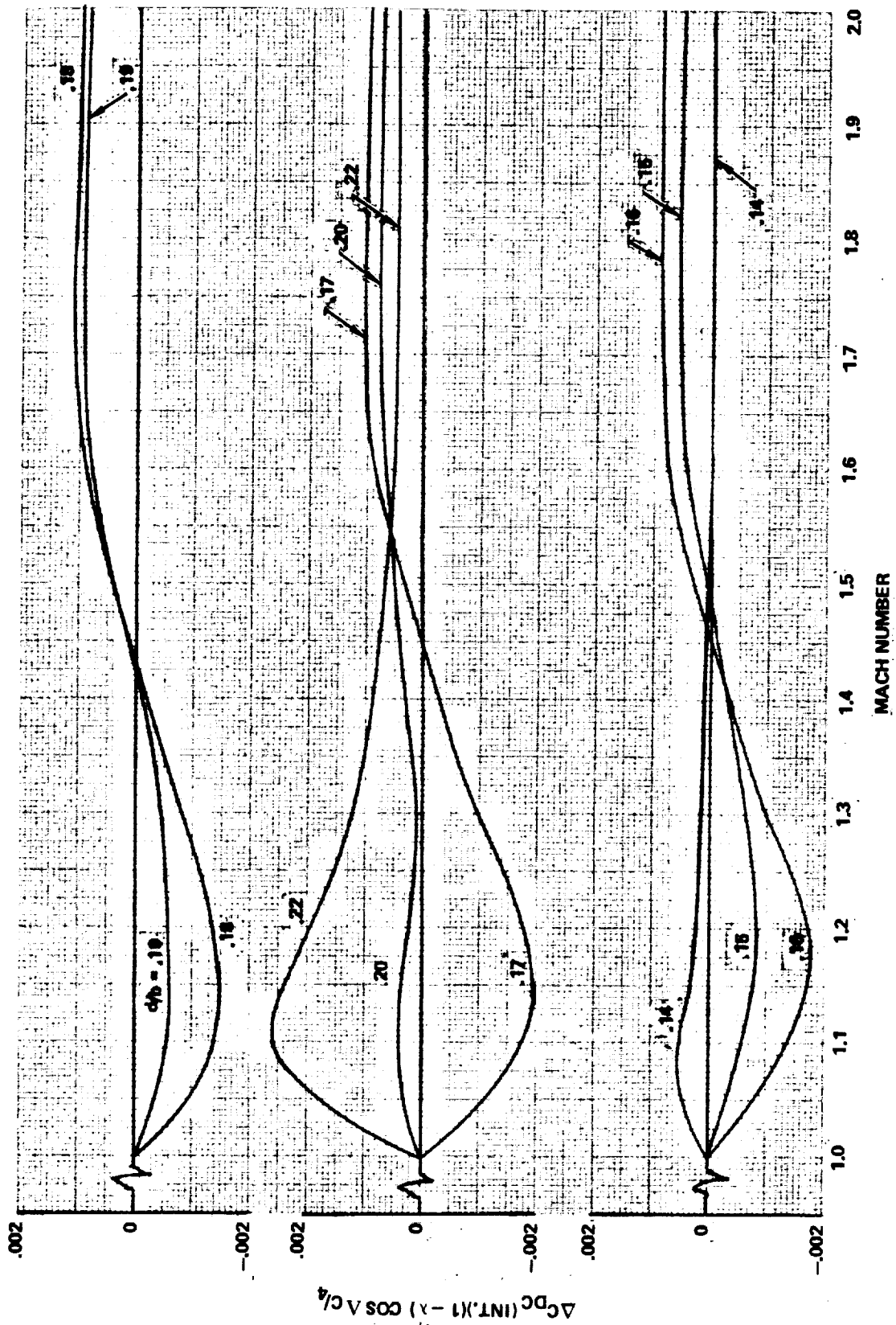
Figure 15. - Wing/body zero lift interference drag.
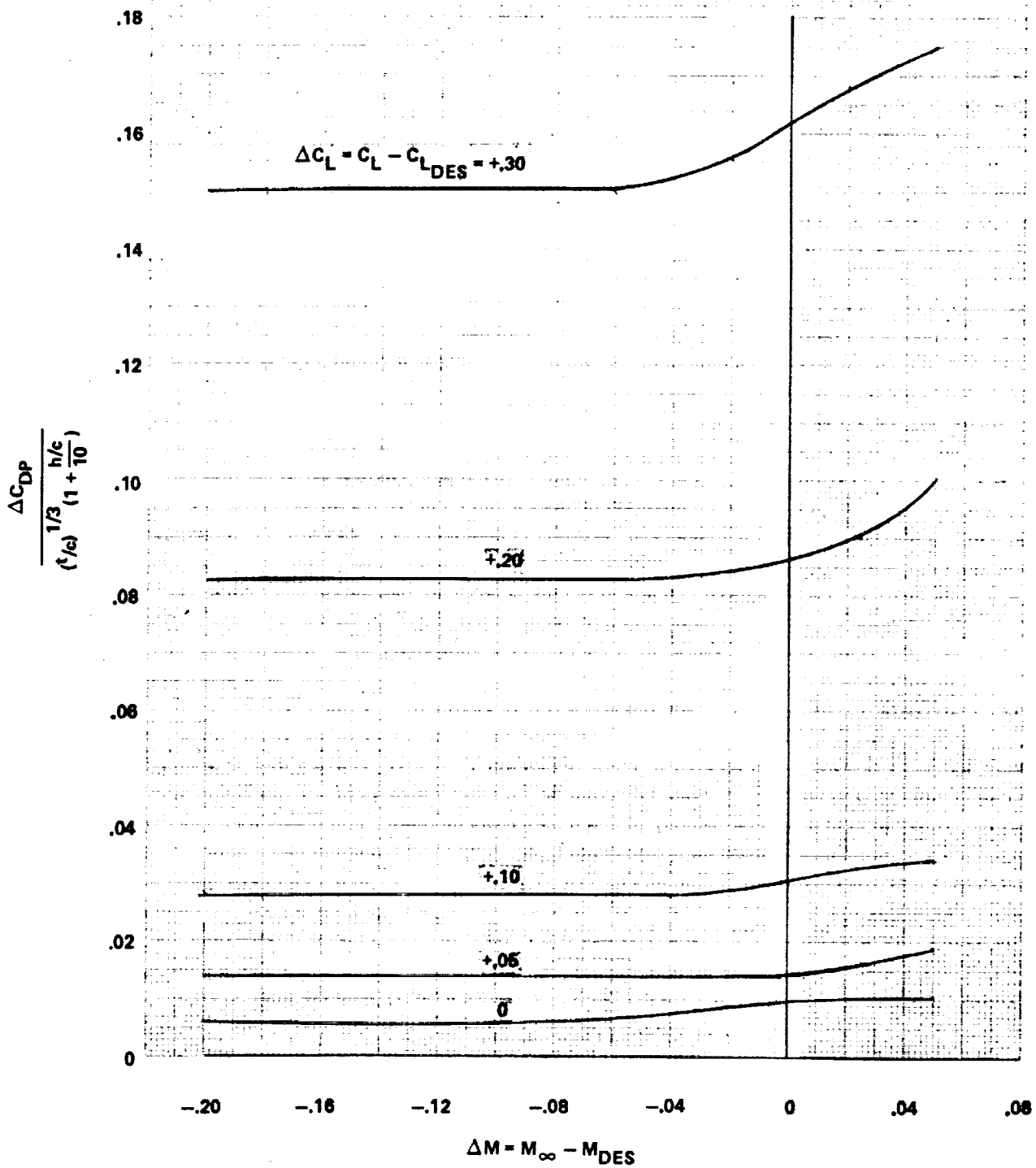
Figure 16. – Subsonic wing pressure drag, $AR \left(\frac{t}{c}\right)^{1/3} = 0.5$.
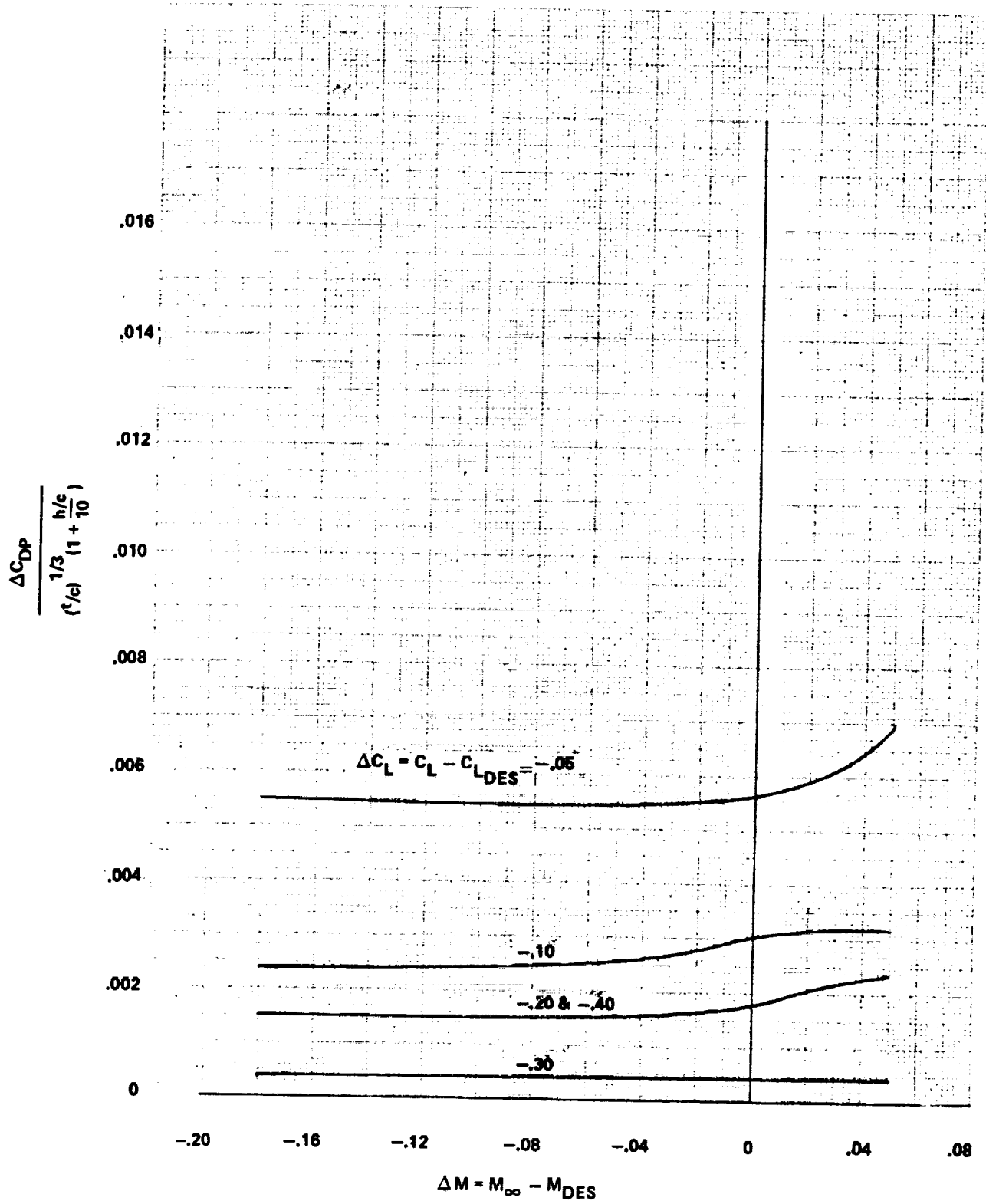
Figure 16. – Concluded.
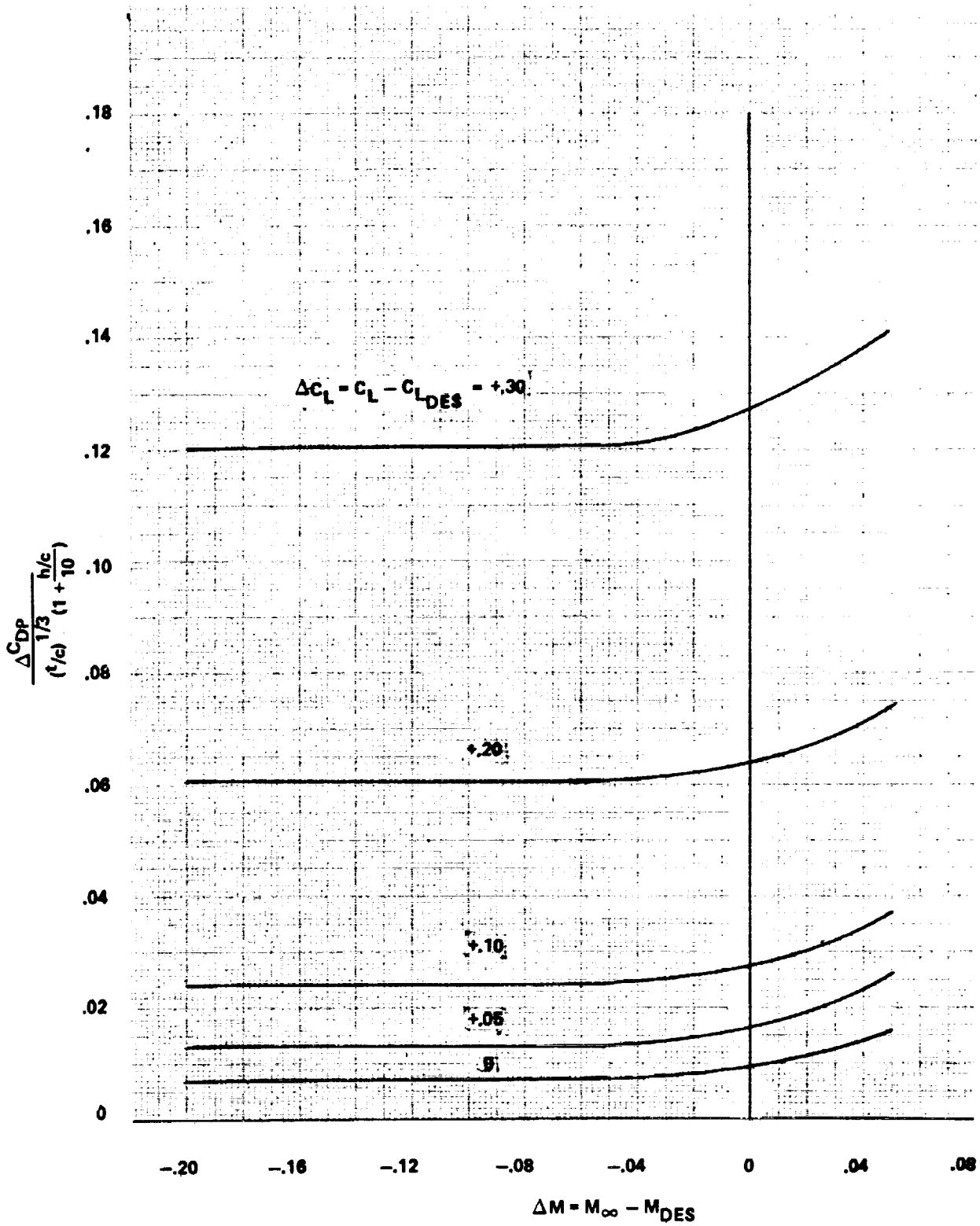
Figure 17. – Subsonic wing pressure drag, AR $(t/c)^{1/3} = 1.0$.
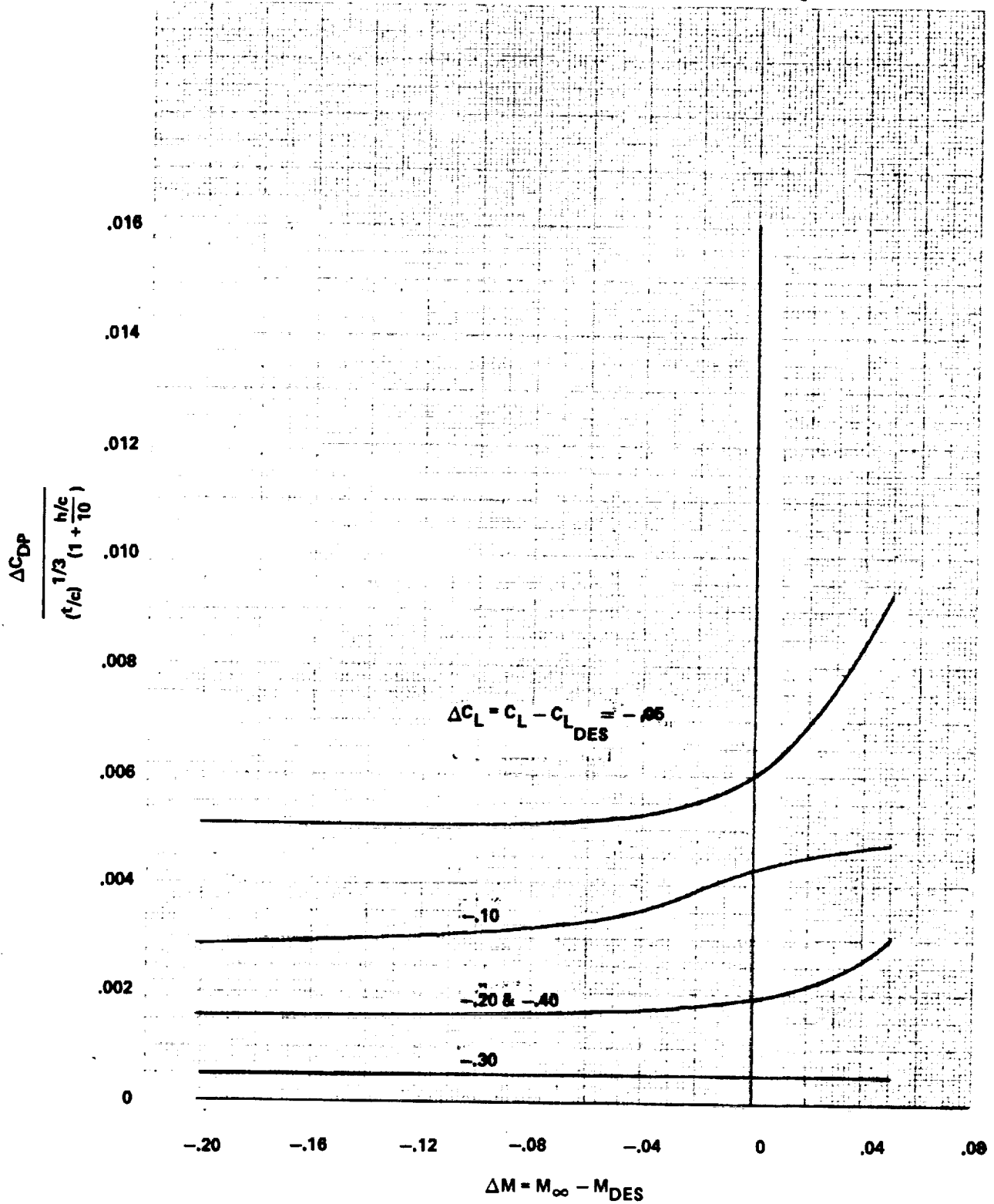
Figure 17. – Concluded.
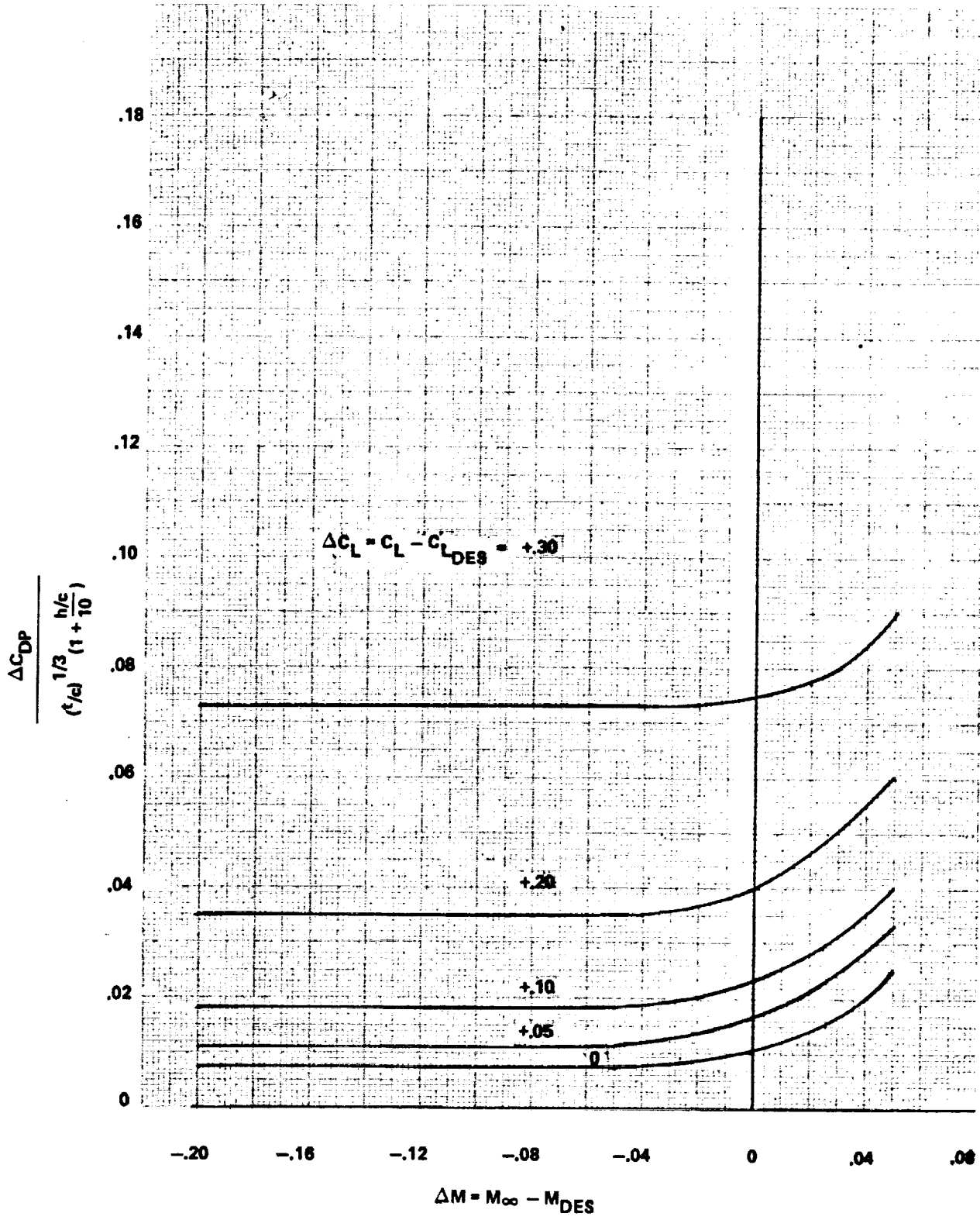
Figure 18. – Subsonic wing pressure drag, AR $(t/c)^{1/3} = 2.0$.

$$\frac{\Delta c_{D_P}}{(^t/c)^{1/3} \, (1 + \frac{h/c}{10})}$$

$\Delta c_L = c_L - c_{L_{DES}} = -.05$

$-.10$

$-.20 \ \& \ -.40$

$-.30$

0

.016

.014

.012

.010

.008

.006

.004

.002

$\bar{0}$

−.20   −.16   −.12   −.08   −.04   0   .04   .08

$\Delta M = M_\infty - M_{DES}$
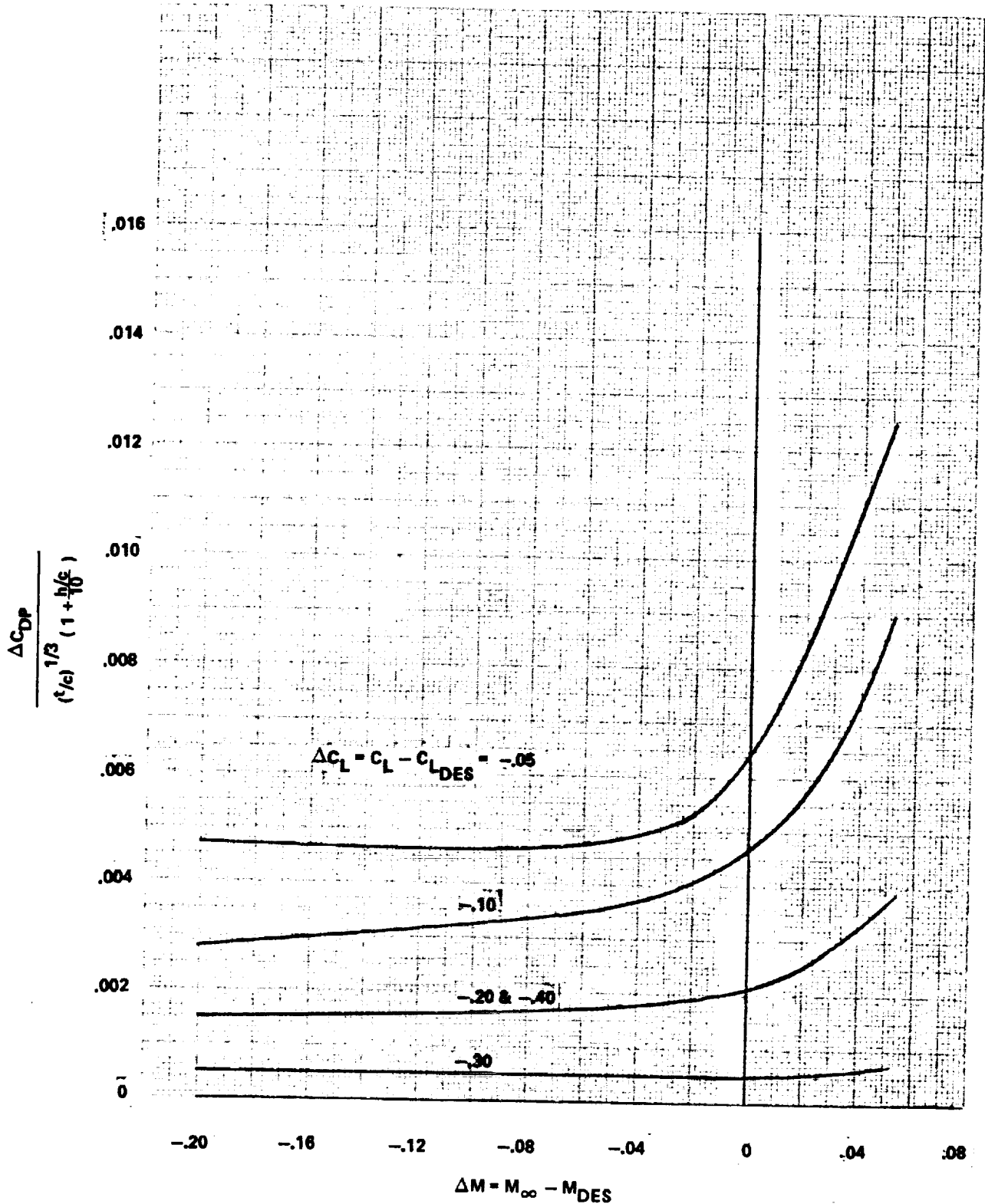
Figure 18. – Concluded.

39
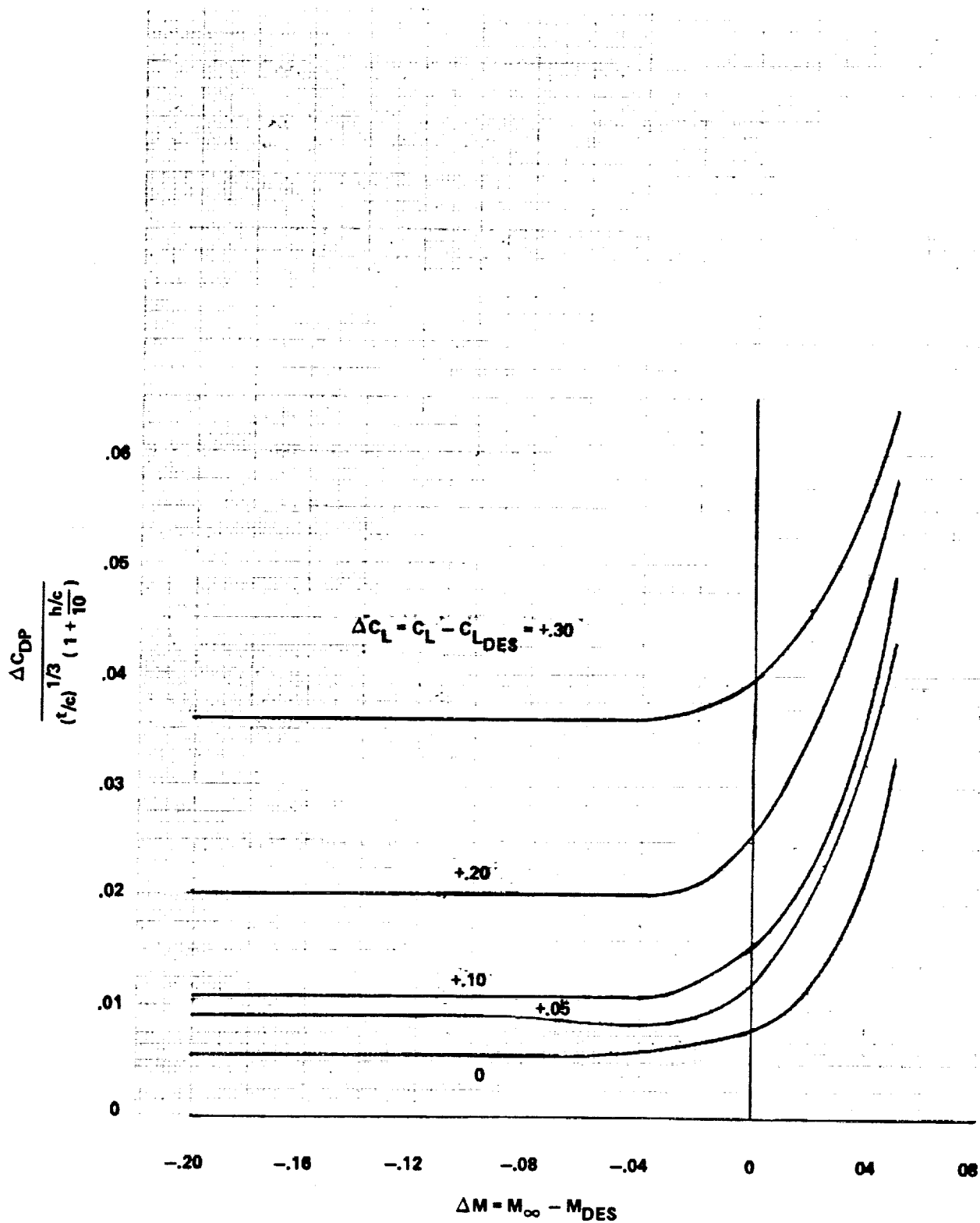
Figure 19. – Subsonic wing pressure drag, AR $(t/c)^{1/3} = 4.0$.

40
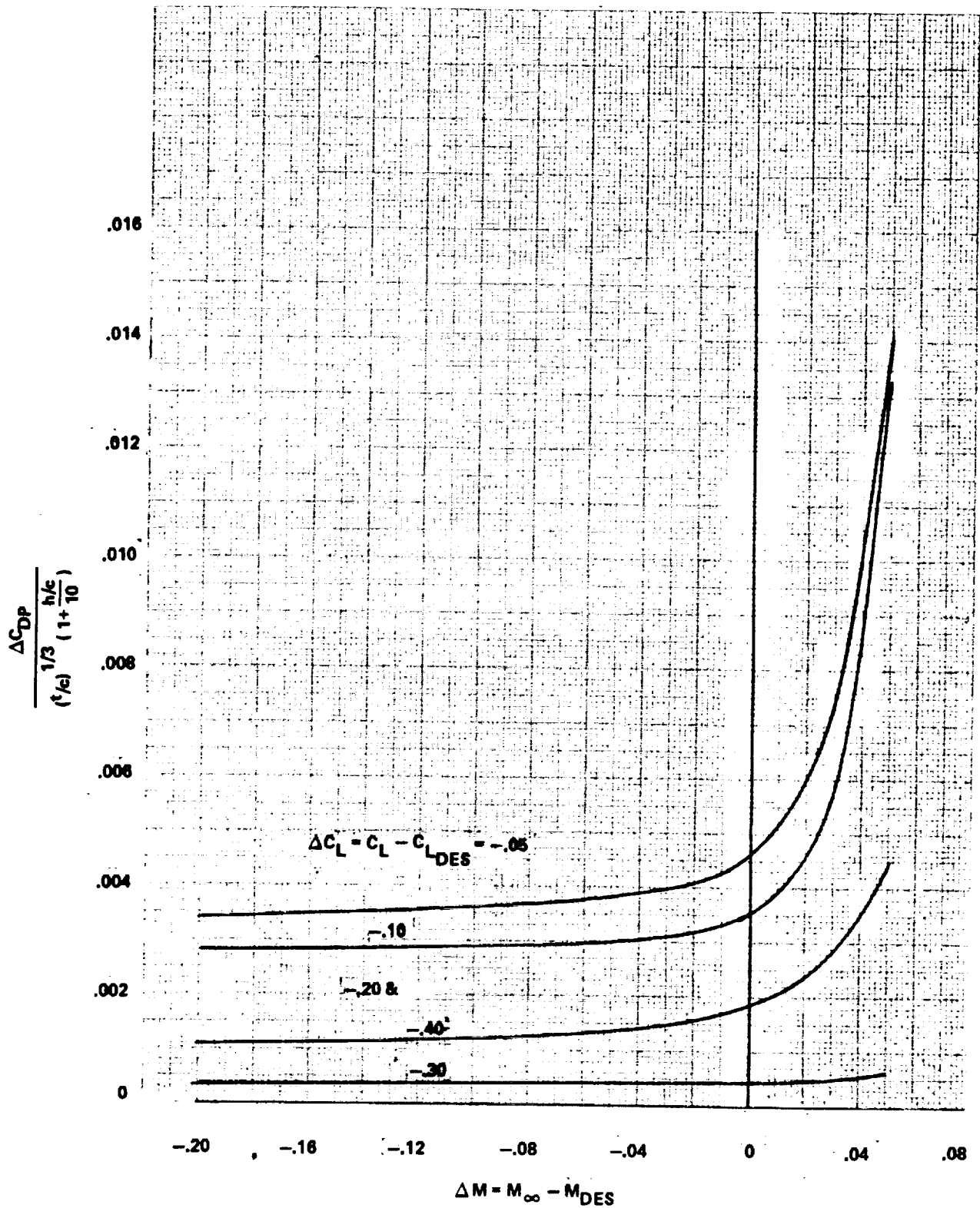
Figure 19. – Concluded.
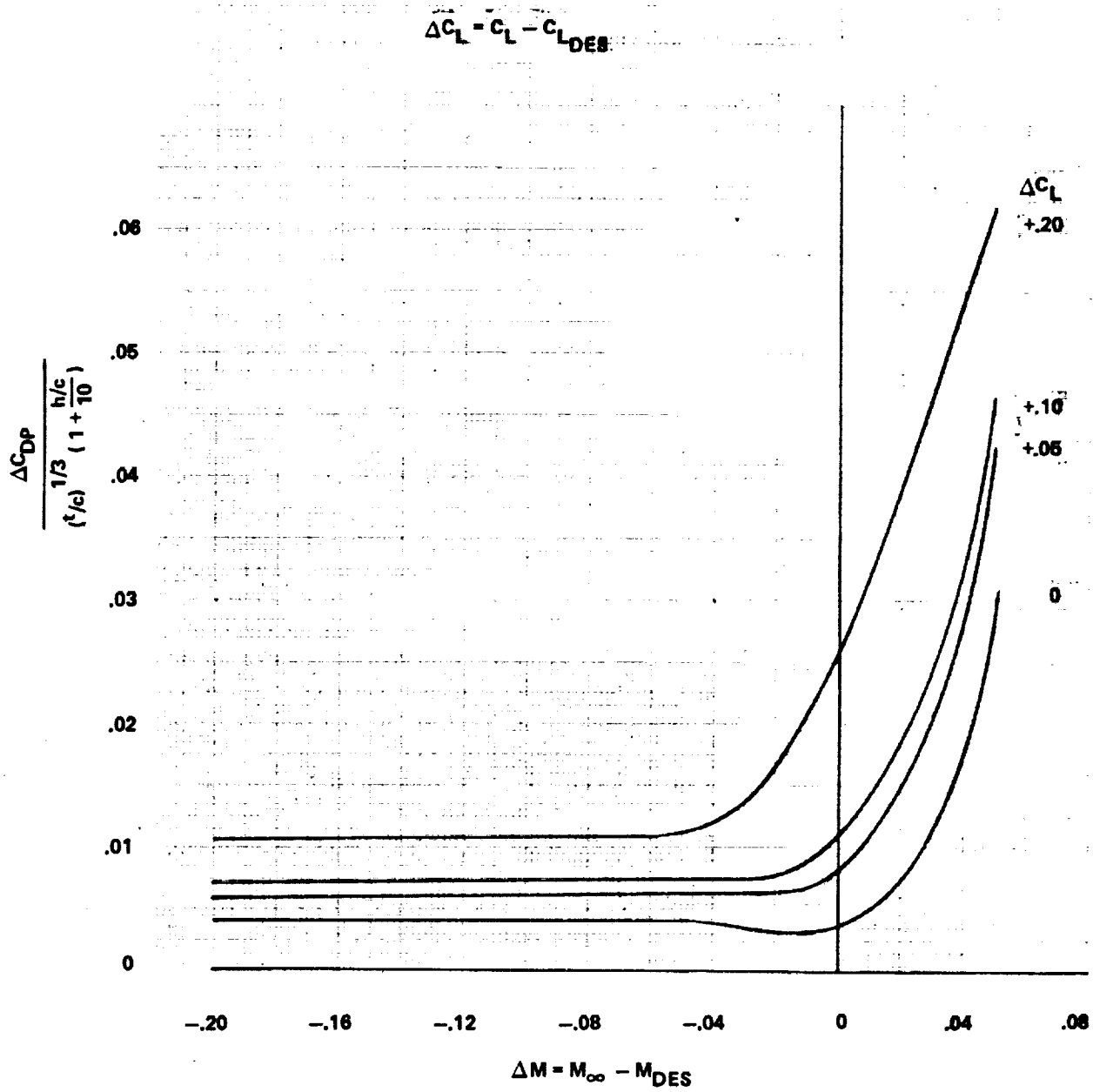
Figure 20. – Subsonic wing pressure drag, AR $({}^t/_c)^{1/3}$ = 6.0.
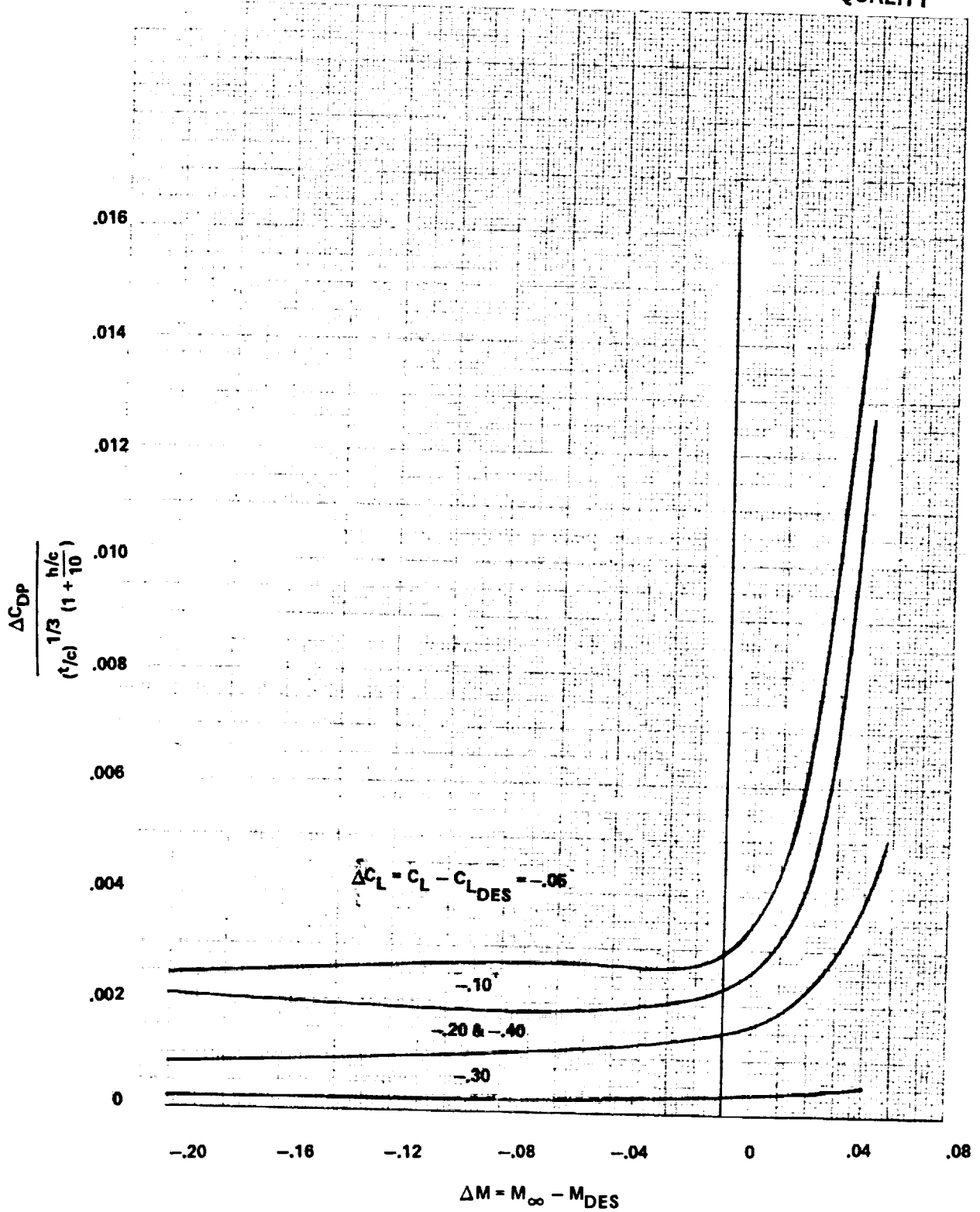
Figure 20. - Concluded.
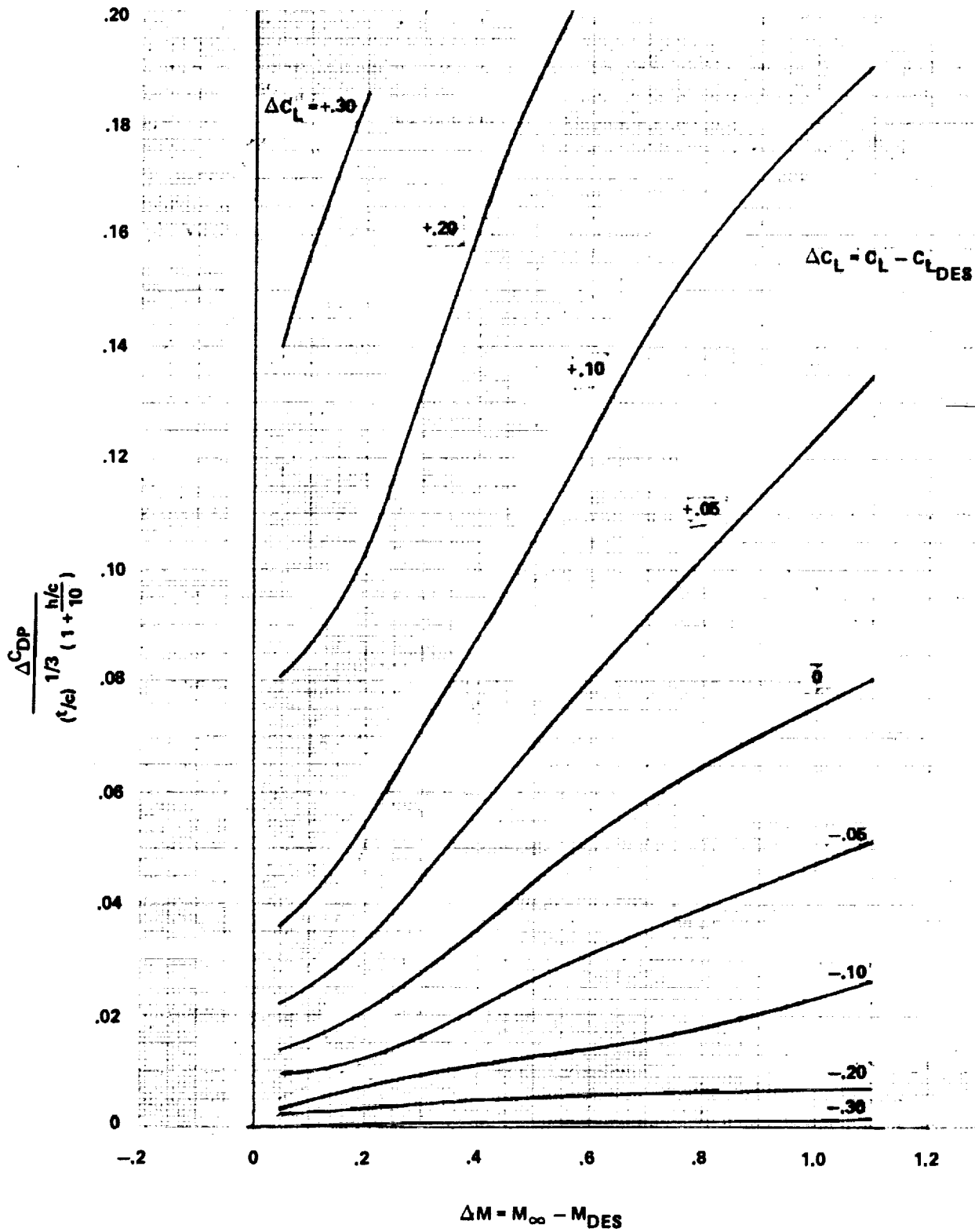
Figure 21. – Supersonic wing pressure drag, AR $(t/c)^{1/3} = 0.8$.
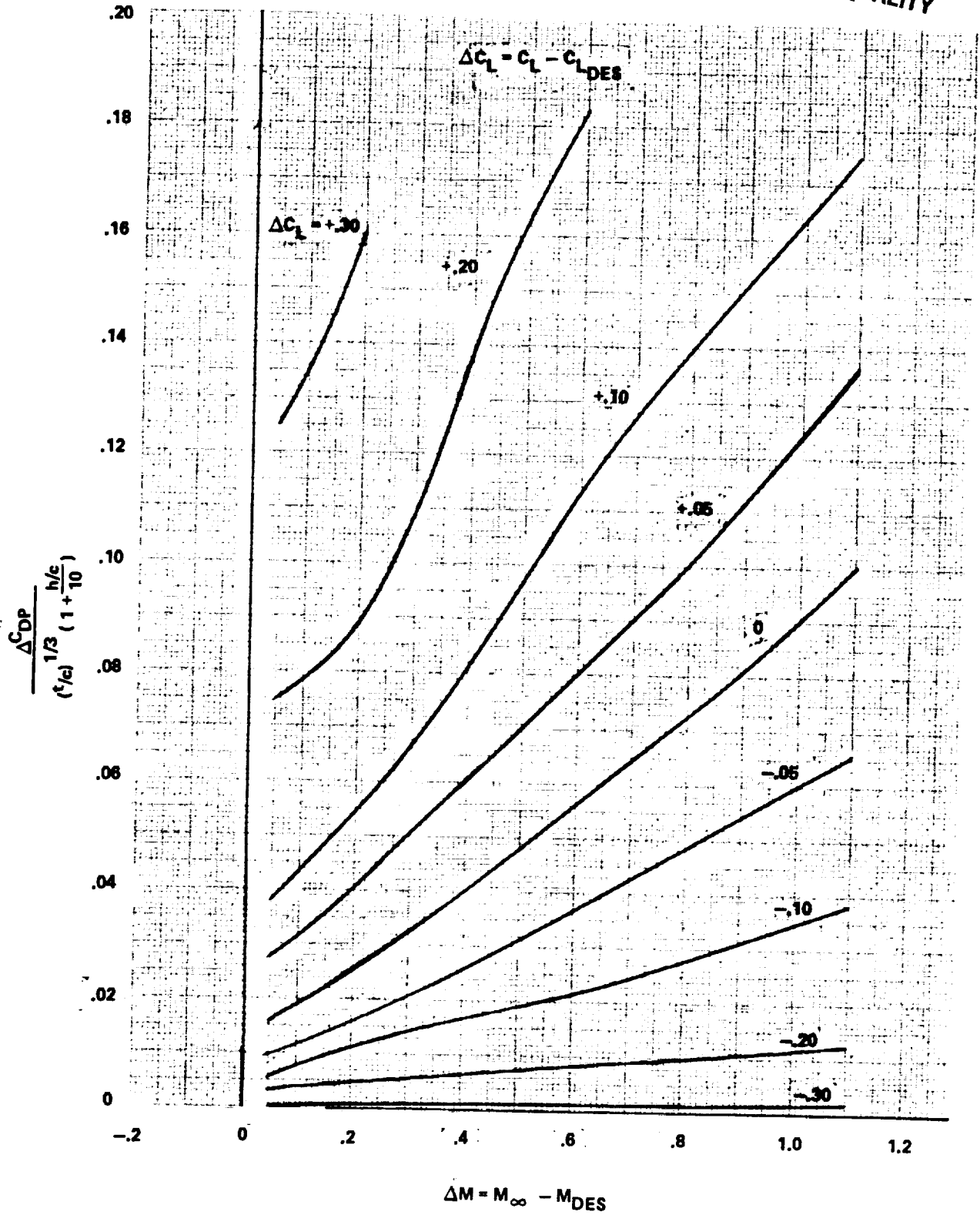
Figure 22. – Supersonic wing pressure drag, AR $(t/c)^{1/3} = 1.00$.
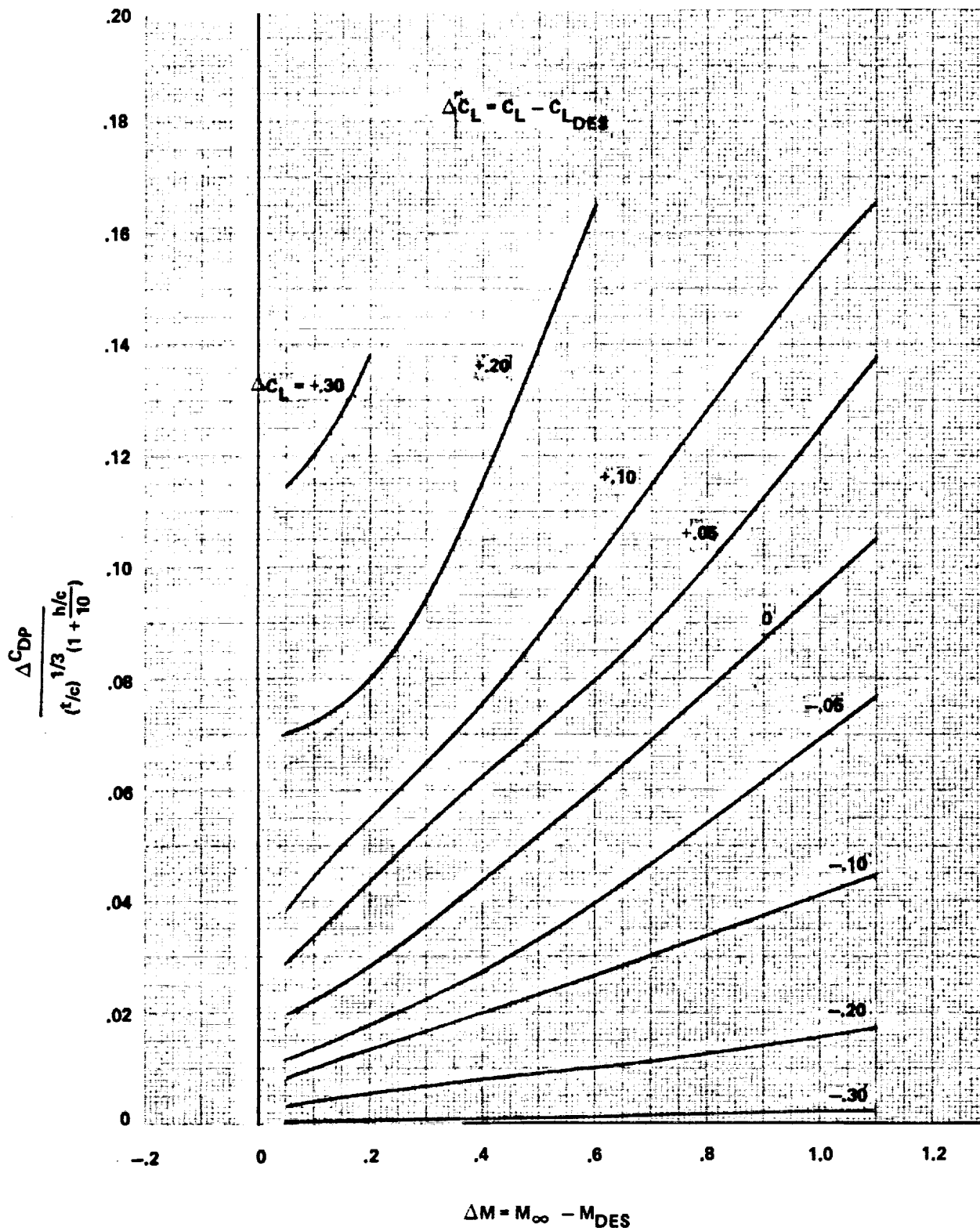
Figure 23. - Supersonic wing pressure drag, AR $(t/c)^{1/3} = 1.20$.
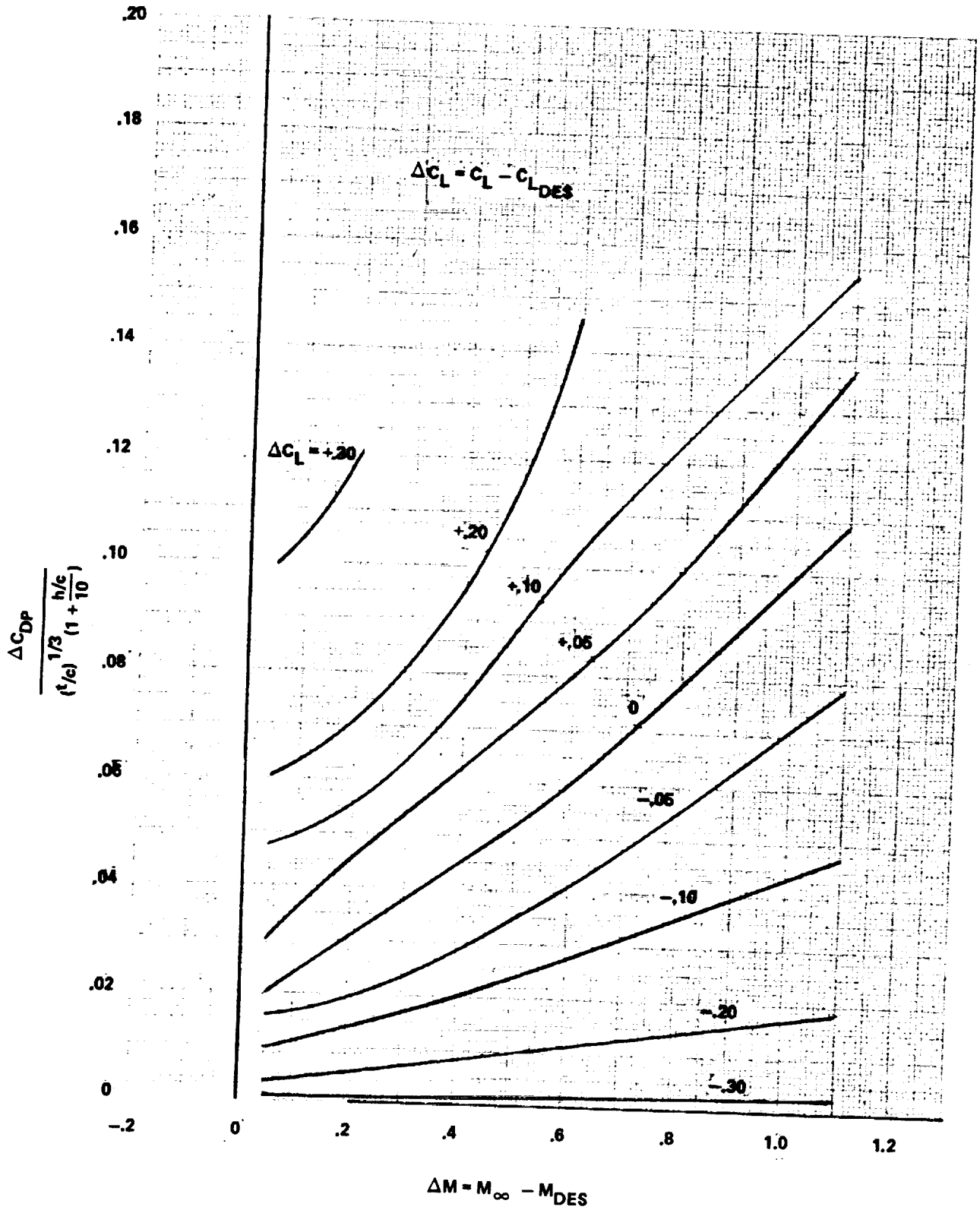
Figure 24. – Supersonic wing pressure drag, AR $(t/c)^{1/3} = 1.40$.
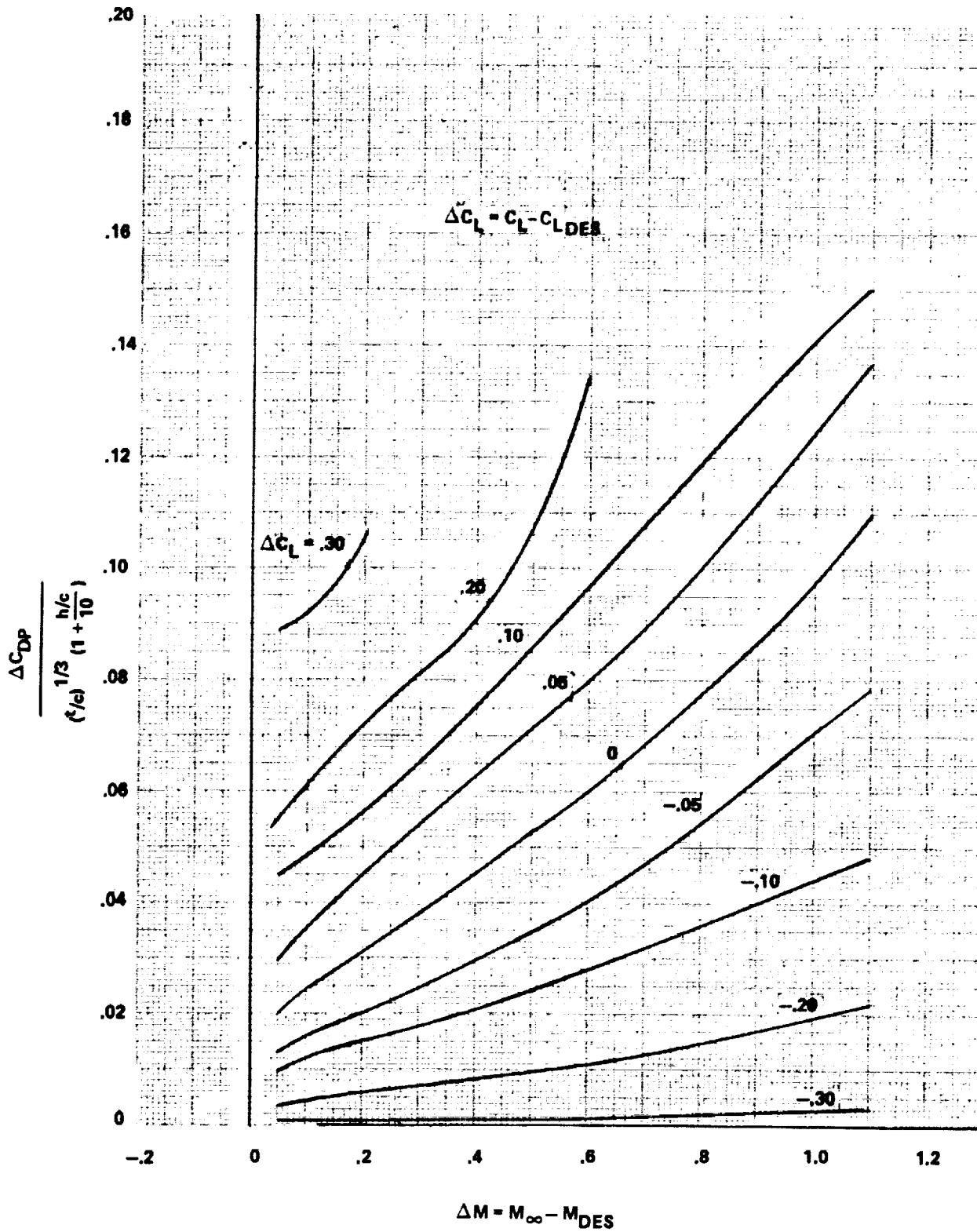
Figure 25. – Supersonic wing pressure drag, $AR \, (t/c)^{1/3} = 1.60$.
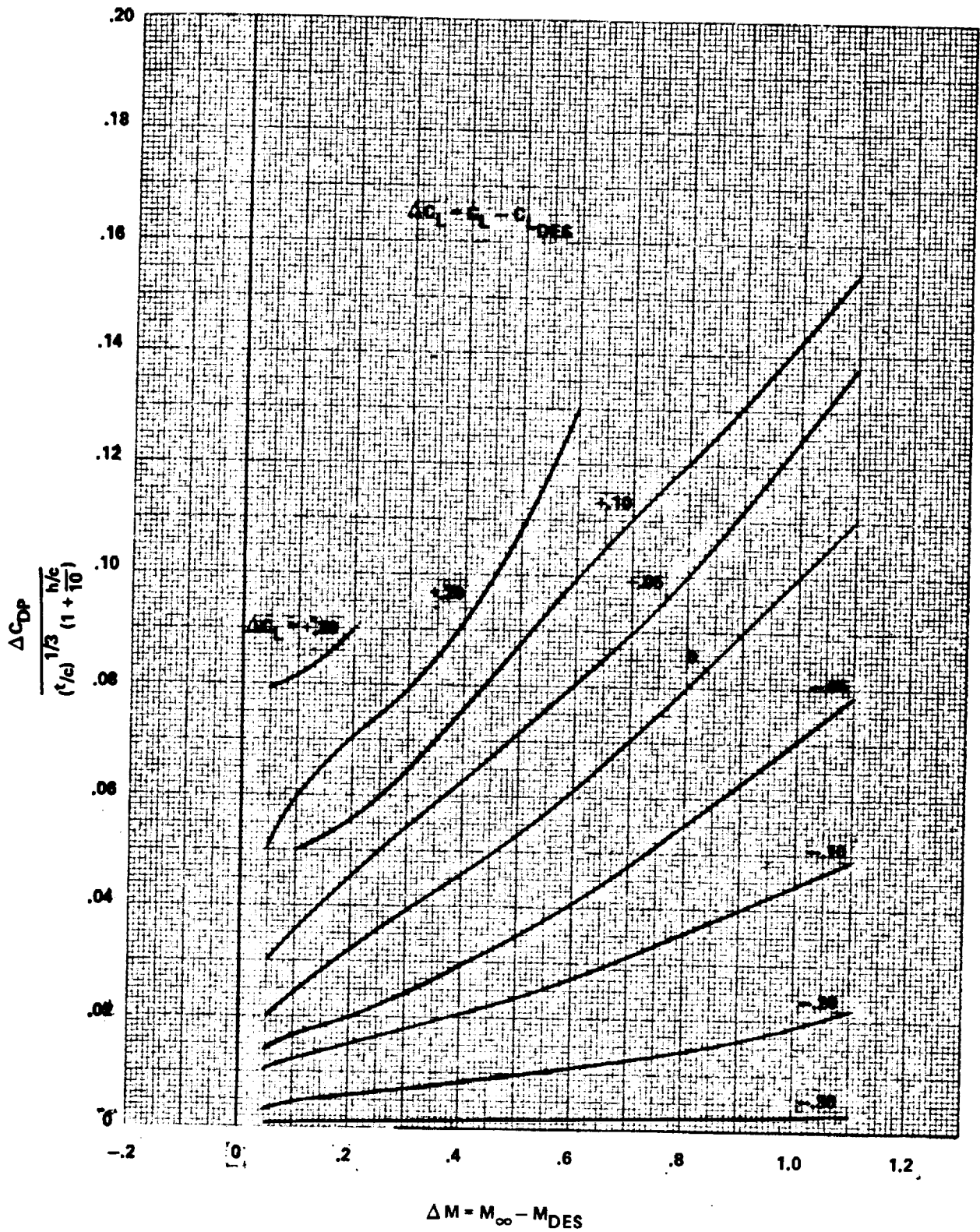
Figure 26. – Supersonic wing pressure drag, AR $(^t/c)^{1/3}$ = 1.80.
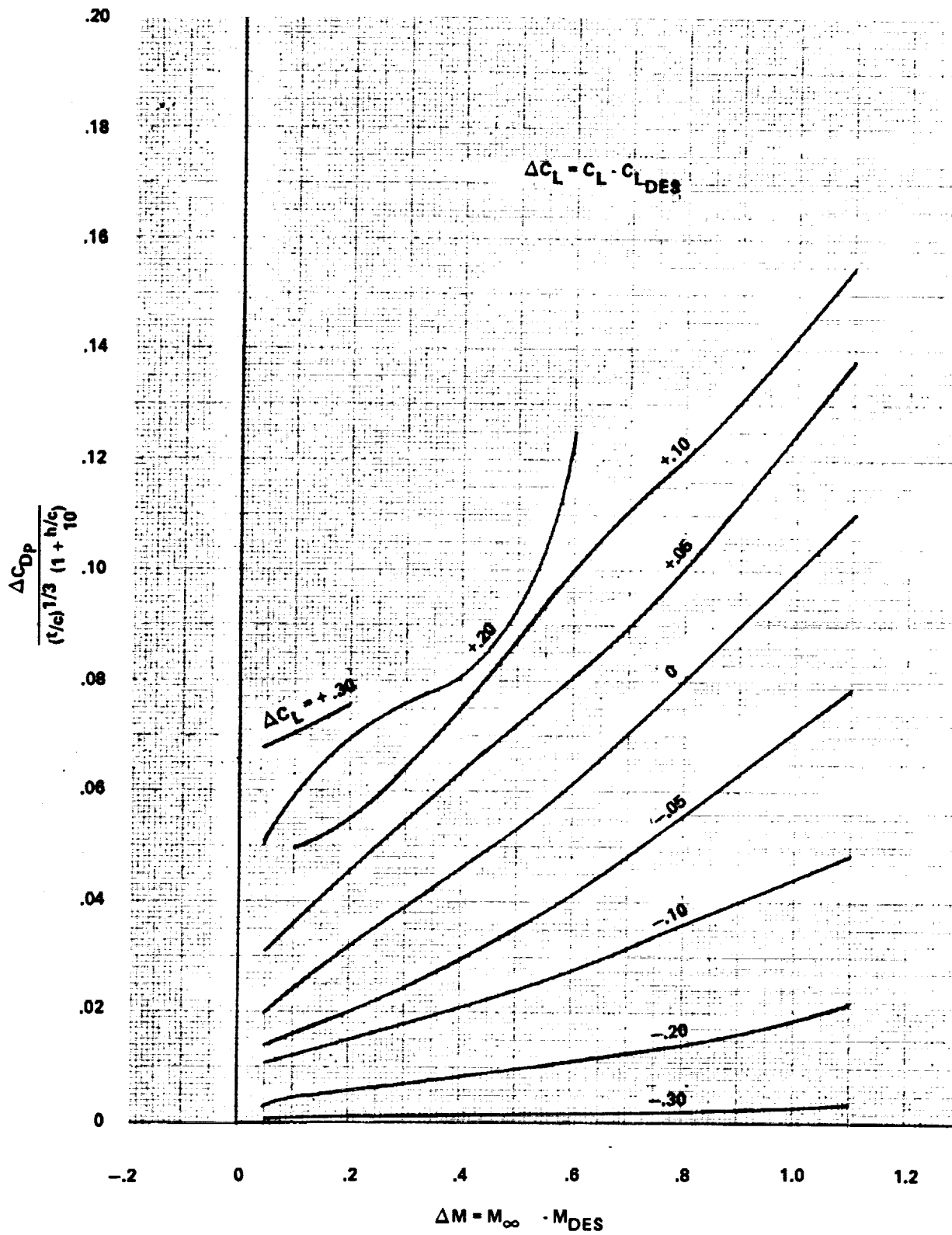
Figure 27. – Supersonic wing pressure drag, AR $(t/c)^{1/3} = 2.0$.

$\Delta M = M_\infty - M_{DES}$

$$\frac{(C_{L_{B.O.}} - C_{L_{DES}}) \cos \Lambda_{c/4}}{AR(1+\frac{h/C}{10})}$$
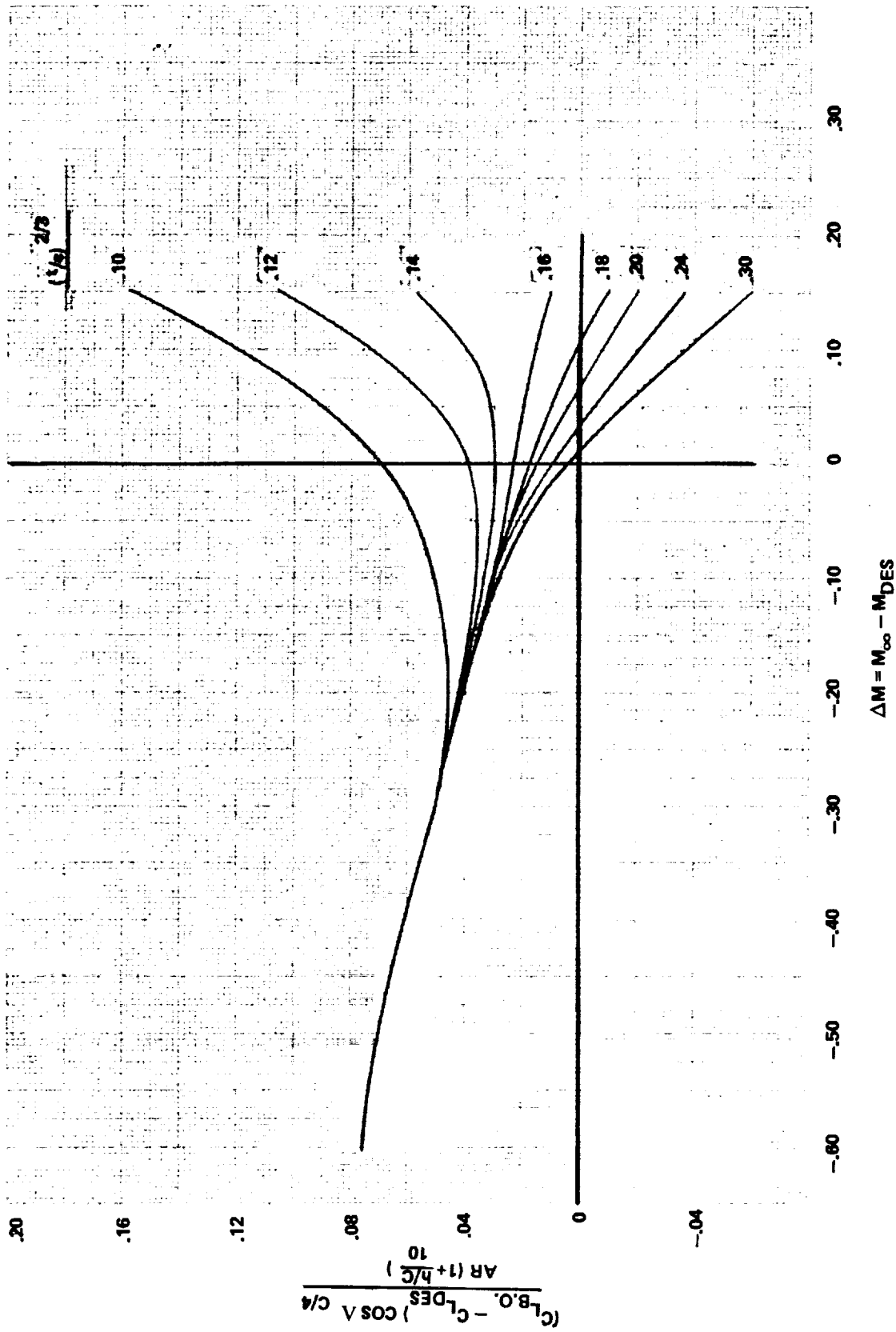
Figure 28. – Buffet onset.

51

2. DATA REDUCTION TECHNIQUE

The aircraft drag information, as presented in references 3 through 22, was analyzed in accordance with procedures as suggested by the Lockheed developed Delta Method of references 1 and 34. This method suggests that when incremental values of component drag are compared in relation to the increment (Δ) in Mach number and lift coefficient from the configuration's aerodynamic optimum values (M_{DES} and $C_{L_{DES}}$), a collapsing of the data is produced when transonic similarity parameters are utilized and a reasonable correlation of the data is therefore possible. The method of drag analysis is presented graphically in figure 29 and outlined in the following discussion.

2.1 Design Lift Coefficient and Mach Numbers

For each aircraft under consideration, the reference drag data were used to construct curves of Mach number times lift-to-drag ratio, M(L/D), for a given value of lift coefficient from the relationship

$$M(L/D) = M(C_L/C_D) \tag{13}$$

These quantities were then plotted versus Mach number and the maximum value of M(L/D) determined for each value of C_L. Ninety-nine percent of this maximum value of $M(\frac{L}{D})$ was then determined and the Mach number at which it occurred noted for each C_L. These quantities were then plotted as $0.99M(\frac{L}{D})_{max}$ versus C_L and M. The peak of the curve of $0.99M(\frac{L}{D})_{max}$ versus C_L was assumed to define the design lift coefficient ($C_{L_{DES}}$) and the corresponding Mach number, the design Mach (M_{DES}). It should be noted that these conditions define the aerodynamic optimums only and may or may not reflect an optimum flight cruise condition when engine SFC is introduced into the maximum range factor $M(\frac{L}{D})/SFC$. Examples of this procedure are given by reference 33 for each of the study aircraft.

2.2 Drag Divergence Mach Number

The three-dimensional Mach number for drag divergence is defined as the point where the rate of change of drag with Mach number, (dC_D/dM), is equal to 0.10. These values of Mach number were noted from curves of total drag coefficient versus Mach number for constant values of lift. Corrections to a two-dimensional value were made using the method contained in reference 34 which is a function of wing aspect ratio and quarter chord sweep angle. Examples of the resulting parameter can be seen for each aircraft in Section 3 of this report.

2.3 Drag Breakdown

The drag of any aircraft configuration can be broken down into two basic components - that which is independent of lift, and that which is the direct result of lift generation or angle of attack. The first of these (lift independent drag) can be thought of basically as the aircraft's resistance to movement and constitutes the minimum drag level of the configuration. The contributors to minimum drag go by many names but generally consist of friction drag, form or pressure drag, and compressibility effects. Friction drag is a function of size, Reynolds Number, and surface roughness and is associated with shear stresses in the configuration boundary layer. Form or pressure drag is affected by shape or volume effects such as thickness, fineness ratio, and contour slopes and is associated with increases in viscous pressure levels due to increases in local Mach numbers. Commpressibility effects become apparent with increased speed as local flows become sonic and the formation of shock waves occur. In the supersonic regime, form, compressibility, and wave drag are synonymous. For the purposes of this study, form and compressibility drag have been lumped together into one term called compressibility drag due to volume (ΔC_{DC}). The minimum drag level, therefore, is assumed as composed of only two parts - friction drag which is easily calculated, and compressibility drag. The procedure by which these two drag levels are determined will be discussed in succeeding paragraphs.

53

The lift dependent (induced) drag level is a function primarily of wing size and shape and is associated with the spanwise load distribution generated and its variation with angle of attack and speed. Depending on the configuration, there is also a certain amount of compressibility or wave drag due to lift produced as angle of attack is increased. This compressibility drag increment is usually small, however, when compared to the total induced drag level but is included as a contributor to lift dependent drag.

For the purpose of this study, induced drag is divided into two components – the theoretical value ($C_L^2/\pi AR$) which assumes an efficiency factor (e) of 1.0 and an elliptical spanwise load distribution, and a wing pressure term (ΔC_{DP}). Compressibility effects due to angle of attack are included in the ΔC_{DP} term. The procedure by which these two drag values are determined is presented in the succeeding discussion.

For each aircraft under consideration, tabulations of total configuration drag were made as a function of Mach number and lift coefficient. These tabulations did not include the effects of wing flaps, landing gear, or external stores and were, therefore, representative of a clean configuration.

As the first step in analysis, the theoretical induced drag term was removed by the relationship

$$C_D' = C_{D_{total}} - C_L^2/\pi AR \qquad (14)$$

where the primed value represents an interim calculation.

A low speed Mach number, usually M = 0.60, approximately ΔM = -0.30 below the design Mach was then chosen and the resulting polar shape obtained from Equation (14) plotted. The minimum value of drag obtained from this operation was designated $C_{D_{P_{MIN}}}$ or minimum parasite drag. It was assumed that this value was composed entirely of friction drag at the Mach number chosen; although it is realized that in actuality, this value usually includes some pressure drag. Skin friction drag at other Mach numbers was then computed using the relationship

54

$$C_{D_F} = C_{D_{P \, min}} \left[\frac{(C_F/C_{F_{INC}})_M}{(C_F/C_{F_{INC}}) \, M \approx 0.60} \right] \qquad (15)$$

Values of $C_F/C_{F_{INC}}$ are presented in figure 8 and are based on information contained in references 34 and 35.

These computed values of skin friction drag were then removed from the results of Equation (14.)

$$\Delta C_{D_C}' = C_D' - C_{D_F} \qquad (16)$$

The resulting lift/drag relationships were plotted for each Mach number and the minimum drag quantity obtained was then identified as the compressibility or zero-lift wave drag (ΔC_{D_C}) of the configuration inclusive of wing, body, and wing/body interference.

Wing pressure drag was then computed from the relation

$$\Delta C_{D_P} = C_D' - C_{D_F} - \Delta C_{D_C} \qquad (17)$$

and its variation with Mach number and lift coefficient noted. As mentioned earlier, the term ΔC_{D_P} includes the combined effects of flow separation, compressibility drag due to lift, and trim drag. Any attempt to further break the term ΔC_{D_P} down into its components was judged to be beyond the scope of this study and would require levels of detail outside the intended preliminary design application. Values of ΔC_{D_P} are presented for each subject aircraft in reference 33.

55

2.4 Component Compressibility Drag

The values of zero-lift wave drag obtained in the above discussion are those of the entire configuration. The three main contributors to total configuration wave drag are the wing, fuselage, and wing/fuselage interference.

$$\Delta C_{D_C} = (\Delta C_{D_C})\text{WING} + (\Delta C_{D_C})\text{FUS.} + (\Delta C_{D_C})\text{INT.} \qquad (18)$$

To separate out these component parts, the following procedure was used;

- The fuselage area distribution, minus capture area, was determined from information as contained in references 3 through 21. Horizontal and vertical tail cross-sectional areas were included as basic fuselage area since their contribution to the total wave drag is usually small but should not be neglected.

- This area distribution was then input to the NASA Wave Drag Program, reference 36, as an equivalent body of circular cross section. The wing was then added to this area distribution and the zero-lift wave drag of the resulting configuration was computed at supersonic speeds.

- From the output of the Wave Drag Program, incremental values of compressibility drag due to the fuselage, wing and wing/fuselage interference were obtained and the percentage of total wave drag for these items determined versus Mach number.

- These percentages were then applied to the values of ΔC_{D_C} obtained from the results of Equation (16) to produce incremental values of supersonic compressibility drag due to fuselage, wing, and fuselage/wing interference.

Subsonic and transonic fuselage compressibility drag and drag divergent Mach number were estimated using results obtained from wind tunnel tests of bodies of various fineness ratio, reference 34. These values were then subtracted from the total value of ΔC_{D_C} derived from the basic data within this Mach range. The remaining quantity was assumed to be wing compressibility drag. Values obtained from this procedure were then faired into existing supersonic drag levels as computed in the preceeding paragraphs. For most of the aircraft considered, the fuselage drag divergence occurred at a Mach number sufficiently high enough to allow the values of ΔC_{D_C} computed to be due entirely to the wing at subsonic speeds. Interference drag was assumed to be zero below Mach 1.0.

56
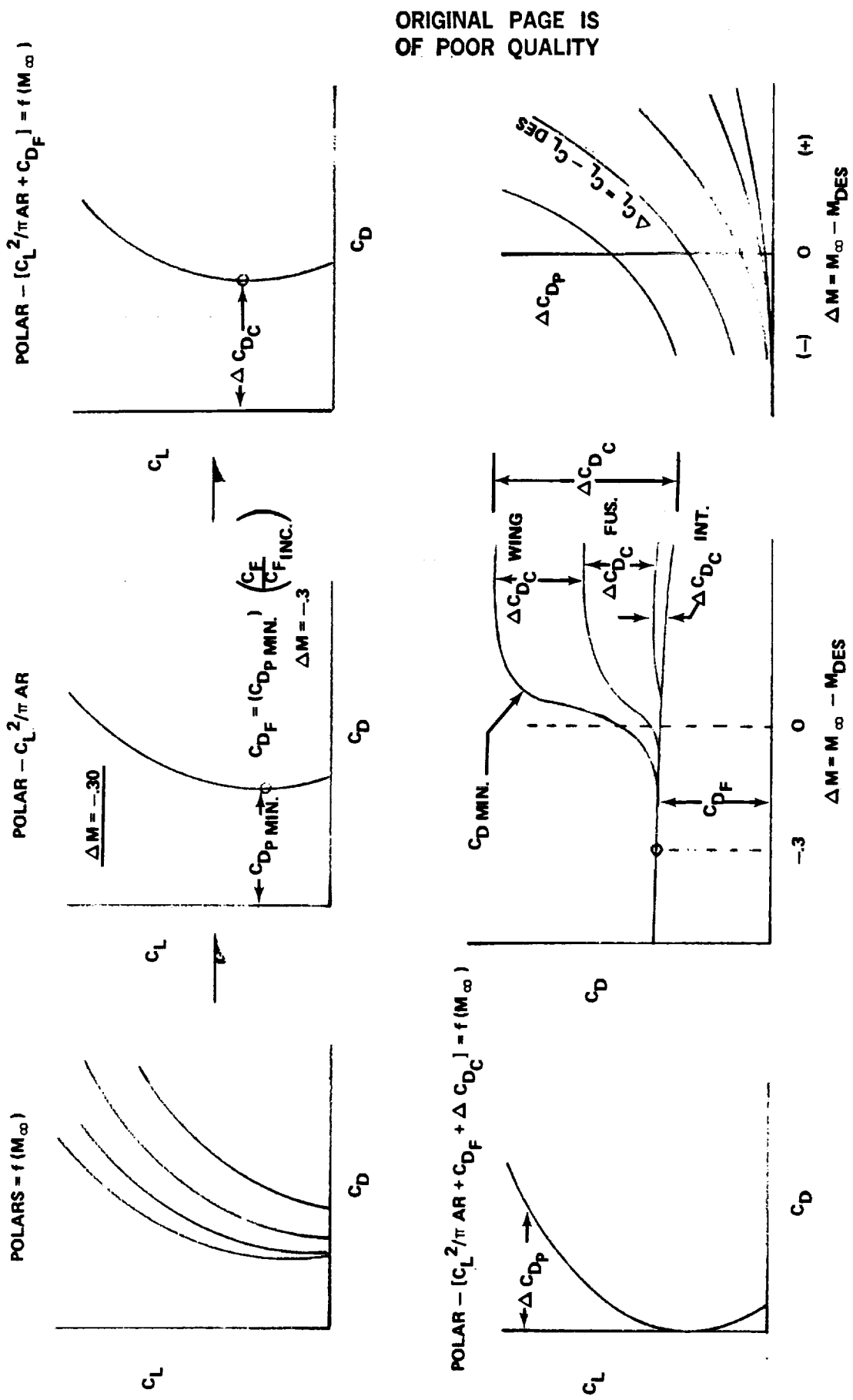
Figure 29 – Drag breakdown procedure.

57

3. DATA CORRELATION

Sections 1 and 2 have presented the Delta Method for estimating total aircraft drag, an overview of final results of the correlation effort, and the method to which the test data were broken down. This section presents the individual aircraft/wind tunnel model data points for each correlated parameter along with the rationale for selection of correlation variables. The original development of the Delta Method Drag correlation technique, described in reference 1, was directed toward determination of drag correlation techniques which would permit preliminary design evaluation of the potential of transonic aircraft incorporating advanced or supercritical airfoils. This current work expands the data base to include conventional and advanced airfoils operating in the transonic flight regime and conventional airfoils operating in the supersonic flight regime. At the present time, the NASA Air Force TACT aircraft represents the only available/known data where advanced airfoil design has been incorporated into a supersonic aircraft. These flight data became available too late to be incorporated into this reporting; however, incorporation at a later date would represent a valuable addition to the Delta Method.

In developing the various component drag correlations, extensive guidance was derived from previous work by McDevitt (reference 37), DATCOM (reference 35), and RAS Data Sheets. The effect of external stores, tip tanks, flaps, cruise droop, and other camber varing devices were not considered. A clean wing was assumed at all times.

The basic geometric properties of all 19 study aircraft are presented in table 1 along with 15 current supercritical or advanced technology experimental wing designs. Included are the values of $C_{L_{DES}}$, M_{DES}, and $C_{D_{P_{MIN}}}$ for the study aircraft calculated by the methods discussed in Section 2 and shown in reference 33. The plotted symbol by which each configuration is recognized is also presented. The flagged symbols indicate wind tunnel model data extracted from reference 1. On the correlation figures to follow, the darkened

58

TABLE 1. – BASIC GEOMETRY

Configuration	Plotted Symbol	AR	$\Lambda_{c/4}$ (deg)	Λ_{LE} (deg)	$(t/c)_{eff}$ (%)	λ	h/c at .7 b/2	S_{REF} ft² (m²)	$\bar{c}$ ft (m)	$C_{L_{DES}}$	M_{DES}	$C_{D_{P_{MIN}}}$	Reference No.
T-2B		5.07	2.00	6.00	12.00	.496	2.00	254.86 (23.68)	7.41 (2.26)	.500	.723	.0229	3
T-37B		6.20	0.00	1.50	16.00	.670	1.88	183.90 (17.08)	5.58 (1.70)	.6075	.675	.0201	4
RA-3B		6.75	35.90	38.58	9.54	.335	–	779.00 (72.37)	11.68 (3.56)	.4275	.823	.0182	5
A-4F		2.91	33.21	41.11	7.48	.226	0.773	260.00 (24.15)	10.80 (3.29)	.350	.805	.0195	6
TA-4F		2.91	33.21	41.11	7.48	.226	0.773	260.00 (24.15)	10.80 (3.29)	.320	.800	.0200	7
RA-5C		3.73	37.50	43.00*	5.00	.190	–	700.00 (65.03)	15.19 (4.63)	.365	.896	.0160	8
A-6A		5.31	25.00	29.47	7.50	.312	1.623	528.90 (49.14)	10.89 (3.32)	.485	.755	.0199	9
A-7A		4.00	35.00	40.37	6.57	.250	1.18	375.00 (34.84)	10.84 (3.30)	.400	.877	.0155	10
F-4E		2.82	45.00	51.40	5.57	.167	–	530.00 (49.24)	16.04 (4.89)	.325	.935	.0215	11
F-5A		3.75	24.00	31.92	4.80	.200	0.735	170.00 (15.79)	7.73 (2.36)	.325	.895	.0192	12
F-8C		3.40	45.00	47.00	5.97	.247	–	375.00 (34.84)	11.79 (3.59)	.300	.872	.0167	13
F-11F		4.00	35.00	38.10	5.35	.500	–	250.00 (23.23)	8.20 (2.50)	.365	.888	.0225	14
F-100		3.86	45.00	49.03	7.00	.260	–	385.20 (35.79)	11.16 (3.40)	.250	.870	.0088	15
F-101		4.28	36.61	41.50	6.50	.290	–	368.00 (34.19)	10.24 (3.12)	.420	.843	.0243	16, 17
F-106C		2.46	18.10	27.08	3.36	.378	0.00	196.10 (18.22)	9.54 (2.91)	.265	.896	.0158	18
F-105B		3.18	45.00	48.09	5.00	.467	–	385.00 (35.77)	11.48 (3.50)	.350	.8875	.0173	19
F-106A		2.20	52.00	60.00	3.91	0.0	–	695.00 (64.57)	23.76 (7.24)	.200	.920	.0109	20
XB-70		1.75	58.79	65.57	2.25	.019	0.00	6297.80 (585.08)	78.53 (23.94)	–	–	.0064	21
S-3A		7.73	15.00	19.00	14.30	.249	2.40	598.00 (55.56)	9.85 (3.00)	.550	.684	.0185	22
CALAC WING 51		8.97	30.00	32.00	12.40	.234	1.94	2.61 (0.242)		.585	.804	.0195	23
VAS		7.20	0.00	3.00	15.80	–	3.00	–	–	.650	.720	–	24
L-1011 SC		6.95	35.00	37.50	10.50	–	1.60	–	–	.450	.867	–	25
L-1011 FLT		6.95	35.00	37.50	10.50	–	1.30	–	–	.460	.850	–	26
VPX-W2		8.63	22.00	24.00	14.60	–	2.60	–	–	.550	.770	–	27
VPX-W3		8.63	22.00	24.00	14.60	–	2.20	–	–	.475	.775	–	27
ATT-W6		7.64	40.00	42.00	9.30	–	1.90	–	–	.470	.916	–	28
T7-CMT		5.07	2.28	6.00	17.00	–	2.10	–	–	.500	.735	–	29
OBLIQUE		6.48	45.00	45.00	7.07	–	0.99	–	–	.325	.970	–	30
F8U VT		6.80	42.24	44.34	9.10	–	2.00	–	–	.450	.963	–	31
BOEING FT.		3.50	39.40	45.00	5.00	–	0.40	–	–	.275	.918	–	32
WHIT. #1		11.48	30.00	32.00	12.22	–	1.12	–	–	.600	.815	–	1
WHIT. #2		10.24	27.00	29.00	12.58	–	1.30	–	–	.600	.795	–	1
WHIT. #3		11.95	27.00	29.00	12.58	–	1.15	–	–	.650	.792	–	1
WHIT. #4		11.95	27.00	29.00	14.58	–	1.38	–	–	.650	.765	–	1

*℄ to W.S. 148   43.15°
W.S. 148 to W.S. 154   39.87°
W.S. 154 to W.S. 247.5   43.23°
W.S. 247.5 to TIP   43.05°

symbols represent the advanced or supercritical model designs on reference 1. Correlation parameters used in the analysis are tabulated in table 2.

It has been assumed that the drag polars presented for all aircraft or models are trimmed, and at the low lift coefficients of interest, trim drag is negligible except at supersonic speeds where it is included in the wing pressure drag term. Considering the diversity of designs, i.e., supersonic fighters, subsonic attack aircraft, surveillance aircraft and transport models varying contractor sources of data, differences in bookkeeping methods, power effects, static margin, and varying test Reynolds numbers, the component data correlation is considered to be quite adequate for the preliminary design of both subsonic and supersonic aircraft.

3.1 $C_{L_{DES}}$ and M_{DES}

Design lift coefficient and design Mach number for each configuration were defined as the subsonic C_L and M at which 0.99 M $(L/D)_{MAX}$ occurs. (Note that these are aerodynamic optimums and may or may not reflect an optimum flight cruise condition where engine SFC must be introduced in the maximum range factor M (L/D)/SFC).

3.1.1 C_L design. - Subsonic wing design techniques consider the variables of aspect ratio, taper ratio, sweep, thickness ratio, camber, and twist in "designing to" optimum pressure distributions in deriving C_L and M design. It was premised that for these subsonic aircraft, an elliptical span load at the design conditions would be attained, therefore, twist and taper need not be considered as unique correlating parameters. Further, subsonic wing design practices rely heavily on a high degree of two dimensional flow for accurate prediction of C_L design, hence some minimum aspect ratio could be anticipated. The correlation on figure 30 reflects the relationship of the remaining primary design variable to C_L design for both advanced and conventional wings. The aircraft represented in this correlation have been tailored for best cruise performance and compromised only by subsonic cruise speed and take off and landing considerations.

60

TABLE 2. – CORRELATION PARAMETERS

OF POOR QUALITY

Configuration	$\left(\frac{t}{c}\right)^{1/3}$	$\left(\frac{t}{c}\right)^{2/3}$	$\left(\frac{t}{c}\right)^{5/3}$	$AR\left(\frac{t}{c}\right)^{1/3}$	$\left(\frac{t}{c}\right)^{1/3}\left(1+\frac{h/c}{10}\right)$	$\left(\frac{t}{c}\right)^{5/3}\left(1+\frac{h/c}{10}\right)$	$AR\,TAN\Lambda_{LE}$	S_π^* ft² (m²)	ℓ ft (m)	ℓ/d^*	S_b ft² (m²)
T-2B	.493	.243	.0292	2.50	.592	.0350	.533	24.10 (2.24)	37.80 (11.52)	6.82	0.0
T-37B	.542	.295	.0472	3.36	.605	.0560	.162	22.90 (2.13)	29.30 (8.93)	5.43	0.0
KA-3B	.456	.209	.0199	3.08	.456	.0199	5.38		71.20 (21.70)		
A-4F	.421	.178	.0133	1.23	.454	.0143	2.54	18.85 (1.75)	40.70 (12.41)	8.31	1.00 (.09)
TA-4F	.421	.178	.0133	1.23	.454	.0143	2.54	20.25 (1.88)	42.60 (12.98)	8.39	1.00 (.09)
RA-5C	.368	.136	.00679	1.37	.368	.00679	3.49	45.25 (4.20)	73.30 (22.34)	9.66	12.00 (1.11)
A-6A	.421	.178	.0133	2.23	.489	.0155	3.00	42.70 (3.97)	54.00 (16.46)	7.47	0.40 (.04)
A-7A	.403	.163	.0107	1.61	.450	.01196	3.40	23.65 (2.20)	45.50 (13.87)	8.29	1.20 (.11)
F-4E	.381	.146	.00812	1.08	.381	.00812	3.53	32.50 (3.02)	60.40 (18.41)	9.39	6.60 (.61)
F-5A	.363	.132	.00634	1.36	.389	.00682	2.33	14.65 (1.36)	45.00 (13.72)	10.42	3.25 (.30)
F-8C	.390	.153	.00912	1.33	.390	.00912	3.65	21.95 (2.04)	53.80 (16.40)	10.17	6.30 (.59)
F-11F	.367	.142	.0076	1.51	.367	.0076	3.14	20.50 (1.90)	44.20 (13.47)	8.65	5.20 (.48)
F-100	.412	.170	.0119	1.59	.412	.0119	4.45	21.70 (2.02)	45.72 (13.94)	8.70	2.22 (.21)
F-101	.402	.162	.0105	1.72	.402	.0105	3.79		67.44 (20.56)		
F-104G	.322	.104	.0035	.792	.322	.0035	1.256	18.00 (1.67)	54.40 (16.58)	11.36	5.20 (.48)
F-105B	.368	.136	.00679	1.17	.368	.00679	3.54	24.60 (2.29)	63.10 (19.23)	11.31	1.10 (.10)
F-106A	.339	.115	.0045	.747	.339	.0045	3.81	30.25 (2.81)	65.90 (20.09)	10.61	7.30 (.68)
XB-70	.282	.080	.0018	.494	.282	.0018	17.02	170.00 (15.79)	194.58 (59.31)	13.23	83.00 (7.71)
S-3A	.522	.273	.0391	4.04	.647	.0022	2.66	54.00 (5.02)	49.42 (15.06)	6.19	0.0
CALAC WING 51	.499	.250	.0313	4.47	.596	.0370	5.60				
VAS	.541	.292	.0462	3.90	.703	.0600	.378				
L-1011 SC	.472	.2226	.0234	3.28	.547	.0271	5.33	301.21 (27.98)**	177.70 (54.16)	18.15	0.0
L-1011 FLT	.472	.2226	.0234	3.28	.533	.0264	5.33	301.21 (27.98)**	177.70 (54.16)	18.15	0.0
VFX-W2	.527	.2773	.0405	4.54	.663	.0510	3.84				
VFX-W3	.527	.2773	.0405	4.54	.642	.0494	3.24				
ATT-W4	.453	.2052	.0191	3.46	.538	.0227	6.88				
T2-CWT	.553	.3069	.0521	2.80	.670	.0631	.533				
OBLIGUE	.414	.1710	.0120	2.68	.454	.0133	6.48				
FBU WT.	.450	.2023	.0184	3.06	.540	.0221	6.65				
BOEING FT.	.368	.1357	.00678	1.29	.383	.00706	3.50				
WHIT. #1	.496	.2463	.0301	5.70	.552	.0335	7.17				
WHIT. #2	.501	.2511	.0316	5.13	.566	.0357	5.68				
WHIT. #3	.501	.2511	.0316	5.99	.558	.0352	6.63				
WHIT. #4	.526	.2770	.0403	6.29	.599	.0460	6.63				

* With Capture Area removed for internally mounted engines

** Based on 235 in. diam fuselage excluding wheel fairings and center engine installation

61

Optimum cruise efficiency for supersonic tactical aircraft geometries may be compromised by maneuver, takeoff and landing, ceiling, external store carriage, and maximum speed. The high dash speed requirement drives those designs to low aspect ratio-highly swept-thin wings with resulting aerodynamic best cruise efficiency occurring at high subsonic speeds, sometimes higher than the best cruise speed for the engine. For this class of aircraft, C_L design (see figure 31), correlates with aspect ratio times thickness ratio to the one-third power. The change over in C_L design relating parameters occurs at approximately an aspect ratio of five. (Note the T-2B and A-6 on figures 30 and 31).

3.1.2 <u>M design</u>. - The original Delta Method derivation (reference 1 and 34) shows that M design and M divergence, i.e., d $C_D/dM = 0.10$, are synonymous at the design lift coefficient. M design for the subsonic configurations (see Figure 32), when adjusted for the three-dimensional effects of aspect ratio and sweep, follow the correlating parameters suggested in the Transonic Similarity Rules (reference 37). The increased drag divergence Mach number for those configurations employing advanced sections is evidenced. For the supersonic aircraft designs, i.e., low aspect ratio-highly swept-thin wings, Mach design corrected for three-dimensional effects, correlates more favorably as a direct function of wing thickness ratio. (See figure 33.)

Referring back to figure 32, this correlation implies that as the wing thickness is increased above a thickness ratio of approximately 20 percent, little benefit in drag divergence Mach number is evidenced for the advanced airfoils. This logic is borne out in the limit case of a cylinder where $t/_c = 1.0$. There would be no way of dictating differences in upper and lower surface pressure distribution and no distributions in section characteristics. Until advanced sections of greater thickness ratio are developed, this diminishing return of advanced over conventional sections appears valid for preliminary design purposes. As the thickness ratio is reduced, the spread in divergence Mach number between the two technologies is increased. Again, in the limit case with thickness ratio approaching zero, no mechanism for prescribing desired upper and lower surface pressure distribution exists.

62

Hence relations of advanced airfoil section drag divergence Mach number should not be extended below the thickness for which data are shown. This airfoil technology level difference for lower thickness ratios does lend emphasis to consideration for advanced section technology application to supersonic fighters for a potential improvement in cruise performance.

3.2 Friction Drag Correction Factor

The Delta Method includes a procedure for determination of the subsonic friction drag on bodies, wings, tails, and nacelles. This theoretic friction estimate must be increased by approximately six percent to produce friction drag levels that agree with flight test results of transport and bomber type aircraft. For attack and fighter type aircraft which might have bubble canopies, weapons, pylons, antenna in flight refueling probes, etc., this factor is much larger. A correlation of average skin friction computed by the theoretic procedure is compared with the actual average skin friction coefficient in figure 34 to derive a simple and more realistic correction factor for fighter/attack type aircraft friction drag. This factor is 28.4 percent. When using the Delta Method, good engineering judgment should be exercised in choosing the procedures for friction drag determination most appropriate to the concept under consideration. The correlation for the friction drag correction factor presented in figure 34 is the same as given by figure 9.

3.3 Compressibility Drag

Compressibility, wave or pressure drag, i.e., all synonymous terms, generally is separated as drag due to volume, i.e., zero lift, and drag due to lift Compressibility drag due to volume for this correlation has been broken down into the contribution of the wing, the fuselage, and a wing body interference contribution (see figure 29, Section 2.0). The compressibility drag due to lift for both the wing and fuselage are included in the pressure drag correlation explained in section 3.3.4.

63

3.3.1 Compressibility drag due to wing volume. - The only transonic and supersonic linear wave drag theories available generally prescribe a systematic series of uncambered wings having specific section characteristics, i.e., diamond, double wedge, biconvex, etc. Since the wave drag required for this method was for real airfoils and no systematic sets of wing variables existed, selection of the correlating parameters suggested by the transonic similarity laws and supersonic drag theory were used on a best fit of data approach. Transonic similarity laws suggest normalizing ΔC_{D_C} WING by $(t/c)^{5/3}$ which was done. Based on previous correlations, reference 1, the wing compressibility or wave drag was also normalized by a camber factor of $(1 + \frac{h}{c}/10)$. In the subsonic/transonic speed regime, compressibility or wave drag for the wings of advanced or conventional sections were found to correlate best as a function of $(t/c)^{2/3}$ (see figure 35). In the supersonic speed regime, AR tan $\Lambda_{L.E.}$ proved to be the correlation parameter that produced the best data fit for all airplanes (see figure 36). The F-104 and F-106, having a major wing geometry difference in sweep and taper only, were the drivers in selecting this correlating parameter. The final data fairings of figures 35 and 36 are summarized in figures 10 and 11.

3.3.2 Compressibility drag due to fuselage volume. - Since fuselage drag characteristics are not dependent on wing design characteristics, fuselage compressibility or wave drag has been correlated at discrete Mach numbers rather than at a ΔM from wing design Mach number. The procedures followed in separating wing and fuselage compressibility or wave drag due to volume from the total aircraft minimum drag have been identified graphically on figure 29. Body or fuselage wave drag normally is divided into three components, i.e., forebody, aftbody, and midbody interference drag. Linear theory provides a guide to data correlation through the relationship $C_D (\ell/d)^2 = (f) \sqrt{M^2 - 1}/(\ell/d)$. Initial correlation attempts to separate total fuselage drag into these components proved fruitless, partially due to the extreme difficulty in defining the extent of forebody, midbody, and aftbody from the area progression curve. Observing the many area progression curves, those parameters that appeared to be consistently definable for all

64

configurations were the overall length, the maximum diameter and a base area. The base area was not interpreted - soley as a base drag contributor - it is also an indicator afterbody closure, i.e., the higher the base area the less severe an aftbody closure and the lower the aftbody wave drag contribution. From these observations and assumptions, fuselage wave drag (ΔC_{D_C} FUS.) was multiplied by the square of the length to diameter ratio, and correlated as a function of one plus the ratio of base area to maximum frontal area (see figures 37 and 38). These data fairings are used in figures 13 and 14 of the methodology.

3.3.3 Wing body interference drag. - Wing-body interference drag was determined from the Lockheed modified NASA wave drag program of reference 36. Interference drag is defined as the difference in total aircraft equivalent body wave drag and the sum of the theoretic component, wing and fuselage drags taken separately. The wing-body interference drag curve on figure 39 exhibits both positive and negative interference. Wing geometries are the major quantifiable contributor to differences in this interference parameter. Various combinations of wing geometries were investigated to achieve the best fit of data. Interference wave drag is normalized by $(1 - \lambda)$ times the Cos $\Lambda_{c/4}$ and correlated as a function of wing span to body diameter. The solid curves of figure 39 show the final data fairings which are summarized in figure 15.

3.3.4 Wing pressure drag due to lift. - The Delta Method defines the pressure drag term as additional lift related drag over and above the classical induced drag represented by $C_L^2/\pi AR$. This pressure drag results from flow separation and shock-induced losses, and in the supersonic speed regime, the drag term ΔC_{D_P} is also comprised of some fuselage lift.

Both transonic and supersonic linear theory predict drag due to lift, $\left(C_D^2/C_L\right)$ to be a function of leading edge suction which suggested that wing geometries that effect leading edge suction would produce the best correlation. Transonic similarity laws gave the clue as to the correlating parameters to use. Best data fit was obtained by first normalizing ΔC_{D_P} by $(t/c)^{1/3}$ times the camber term $(1 + \frac{h}{c}/10)$, and correlating versus AR $(t/c)^{1/3}$. Correlation

of this ΔC_{D_p} term is presented on figures 40 through 48 for subsonic con-
figurations and on figures 49 through 57 for supersonic configurations.
The solid curves showing the final data fairings are used in figures 16
through 27 of the Delta Method. Pressure drag due to lift correlation is
continuous throughout the Mach number range and no difference exists be-
tween conventional and advanced airfoil pressure drags when compared for
identical geometries.

3.4 Buffet Onset

The buffet onset data were available for only a limited number of
configurations and are restricted to wings of conventional sections with
the exception of wind tunnel buffet measurement on the T-2C supercritical
wind tunnel model. Buffet onset is very difficult to define due to diffi-
culty in determining "g" intensity and the lack of common threshold in-
tensity definition. Considering this, the correlations shown on
figure 58 are considered excellent. Until more advanced section buffet data
becomes available, it may be premised that this correlation is appropriate
for both conventional and advanced or supercritical wings. Data are shown
as a function of wing sweep, thickness, aspect ratio, camber, $C_{L_{DES}}$, and
ΔM. The Mach number range for this analysis is $-0.6 < \Delta M < +0.20$. The
solid curves represent the final data fairings which are summarized in
figure 28.

66
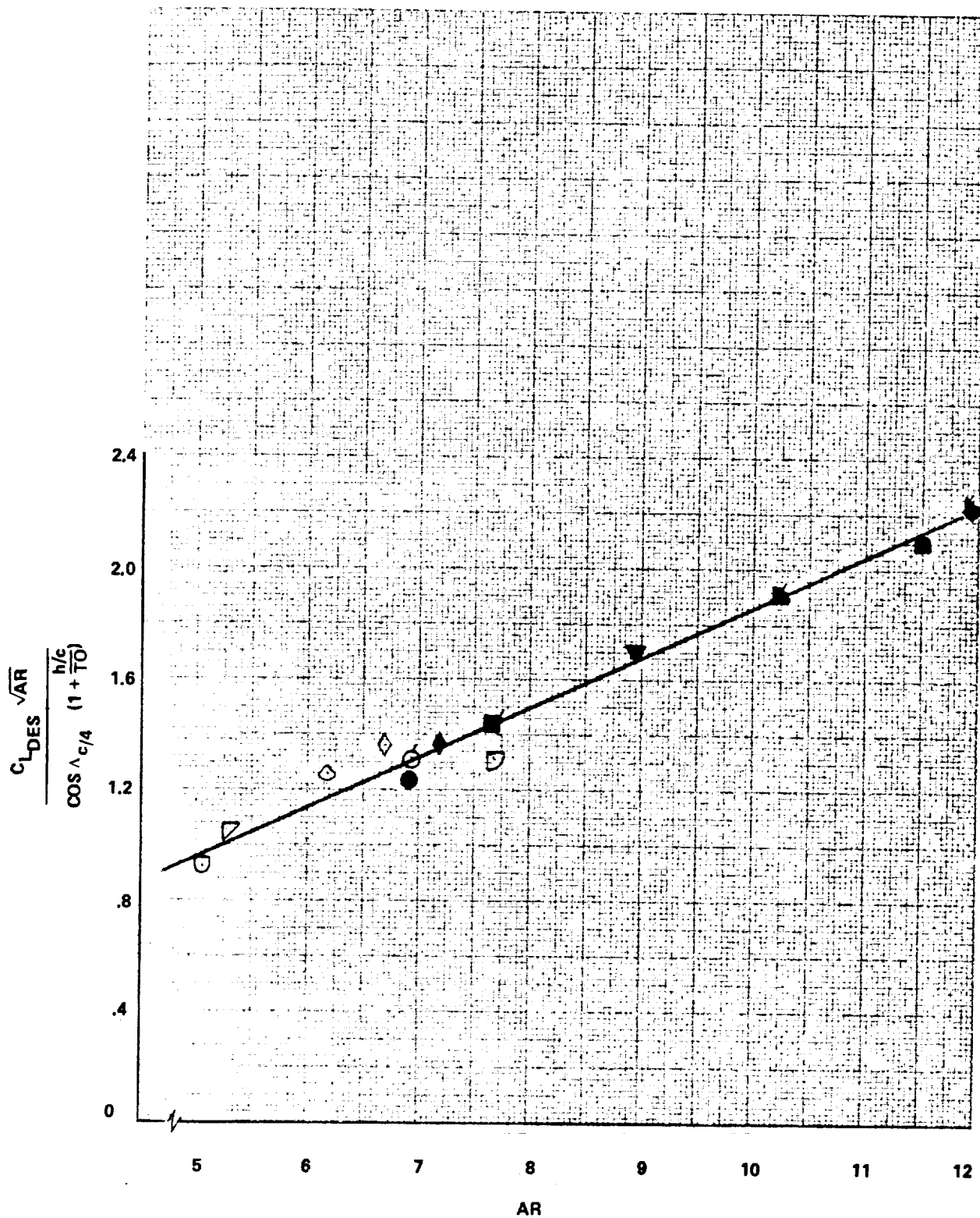
Figure 30. – $C_{L_{DES}}$ correlation, supersonic aircraft.
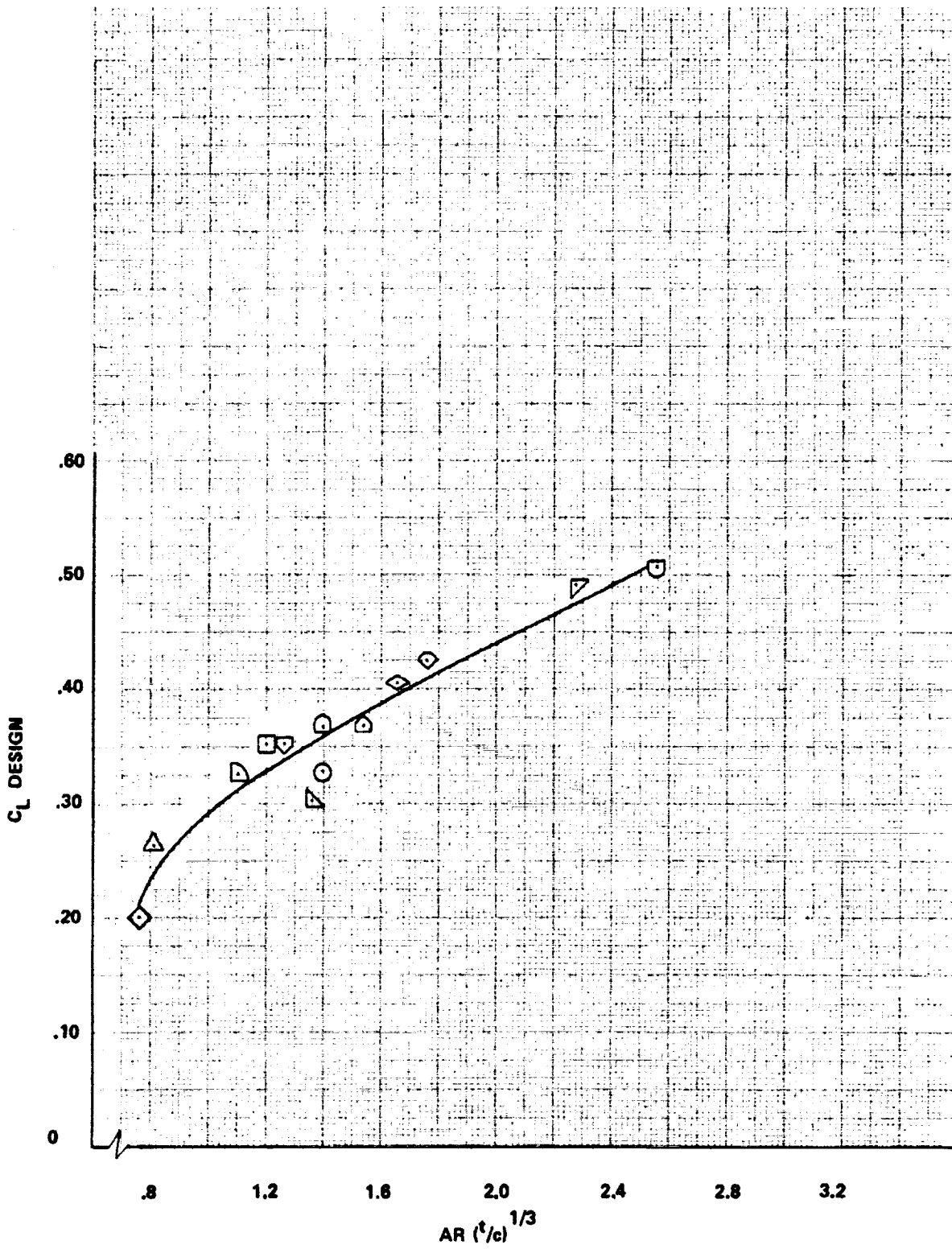
Figure 31. – $C_{L_{DES}}$ correlation, subsonic aircraft.

68
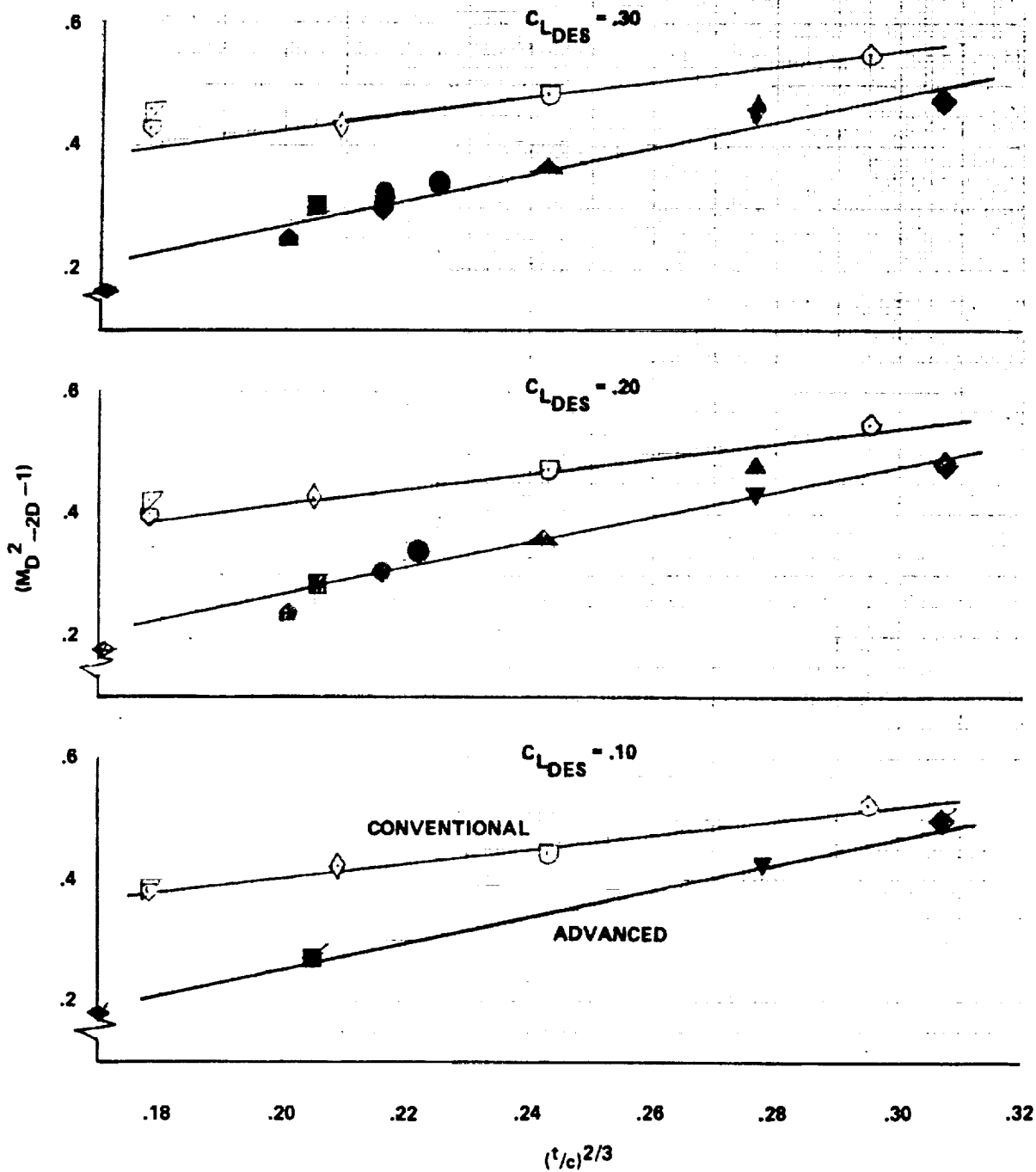
Figure 32. - M_{D2-D} data correlation, subsonic configurations.

$C_{L_{DES}} = .60$

$C_{L_{DES}} = .50$

$C_{L_{DES}} = .40$

$(M^2 D_{2-D} - 1)$

$(t/c)^{2/3}$

.18　.20　.22　.24　.26　.28　.30　.32
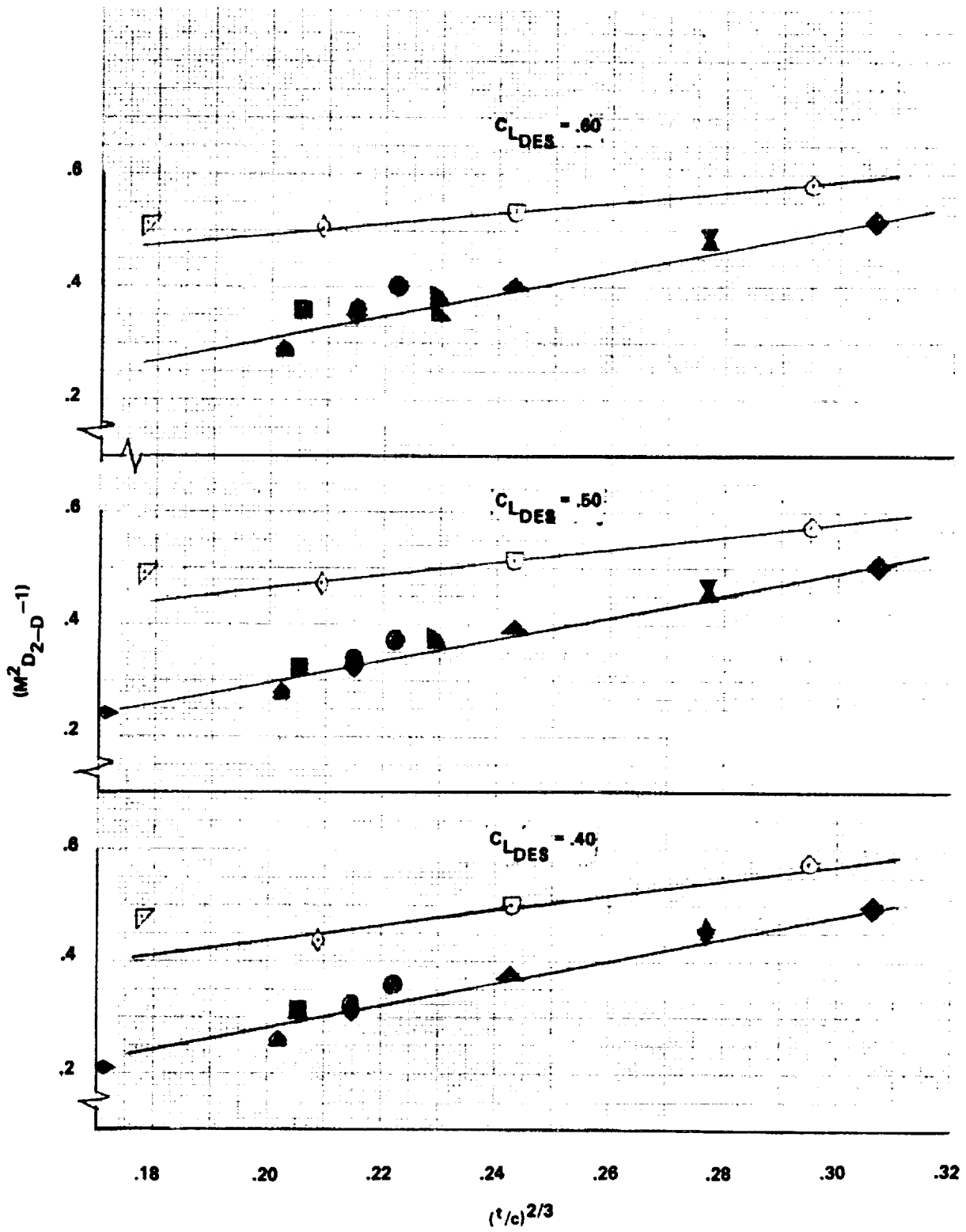
Figure 32 - Continued.
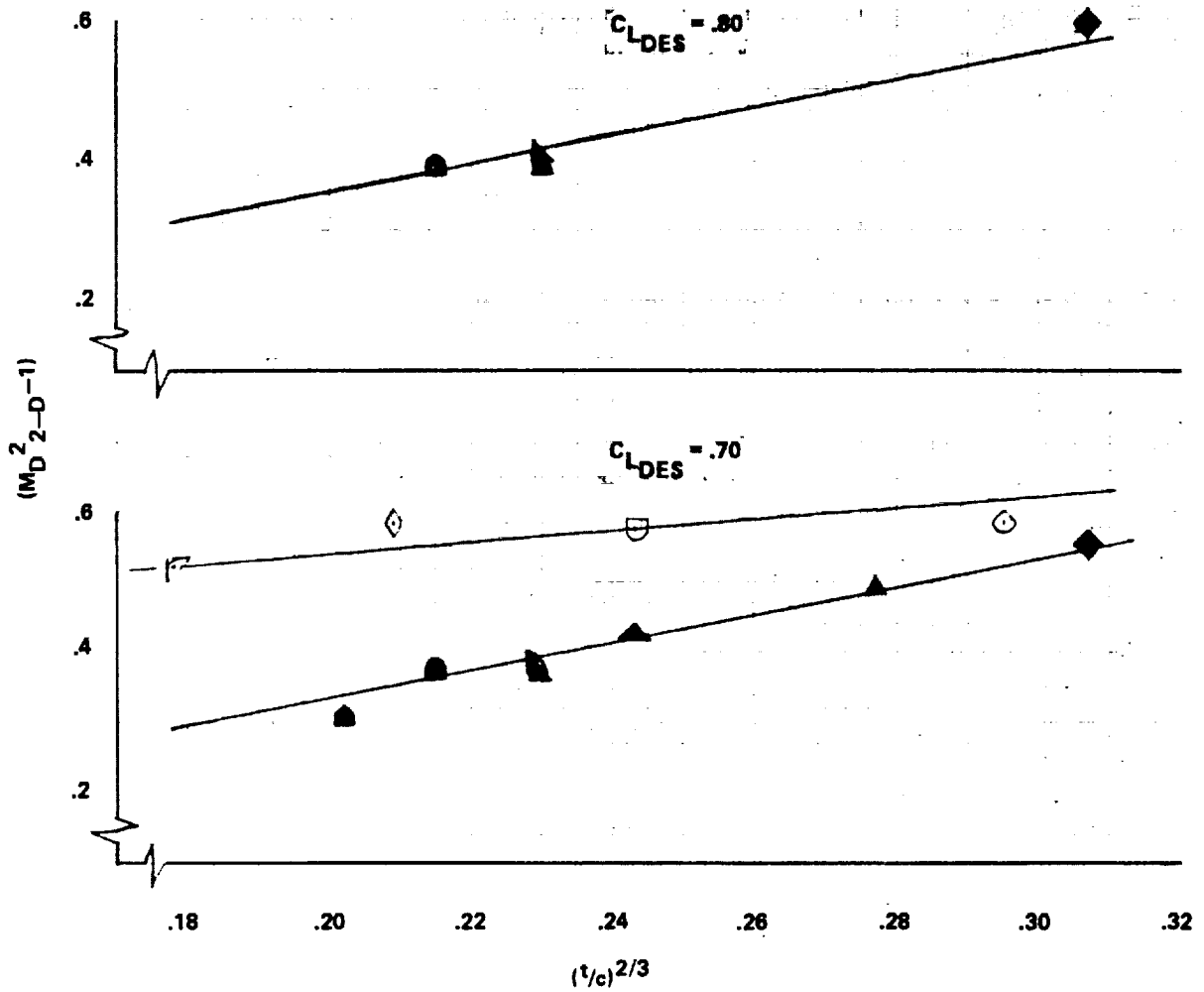
Figure 32. – Concluded.
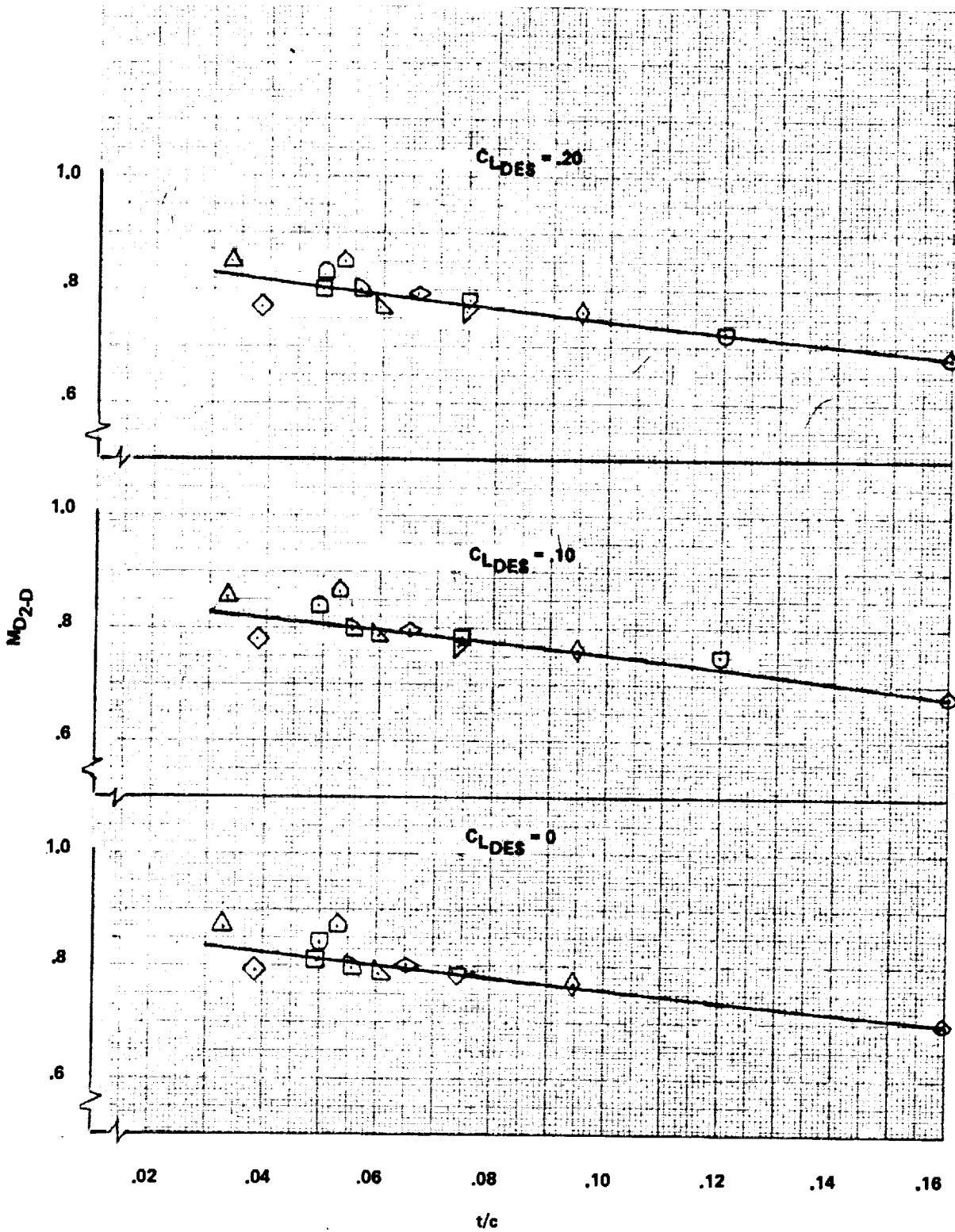
Figure 33. – $M_{D_{2-D}}$ data correlation, conventional and supersonic airfoil sections.

72

Figure 33. – Concluded.

$$C_F \text{ (COMPUTED)} = C_{D_F} \left(\frac{S_{REF}}{S_{WET}} \right)$$
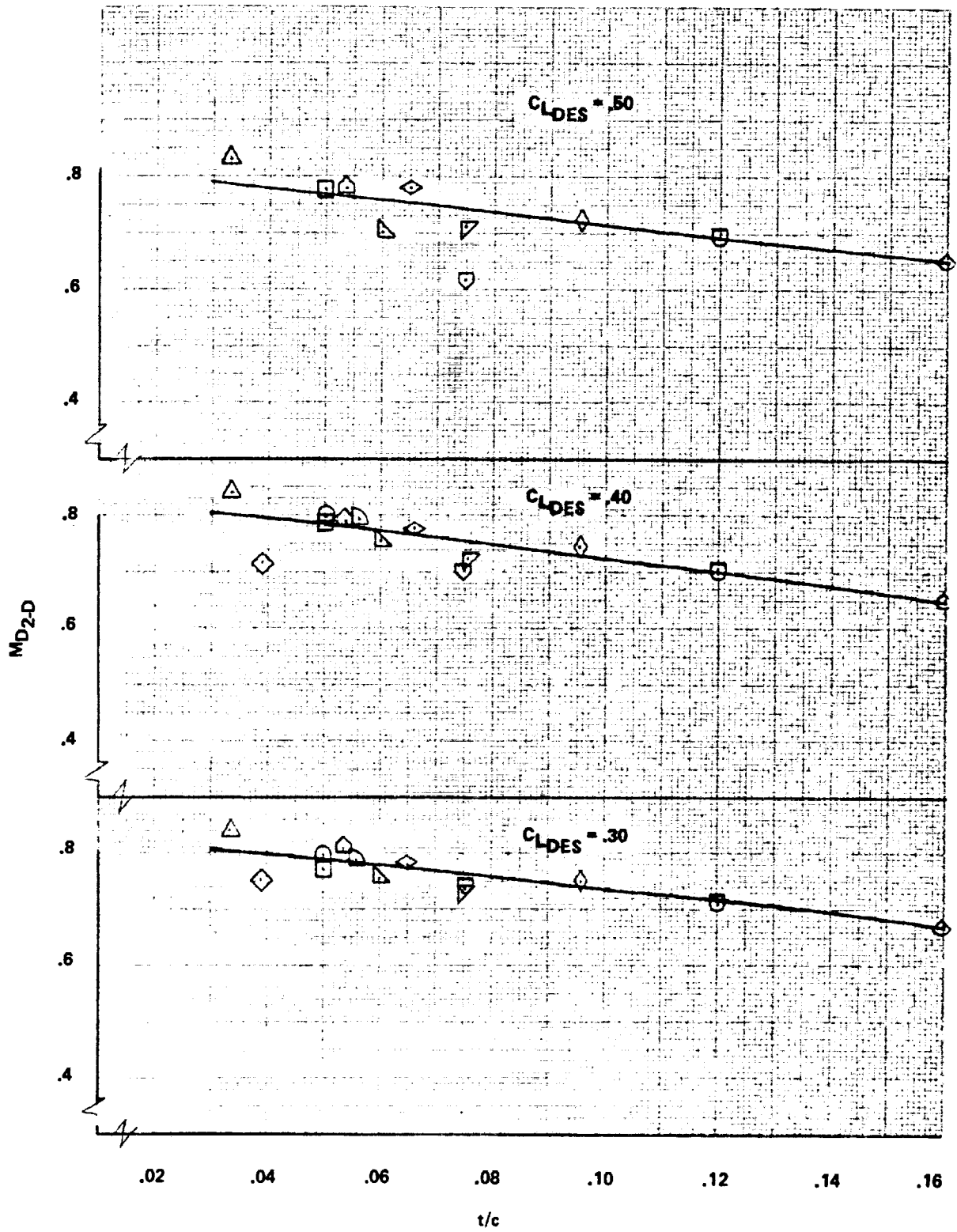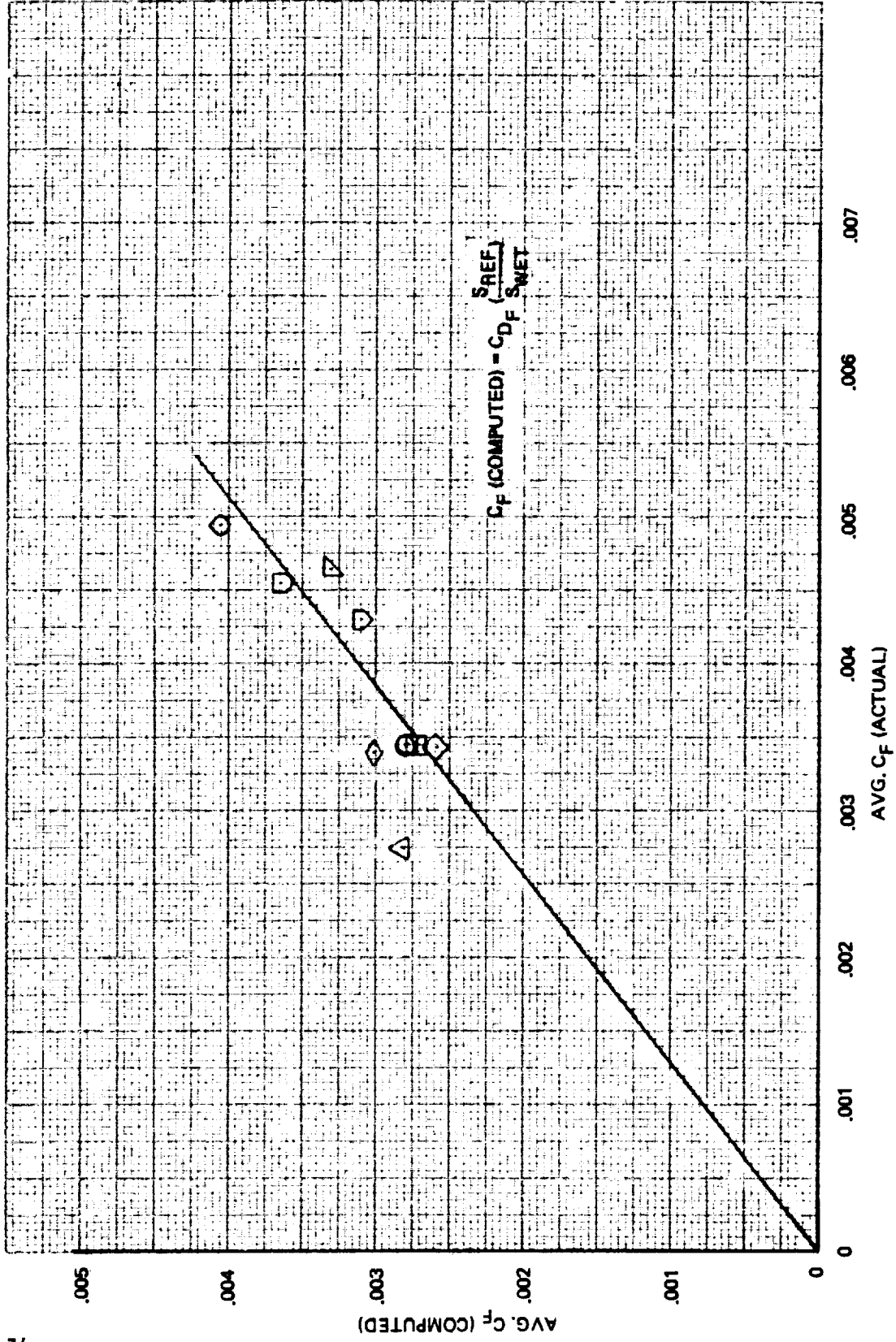
Figure 34. – Friction drag correction parameter correlation.

74
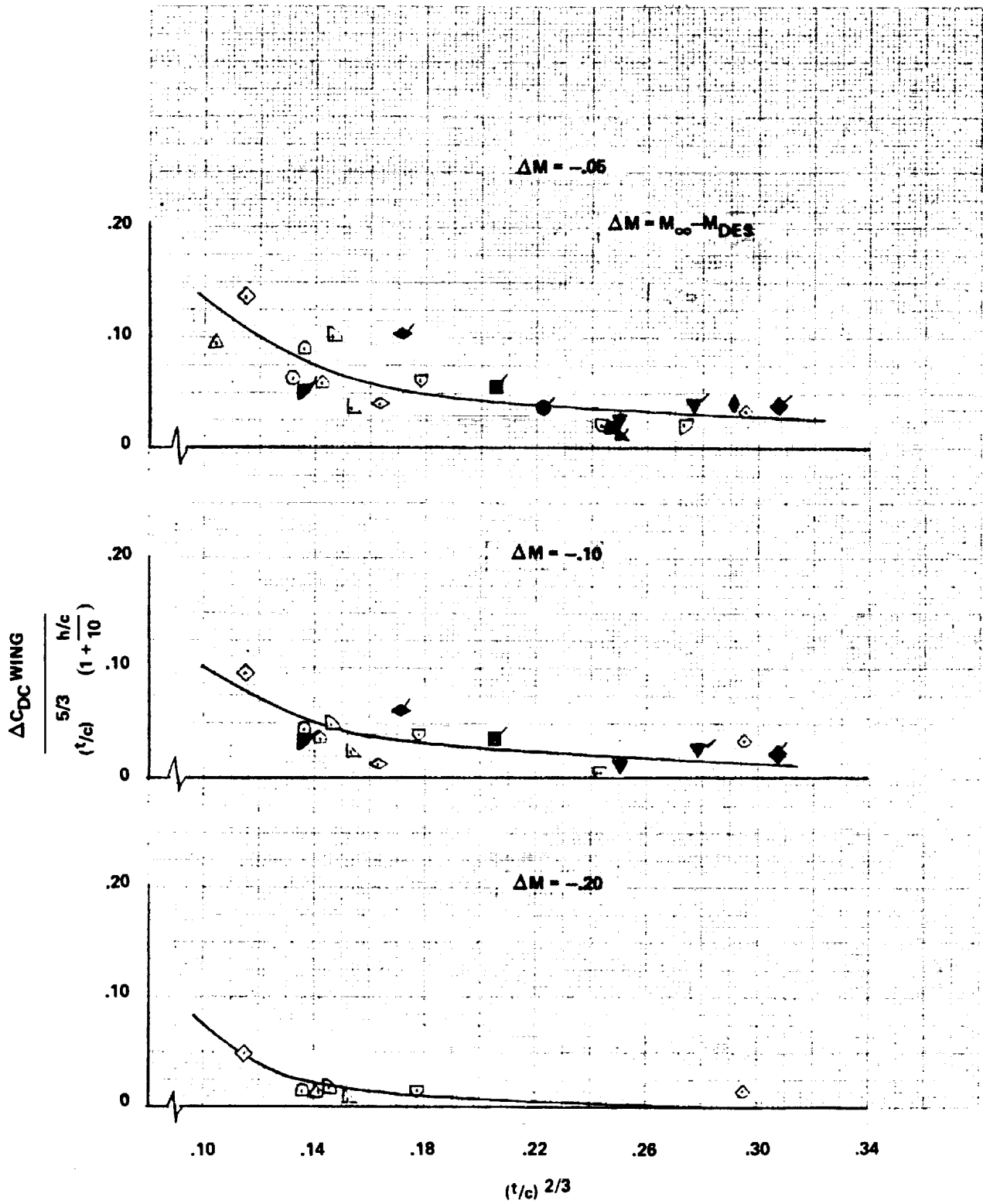
Figure 35. - Subsonic wing compressibility drag correlation.
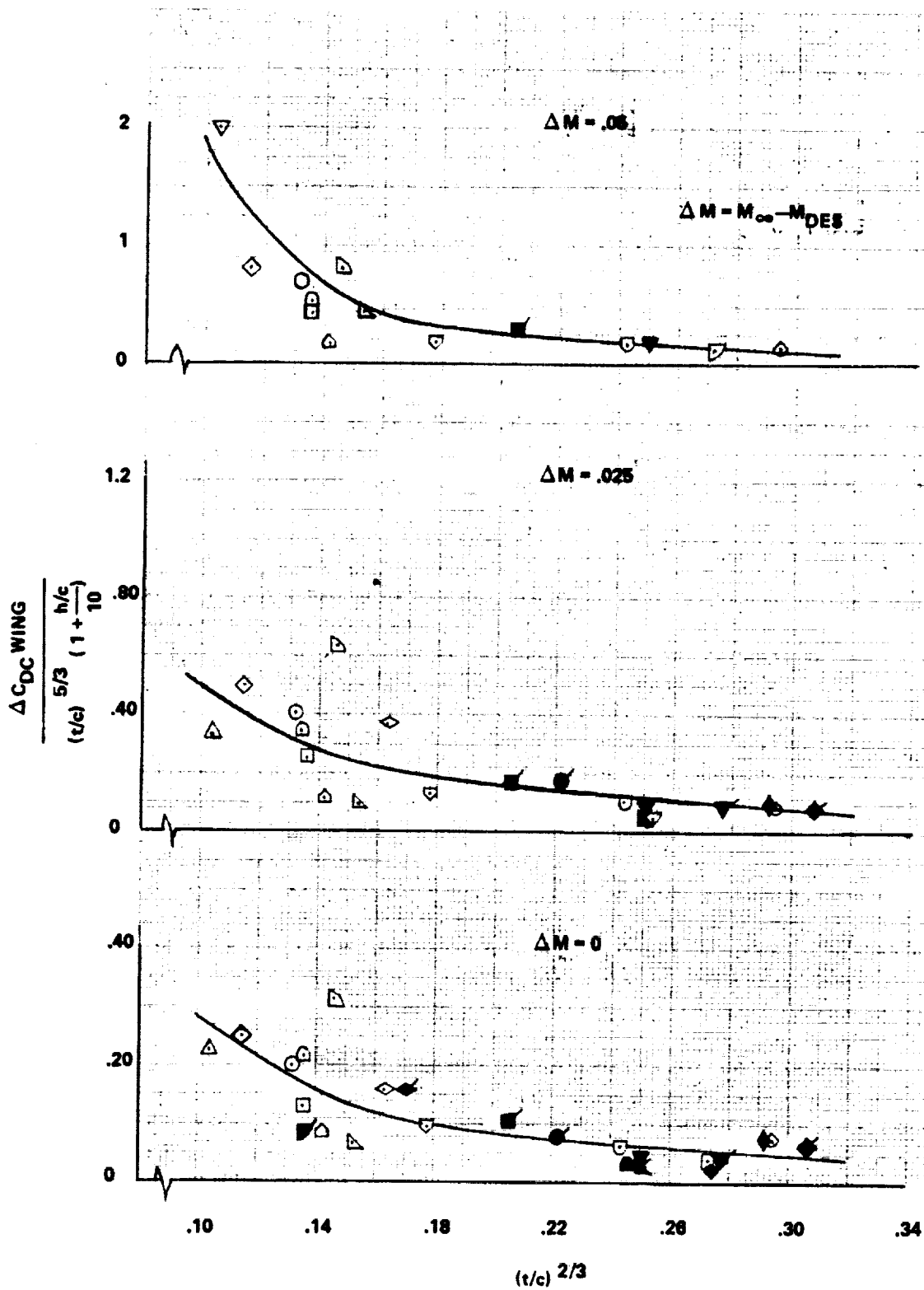
Figure 35. – Concluded.

76
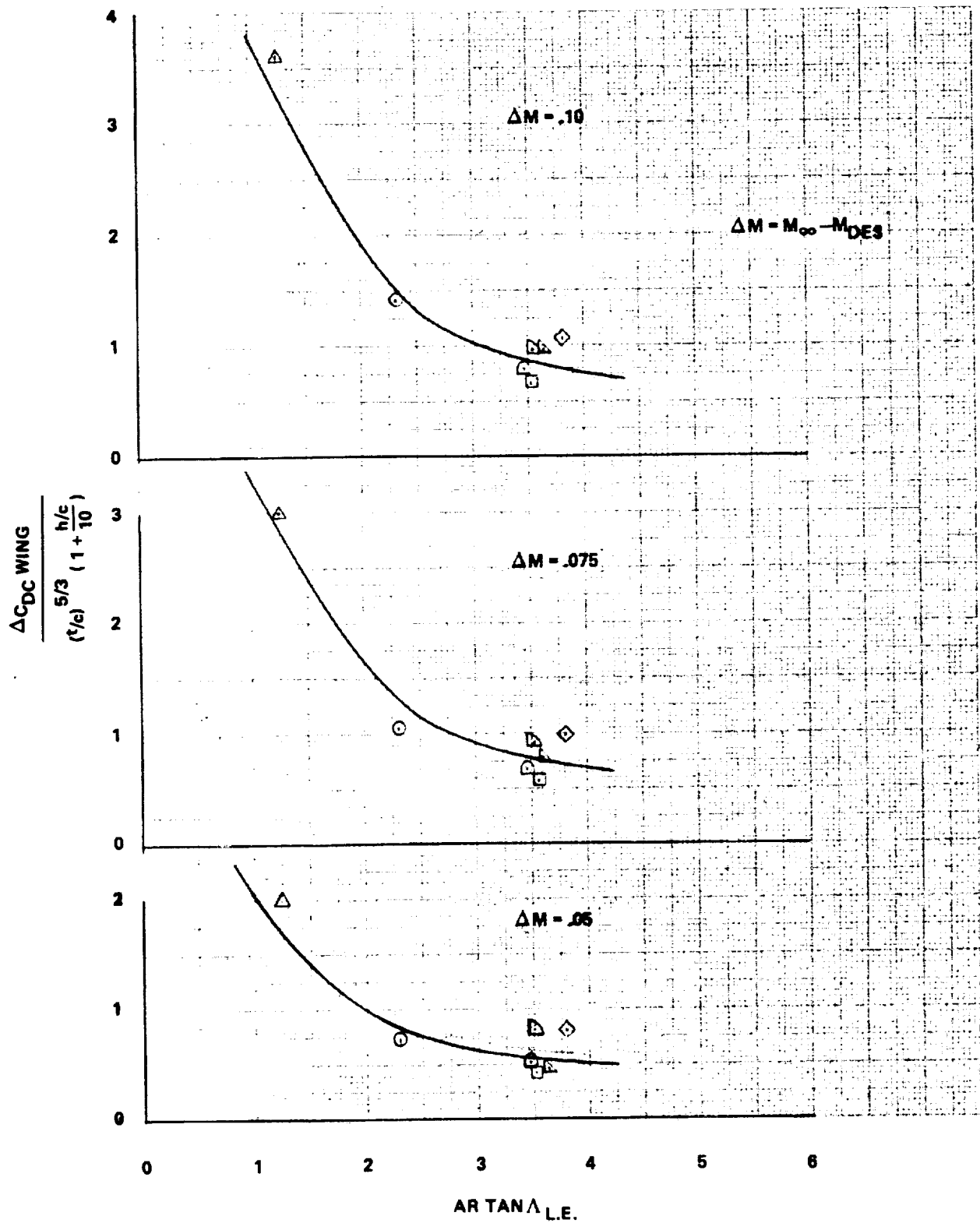
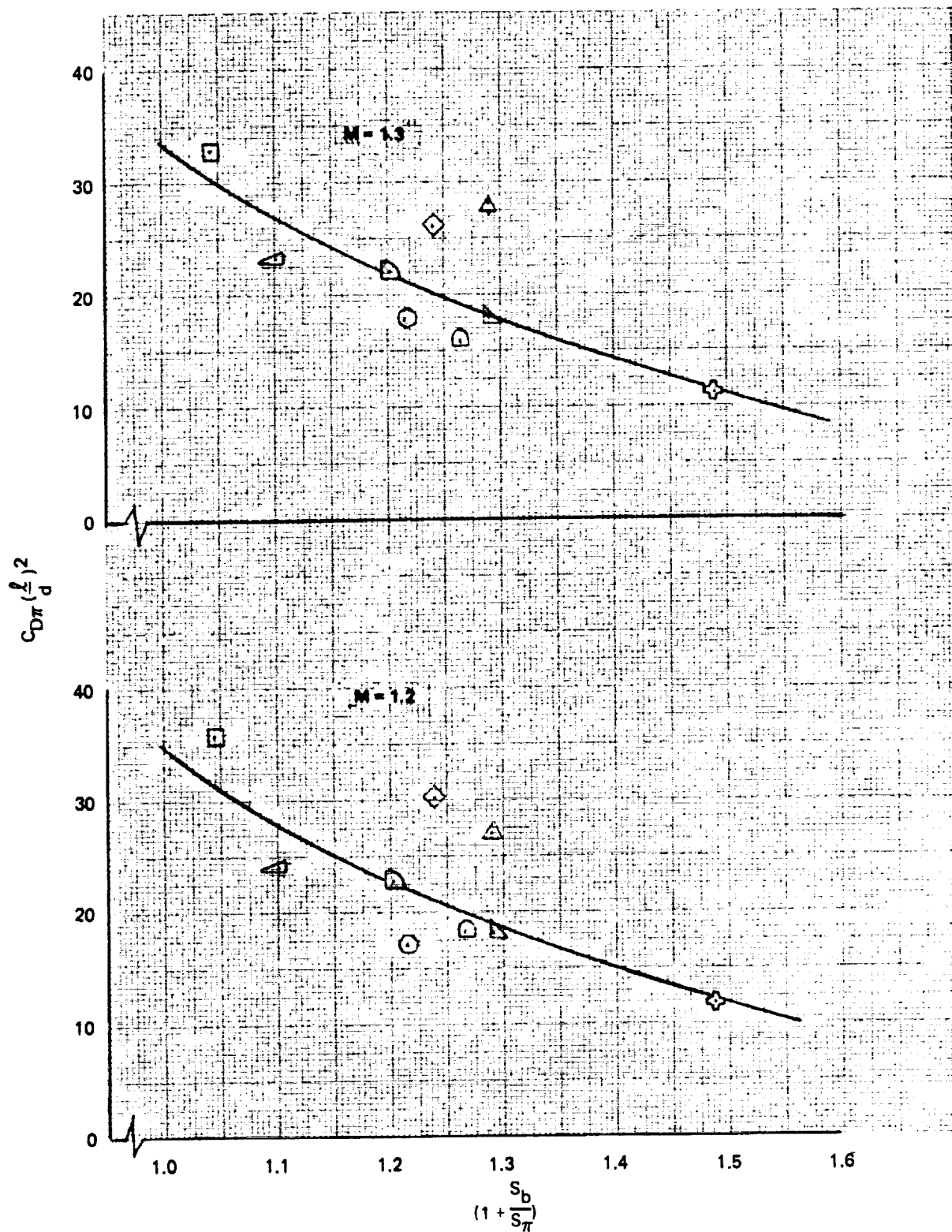Figure 36. — Supersonic wing compressibility drag correlation.

Figure 36. - Continued.

ORIGINAL PAGE IS
OF POOR QUALITY
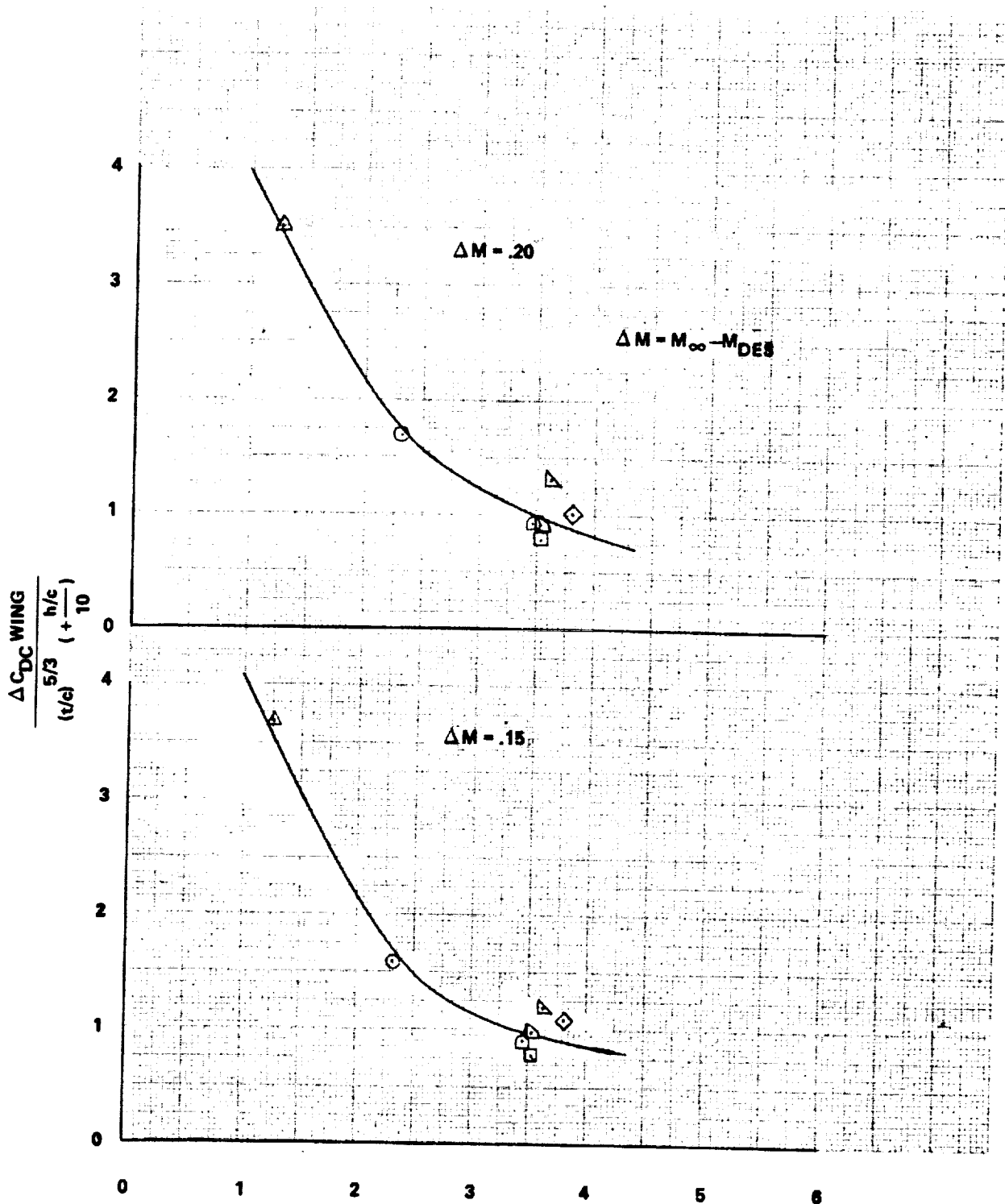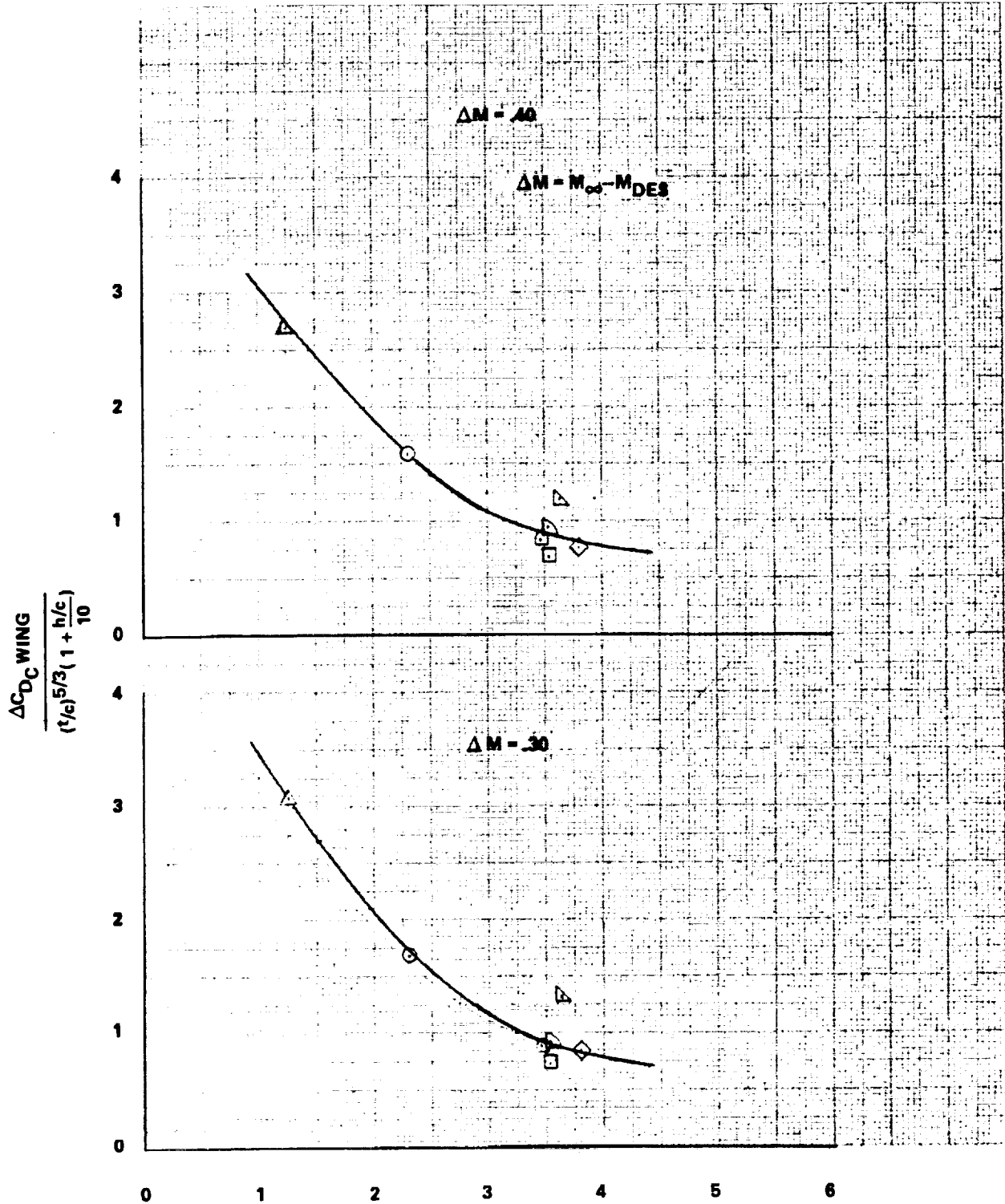
Figure 36. – Continued.
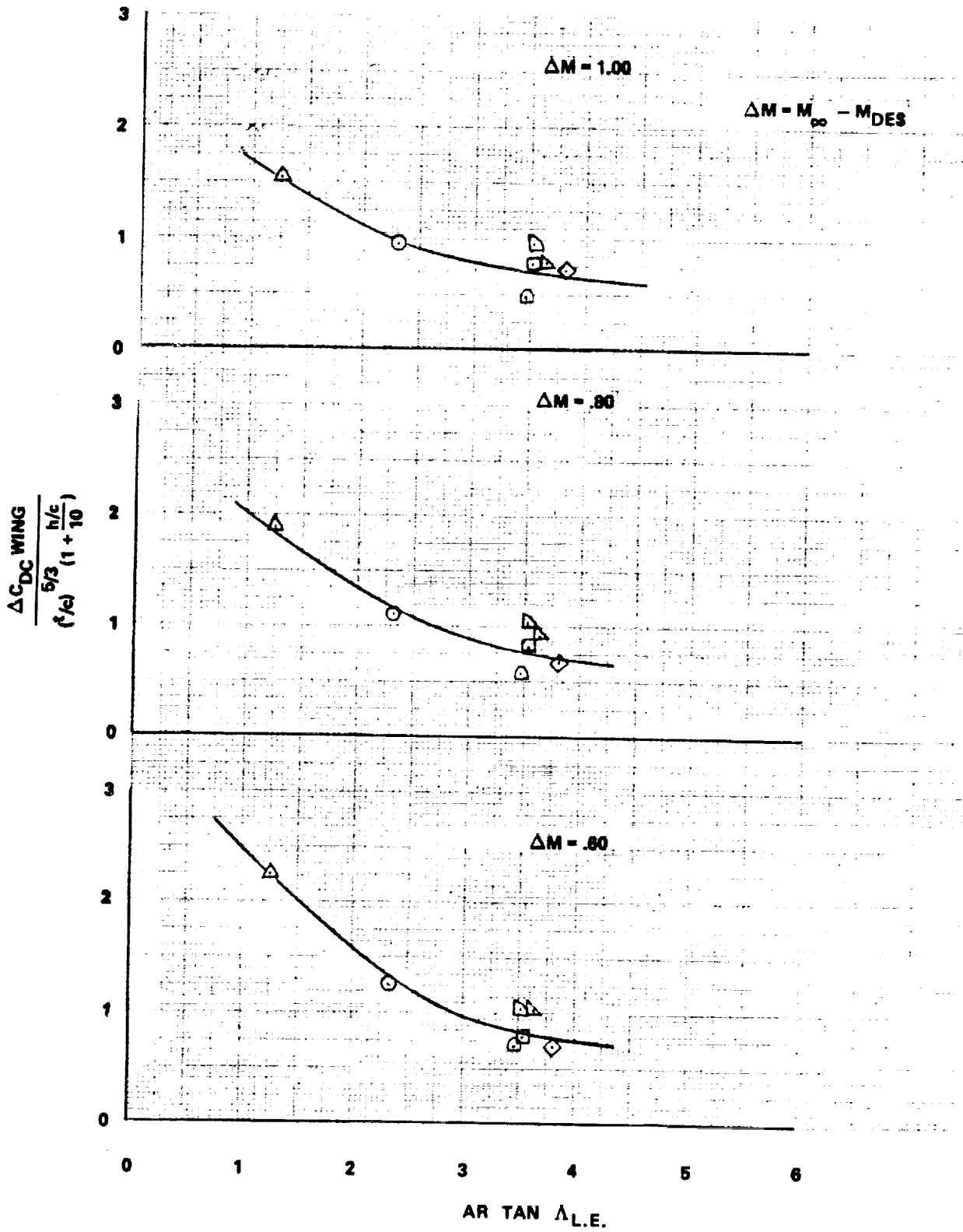
Figure 36. – Concluded.
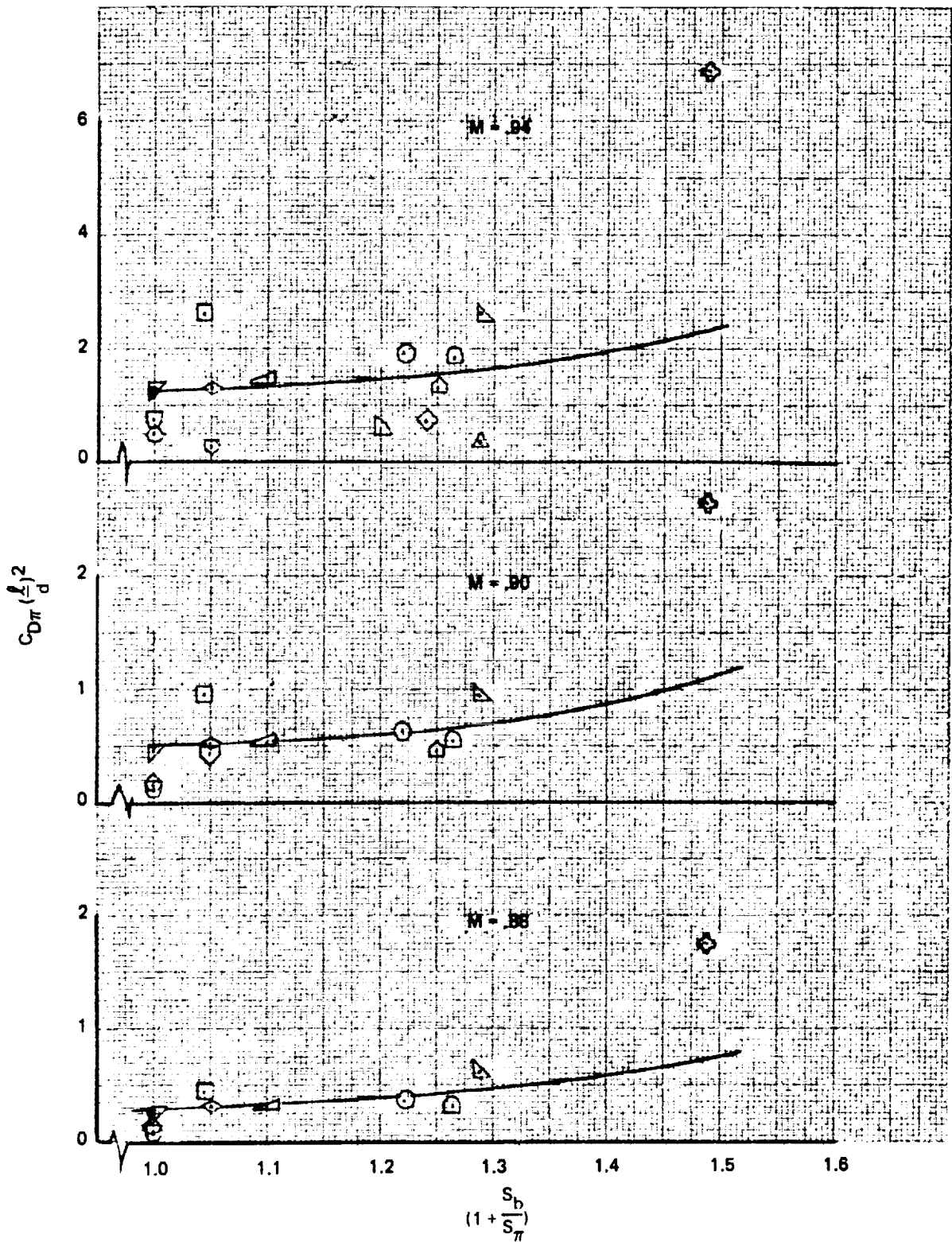
Figure 37. - Subsonic fuselage compressibility drag correlation.
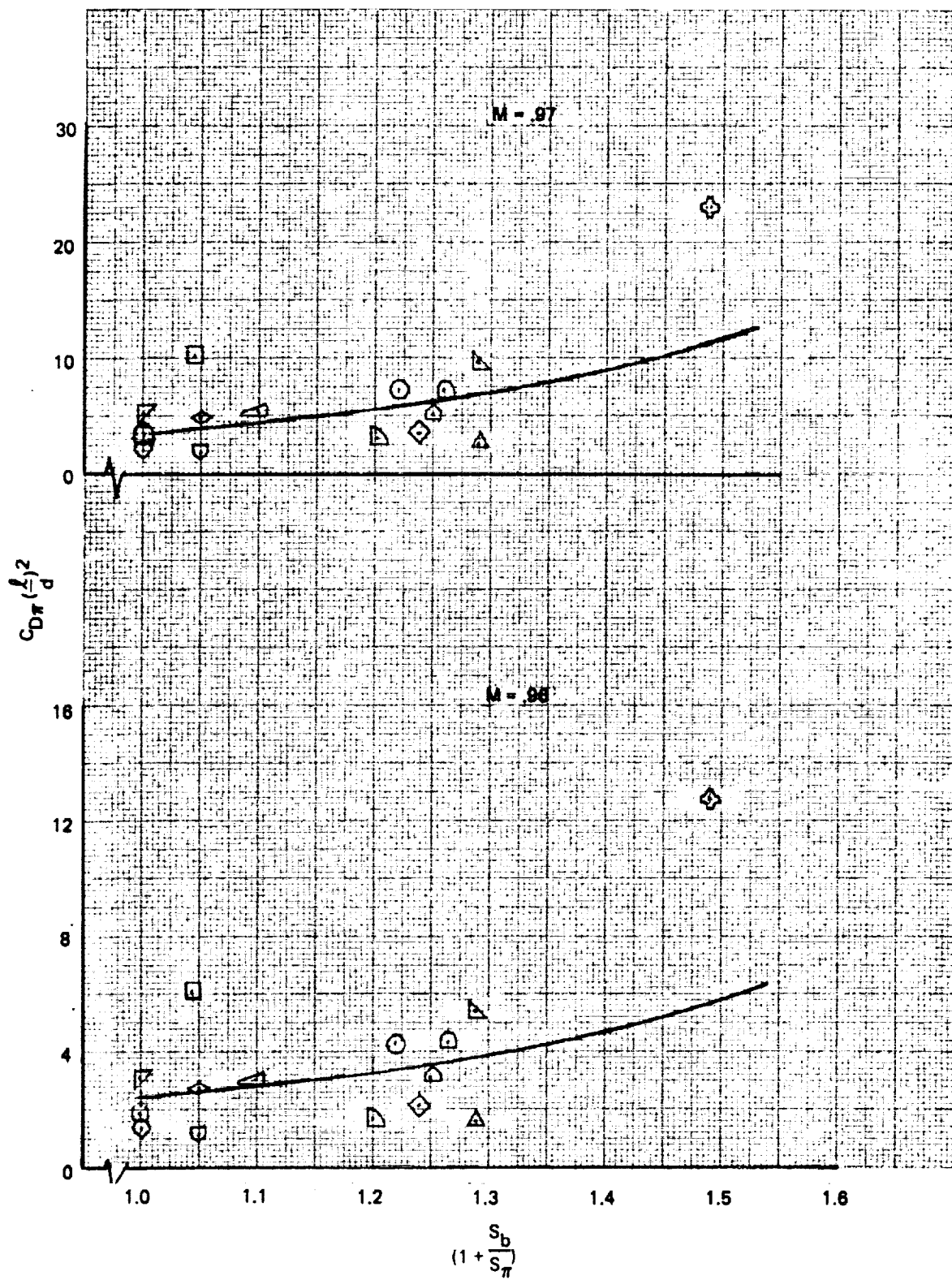
Figure 37. – Concluded.
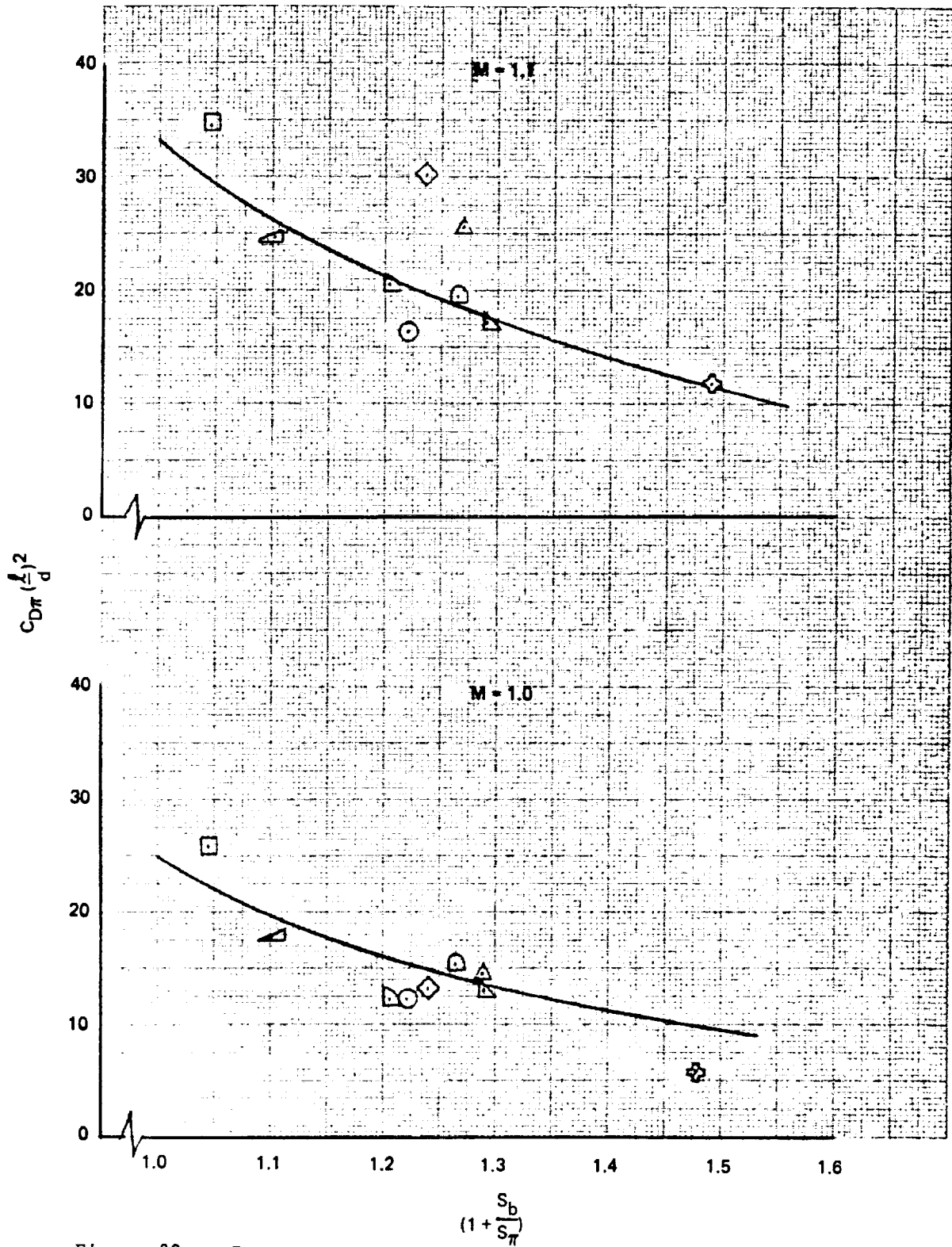
Figure 38. - Supersonic fuselage compressibility drag correlation.
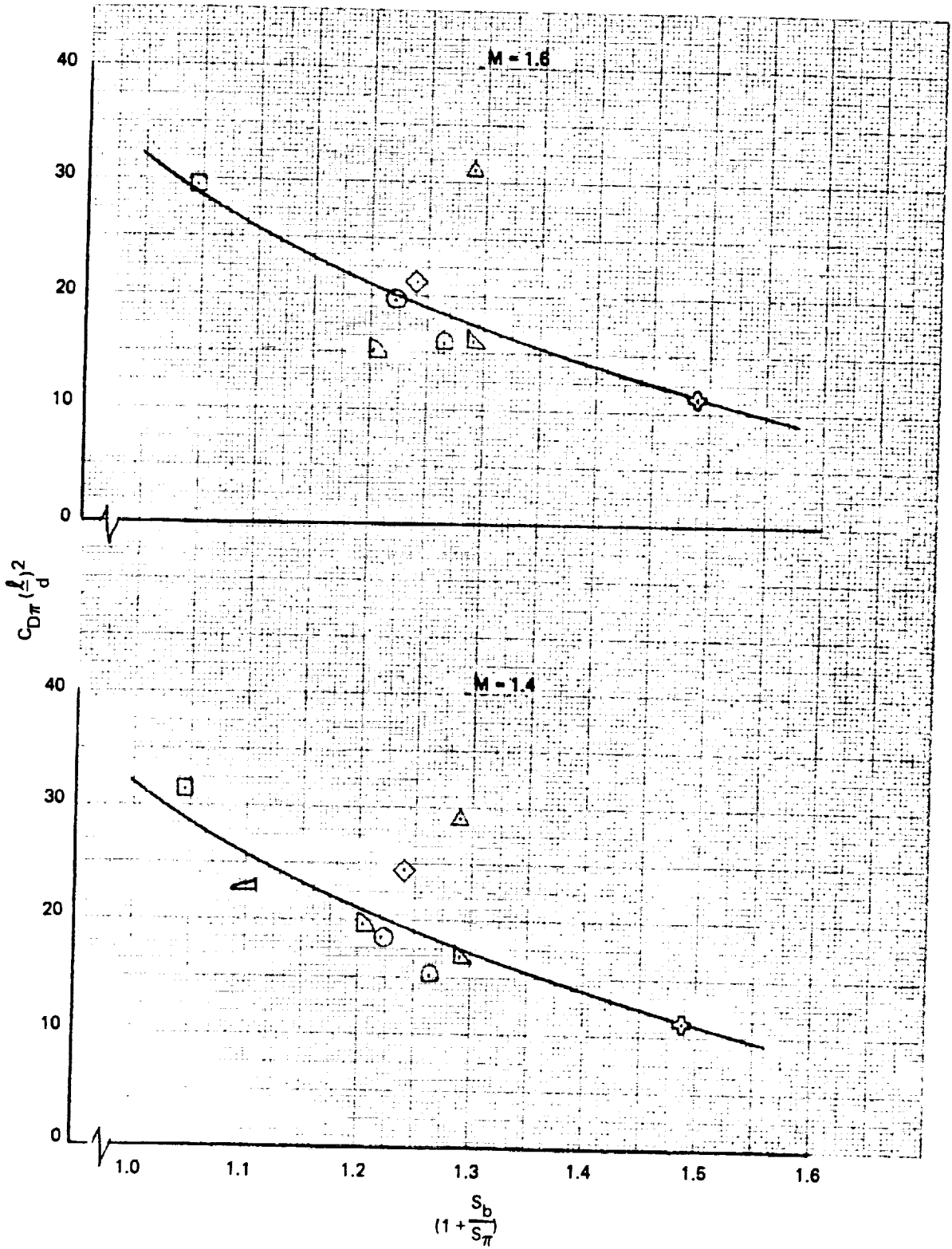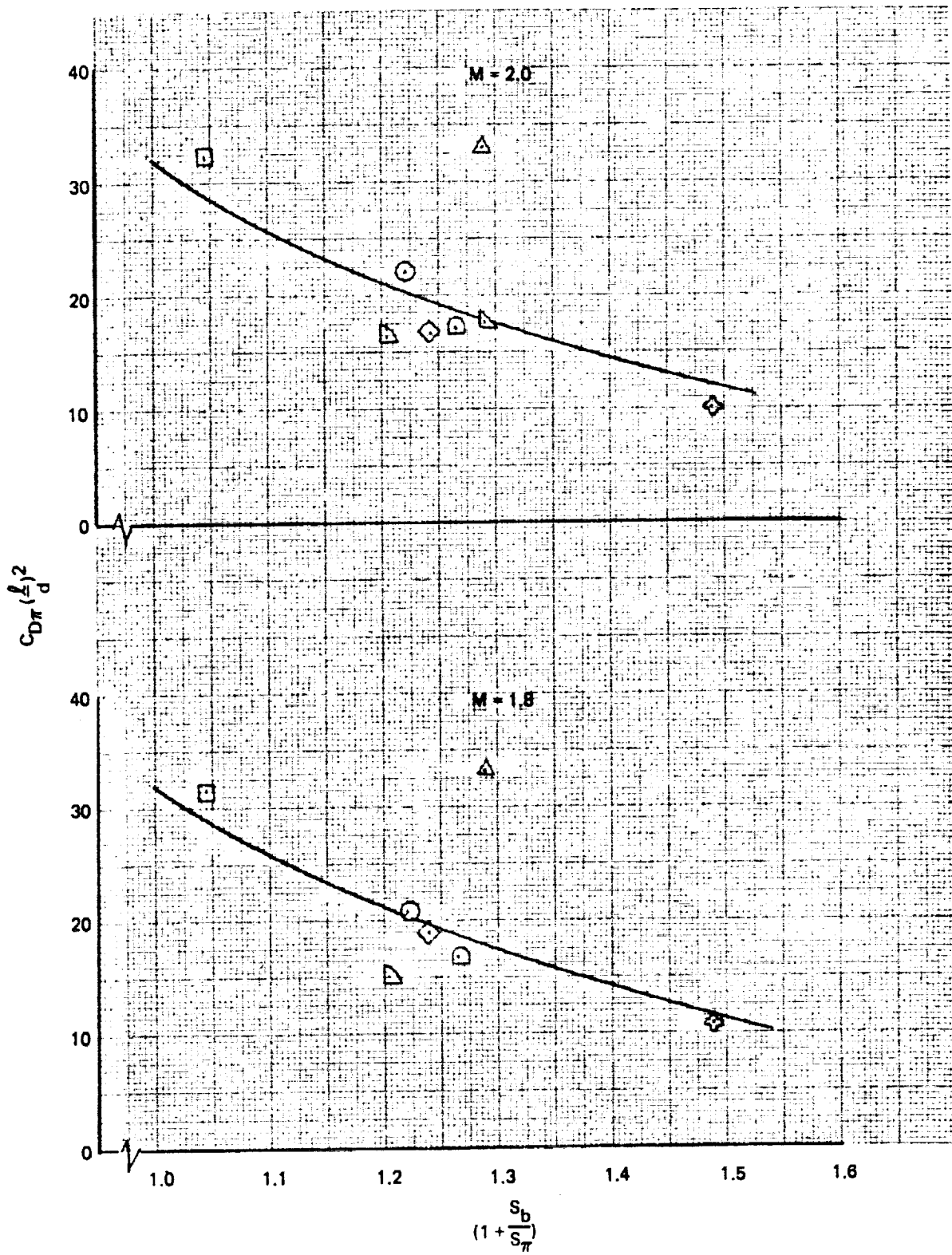
83

Figure 38. - Continued.

Figure 38. - Continued.
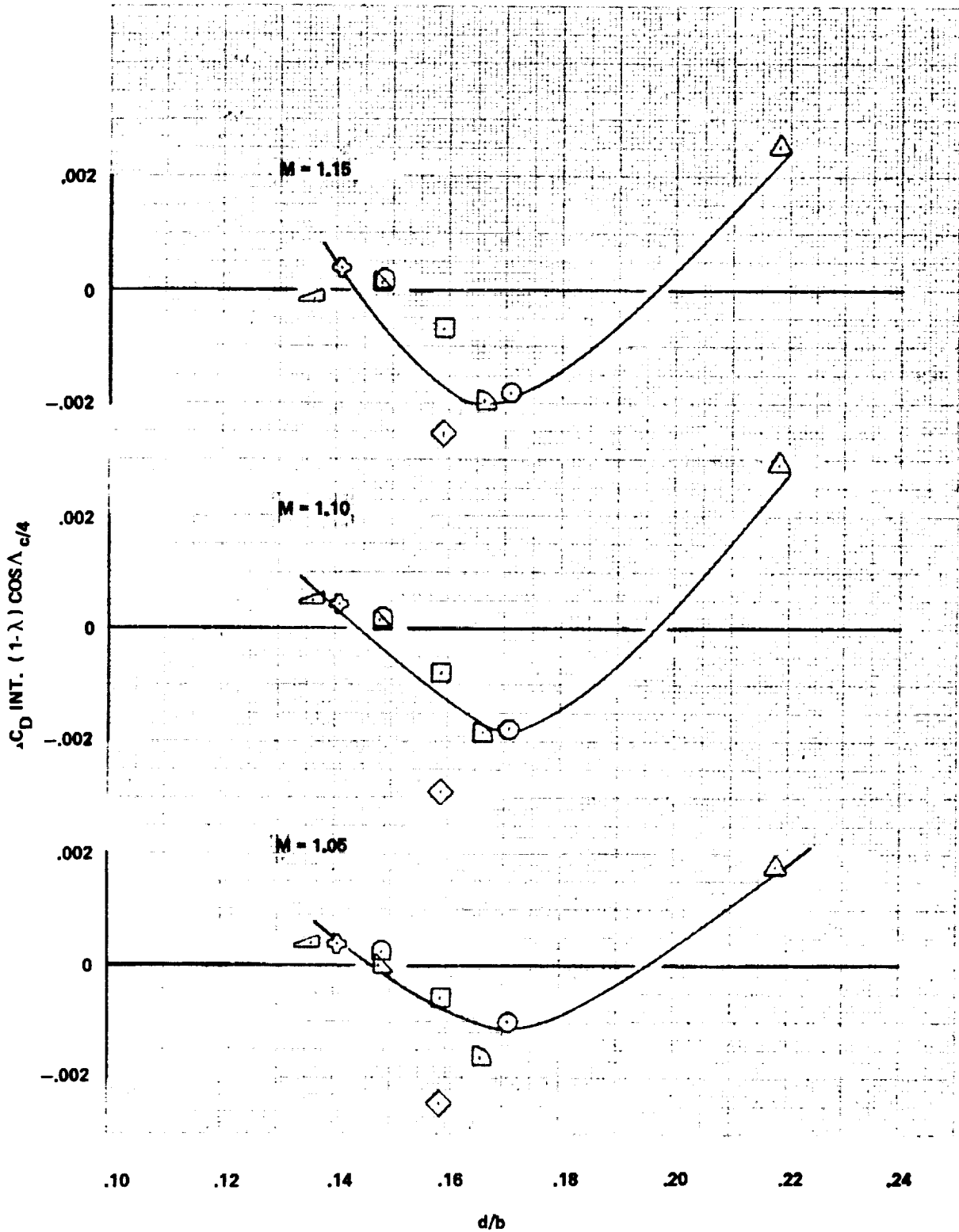
Figure 38. - Concluded.

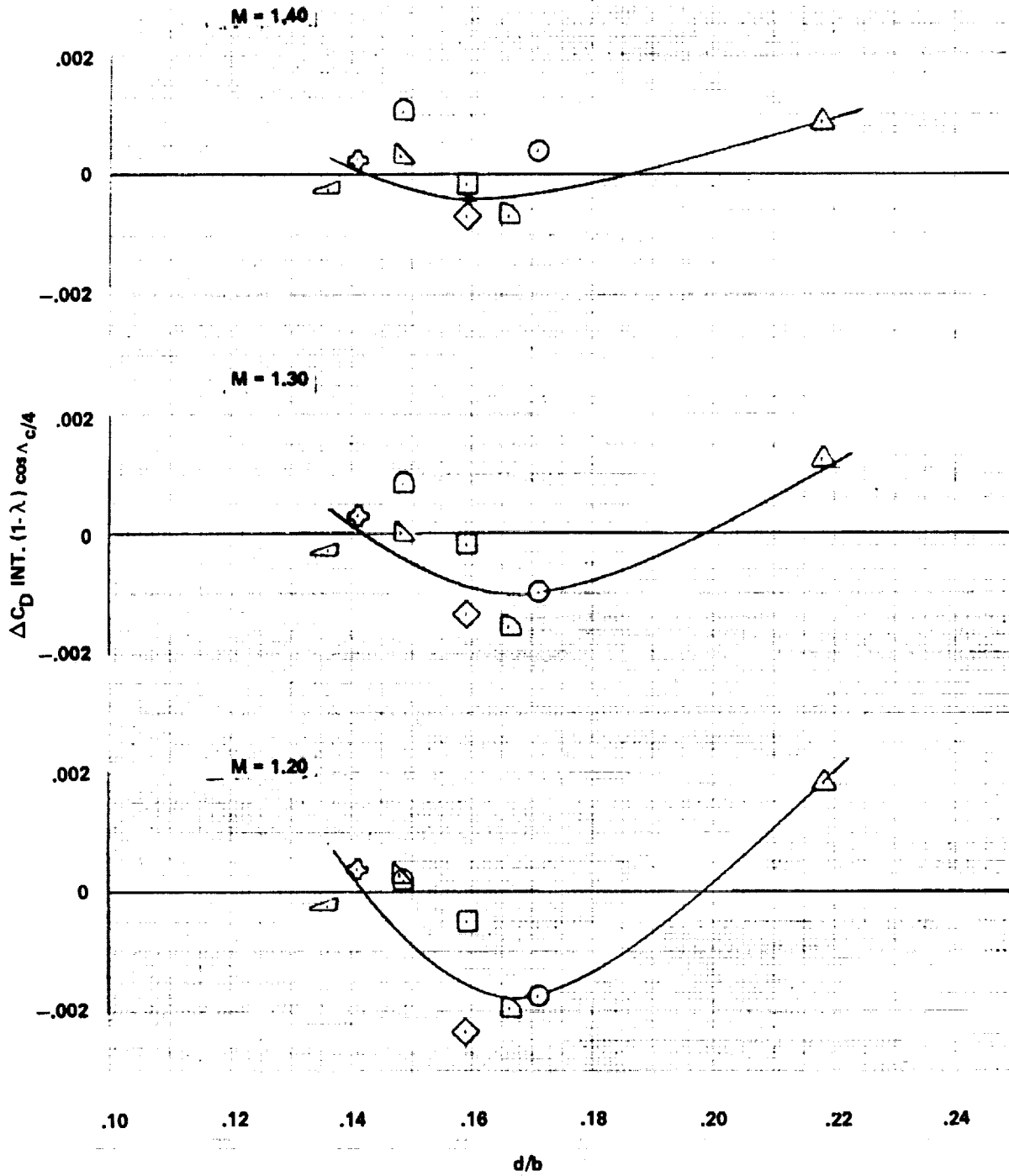Figure 39. – Wing/body interference drag correlation.
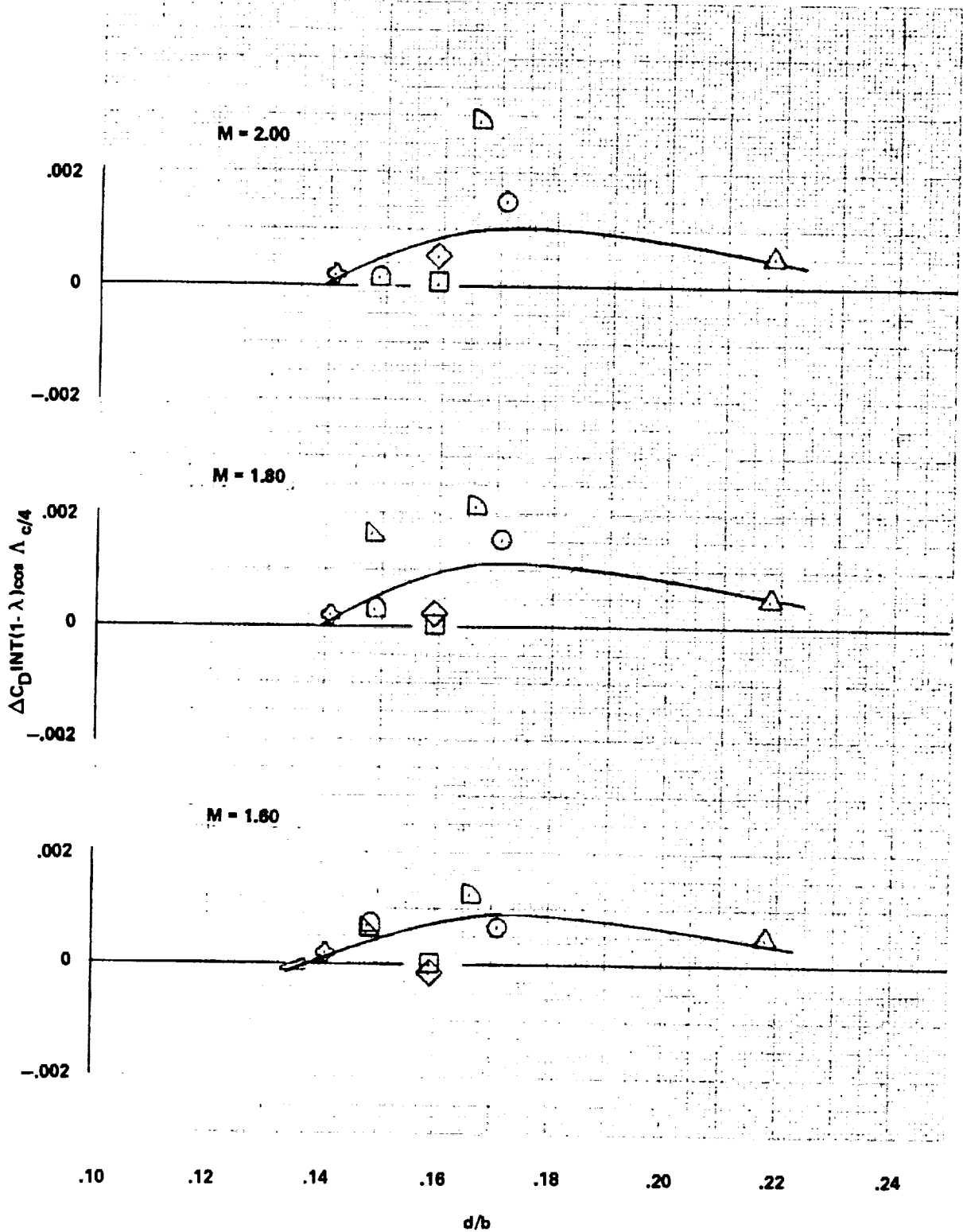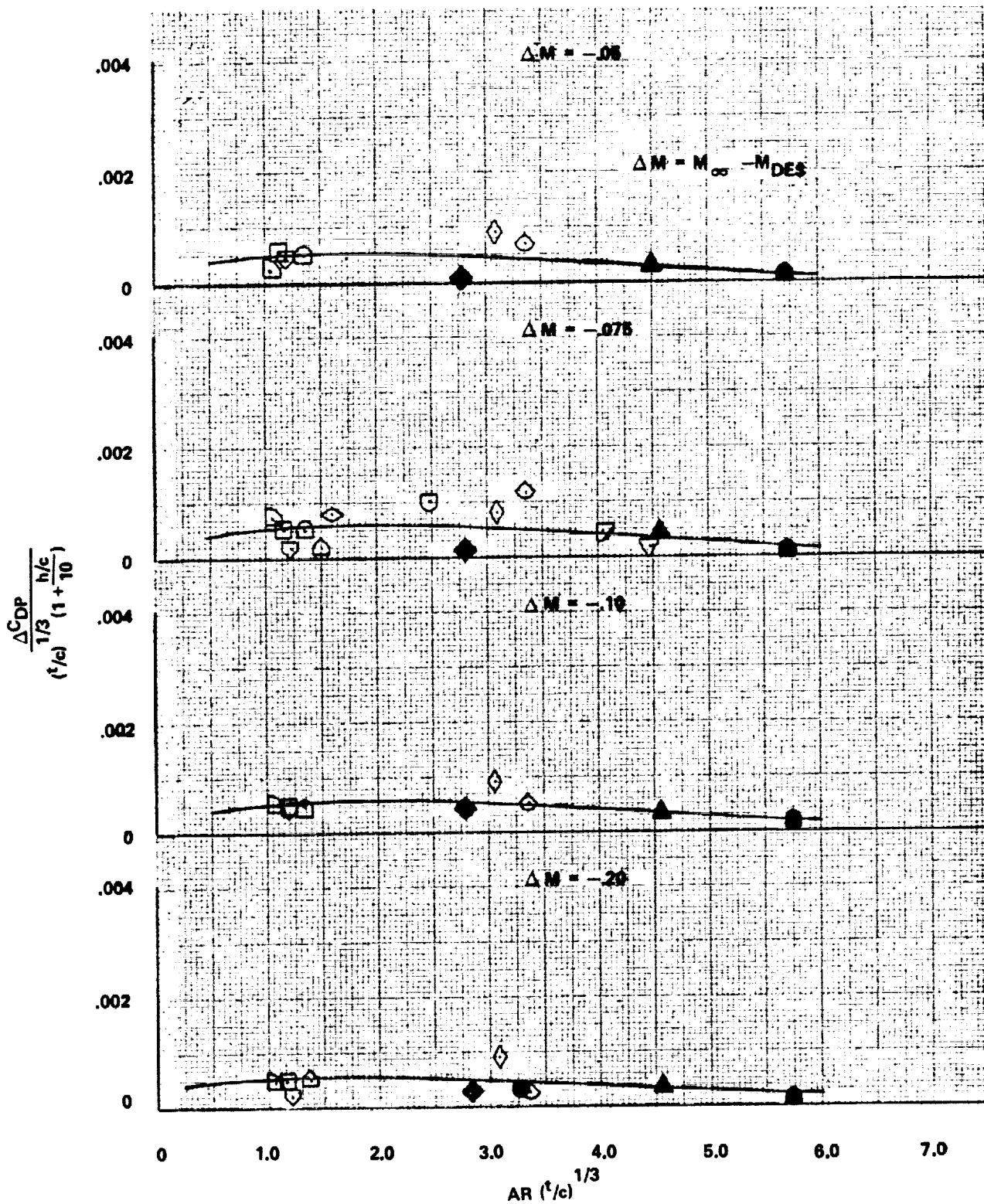
Figure 39. - Continued.

Figure 39. - Concluded.

Figure 40. – Subsonic ΔC_{DP} correlation, ΔC_L = -0.30.

ORIGINAL PAGE IS
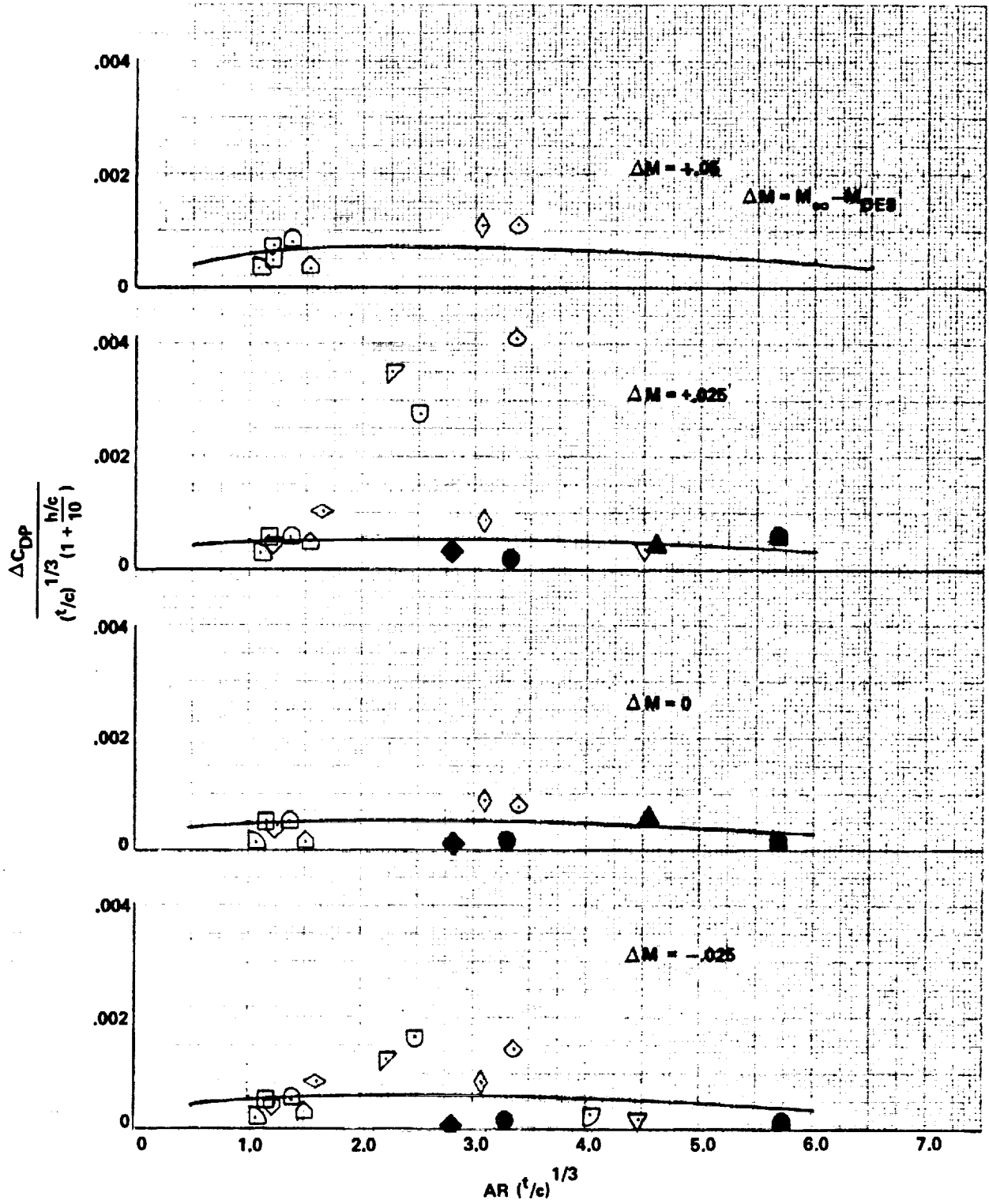OF POOR QUALITY

Figure 40. – Concluded.
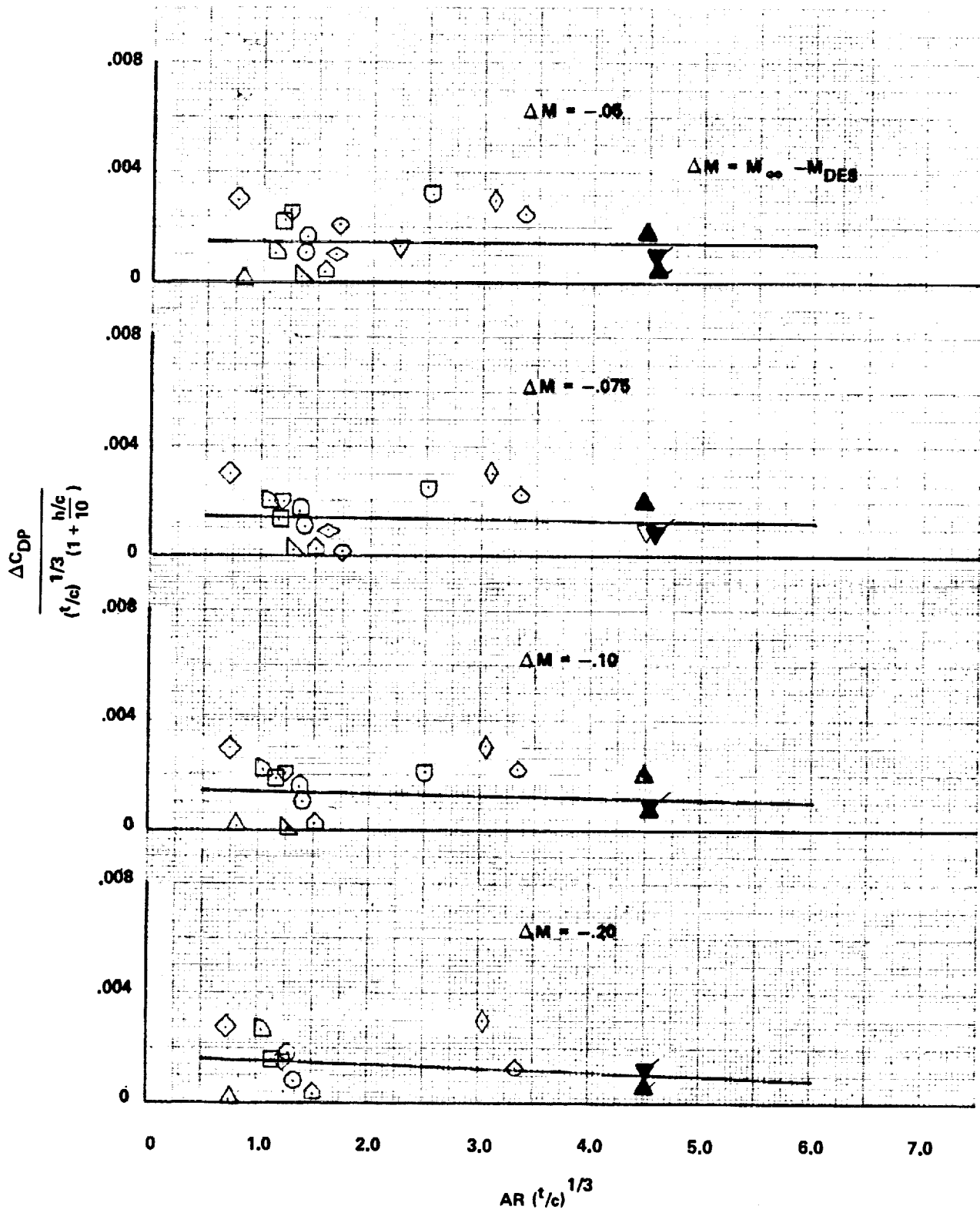
Figure 41. - Subsonic ΔC_{DP} correlation, ΔC_L = -0.20.

Figure 41. - Concluded.
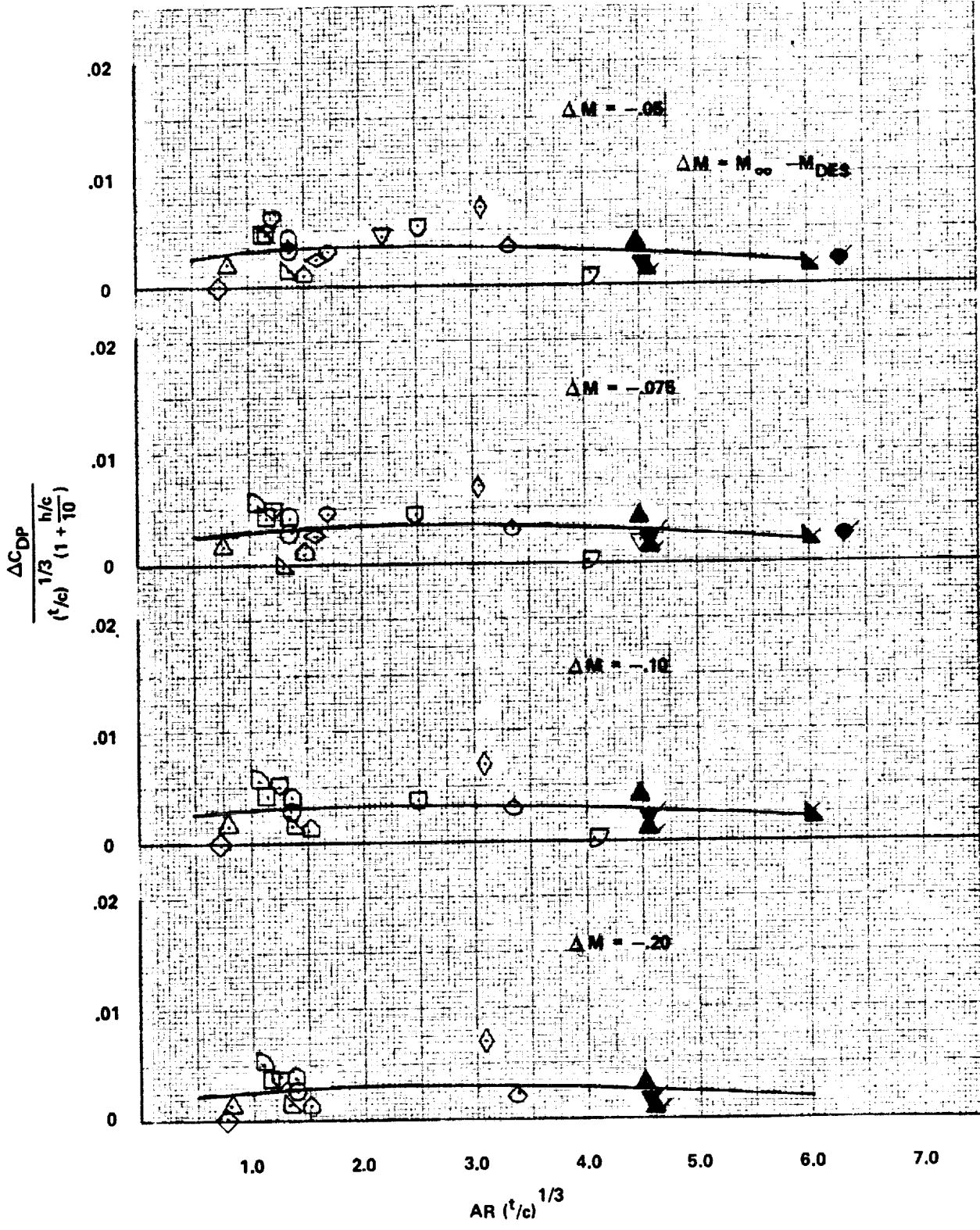
Figure 42. – Subsonic ΔC_{DP} correlation $\Delta C_L = -0.10$.

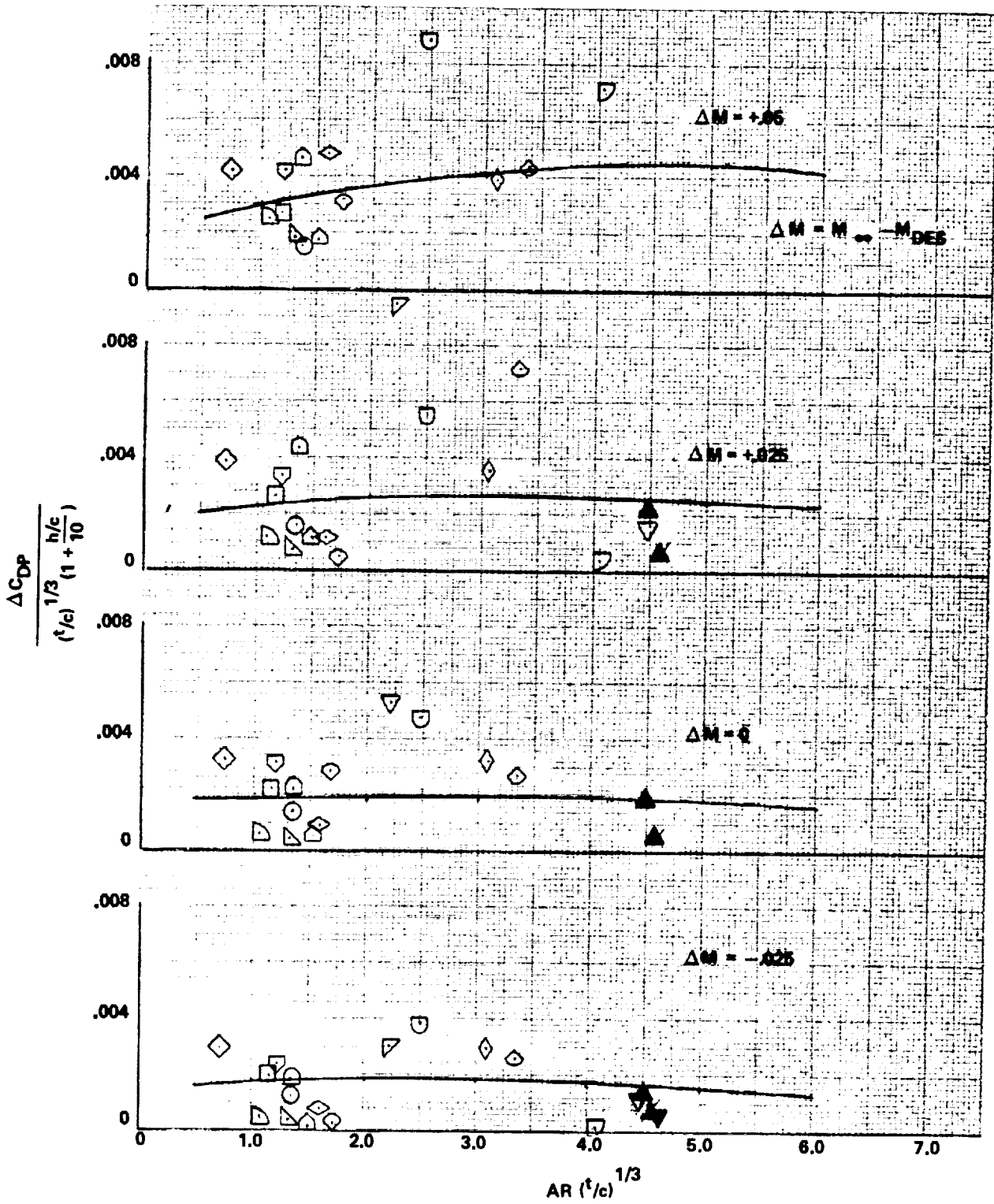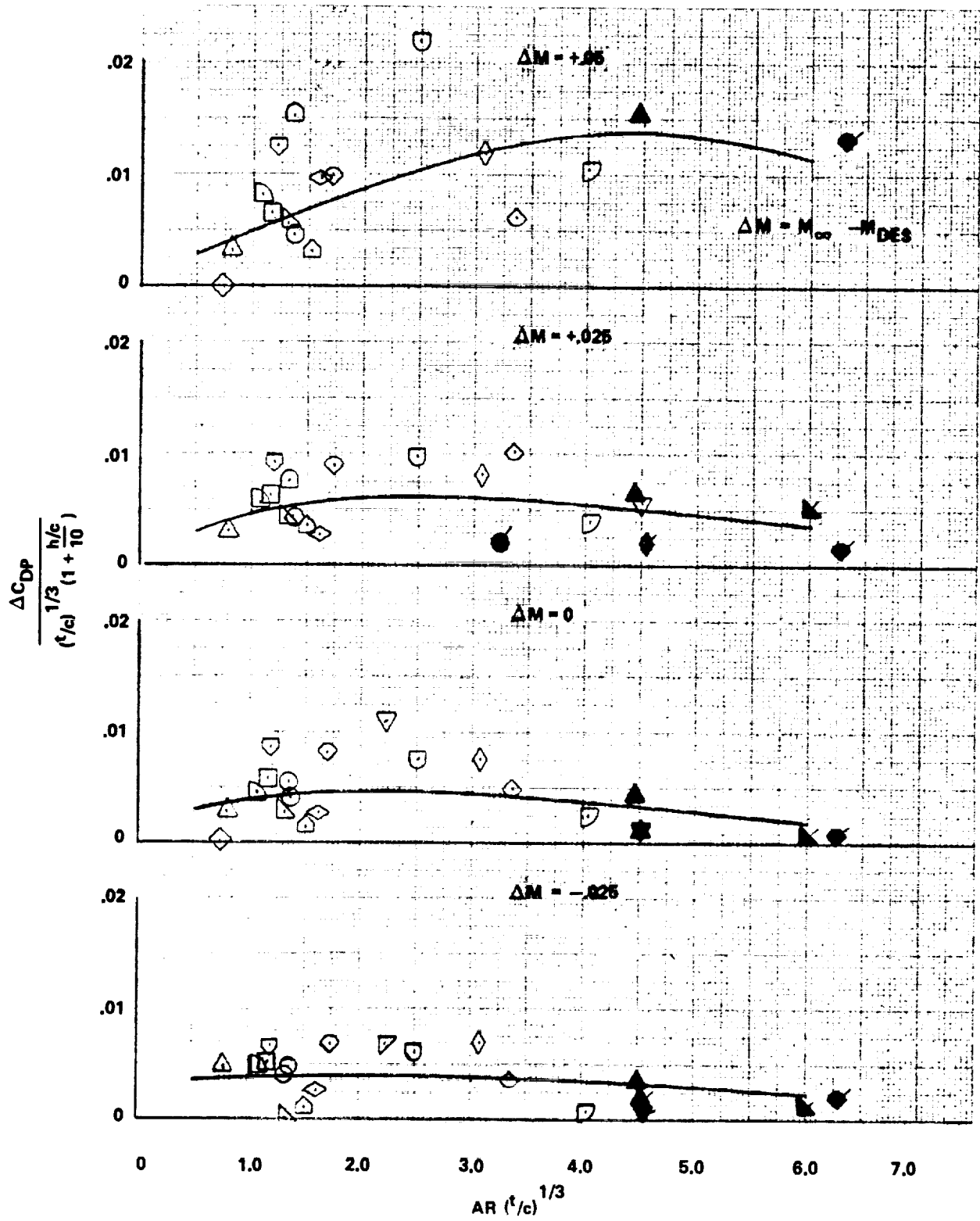Figure 42. - Concluded.
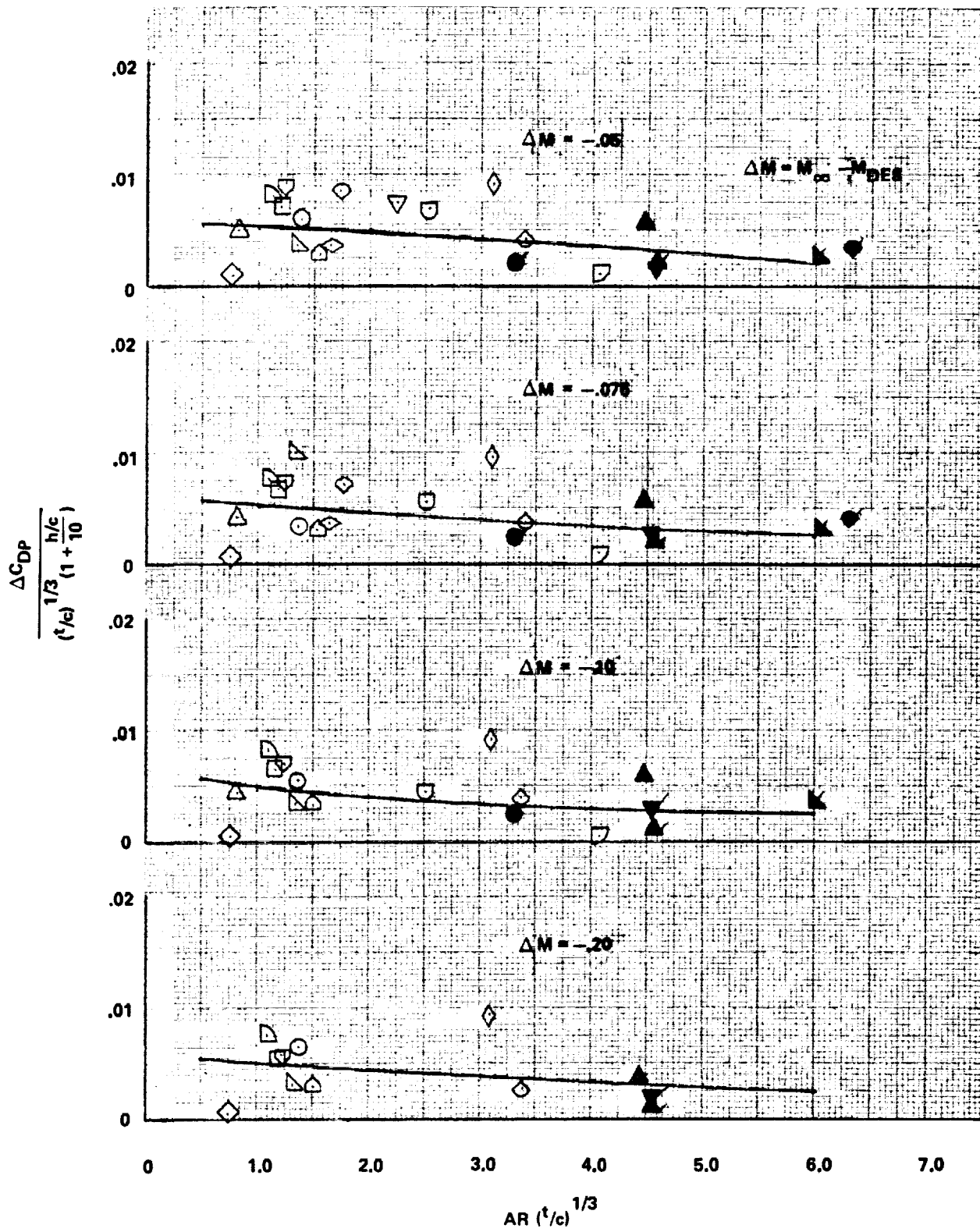
Figure 43. – Subsonic ΔC_{DP} correlation, $\Delta C_L = -0.05$.
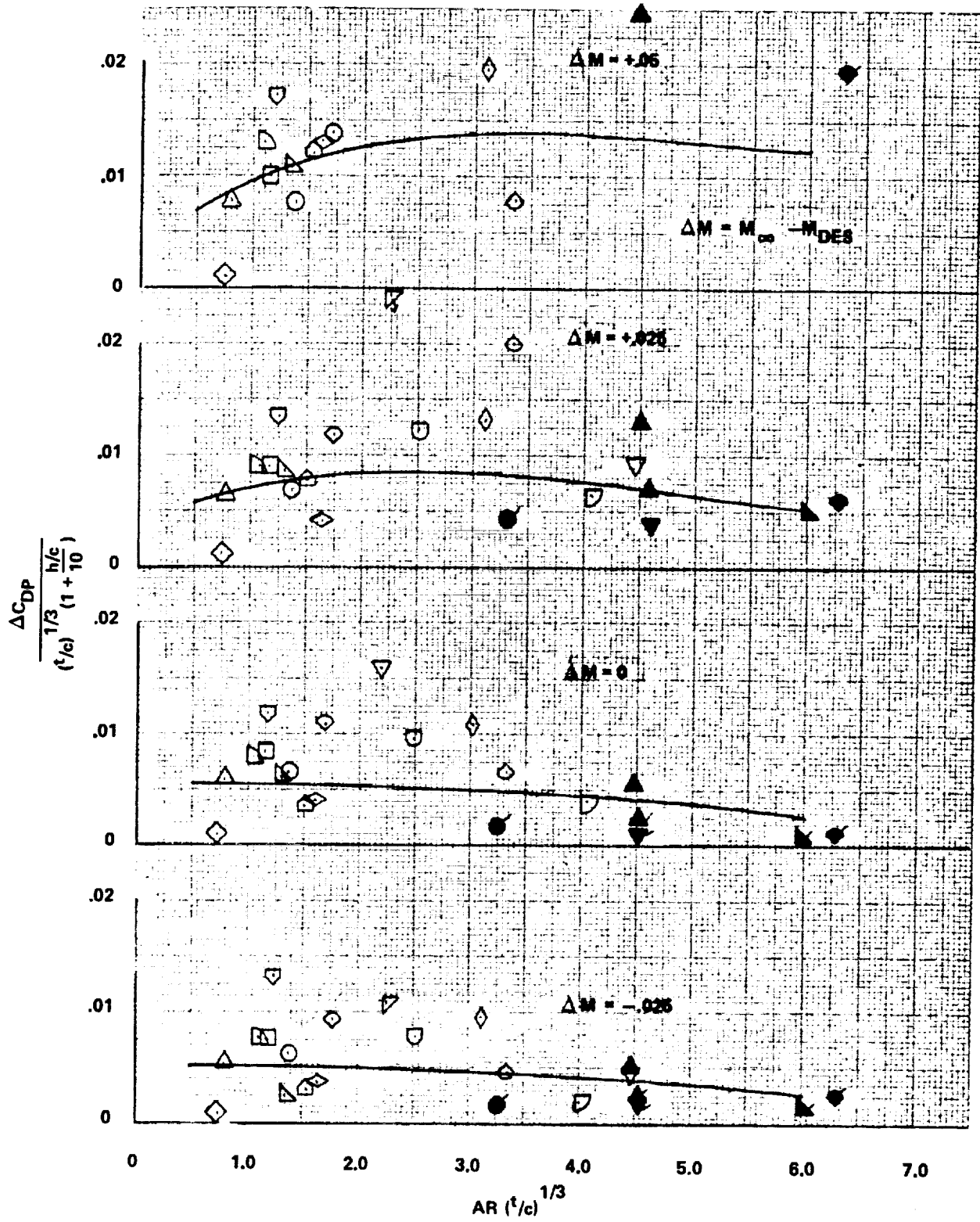
Figure 43. - Concluded.
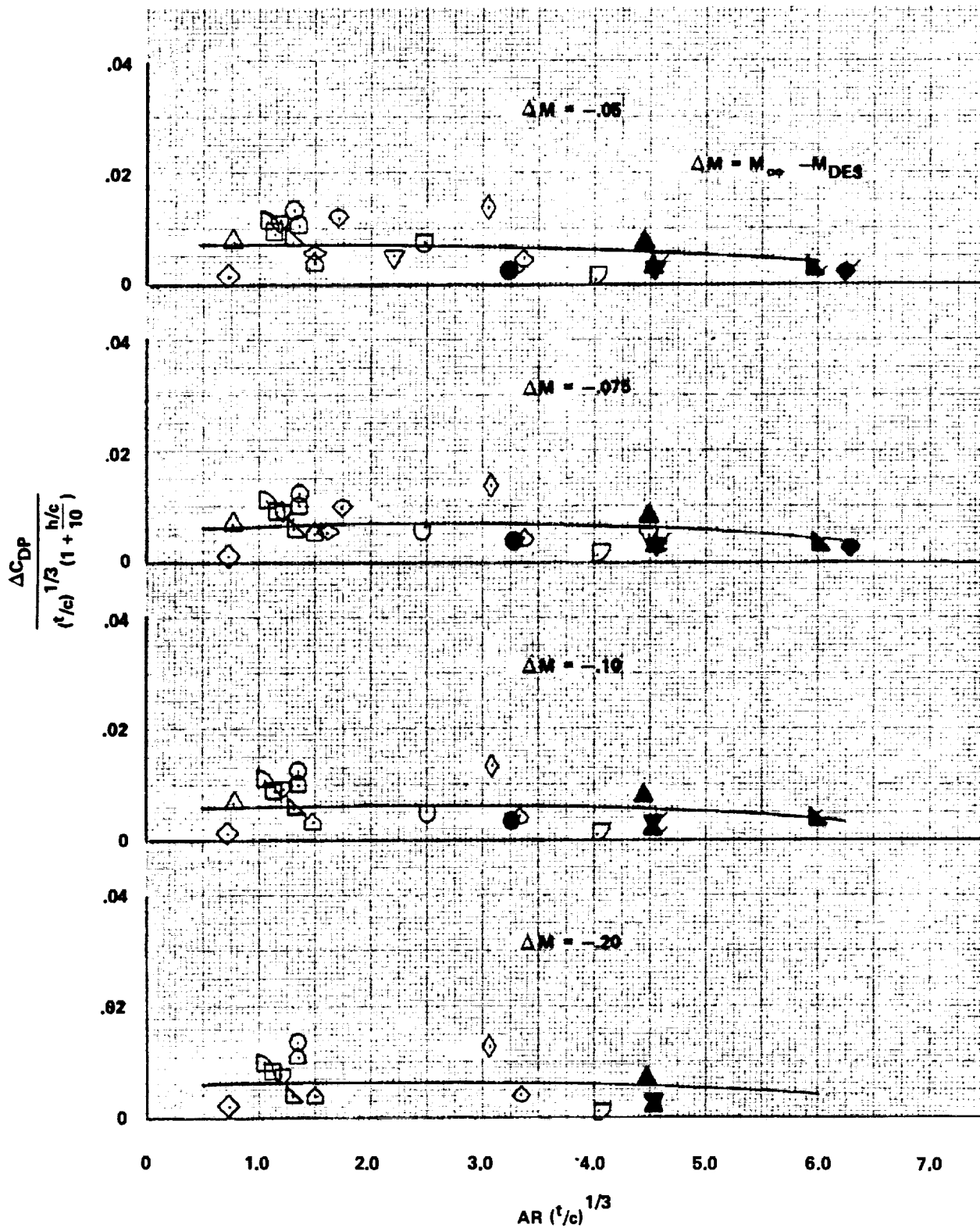
Figure 44. – Subsonic ΔC_{DP} correlation, $\Delta C_L = 0$.

$$\frac{\Delta C_{DP}}{(^t/c)^{1/3}(1+\frac{h/c}{10})}$$
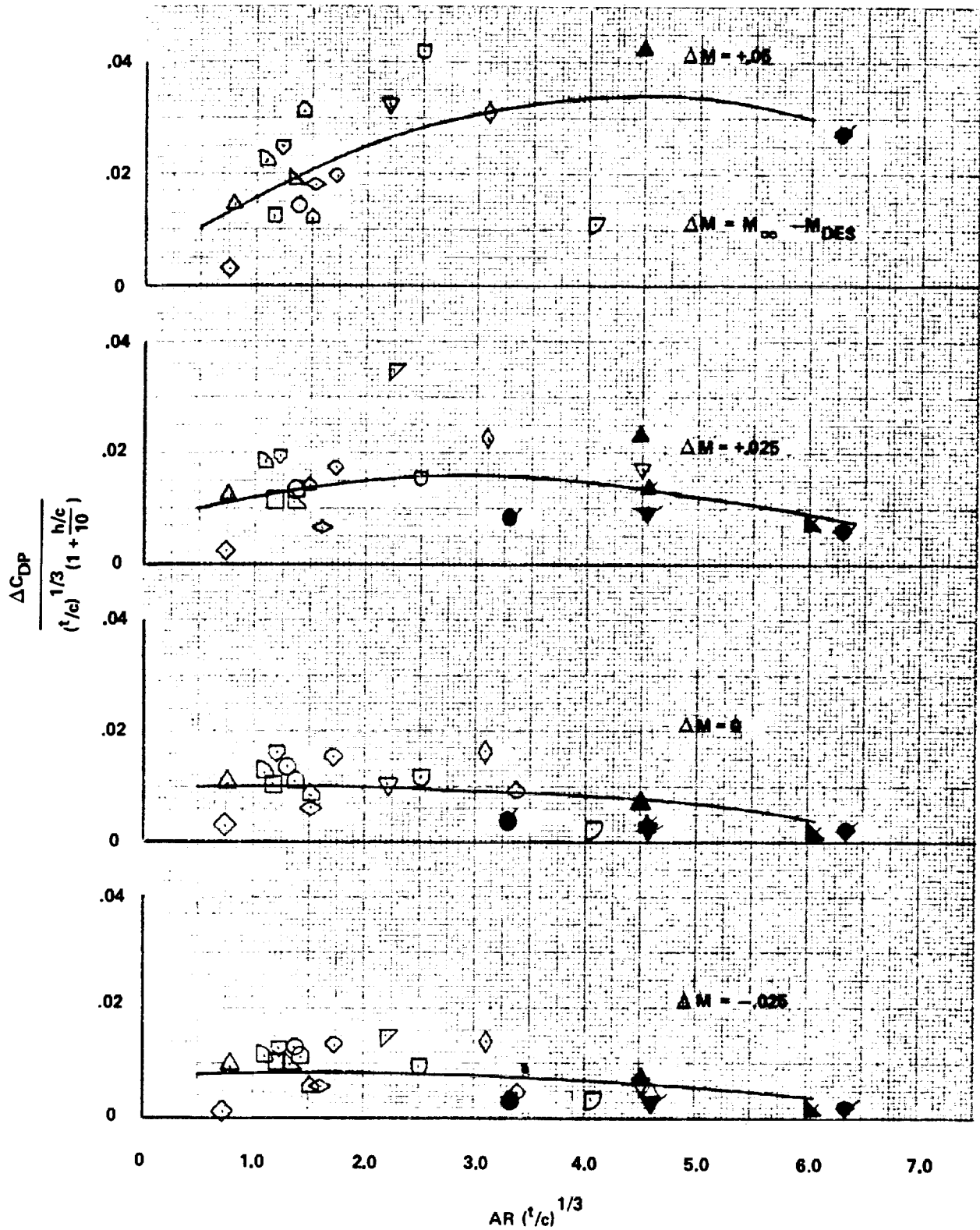
Figure 44. – Concluded.

Figure 45. – Subsonic ΔC_{DP} correlation, $\Delta C_L = +0.05$.

100

$$\frac{\Delta c_{DP}}{(t/c)^{1/3}(1 + \frac{h/c}{10})}$$

$AR \ (t/c)^{1/3}$
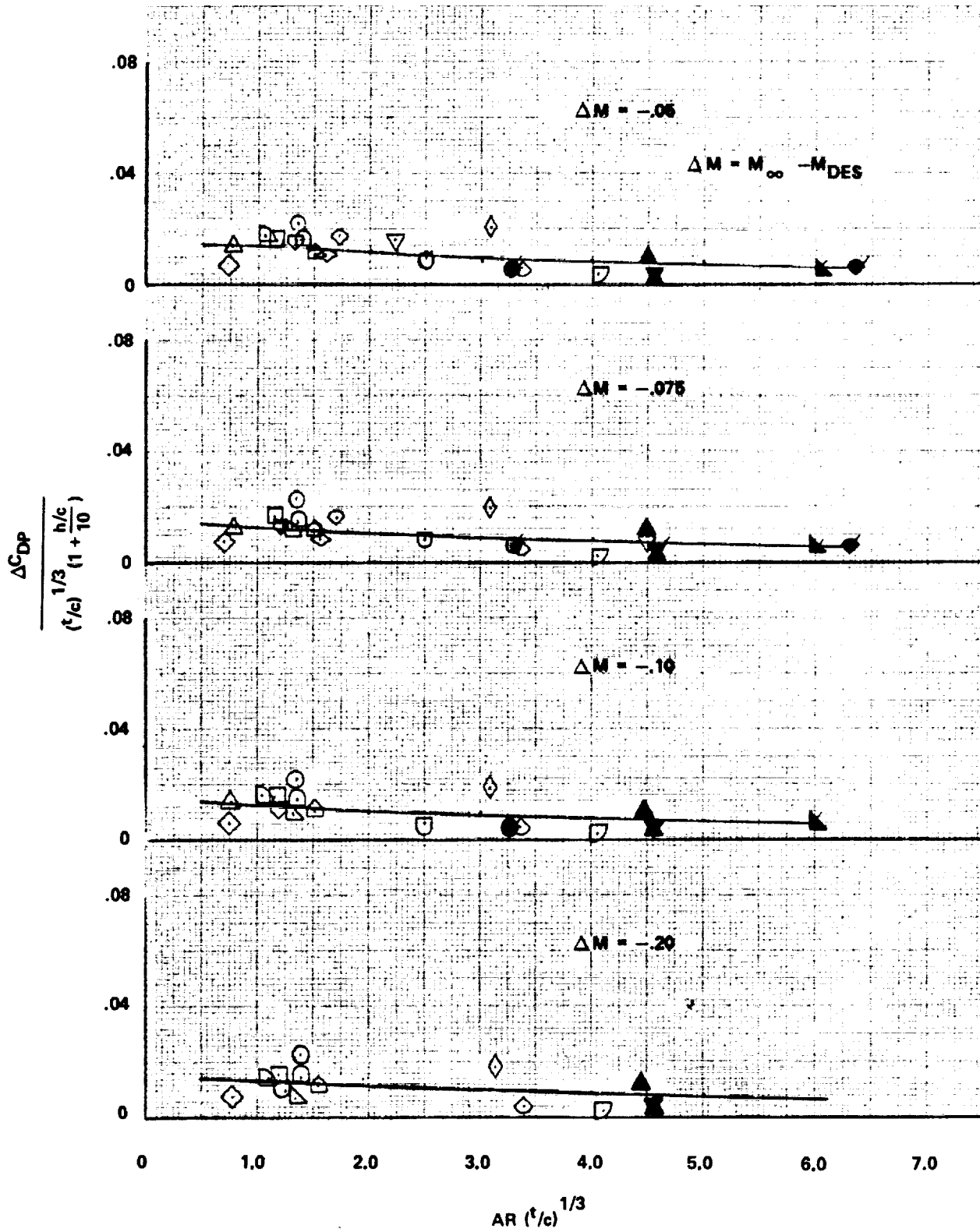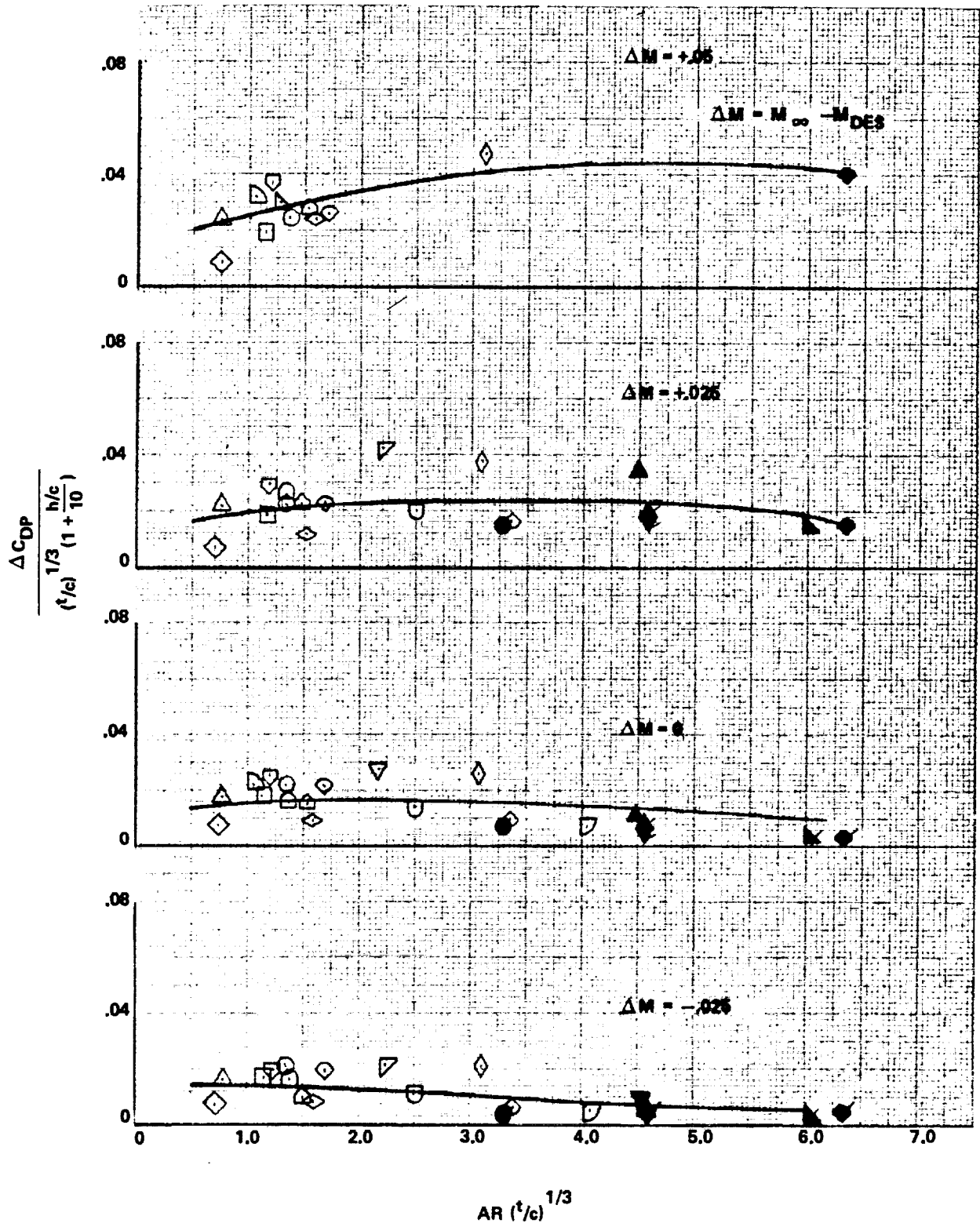
Figure 45. – Concluded.
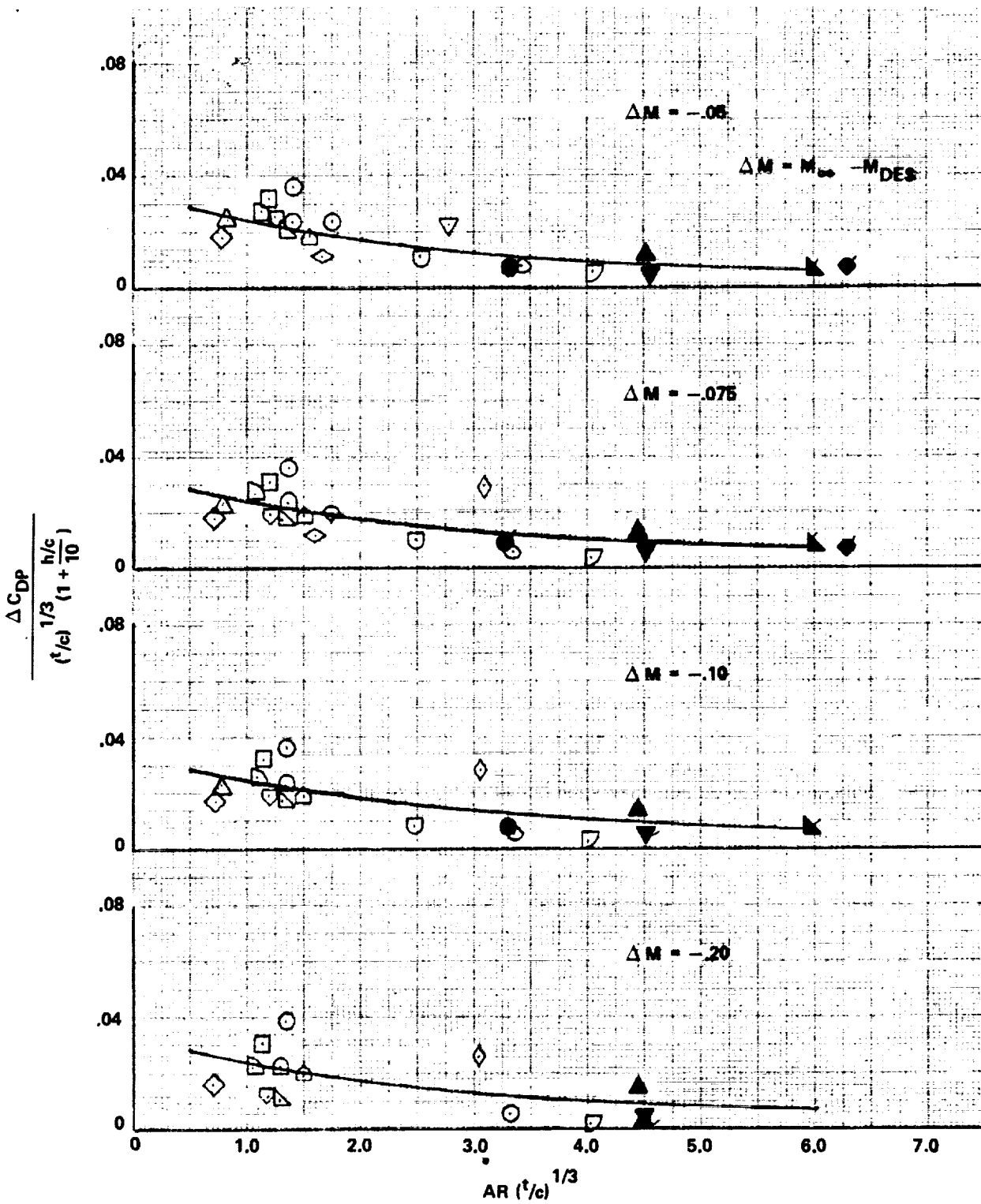
Figure 46. – Subsonic ΔC_{DP} correlation, $\Delta C_L = +0.10$.

102

$$\frac{\Delta c_{DP}}{(t/c)^{1/3}(1 + \frac{h/c}{10})}$$

AR $(t/c)^{1/3}$

Figure 46. – Concluded.
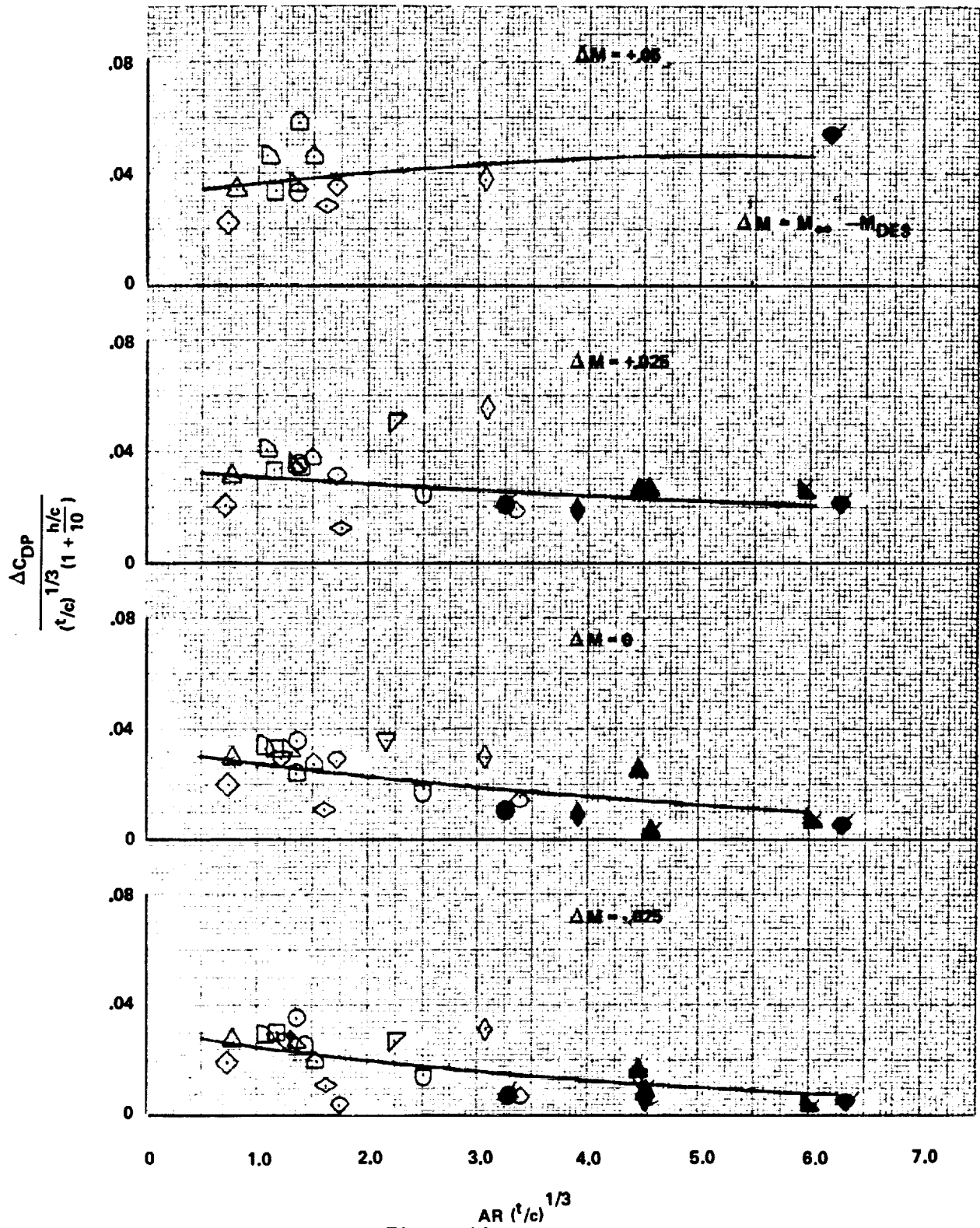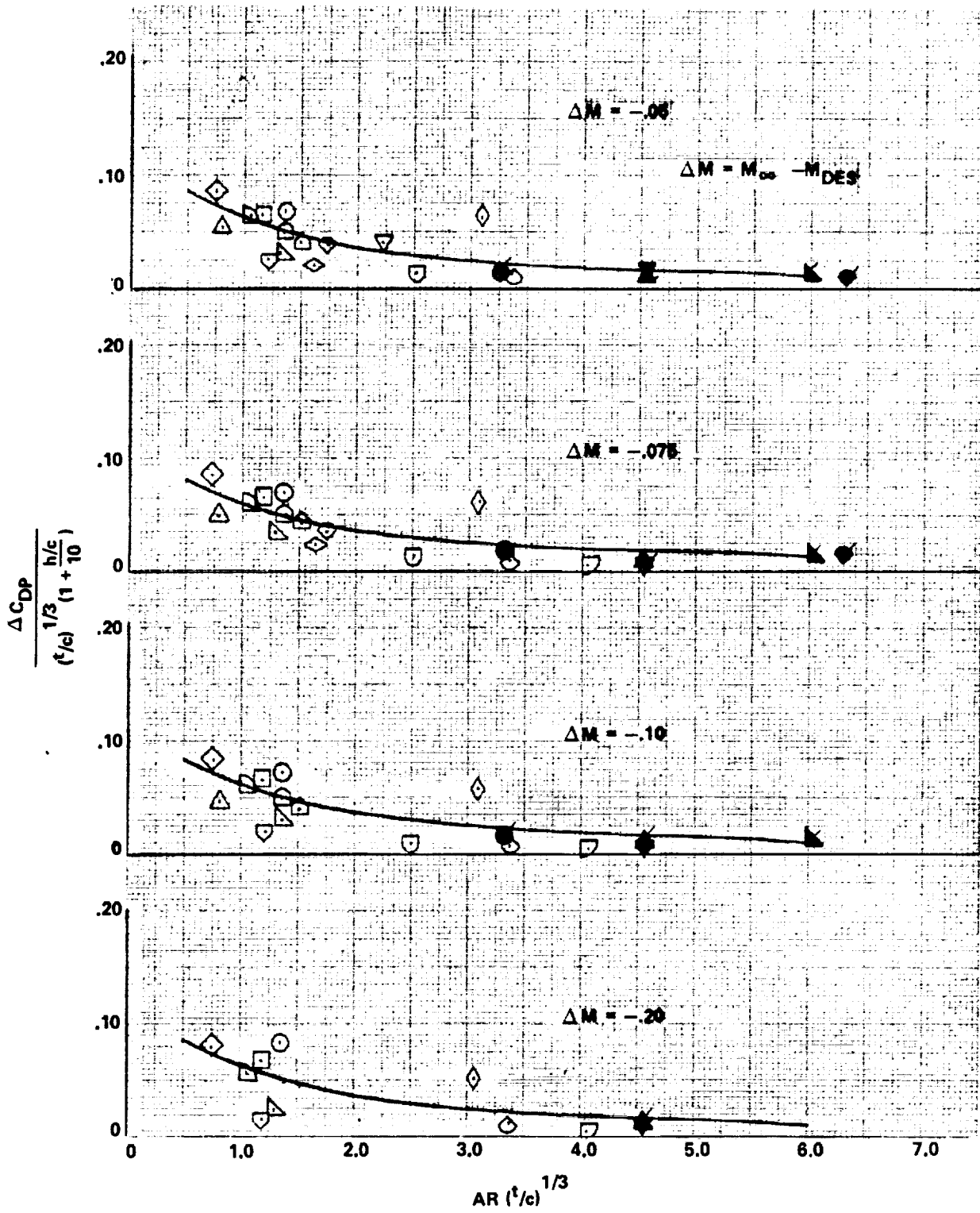
Figure 47. – Subsonic ΔC_{DP} correlation, $\Delta C_L = +0.20$.

104
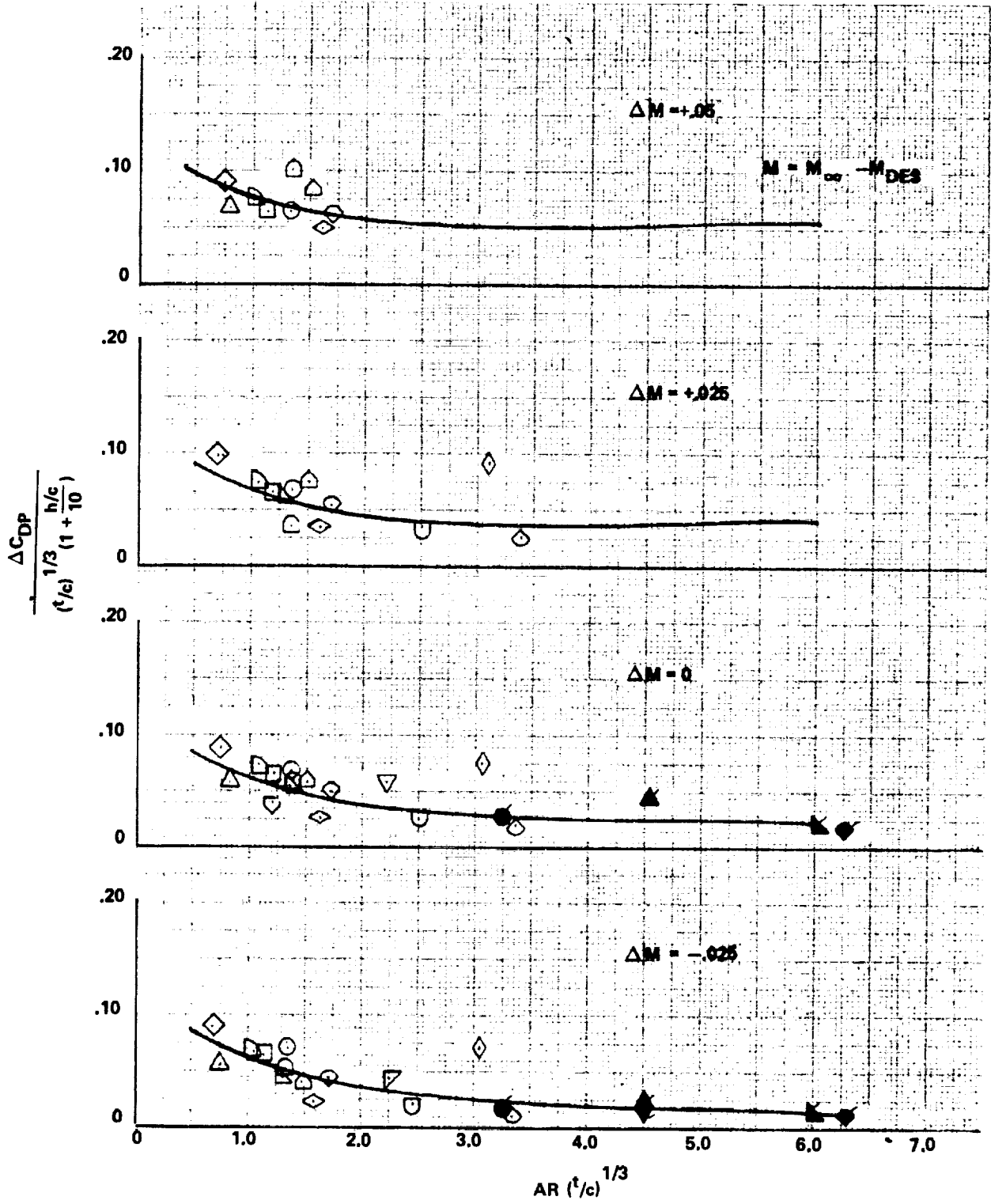
Figure 47. – Concluded.

Figure 48. – Subsonic ΔC_{DP} correlation, ΔC_L = +0.30.

106

$$\frac{\Delta c_{DP}}{(^t/c)^{1/3}(1 + \frac{h/c}{10})}$$

$\Delta M = +.05$

$\Delta M = M_{\infty} - M_{DES}$

$\Delta M = +.025$

$\Delta M = 0$

$\Delta M = -.025$

$AR \left(^t/c\right)^{1/3}$
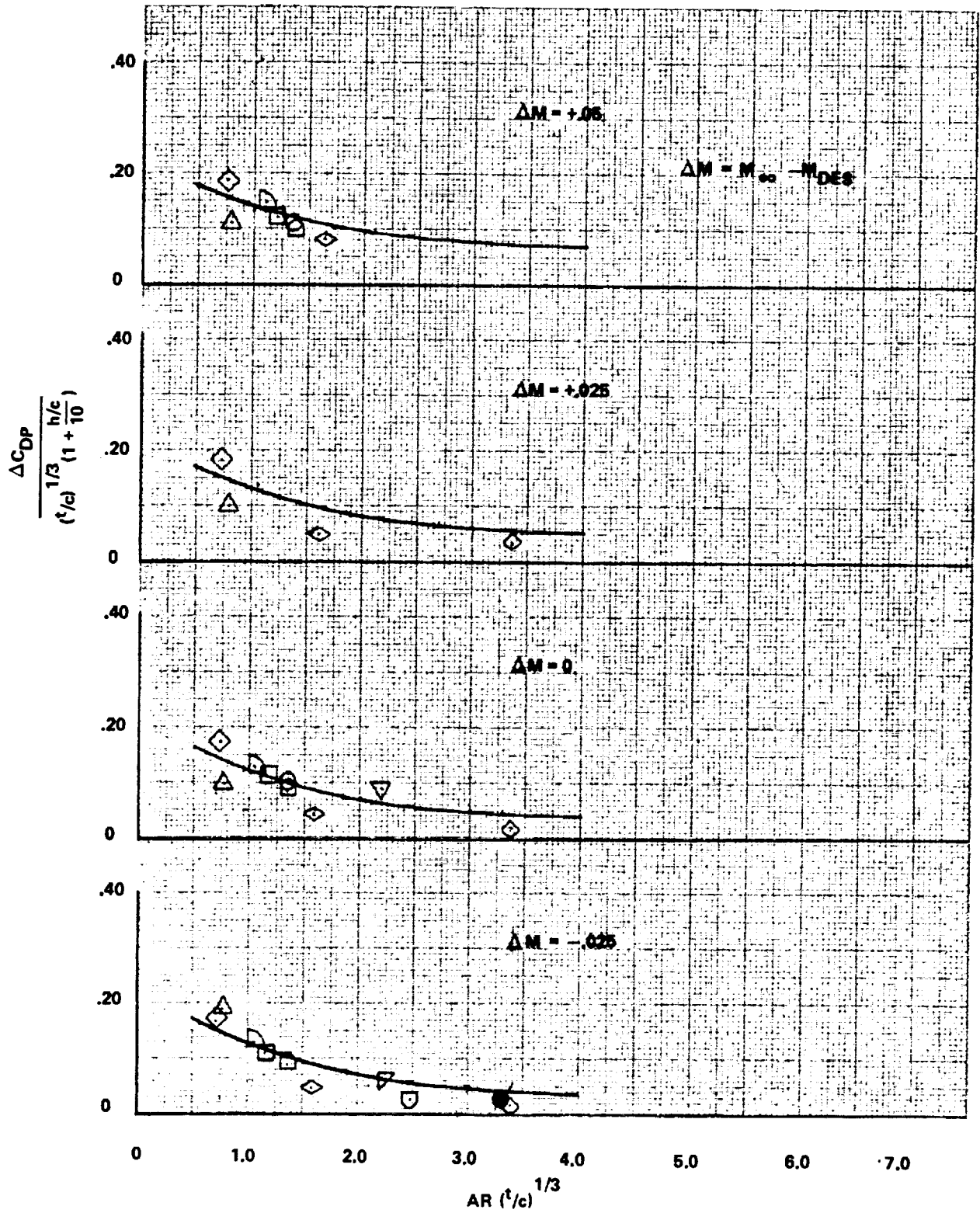
Figure 48. – Concluded.

Figure 49. — Supersonic wing pressure drag correlation, $\Delta C_L = -0.30$.

Figure 49. - continued.

109

$$\Delta M = M_\infty - M_{DES}$$

$$\Delta M = +1.20$$

$$\Delta M = +1.10$$

$$\frac{\Delta C_{DP}}{(t/c)^{1/3}\left(1 + \frac{h/c}{10}\right)}$$

.004

.002

0

.004

.002

0

.8   1.2   1.6   2.0   2.4   2.8   3.2   3.6

$$AR\,(t/c)^{1/3}$$
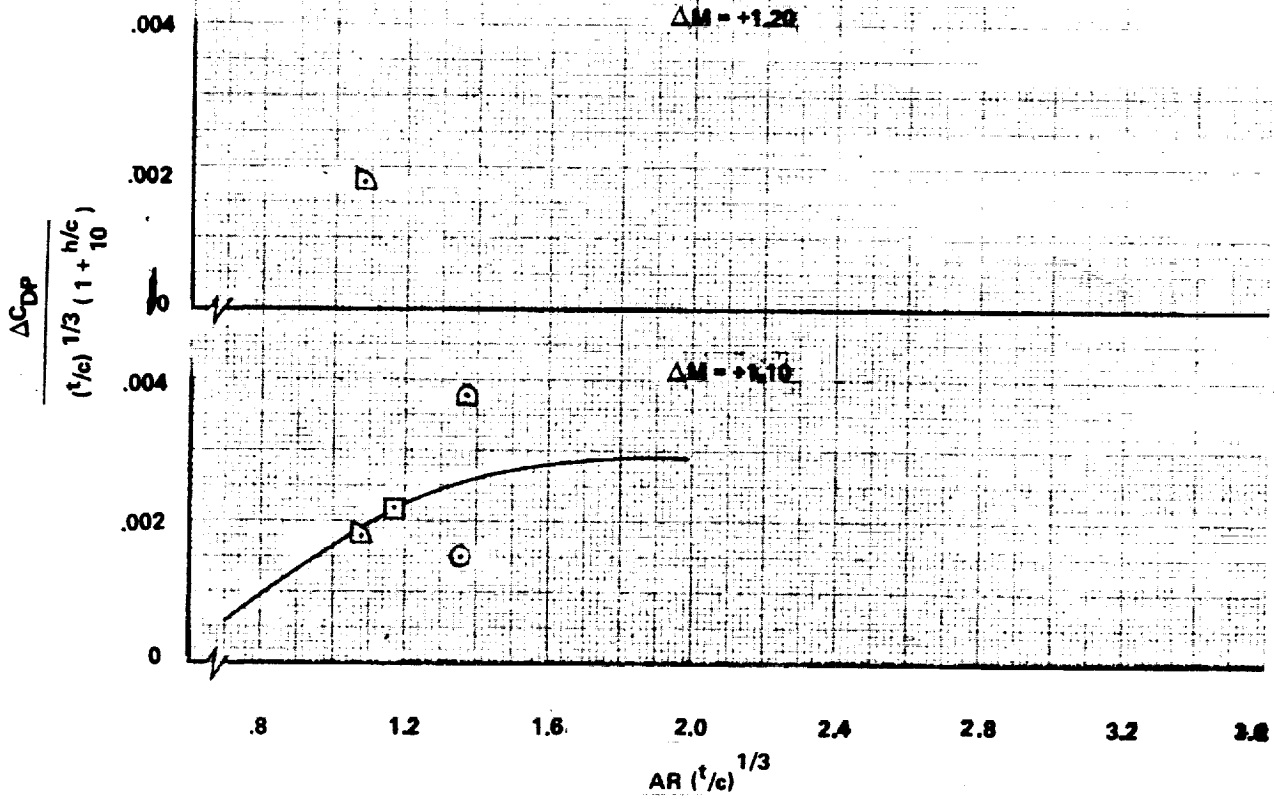
Figure 49. – Concluded.

110

Figure 50. – Supersonic wing pressure drag correlation, $\Delta C_L = -0.20$.

$$\frac{\Delta c_{D_P}}{(t/c)^{1/3}(1+\frac{h/c}{10})}$$

$\Delta M = +1.08$

$\Delta M = M_\infty - M_{DES}$

$\Delta M = +.80$

$\Delta M = +.60$

$\Delta M = +.40$

$AR \left(\frac{t}{c}\right)^{1/3}$

Figure 50. – Continued.

112

Figure 50. – Concluded.

Figure 51. – Supersonic wing pressure drag correlation, $\Delta C_L = -0.10$.

Figure 51. - Continued.

115

$$\Delta M = M_{\delta \alpha} - M_{DES}$$

$$\Delta M = +1.20$$

$$\Delta M = +1.10$$

$$AR \left(\frac{t}{c}\right)^{1/3}$$

Figure 51. – Concluded.

116
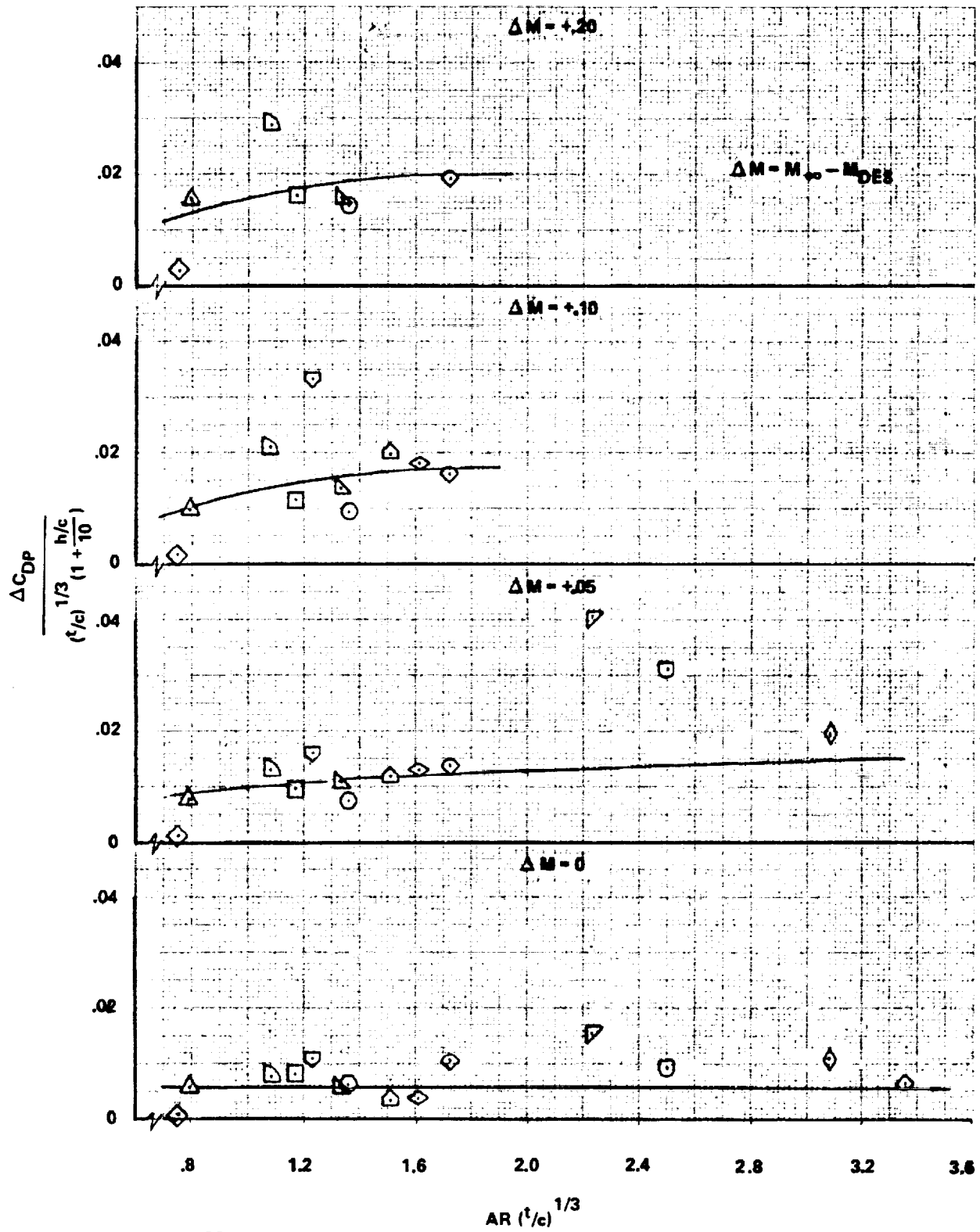
Figure 52. — Supersonic wing pressure drag correlation, $\Delta C_L = -0.05$.
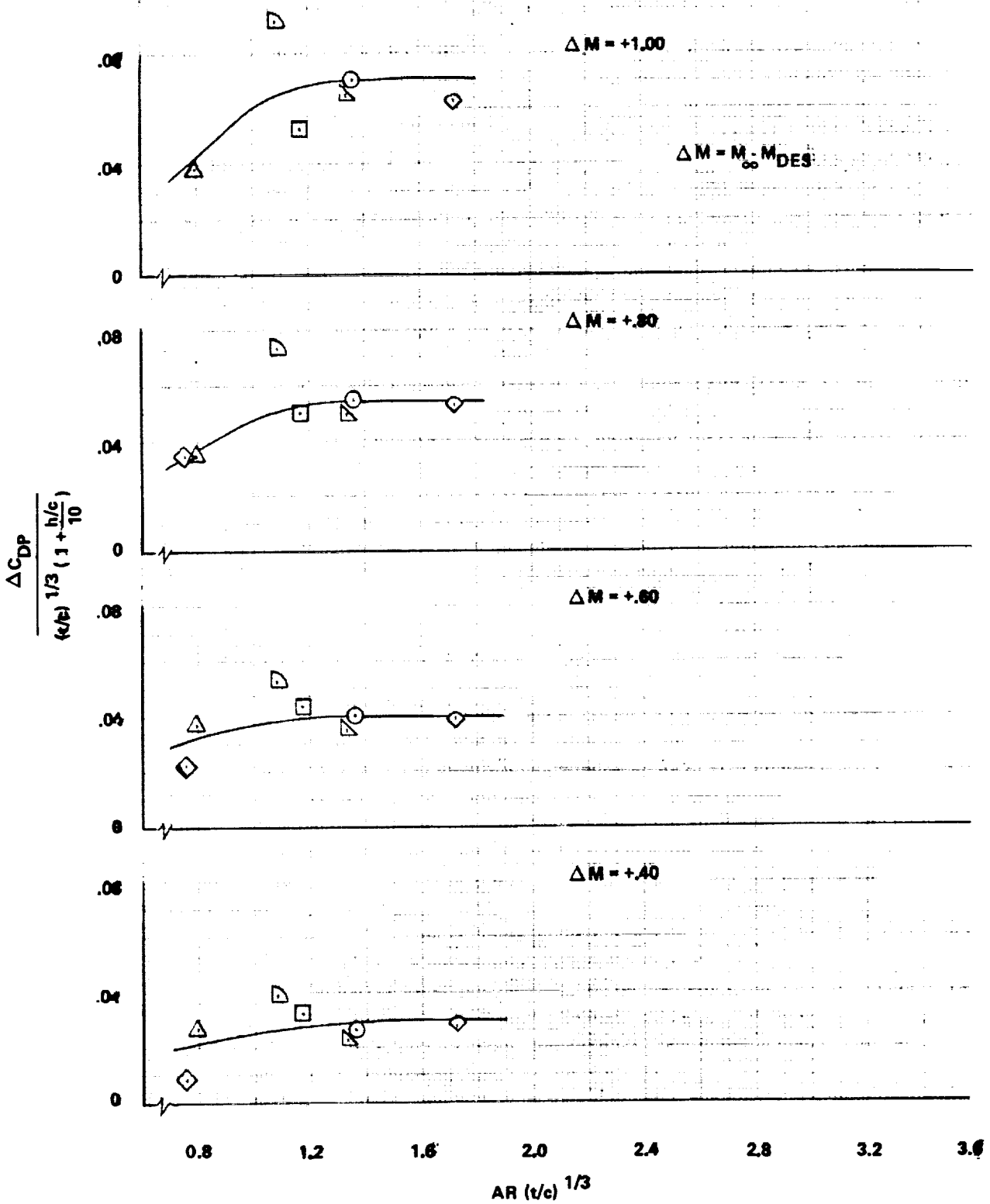
Figure 52. - Continued.
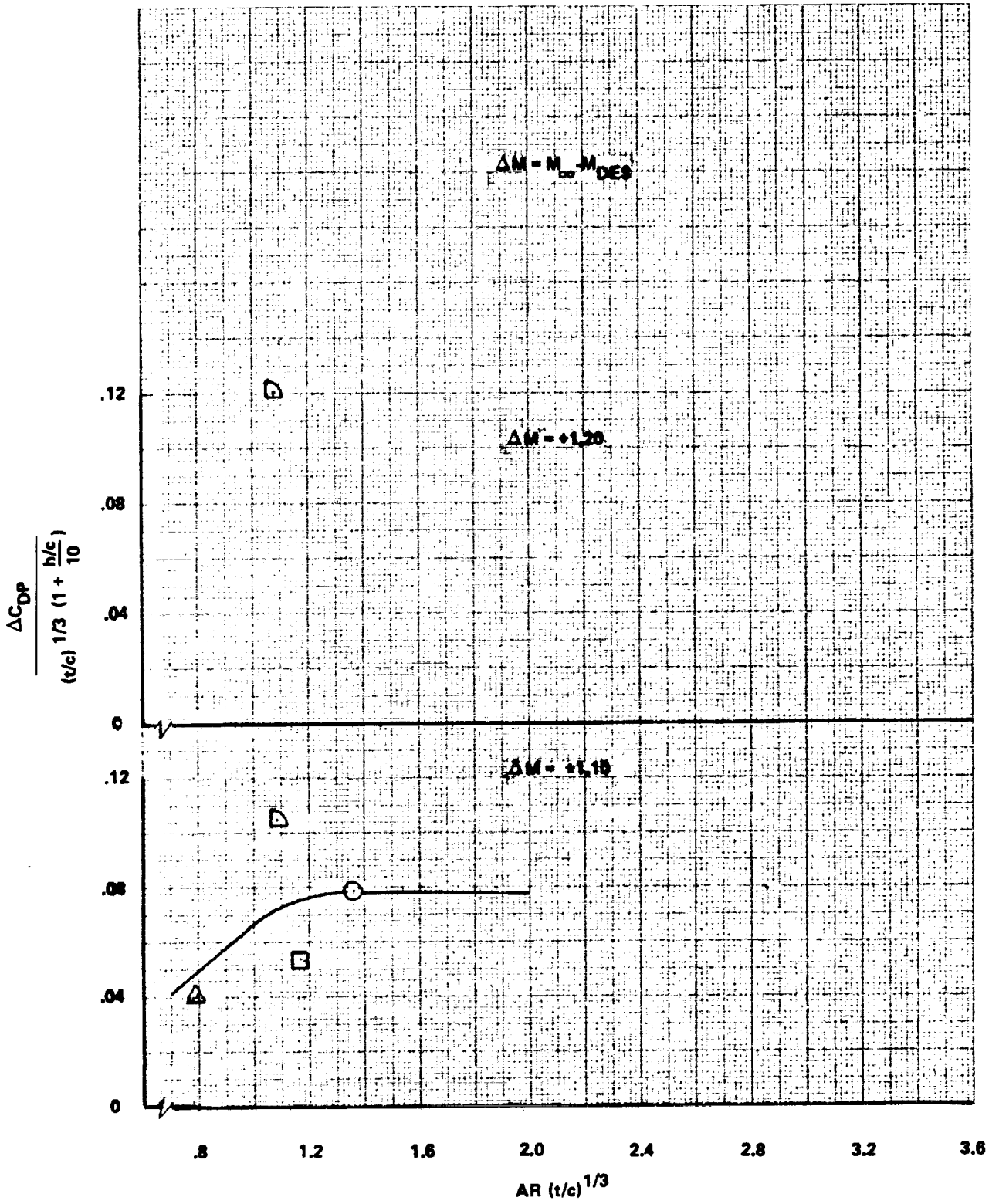
Figure 52. — Concluded.
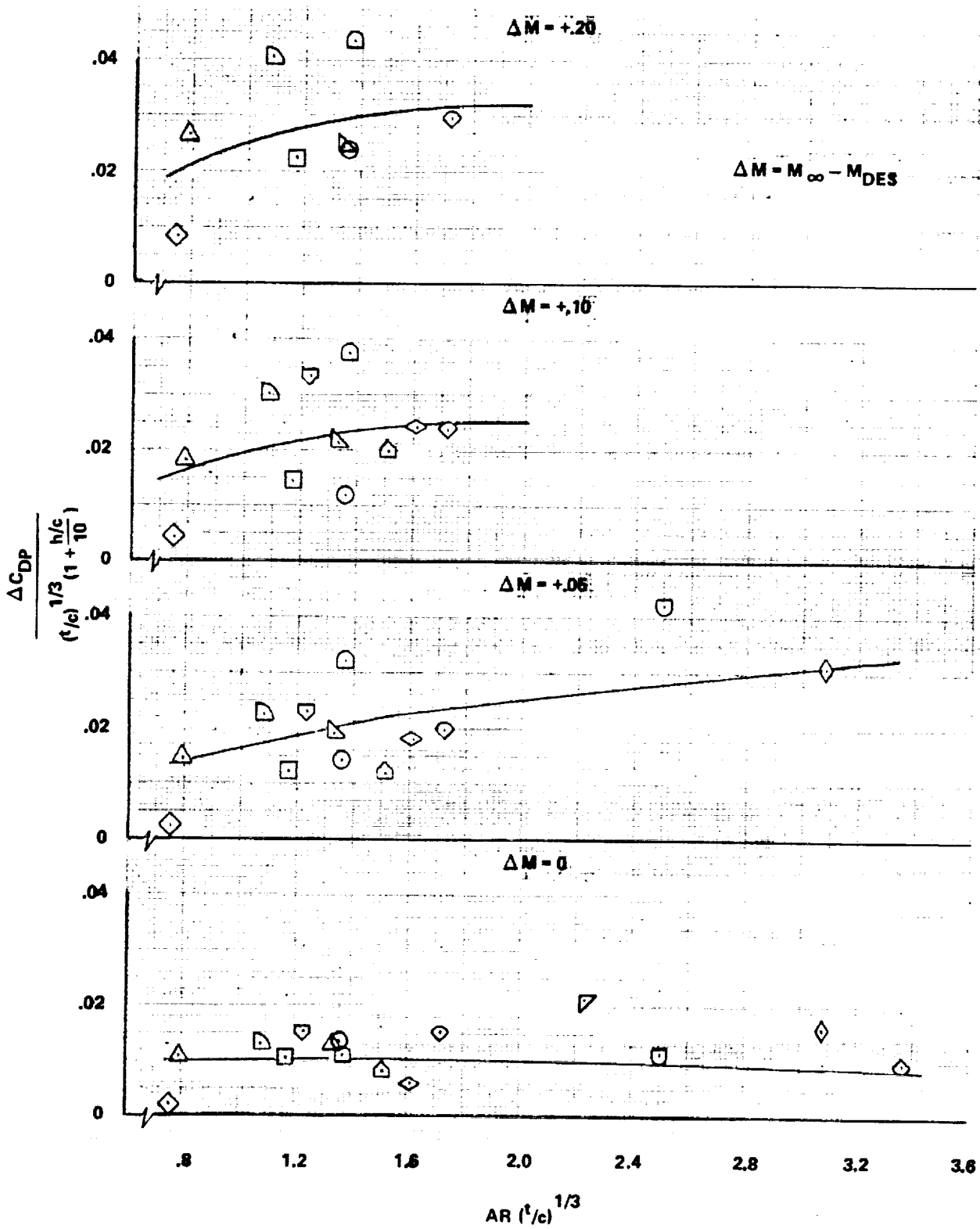
Figure 53. – Supersonic wing pressure drag correlation, $\Delta C_L = 0$.

Figure 53. - Continued.

$$\Delta M = M_\infty - M_{DES}$$

$$\Delta M = +1.2$$

$$\Delta M = +1.1$$

$$\frac{\Delta c_{DP}}{(^t/c)^{1/3}(1+\frac{h/c}{10})}$$

AR $(^t/c)^{1/3}$
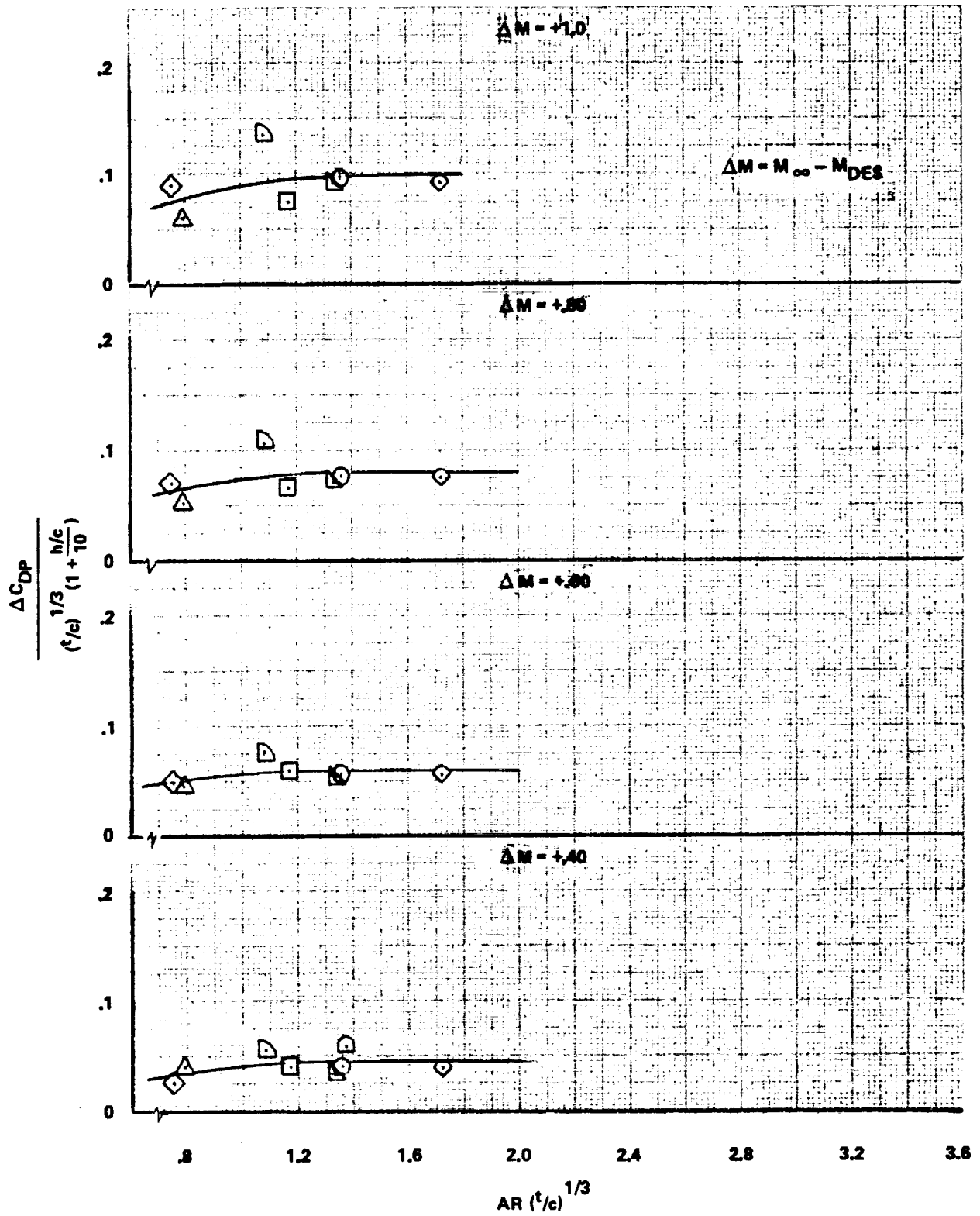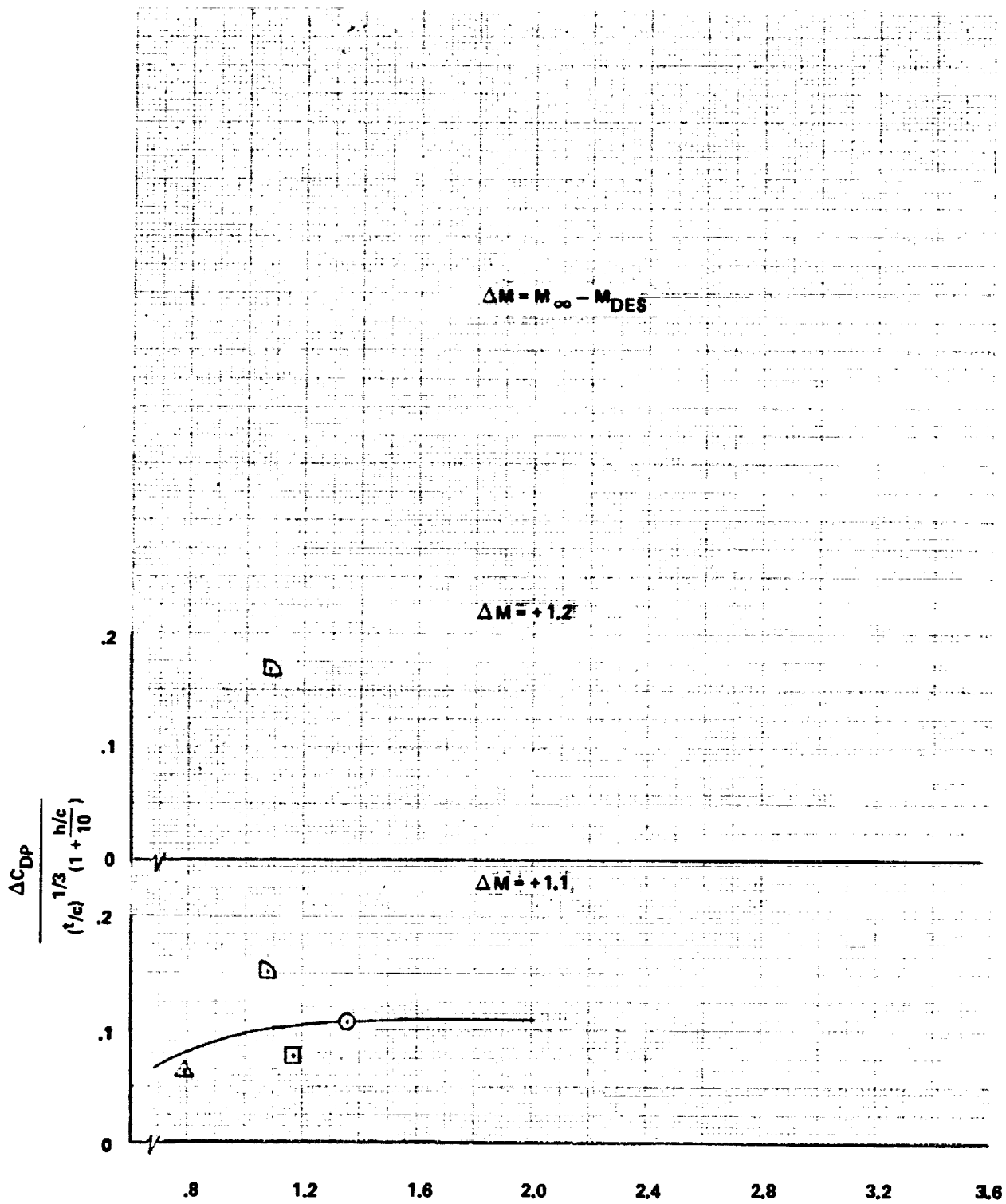
Figure 53. – Concluded.

122
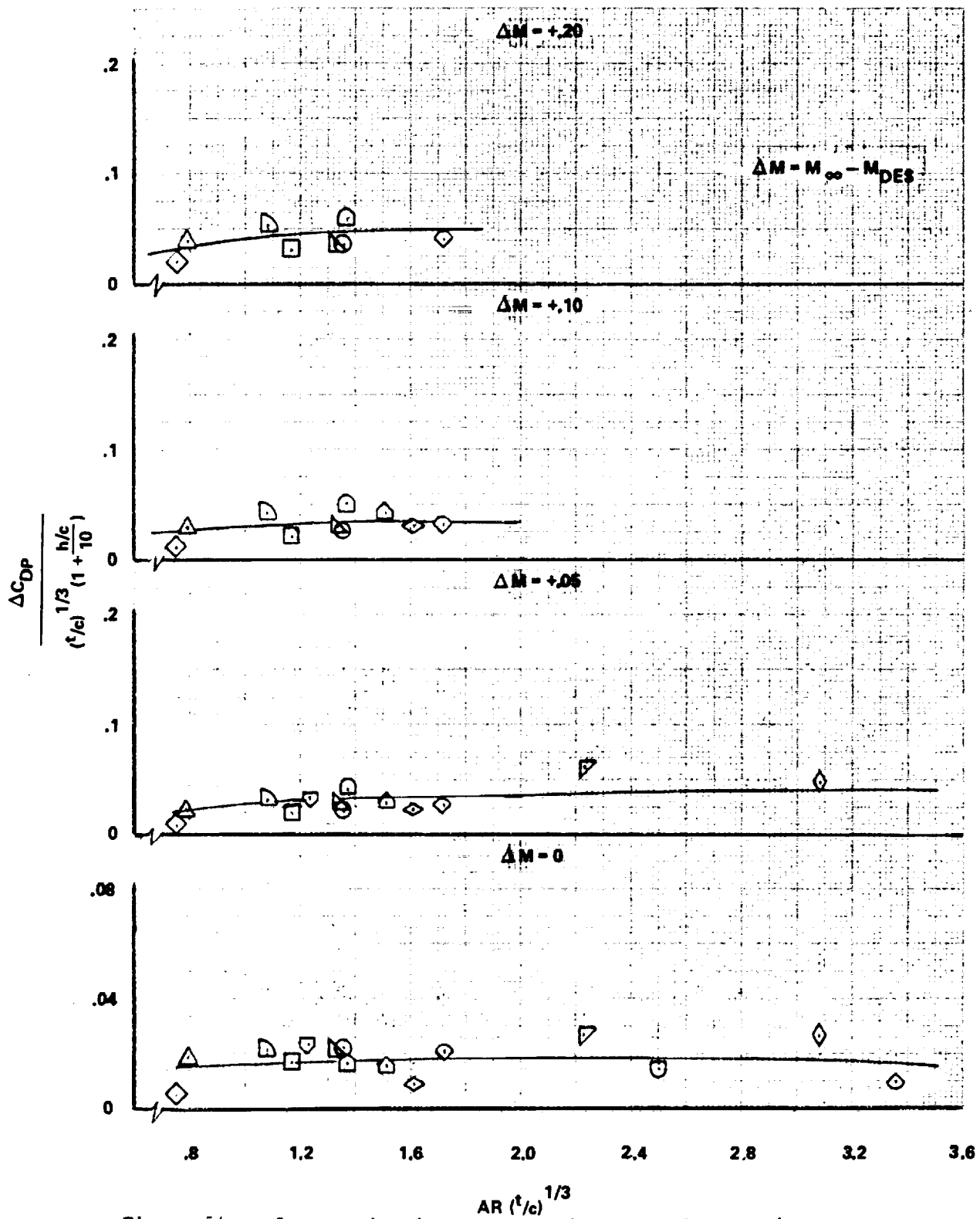
Figure 54. – Supersonic wing pressure drag correlation, $\Delta C_L = +0.05$.

123
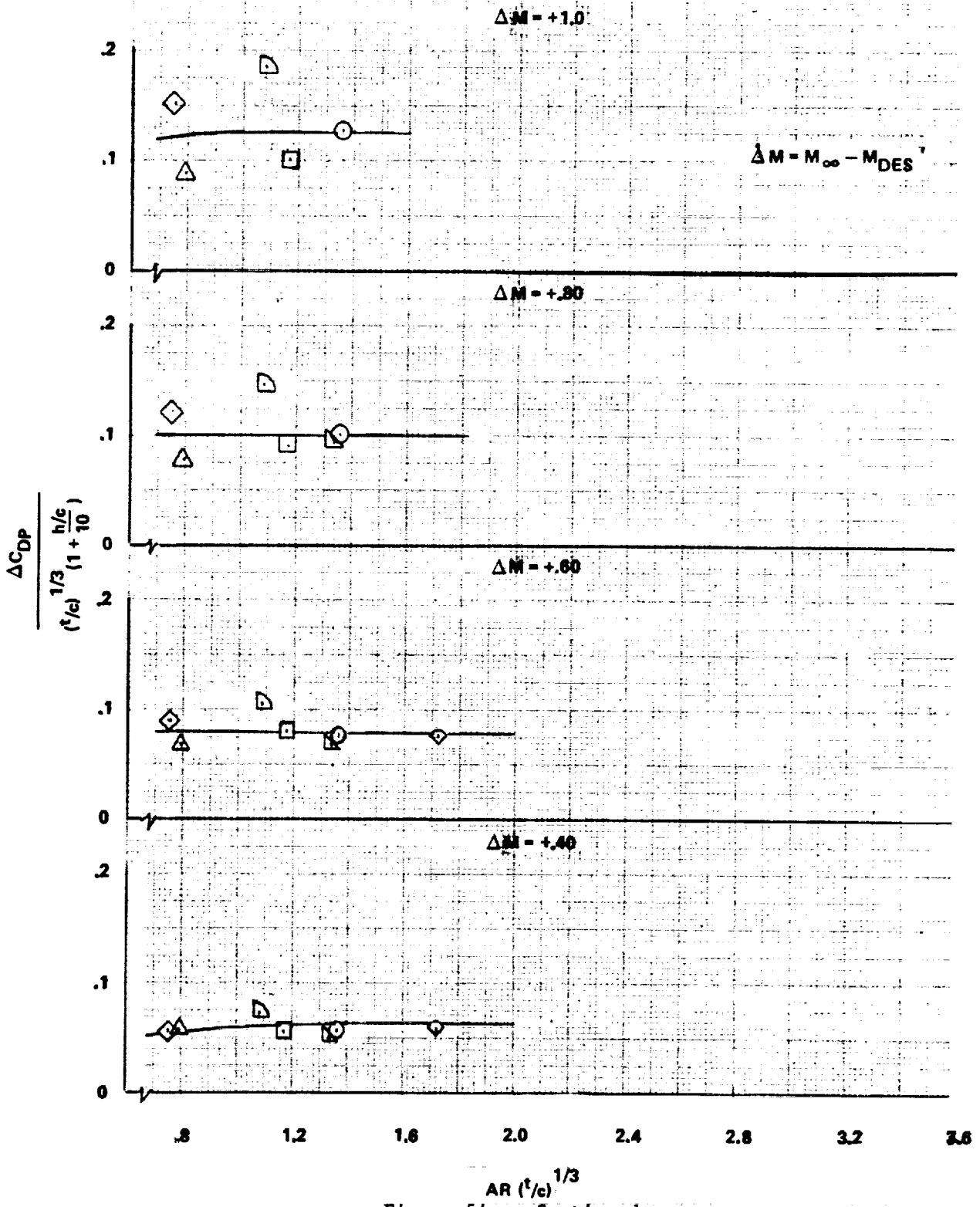
Figure 54. — Continued.

124
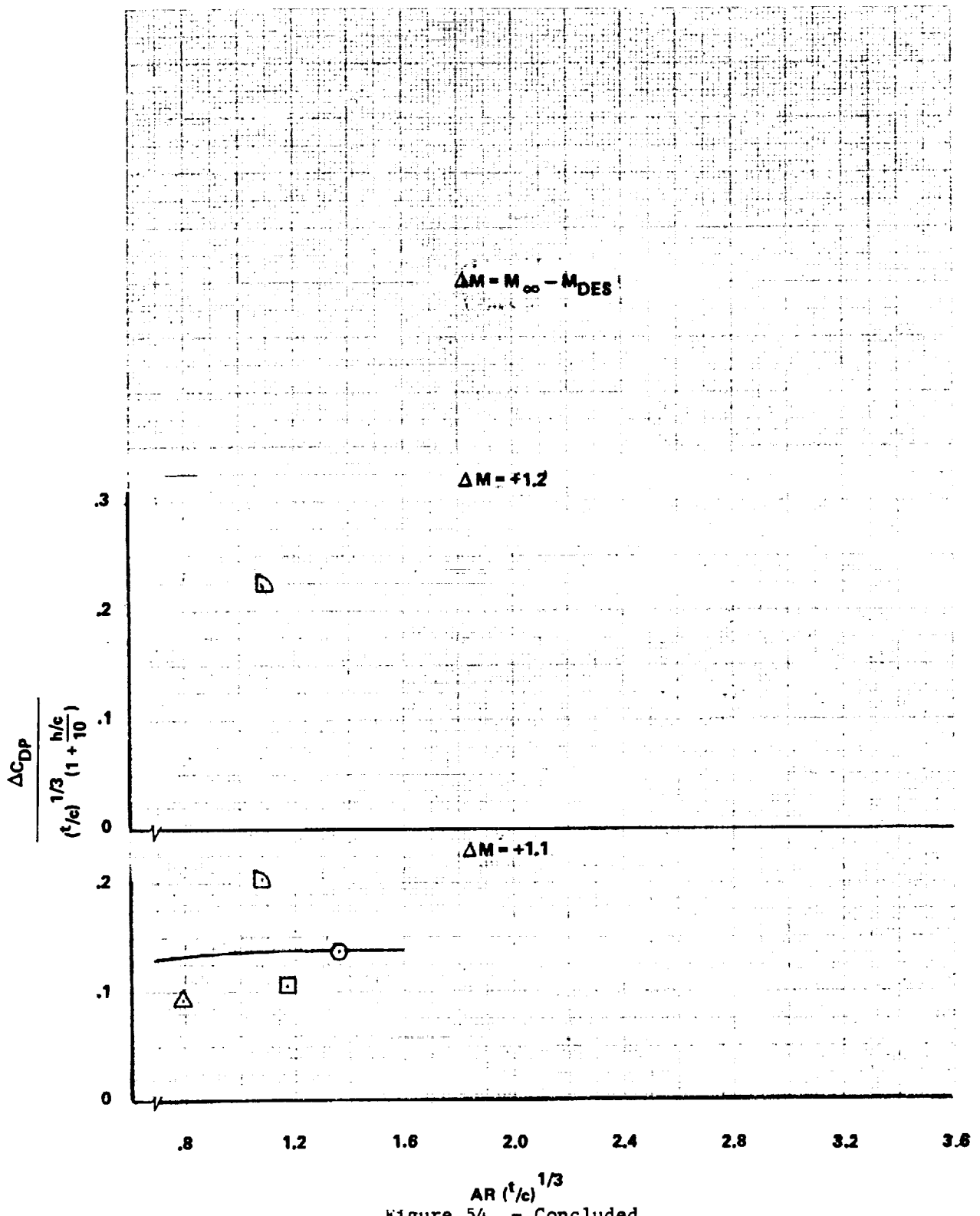
Figure 54. – Concluded.
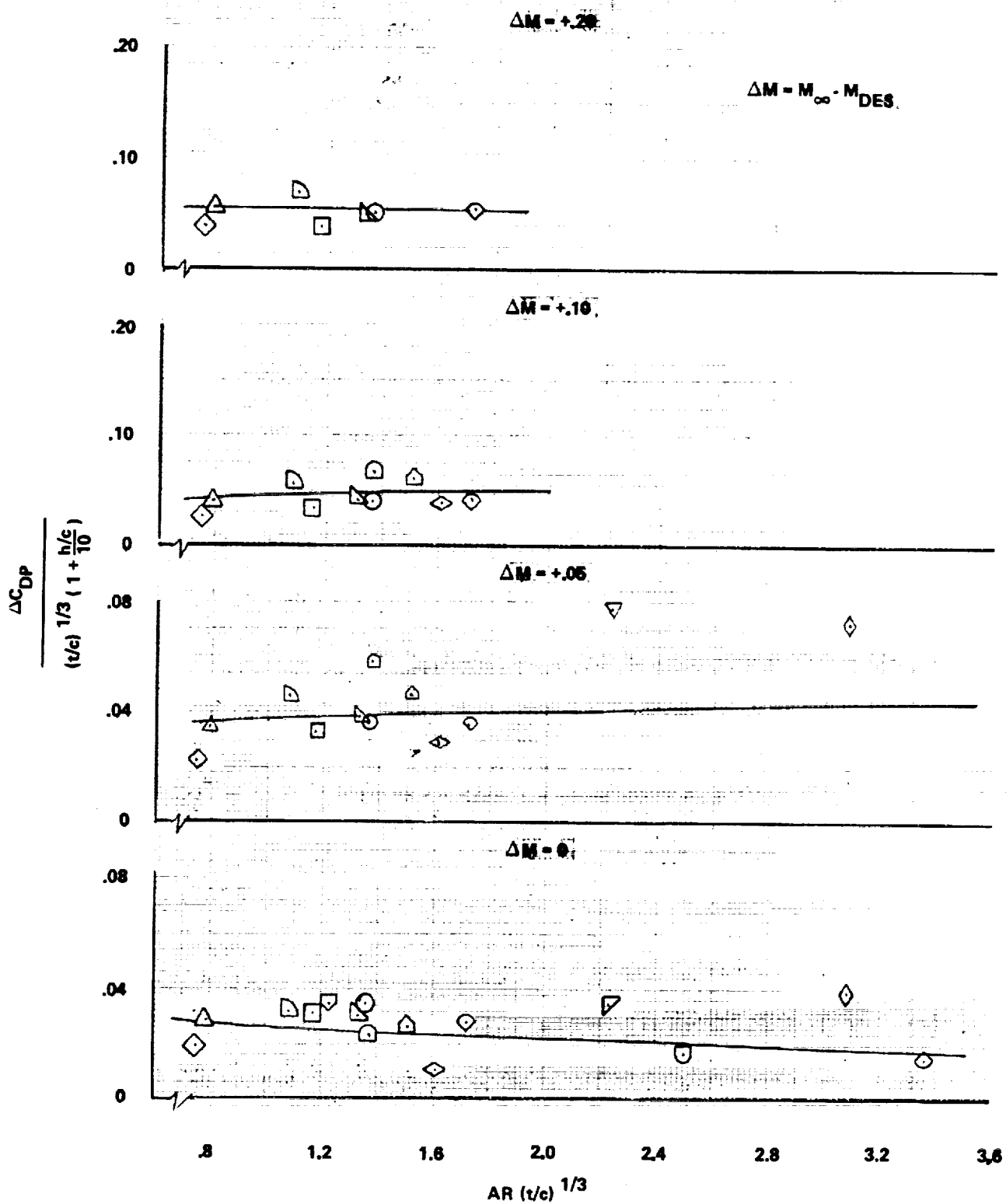
Figure 55. – Supersonic wing pressure drag correlation, $\Delta C_L = +0.10$.

126
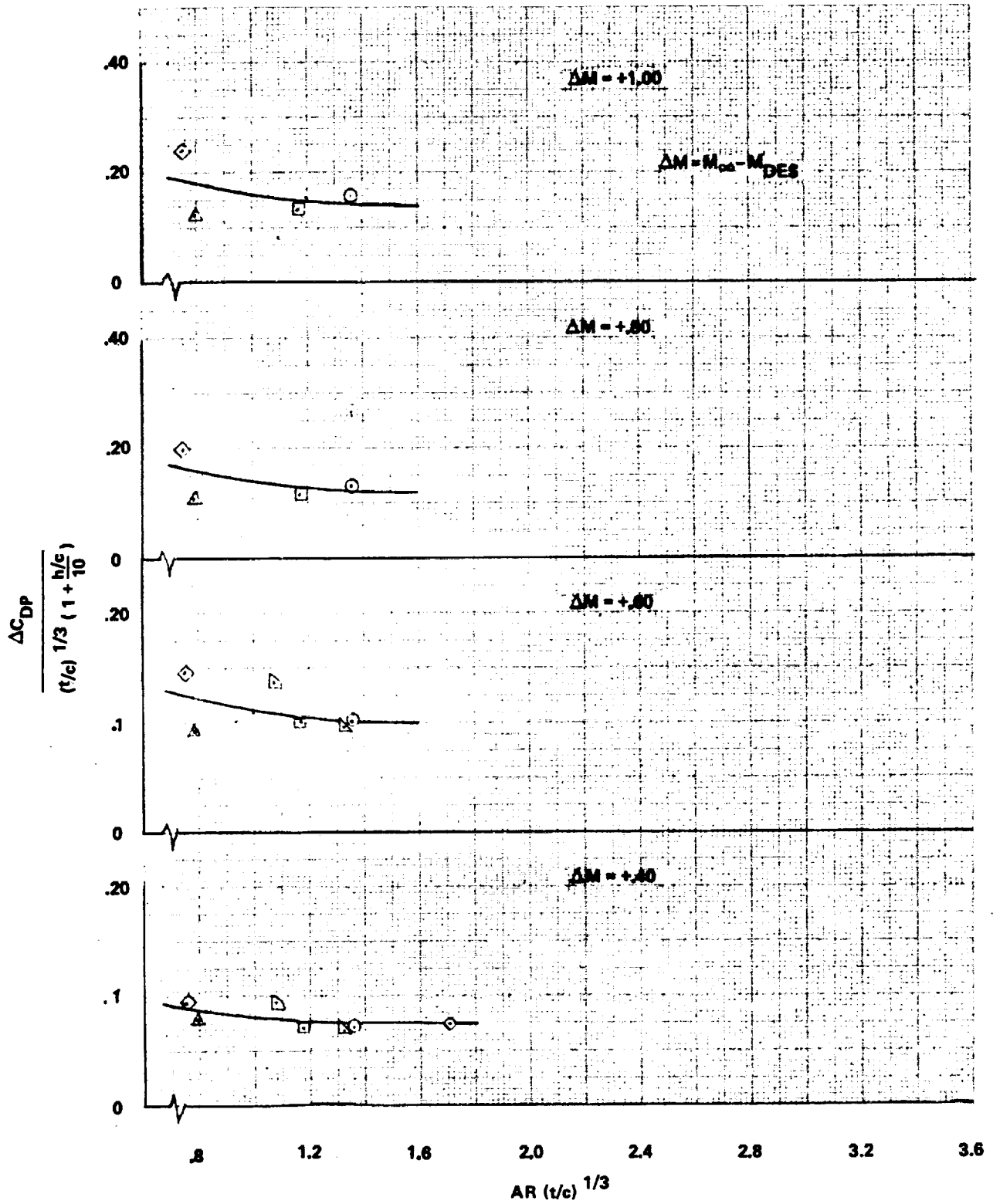
Figure 55. – Continued.

127

$$\Delta M = M_\infty - M_{DES}$$

$$\Delta M = +1.10$$
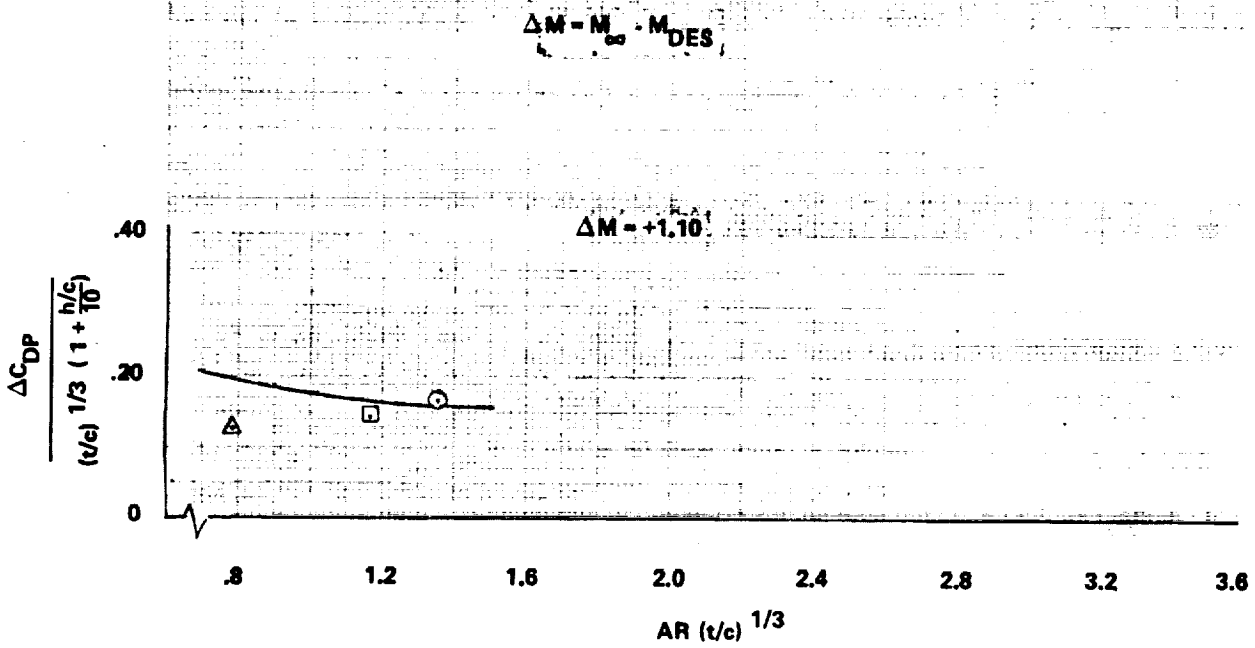
Figure 55. — Concluded.

128
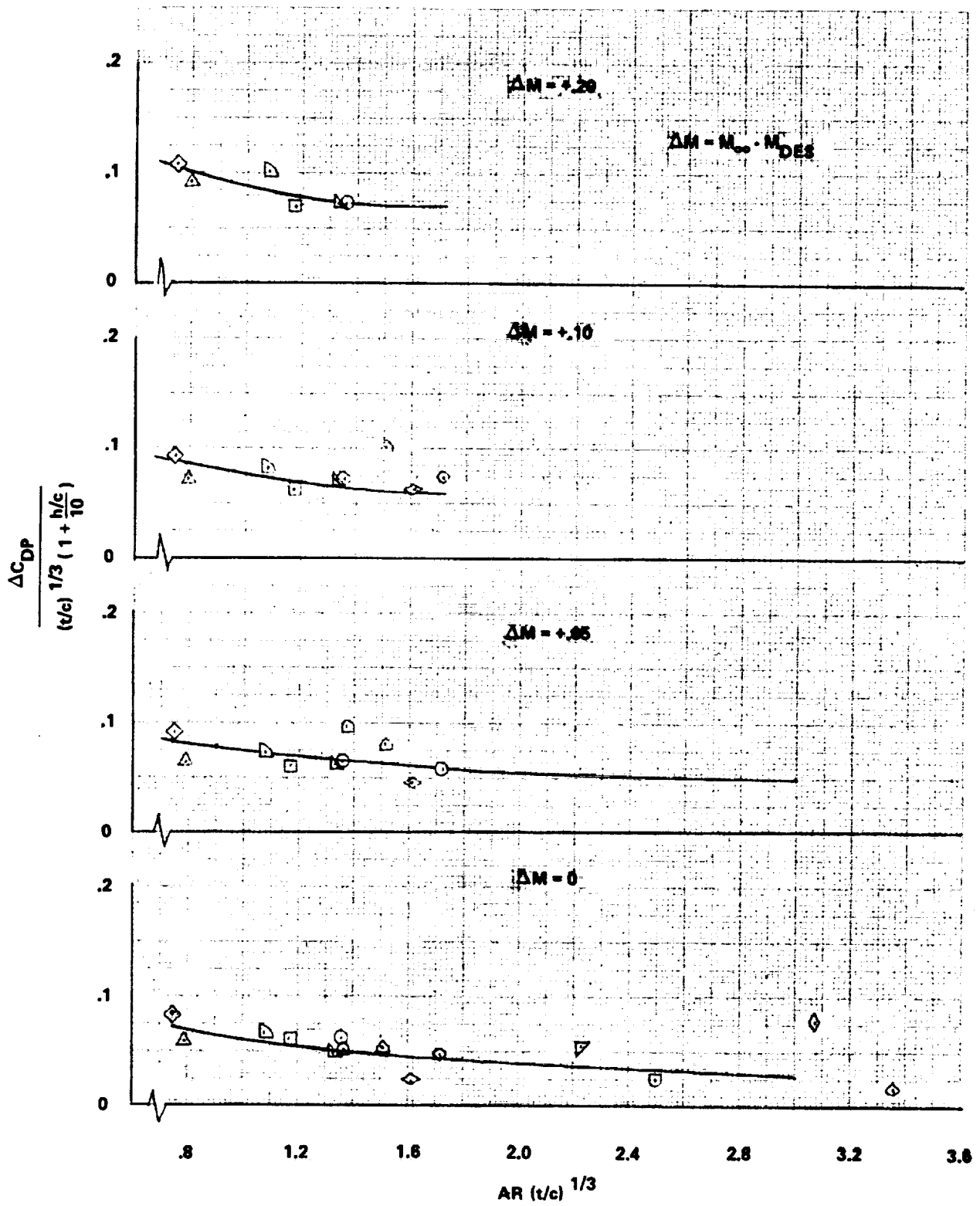
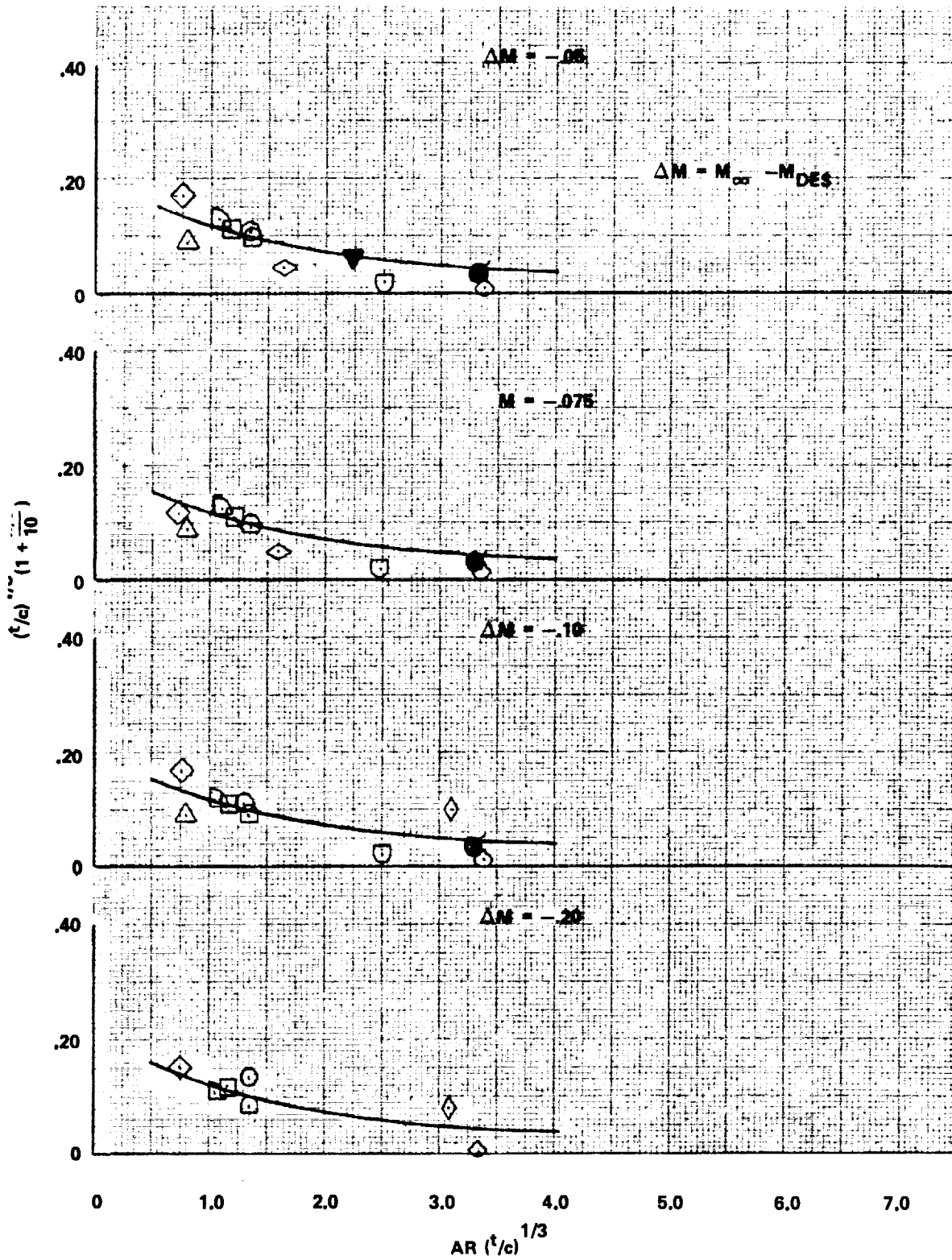Figure 56. – Supersonic wing pressure drag correlation, $\Delta C_L = +0.20$.
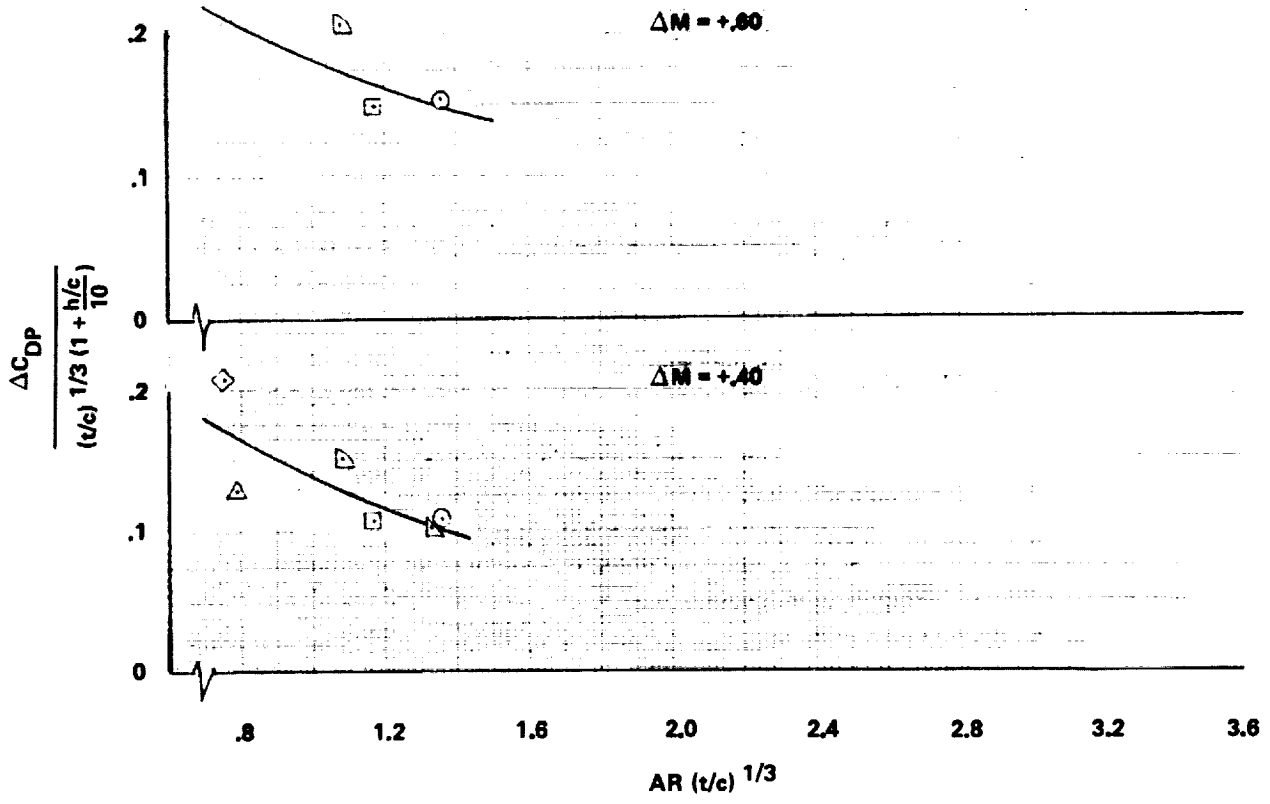
Figure 56. – Concluded.

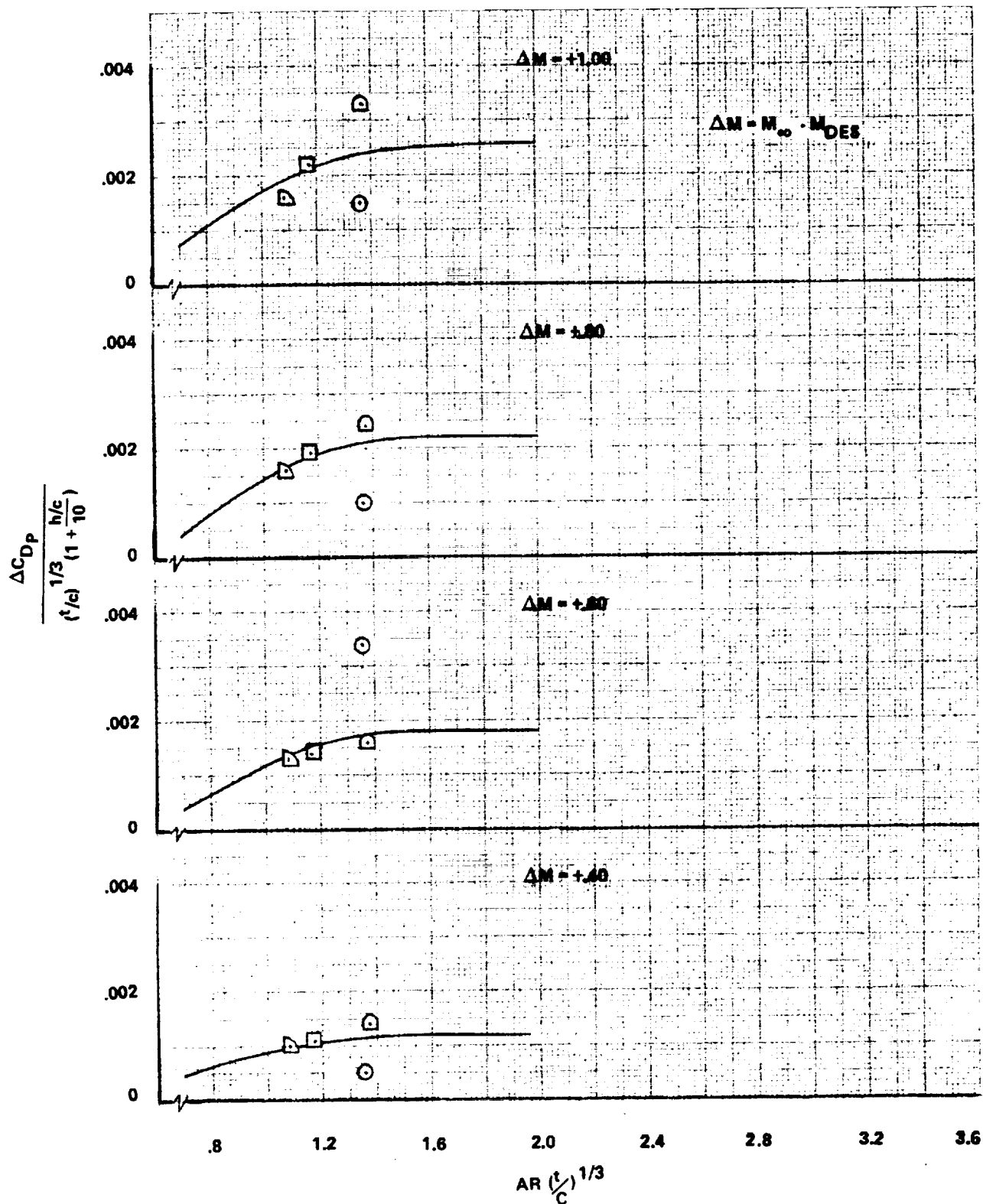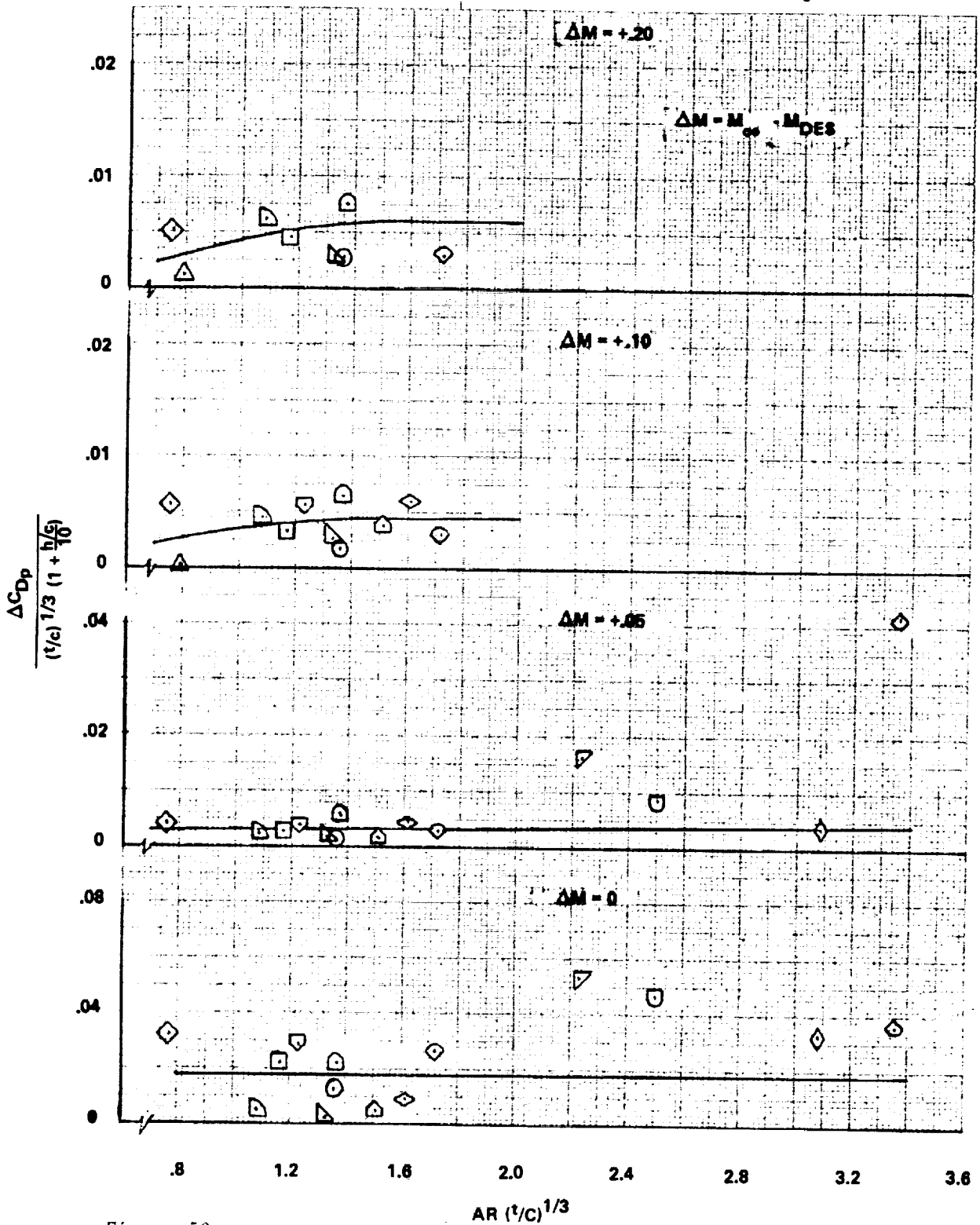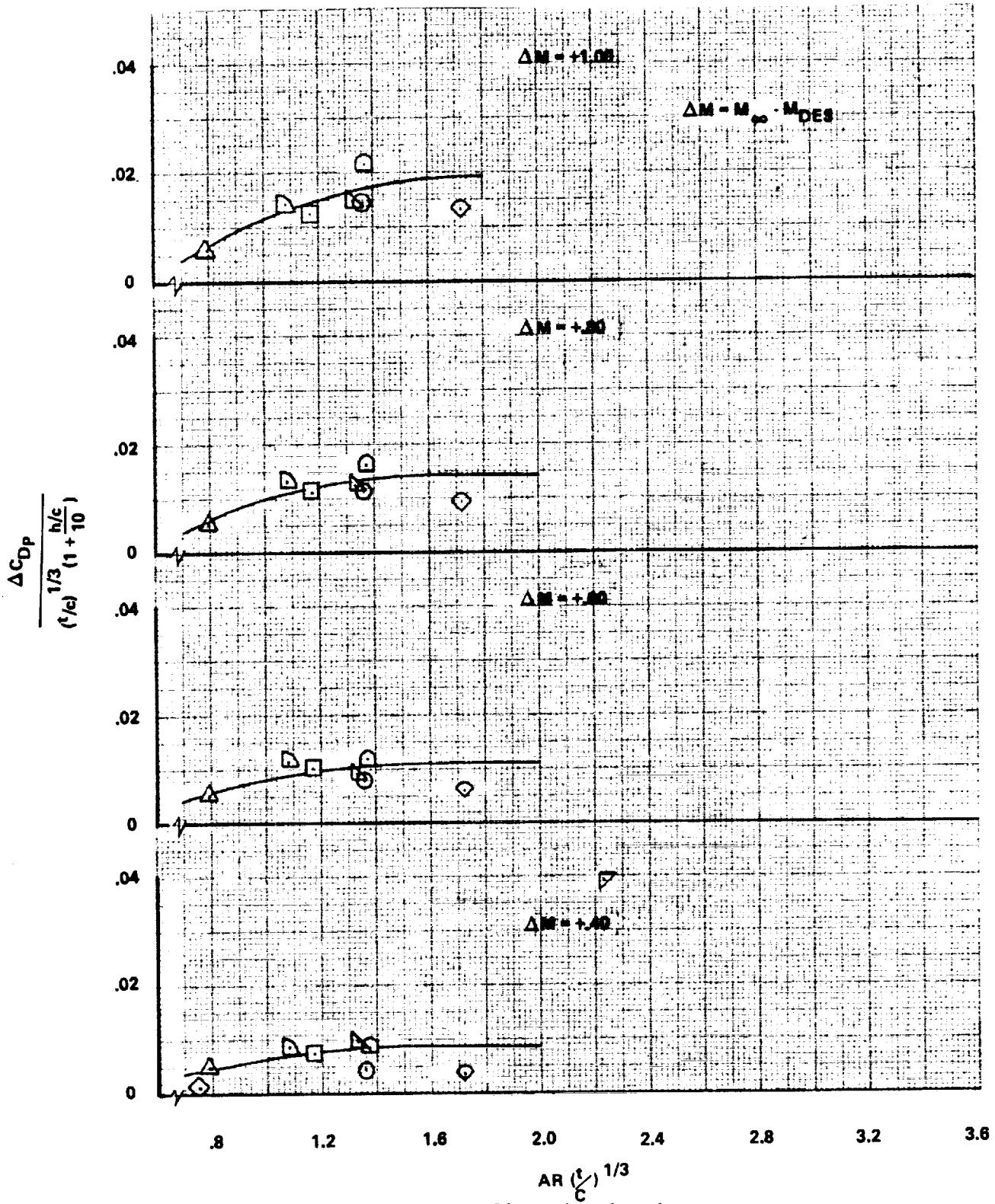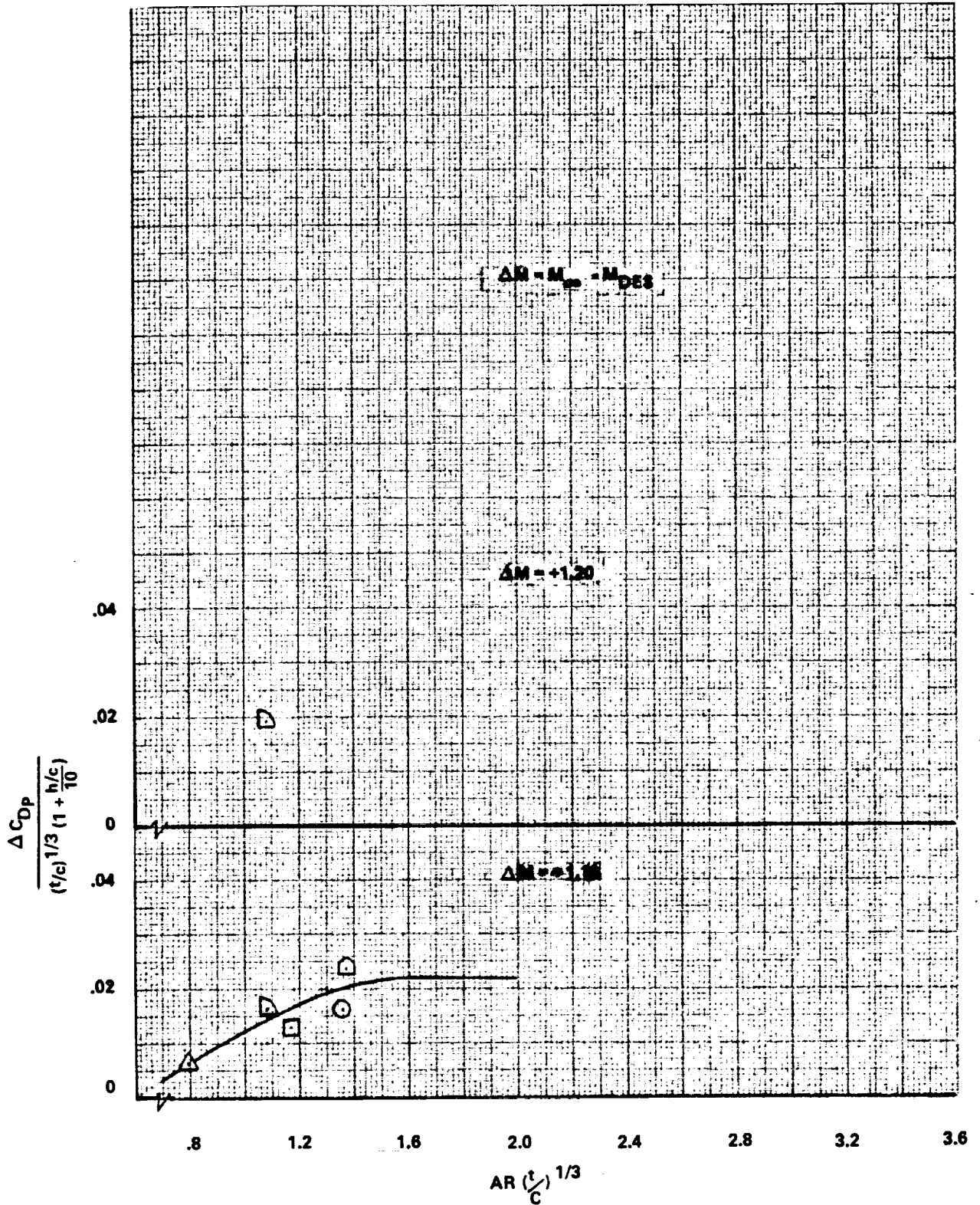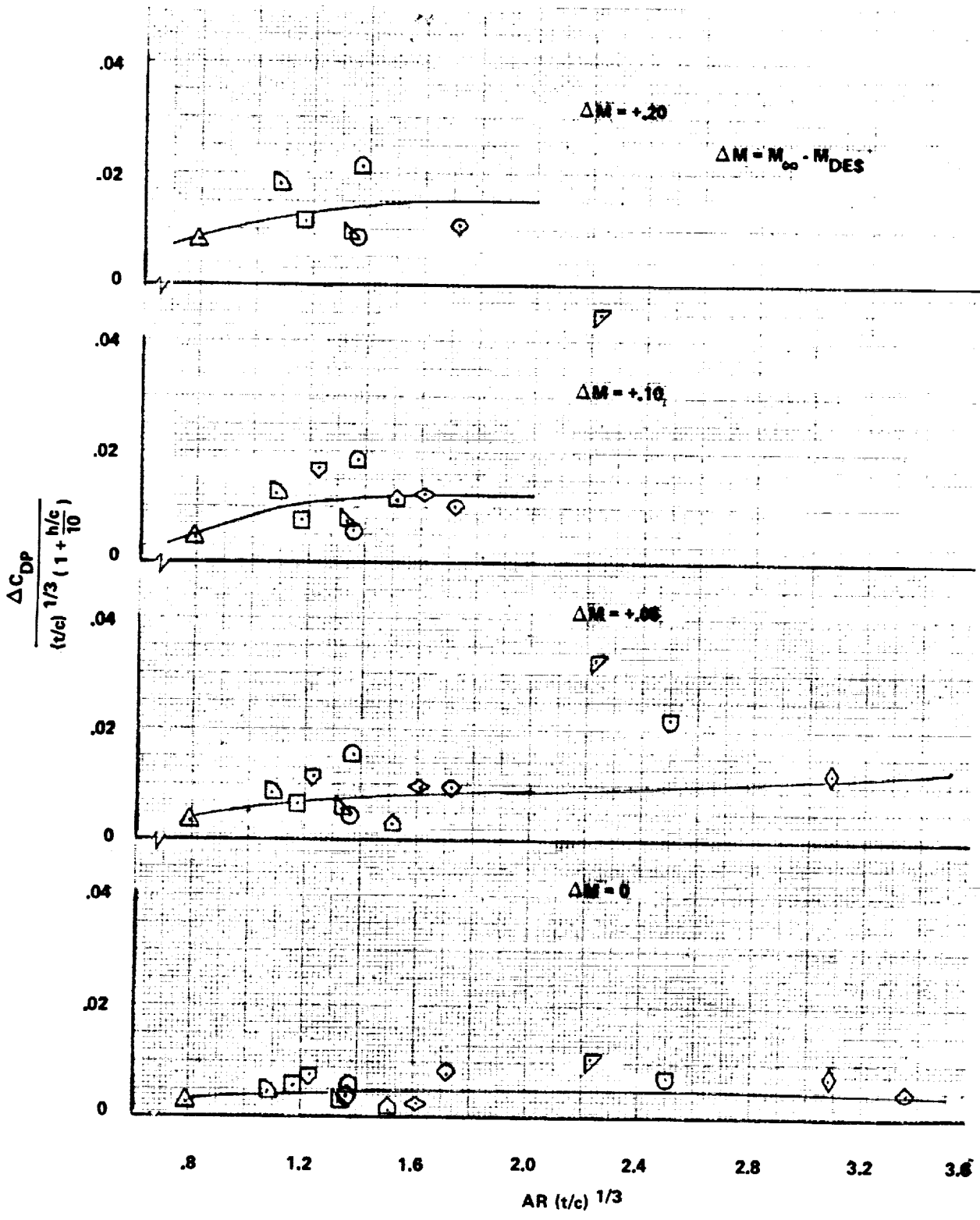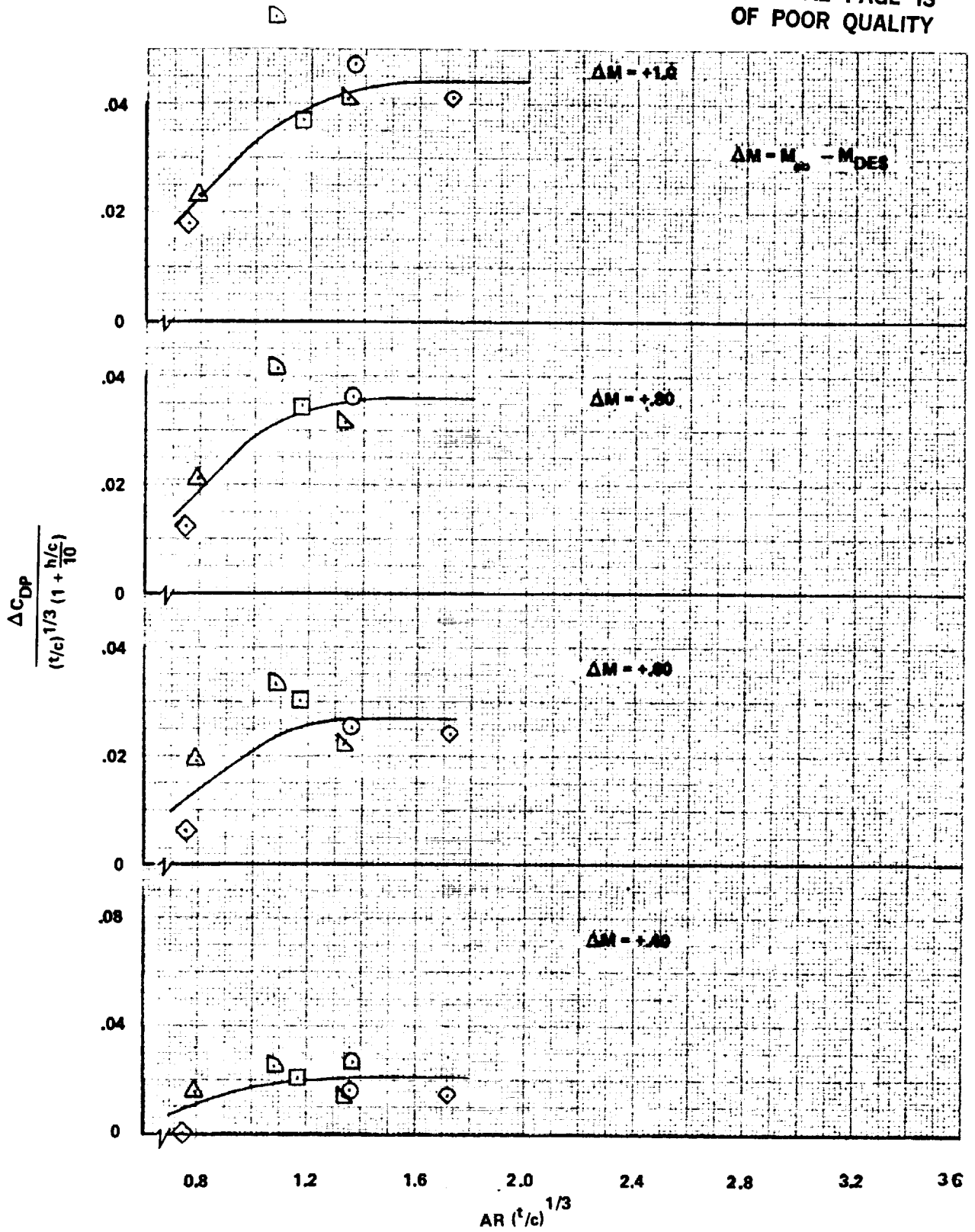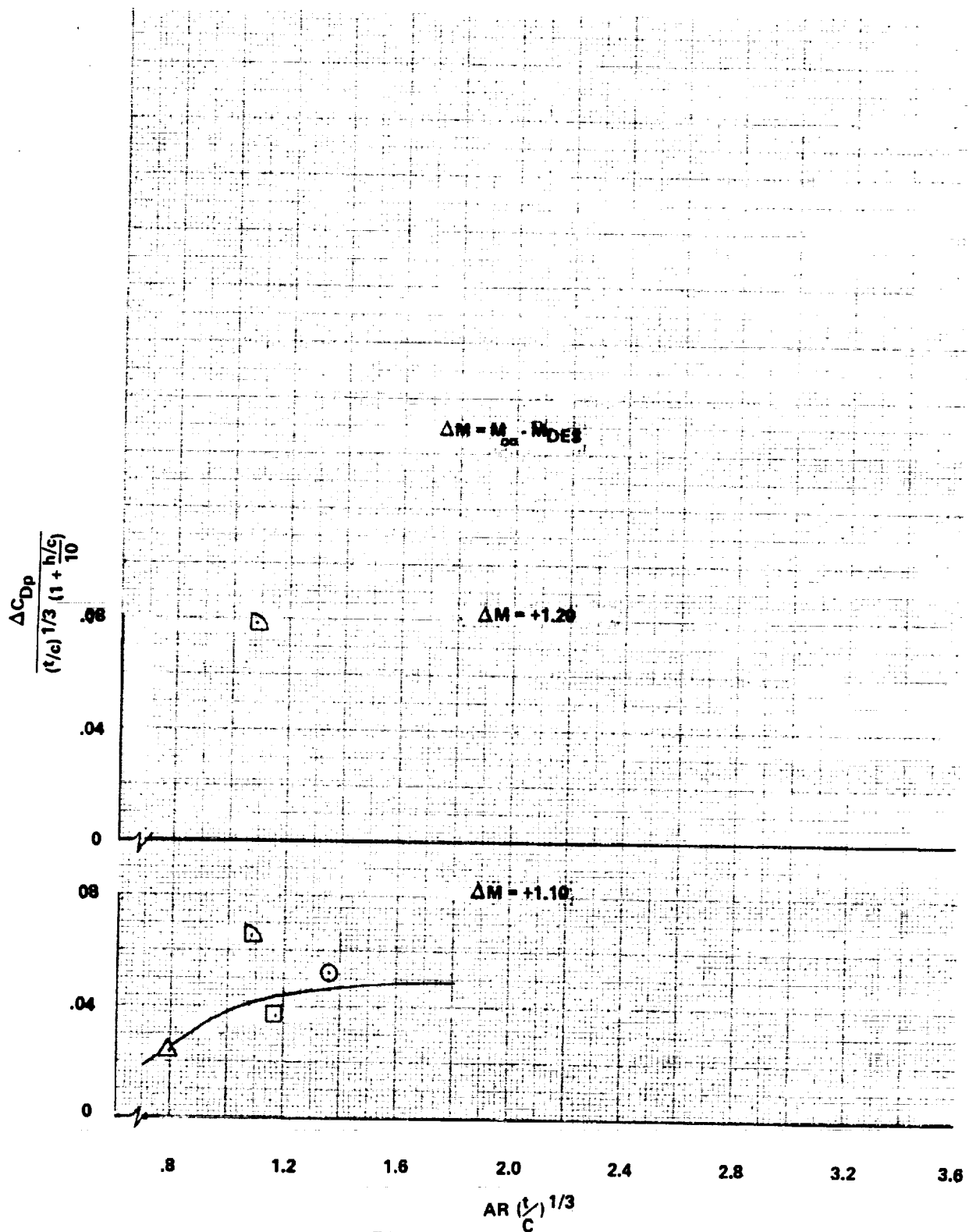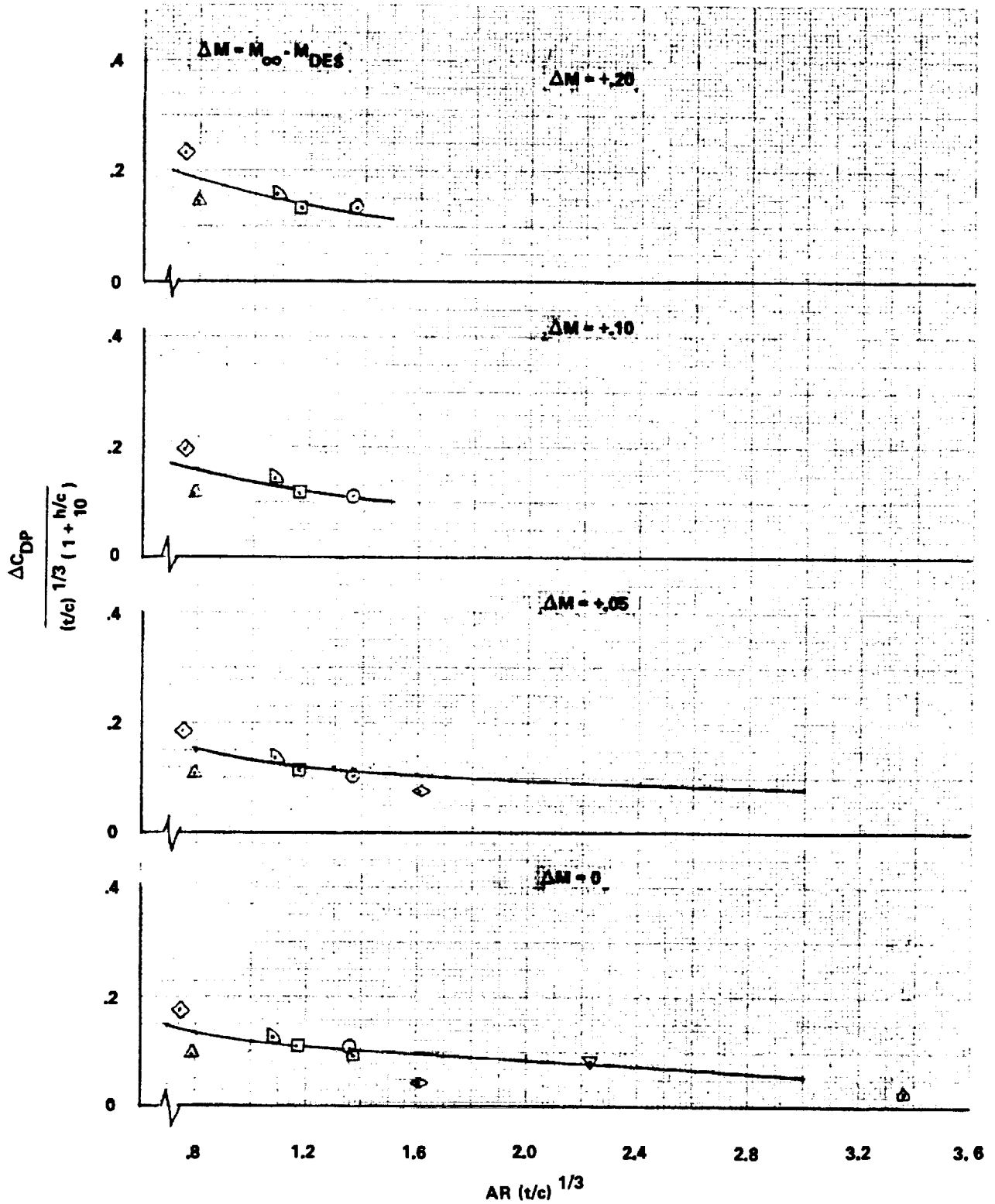Figure 57. — Supersonic wing pressure drag correlation, $\Delta C_L = +0.30$.

131
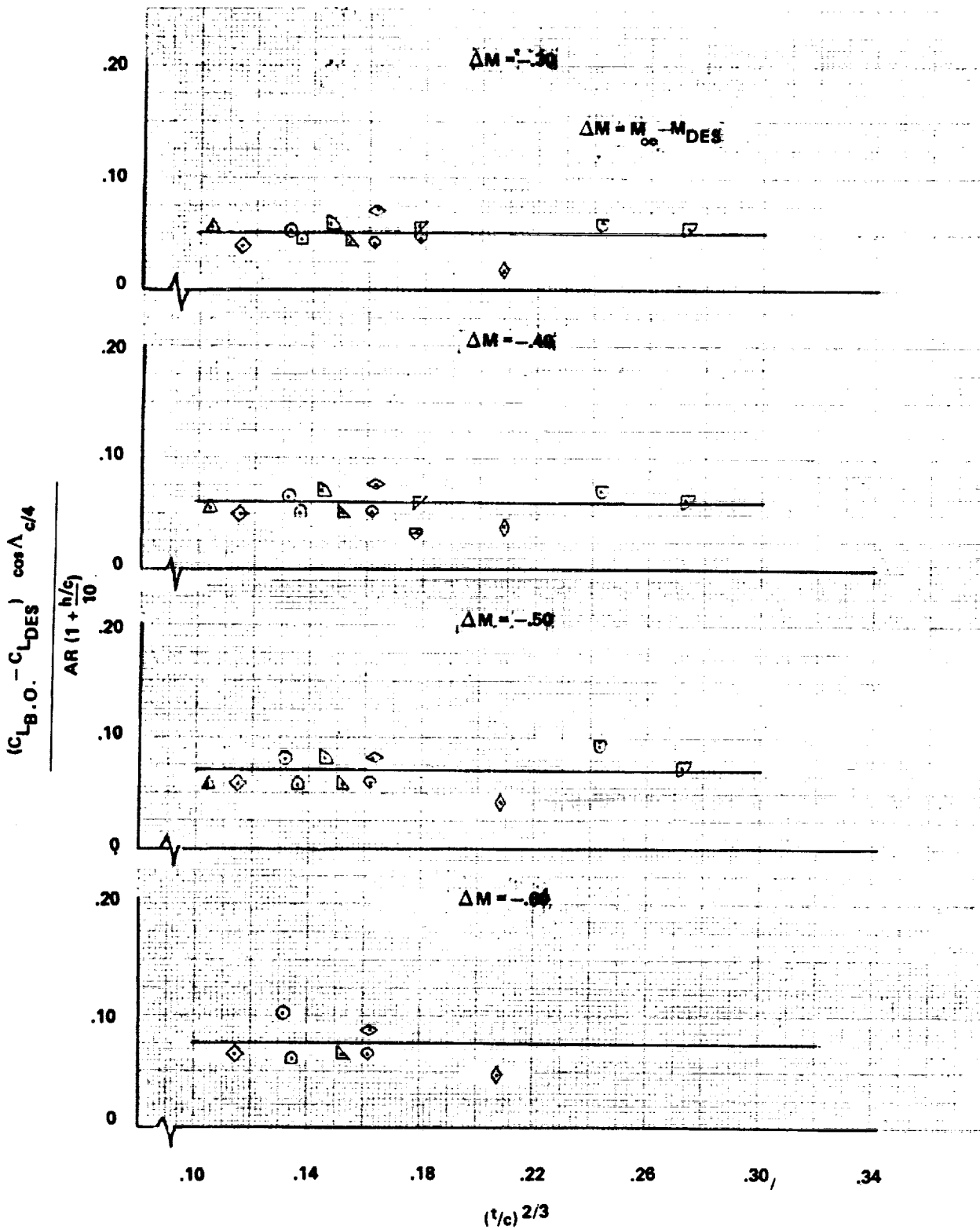
Figure 58. – Buffet onset correlation.

132
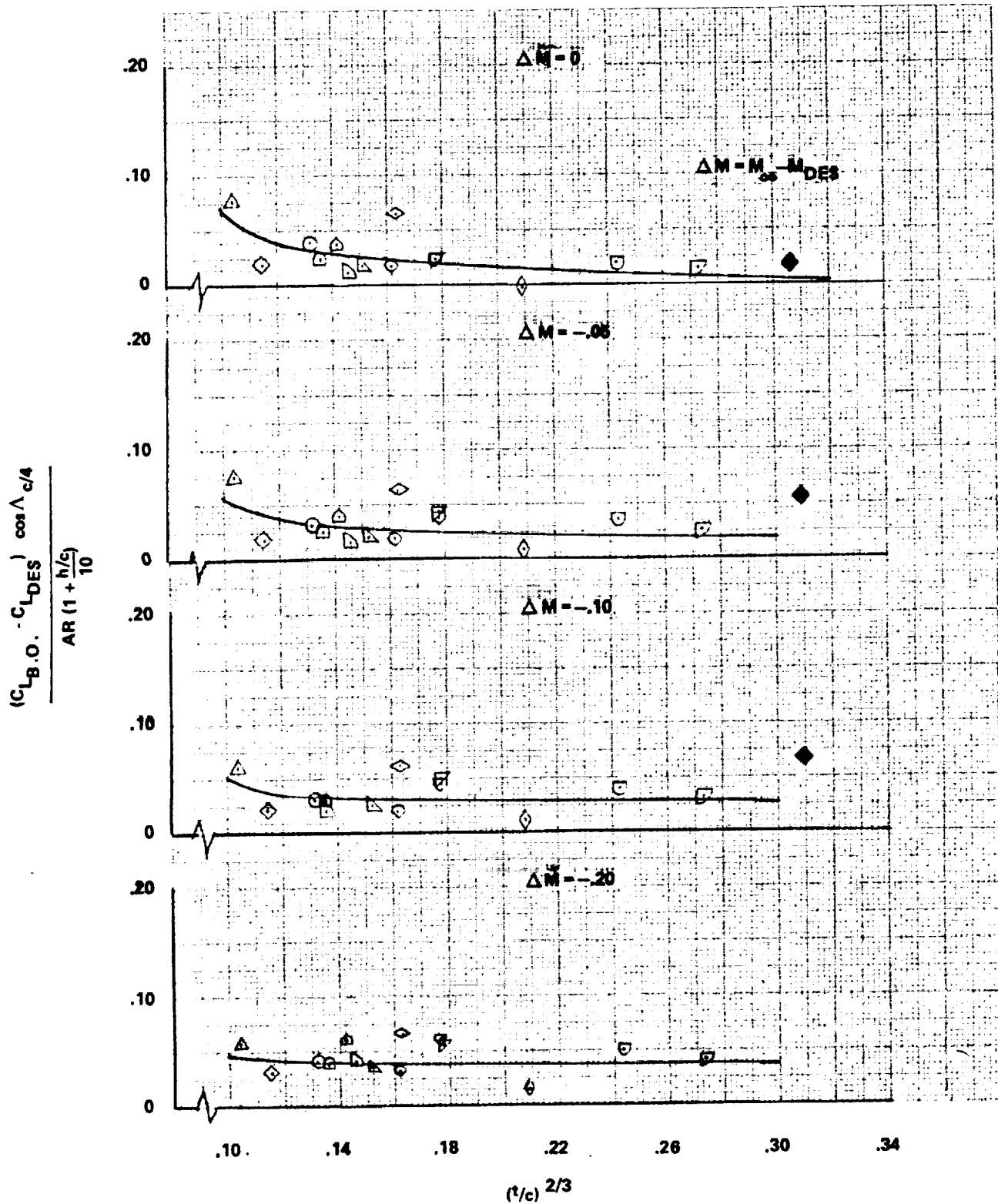
Figure 58. - Continued.

$$M = M_\infty - M_{DES}$$
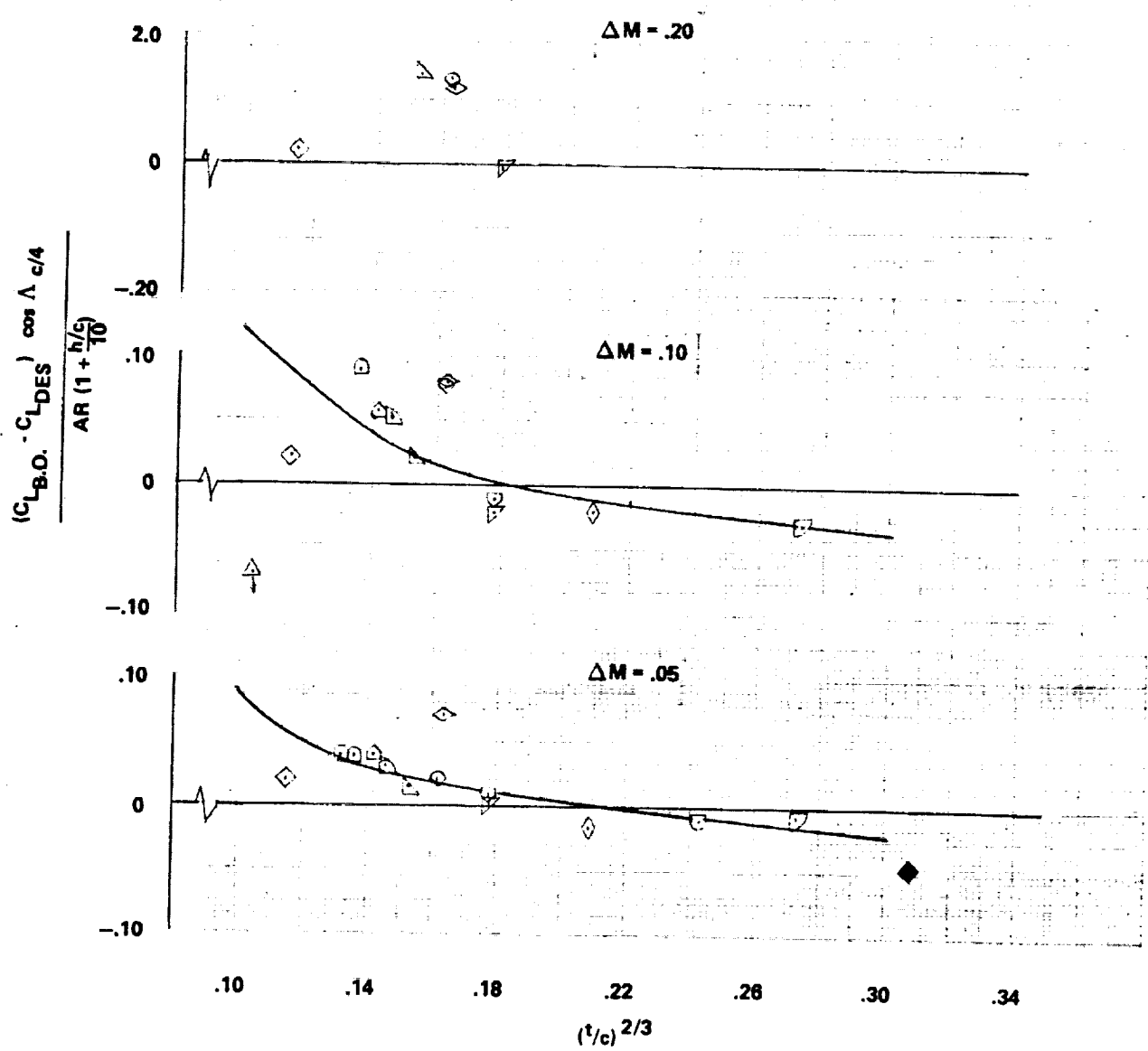
Figure 58. – Concluded.

4. EXAMPLE AIRCRAFT DRAG BUILDUP

The Delta Method drag prediction technique, as presented in Section 1, is used in this section to compute the drag polars of several of the subject aircraft at selected Mach numbers. These examples are then compared to the basic data for the subject aircraft as presented in references 3 through 21 and discrepancies noted. Included also is a comparison of certain drag levels for an advanced supersonic configuration which was not included in the original stable of subject aircraft. This method has also been converted into a computer code named Emperical Drag Estimates Techniques (EDET). This code is compatible with the NASA-Ames computer facilities and is detailed in reference 2.

4.1 Design Lift Coefficient and Mach Number

The first step in the Delta Method is the determination of the design lift coefficient and Mach number of the configuration in question. This is determined from the values of aspect ratio, thickness, sweep, and camber of the configuration being analyzed.

The calculation for $C_{L_{DES}}$ is given in table 3. The curves of figure 1 are entered at the appropriate value of AR $(t/c)^{1/3}$ for supersonic and AR for subsonic designs and the values of $C_{L_{DES}}$ noted. For the subsonic configurations, the value taken from the curve must be multiplied by the expression $\cos \Lambda c/4 \ (1 + \frac{h/c}{10})/\sqrt{AR}$. Also included in table 3 are the values of $C_{L_{DES}}$ derived from the basic data and used in figures 30 and 31 to correlate $C_{L_{DES}}$.

It can be seen that the deviation between these values and those derived from figure 1 are (with three exceptions) within a band of $\Delta C_L = \pm 0.05$ which is considered acceptable.

TABLE 3. - DESIGN LIFT COEFFICIENT CALCULATION

Configuration	AR	t/c	$\Lambda_{c/4}$ (deg)	h/c (%)	$AR\left(\dfrac{t}{c}\right)^{1/3}$	① $C_{L_{DES}}$ Fig. 1 vs $AR(t/c)^{1/3}$	$\dfrac{C_{L_{DES}}\sqrt{AR}}{\cos\Lambda_{c/4}\left(1+\dfrac{h/c}{10}\right)}$	① $C_{L_{DES}}$	② $C_{L_{DES}}$ FROM BASIC DATA	$\Delta=$ ① - ②
T-2B	5.07	.1200	2.00	2.00	2.50	–	.970	.517	.500	.017
T-37B	6.20	.1600	0.00	1.88	3.36	–	1.17	.559	.6075	-.049
KA-3B	6.75	.0954	35.90	–	3.08	–	1.27	.396	.4275	-.032
A-4F	2.91	.0748	33.21	0.773	1.23	–	.566	.299	.350	-.051
TA-4F	2.91	.0748	33.21	0.773	1.23	–	.566	.299	.320	-.021
RA-5C	3.73	.0500	37.50	–	1.37	.352	–	–	.365	-.013
A-6A	5.31	.0750	25.00	1.623	2.23	–	1.01	.461	.485	-.024
A-7A	4.00	.0657	35.00	1.180	1.61	.389	–	–	.400	-.011
F-4E	2.82	.0557	45.00	–	1.08	.310	–	–	.325	-.015
F-5A	3.75	.0480	24.00	0.735	1.36	.352	–	–	.325	.027
F-8C	3.40	.0597	45.00	–	1.33	.350	–	–	.300	.050
F-11F	4.00	.0535	35.00	–	1.51	.377	–	–	.365	.012
F-100	3.86	.0700	45.00	–	1.59	–	–	–	.365	.017
F-101	4.28	.0650	36.61	–	1.72	.405	.742	.267	.420	-.015
F104G	2.46	.0336	18.10	0.00	0.792	.235	–	–	.265	-.030
F-105B	3.18	.0500	45.00	–	1.17	.323	–	–	.350	-.027
F-106A	2.20	.0391	52.00	–	0.747	.215	–	–	.200	.015
XB-70	1.75	.0225	58.79	0.00	0.494	–	–	–	.200	–
S-3A	7.73	.1430	15.00	2.40	4.04	–	1.459	.629	.550	.079
Wing 51	8.97	.1240	30.20	1.94	4.47	–	1.68	.581	.585	-.004
VA5	7.20	.1580	0.00	3.00	3.90	–	1.36	.657	.650	.007
L-1011 SC	6.95	.1050	35.00	1.60	3.28	–	1.31	.472	.450	.022
L-1011 FLT	6.95	.1050	35.00	1.30	3.28	–	1.31	.460	.460	0
VPX-W2	8.63	.1460	22.00	2.60	4.54	–	1.62	.644	.550	.094
VPX-W3	8.63	.1460	22.00	2.20	4.54	–	1.62	.624	.475	.149
ATT-W4	7.64	.0930	40.00	1.90	3.46	–	1.42	.474	.470	-.004
T2-CWT	5.07	.1700	2.28	2.10	2.80	–	.970	.521	.500	.021
OBLIGUE	6.48	.0707	45.00	0.99	2.68	–	1.225	.373	.325	.048
FBU WT.	6.80	.0910	42.24	2.00	3.06	–	1.28	.437	.450	-.013
BOEING FT.	3.50	.0500	39.40	0.40	1.29	.344	–	–	.275	.069
WHIT. #1	11.48	.1222	30.00	1.12	5.70	–	2.14	.610	.600	.010
WHIT. #2	10.24	.1258	27.00	1.30	5.13	–	1.92	.603	.600	.003
WHIT. #3	11.95	.1258	27.00	1.15	5.99	–	2.23	.644	.650	-.006
WHIT. #4	11.95	.1458	27.00	1.38	6.29	–	2.23	.655	.650	.005

Known Parameters REF: Table 1

Fig. 1 vs AR

The calculation for M_{DES} is given by table 4. The curves of figures 2 and 3 are entered at the appropriate value of $^t/c$ for supersonic and $(^t/c)^{2/3}$ for subsonic designs and the corresponding value of M_{D2-D} noted. For subsonic configurations the distinction must be made between advanced or conventional airfoil sections. The above value of two-dimensional drag divergent Mach is then corrected for sweep and aspect ratio using figure 4 and equation (5). The resulting three-dimensional drag divergent Mach number is, then, the design Mach (M_{DES}). It can be seen from table 4 that the deviation between these calculated values and those derived from the basic data are (with two exceptions) within a band of $M = \pm 0.05$ which is considered acceptable.

4.2 Friction Drag

Once the configuration design lift and Mach number have been determined, the next step is to calculate those drag values which are independent of lift and which make up the minimum drag level. The first of these items is friction drag.

Friction drag is calculated as discussed in Section 1.2 using equation (7). Two aircraft (A4-F and RA-5C) are chosen as examples to demonstrate the method. Component wetted areas and reference lengths are either obtained from the geometric data of these aircraft or measured from the three-views as presented in references 3 through 21. The computation is shown in the following paragraphs. First, the required geometric parameters are computed as follows:

Component	A-4F			RA-5C		
	S_{WET} ft^2 (m^2)	ℓ = ft ft (m)	S_{WET}/S_{REF}	S_{WET}/S_{REF} ft^2 (m^2)	ℓ - ft (m)	S_{WET}/S_{REF}
Wing	430.0 (39.95)	9.48 (2.89)	1.65	1144.08 (106.29)	13.95 (4.25)	1.63
Horz. Tail	84.40 (7.84)	4.66 (1.42)	0.32	388.72 (36.11)	9.73 (2.97)	0.56
Vert. Tail	49.95 (4.64)	7.38 (2.25)	0.19	235.33 (21.86)	8.34 (2.54)	0.34
Fuselage	547.65 (50.88)	40.70 (12.41)	2.11	1474.00 (136.91)	73.30 (22.34)	2.11

TABLE 4. DESIGN MACH NUMBER CALCULATION

Configuration	Known Parameters REF: Tables 1 and 3						$M_{D_{2\text{-}D}}$ Fig.①	$M^2_{D_{2\text{-}D}} - 1$ (Fig. 3)	① $M_{D_{2\text{-}D}}$ (Fig. 3)	② ΔM_{AR} (Fig. 4)	③ $\Delta \Lambda_{c/4}$ (Fig. 4)	④ M_{DES} = ①+②+③	⑤ M_{DES} From Basic Data	Δ = ④ − ⑤
	AR	t/c	$\Lambda_{c/4}$ (deg)	$C_{L_{DES}}$	$\frac{1}{AR}$	$(\frac{t}{c})^{2/3}$								
T-2B	5.07	.1200	2.00	.517	.197	.243	–	-.527	.688	.0275	0	.7155	.723	-.008
T-37B	6.20	.1600	0.00	.559	.161	.295	–	-.580	.648	.022	0	.670	.675	-.005
KA-1B	6.75	.0954	35.90	.396	.148	.209	–	-.464	.732	.0205	.060	.8125	.823	-.011
A-4F	2.91	.0748	33.21	.299	.344	.178	–	-.399	.775	.049	.052	.875	.805	.070
TA-4F	2.91	.0748	33.21	.299	.344	.178	–	-.399	.775	.049	.052	.875	.800	.075
RA-5C	3.73	.0500	37.50	.352	.268	.136	.785	–	–	.0378	.066	.889	.896	-.007
A-6A	5.31	.0750	25.00	.461	.188	.178	–	-.425	.758	.026	.028	.812	.755	.057
A-7A	4.00	.0657	35.00	.389	.250	.163	.770	–	–	.035	.057	.862	.877	-.015
F-4E	2.82	.0557	45.00	.310	.355	.146	.781	–	–	.060	.094	.935	.935	0
F-5A	3.75	.0480	24.00	.352	.267	.132	.788	–	–	.037	.025	.850	.895	-.045
F-8C	3.40	.0597	45.00	.350	.294	.153	.775	–	–	.042	.094	.911	.950	-.039
F-11F	4.00	.0535	35.00	.377	.250	.142	.778	–	–	.035	.057	.870	.888	-.018
F-100	3.86	.0700	45.00	.267	.259	.170	–	-.320	.825	.035	.094	.954	.870	.084
F-101	4.28	.0650	36.61	.405	.234	.162	.783	–	–	.033	.063	.879	.843	.036
F-104C	2.46	.0336	18.10	.235	.407	.104	.820	–	–	.058	.014	.892	.896	-.004
F-105B	3.18	.0500	45.00	.323	.314	.136	.801	–	–	.044	.094	.939	.8875	.052
F-106A	2.20	.0391	52.00	.215	.455	.115	.805	–	–	.065	.124	.994	.920	.074
XB-70	1.75	.0225	58.79	–	.571	.080	–	–	–	–	–	–	–	–
S-3A	7.73	.1430	15.00	.629	.129	.273	–	-.575	.652	.018	.009	.679	.684	-.005
WING 51	8.97	.1240	30.00	.581	.111	.250	–	-.405*	.771	.015	.042	.828	.804	.024
VA-5	7.20	.1580	0.00	.657	.139	.292	–	-.503*	.705	.019	0	.724	.720	.004
L-1011 SC	6.95	.1050	35.00	.472	.144	.223	–	-.339*	.813	.020	.057	.890	.867	.023
L-1011 FLT	6.95	.1050	35.00	.460	.144	.223	–	-.476	.724	.020	.057	.801	.850	-.049
VPX-W2	8.63	.1460	22.00	.644	.116	.277	–	-.470*	.728	.016	.021	.765	.770	-.005
VPX-W3	8.63	.1460	22.00	.624	.116	.277	–	-.467*	.730	.016	.021	.767	.775	-.008
ATT-W4	7.64	.0930	40.00	.474	.131	.205	–	-.304*	.834	0	.075	.909	.916	-.007
T2-CWT	5.07	.1700	2.28	.521	.197	.307	–	-.513*	.698	.0275	0	.725	.735	-.010
OBLIQUE	6.48	.0707	45.00	.373	.154	.171	–	-.212*	.888	.022	.094	1.004	.970	.034
FBU WT.	6.80	.0910	42.24	.437	.147	.202	–	-.292*	.861	.021	.084	.946	.963	-.017
BOEING FT.	3.50	.0500	39.40	.344	.286	.136	–	-.382*	.786	.040	.073	.899	.918	-.019
WHIT. #1	11.48	.1222	30.00	.610	.087	.246	–	-.451*	.741	.012	.042	.795	.815	-.020
WHIT. #2	10.24	.1258	27.00	.603	.098	.251	–	-.4175*	.763	.014	.033	.810	.795	.015
WHIT. #3	11.95	.1258	27.00	.644	.084	.251	–	-.420*	.762	.012	.033	.807	.792	.015
WHIT. #4	11.95	.1458	27.00	.655	.084	.277	–	0.470*	.728	.012	.033	.773	.765	.008

*Advanced Airfoils

Reference lengths for the wing and tail surfaces are chosen as the exposed aerodynamic chord lengths. The actual fuselage length is used for the fuselage.

Form factors are computed from figures 6 and 7 as follows:

Component	A – 4F		RA – 5C	
Wing	$t/c = 0.0748$	FF = 1.255	$t/c = 0.050$	FF = 1.165
Horz. Tail	$t/c = 0.055$	FF = 1.185	$t/c = 0.040$	FF = 1.13
Vert. Tail	$t/c = 0.055$	FF = 1.185	$t/c = 0.040$	FF = 1.13
Fuselage	$\ell/d = 7.81$	FF = 1.191	$\ell/d = 8.52$	FF = 1.155

Fuselage fineness ratio (ℓ/d) is computed with the effects of inlet capture area included in order to obtain a true representation of fuselage geometry. Conventional airfoil sections are assumed for both aircraft.

A reference altitude of 36,152 feet (11,019 meters) and a Mach number of 0.60 is selected for computation. A value of compressible to incompressible drag ($C_F/C_{F_{INC}}$) is taken from figure 8 as 0.966. A Reynolds Number per foot of 1.381×10^6 is obtained from the atmospheric tables. For the case of wind tunnel model evaluation, a desired Reynolds Number and transition location in percent length must be specified. Here it is zero.

Calculation of the friction drag is then obtained as follows:

(Equation 7)

Component	RN x 10^6	C_F (Fig. 5)	$\frac{S_{WET}}{S_{REF}}\left(\frac{C_F}{C_{F_{INC}}}\right)CF(FF)$ $= \Delta C_{DF}$	RN x 10^6	C_F (Fig. 5)	$\frac{S_{WET}}{S_{REF}}\left(\frac{C_F}{C_{F_{INC}}}\right)CF(FF)$ $= \Delta C_{DF}$
		A-4F			RA-5C	
Wing	13.10	0.00281	0.00562	19.27	0.00264	0.00484
Horz. Tail	6.44	0.00319	0.00117	13.44	0.00280	0.00171
Vert. Tail	10.19	0.00294	0.00064	11.52	0.00287	0.00110
Fuselage	56.21	0.00225	0.00585	95.29	0.00219	0.00516
Total C_{D_F}			0.01328			0.01281

These values are then corrected for configuration effects by the use of figure 9 as follows: (Equation (9))

	A-4F	RA-5C
C_{D_F} (Computed)	0.01328	0.01281
① = From Figure 9	1.284*	1.284*
C_{D_F} = C_{D_F} (Computed) x ①	0.01705	0.01645
*This is the slope of the curve given by Figure 9.		

4.3 Compressibility Drag

The second major contributor to zero-lift drag is that level due to compressibility effects. As discussed in Section 3, compressibility drag is estimated from the sum of the three major contributing parts. For this calculation the same two aircraft are chosen as were for the friction drag computation. Compressibility drag is calculated at Mach numbers of 0.9 and 2.0 for the RA-5C and at 0.8 Mach only for the A-4F.

4.3.1 <u>Fuselage compressibility drag</u>. - Compute the required fuselage parameters as follows:

Using Tables 1 and 2:	A-4F	RA-5C
$1 + S_b/S_\pi$	1.05	1.27
$(\ell/d)^2$ = ①	69.06	93.32
S_π/S_{REF} = ②	0.073	0.065

Fuselage compressibility is then computed as shown.

Using Figures 13 and 14	A – 4F	RA – 5C	
	$M_\infty = 0.80$	$M_\infty = 0.90$	$M_\infty = 2.00$
$C_{D_\pi} (\frac{\ell}{d})^2$ (Fig. 13)	0	0.680	–
$C_{D_\pi} = C_{D_\pi} (\ell/d)^2 / ①$	0	0.00729	–
ΔC_{D_C} FUS $= C_{D_\pi} \times ②$	0	0.00047	–
$C_{D_\pi} (\frac{\ell}{d})^2$ (Fig. 14)	–	–	18.25
$C_{D_\pi} = C_{D_\pi} (\ell/d)^2 / ①$	–	–	0.19556
ΔC_{D_C} FUS $= C_{D_\pi} \times ②$	–	–	0.01271

It should be noted that the calculation for S_π and fuselage fineness ratio (ℓ/d) do not include the effects of inlet capture area.

4.3.2 <u>Wing compressibility drag.</u> – The following parameters are tabulated either from table 2 or 4:

	A – 4F	RA – 5C
M_{DES} From Table 4	0.875	0.889
$(t/c)^{5/3} (1 + \frac{h/c}{10}) = ①$	0.01430	0.00679
AR Tan Λ_{LE}	2.54	3.49
$(t/c)^{2/3}$	0.178	0.136

Wing compressibility drag is then calculated as follows:

	A – 4F	RA – 5C	
	$M_\infty = 0.80$	$M_\infty = 0.90$	$M_\infty = 2.00$
$\Delta M = M_\infty - M_{DES}$	-0.075	0.011	1.111
$\Delta C_{D_C} / \textcircled{1}$ (Fig. 10)	0.037	0.220	–
ΔC_{D_C} WING = Fig. 10 x $\textcircled{1}$	0.00053	0.00149	–
$\Delta C_{D_C} / \textcircled{1}$ (Fig. 11)	–	–	0.675
ΔC_{D_C} WING = Fig. 11 x $\textcircled{1}$	–	–	0.00458

4.3.3 <u>Wing/body interference drag</u>. – Interference drag is assumed to occur only above Mach 1.0; therefore, only the supersonic calculation for the RA-5C is required. This is accomplished as follows:

$$M_\infty = 2.0$$
$$d/_b = 0.1485$$
$$(1 - \lambda)\, Cos\Lambda_{c/4} = 0.6427 = \textcircled{1}$$
$$\text{from Figure 15: } \Delta C_{D_C} (INT) \times \textcircled{1} = 0.00048$$
$$\Delta C_{D_C} (INT) = 0.00048/\textcircled{1} = 0.00075$$

4.3.4 <u>Total compressibility drag</u>. – The three components of compressibility drag are then summed to obtain the total compressibility drag using equation 10. These are compared with the original values of ΔC_{D_C} obtained from the basic data (Equation 10).

142

	A – 4F		RA – 5C
	$M_\infty = 0.80$	$M_\infty = 0.90$	$M_\infty = 2.00$
ΔC_{D_C} FUS	0	0.00047	0.01271
ΔC_{D_C} WING	0.00053	0.00149	0.00458
ΔC_{D_C} INT.	0	0	0.00075
TOTAL ΔC_{D_C}	0.00053	0.00196	0.01804
ΔC_{D_C} From Data	0.00130	0.00190	0.01530
Difference	-0.00077	+0.00006	+0.00274

Values of computed aircraft compressibility drag versus those obtained from the basic data of references 3 through 21 are compared in figures 59 and 60 for some of the subject aircraft. It should be noted that the trends shown follow very well the reduced data, which is critical for methods used in design work. The compressibility drag of a more advanced technology fighter configuration, which is not included in the subject aircraft, was computed as 0.00194 at Mach 0.90 and 0.02493 at Mach 1.6 by this procedure. Analysis of available drag data on the aircraft reveal thse values to be 0.0017 and 0.2610 respectively.

4.4 Total Minimum Drag

The total drag level for the configuration which is independent of lift (minimum) is now determined from a summation of the component drags computed in the preceeding paragraphs. This calculation is as follows: (Equations (2) and (15)).

	A-4F	RA-5C	
	$M_\infty = 0.80$	$M_\infty = 0.90$	$M_\infty = 2.0$
C_{D_F} @ $M_\infty = 0.60 = C'_{D_F}$	0.01705	0.01637	0.01637
$C_F/C_{F_{INC}}$ @ $M_\infty = 0.60 = $ ①	0.966	0.966	0.966
$C_F/C_{F_{INC}}$ @ $M_\infty = $ ②	0.949	0.939	0.768
② / ① = ③ } Equation (15)	0.982	0.972	0.795
$\Delta C_{D_F} = C'_{D_F} \times$ ③ $=$ ④	0.01675	0.01591	0.01301
$\Delta C_{D_C} = $ ⑤	0.00053	0.00196	0.01804
$\Delta C_D = $ ⑥	0.00100*	0	0
$C_{D_{MIN}} = $ ④ $+$ ⑤ $+$ ⑥	0.01828	0.01787	0.03105
$C_{D_{MIN}}$ from basic data	0.02040	0.01599	0.02800
Difference	-0.00212	0.00188	0.00305
Error	-10%	11.7%	11%

*The miscellaneous drag item (ΔC_D) for the A-4F in the above calculation represents an estimation of the drag for a centerline rack and IFR probe which are included in the basic drag data as presented in reference 6.

Agreement is acceptable for the two aircraft shown.

4.5 Wing Pressure Drag

The calculations so far have defined those drag items which are independent of angle of attack and which compose the configuration's minimum drag level. The next step in determining the total drag is, to determine the variation of drag with lift and thereby define the polar shape. For the method herein described, polar shape is defined as a combination of the theoretical induced drag ($C_L^2/\pi AR$) and the corresponding value of wing pressure drag (ΔC_{D_P}) which varies as a function of wing lift and Mach number.

144

The calculation of wing pressure drag for the two representative configurations is begun by the tabulation of the required wing parameters from tables 2, 3, and 4:

	A-4F	RA-5C
$C_{L_{DES}}$	0.299	0.365
M_{DES}	0.875	0.889
AR $(t/c)^{1/3}$	1.23	1.37
$(t/c)^{1/3} (1 + \frac{h/c}{10})$	0.454	0.368

Using these values, the curves of figures 16 through 27 are interpolated between for the appropriate value of ΔM and the resultant value of ΔC_{D_p} calculated as a function of ΔC_L as shown below. The corresponding value of wing lift coefficient, C_L, is then determined by the expression:

$$C_L = \Delta C_L + C_{L_{DES}} \tag{19}$$

These calculations are as follows:

A-4F

M = 0.80			
ΔC_L	C_L	$\dfrac{\Delta C_{D_p}}{(t/c)^{1/3} (1 + \frac{h/c}{10})}$	ΔC_{D_p}
-0.3	-0.001	0.00050	0.00023
-0.2	0.099	0.00140	0.00064
-0.1	0.199	0.00315	0.00143
-0.05	0.249	0.00498	0.00226
0	0.299	0.00625	0.00284
0.05	0.349	0.01205	0.00547
0.1	0.399	0.02200	0.00999
0.2	0.499	0.05500	0.02497
0.3	0.599	0.11000	0.04994

M = 0.80 ΔM = 0.80 - 0.875 = -0.075

RA-5C:

ΔC_L	C_L	$M_\infty = 0.90 \; \Delta M = 0.90 - 0.889 = 0.011$		$M_\infty = 2.0 \; \Delta M = 2.0 - 0.889 = 1.111$	
		$\dfrac{\Delta C_{D_P}}{(t/c)^{1/3} (1 + \frac{h/c}{10})}$	ΔC_{D_P}	$\dfrac{\Delta C_{D_P}}{(t/c)^{1/3} (1 + \frac{h/c}{10})}$	ΔC_{D_P}
-0.3	0.065	0.0005	0.00018	0.00258	0.00095
-0.2	0.165	0.00205	0.00075	0.0202	0.00743
-0.1	0.265	0.00465	0.00171	0.0465	0.01711
-0.05	0.315	0.00575	0.00212	0.0780	0.02870
0	0.365	0.01090	0.00401	0.1070	0.03938
0.05	0.415	0.0170	0.00626	0.1400	0.05152
0.1	0.465	0.0280	0.01030	0.1580	0.05814
0.2	0.565	0.0510	0.01877	-	-
0.3	0.665	0.1020	0.03754	-	-

The computation of total drag-due-to-lift (C_{D_L}) is now accomplished by using the equation

$$C_{D_L} = \Delta C_{D_P} + C_L^2 / \pi AR \qquad (20)$$

A comparison of results from this procedure versus that obtained from the basic data for the A-4F and RA-5C are given in figures 61 and 62. Figures 63 through 66 present similar comparisons for a representative sampling of the other study aircraft.

4.6 Total Configuration Polar

The total drag polar at the example Mach number is now computed for both configurations by the summation of the lift dependent and the minimum drag values as previously computed. This calculation is as follows: (Equations (2), (12)).

ΔA-4F				RA – 5C					
$M_\infty = 0.80$						$M = 0.90$		$M_\infty = 2.0$	
$C_{D_{MIN}} = 0.01828$						$C_{D_{MIN}} = 0.01787$		$C_{D_{MIN}} = 0.03105$	
C_L	$C_L^2/\pi AR$	ΔC_{D_P}	C_D	C_L	$C_L^2/\pi AR$	ΔC_{D_P}	C_D	ΔC_{D_P}	C_D
-0.001	0.0	0.00023	0.01851	0.065	0.00036	0.00018	0.01841	0.00095	0.03236
0.099	0.00107	0.00064	0.01999	0.165	0.00232	0.00075	0.02094	0.00743	0.04080
0.199	0.00433	0.00143	0.02404	0.265	0.00599	0.00171	0.02557	0.01711	0.05415
0.249	0.00678	0.00226	0.02732	0.315	0.00847	0.00212	0.02846	0.02870	0.06822
0.299	0.00978	0.00284	0.03090	0.365	0.01137	0.00401	0.03325	0.03938	0.08180
0.349	0.01332	0.00547	0.03707	0.415	0.01470	0.00626	0.03883	0.05152	0.09727
0.399	0.01741	0.00999	0.04568	0.465	0.01845	0.01030	0.04662	0.05814	0.10764
0.499	0.02724	0.02497	0.07049	0.565	0.02724	0.01877	0.06388	–	–
0.599	0.03925	0.04994	0.10747	0.665	0.03774	0.03754	0.09315	–	–

Comparison of these data to that of the reference basic data is given by figures 67 and 68.

4.7 BUFFET ONSET

The ability to predict quickly the buffet onset characteristics of a configuration to within an acceptable tolerance level is of equal importance to the drag calculation herein described. To this end, the computer code (EDET) has been structured to include the correlation of buffet onset information so that the lift coefficient for this occurance ($C_{L_{B.O.}}$) can be estimated.

The calculation for buffet onset is accomplished in the following manner for the two representative aircraft. First, the following data must be assembled:

Aircraft	$AR \left(1 + \frac{h/c}{10}\right)$	$\cos \Lambda_{c/4}$	$(t/c)^{2/3}$	$C_{L_{DES}}$	M_{DES}	$\dfrac{\cos \Lambda_{c/4}}{AR \left(1 + \frac{h/c}{10}\right)} = \text{①}$
A-4F	3.135	0.8367	0.1775	0.299	0.875	0.2669
RA-5C	3.730	0.7934	0.1357	0.365	0.889	0.2127

147

Using figure 28 at the appropriate value of M and (t/c), the calculation proceeds as follows:

M_∞	A-4F				RA-5C			
	ΔM	$C_{L_{B.O.}} - C_{L_{DES}}$ $\times$ ①	$C_{L_{B.O.}} - C_{L_{DES}}$	$C_{L_{B.O.}}$	ΔM	$C_{L_{B.O.}} - C_{L_{DES}}$ $\times$ ①	$C_{L_{B.O.}} - C_{L_{DES}}$	$C_{L_{B.O.}}$
0.40	-0.475	0.0680	0.2548	0.5538	-0.489	0.0695	0.3268	0.6918
0.60	-0.275	0.0480	0.1798	0.4788	-0.289	0.050	0.2351	0.6001
0.80	-0.075	0.0279	0.1045	0.4035	-0.089	0.0340	0.1598	0.5248
0.90	0.025	0.0158	0.0592	0.3582	0.011	0.0320	0.1504	0.5154

These computed values are compared to those presented in the basic data of references 3 through 21 in figure 69. Also included are similar data computed for a representative sampling of the other subject aircraft.

148
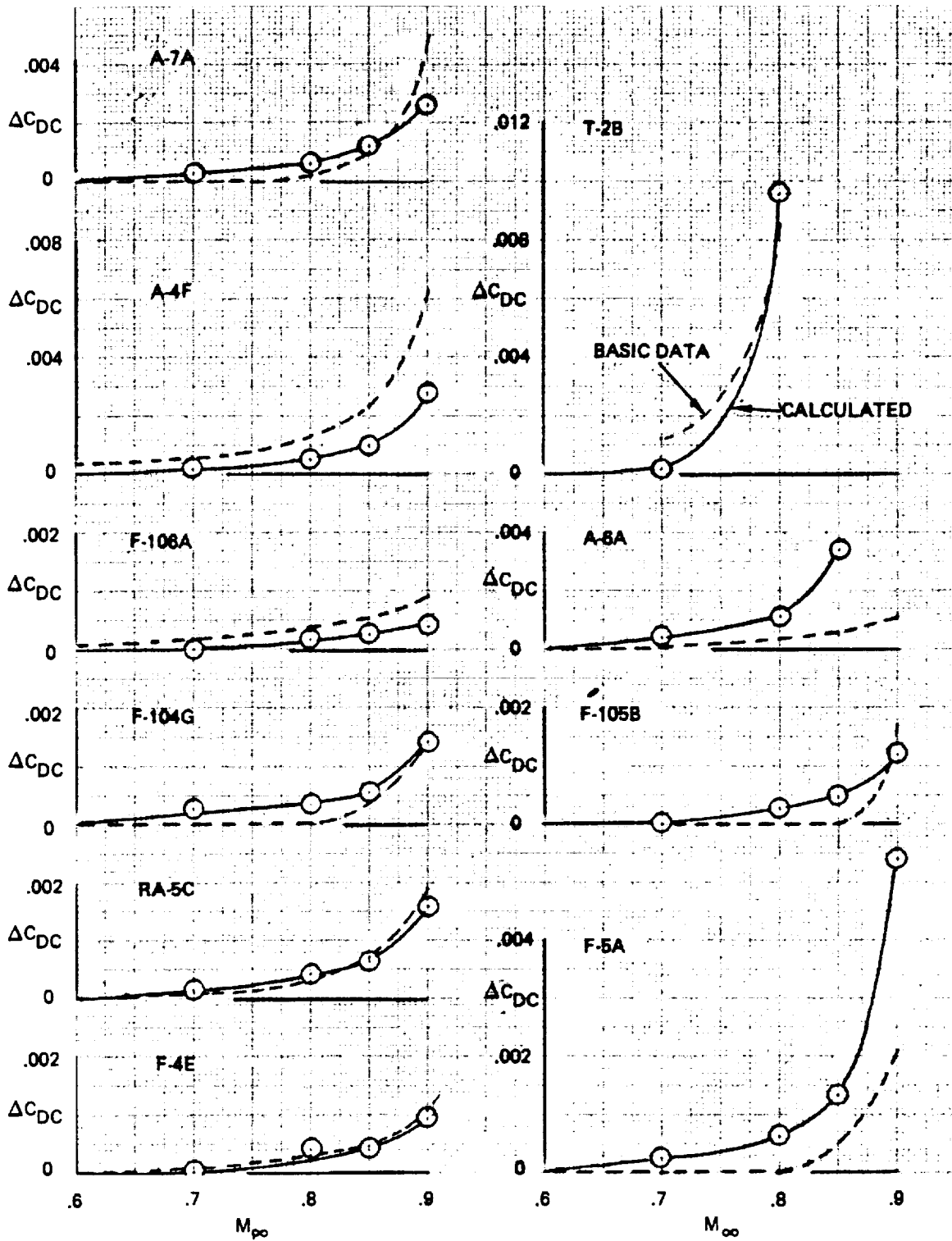
Figure 59. – Subsonic compressibility drag comparison.
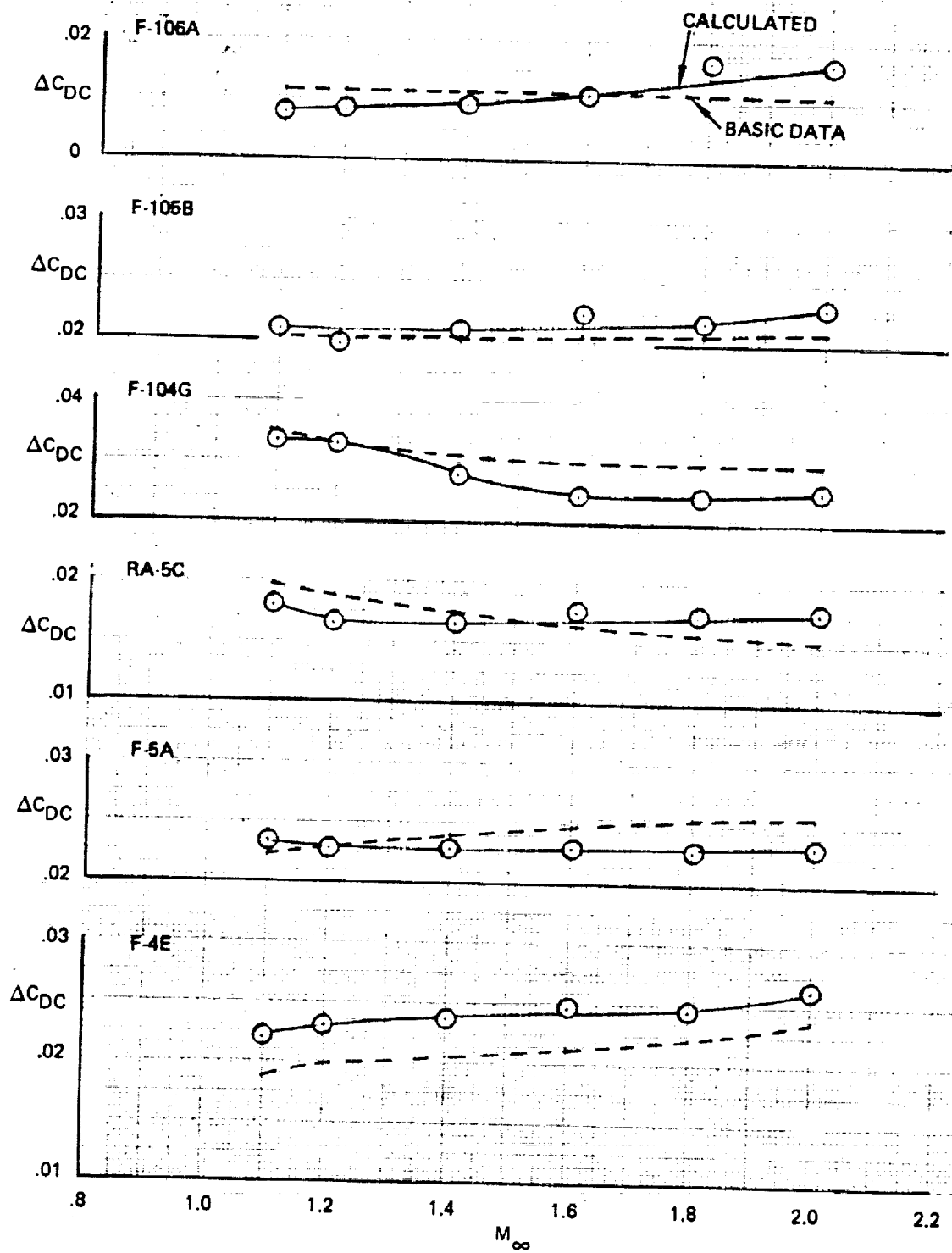
Figure 60. - Supersonic compressibility drag comparison.
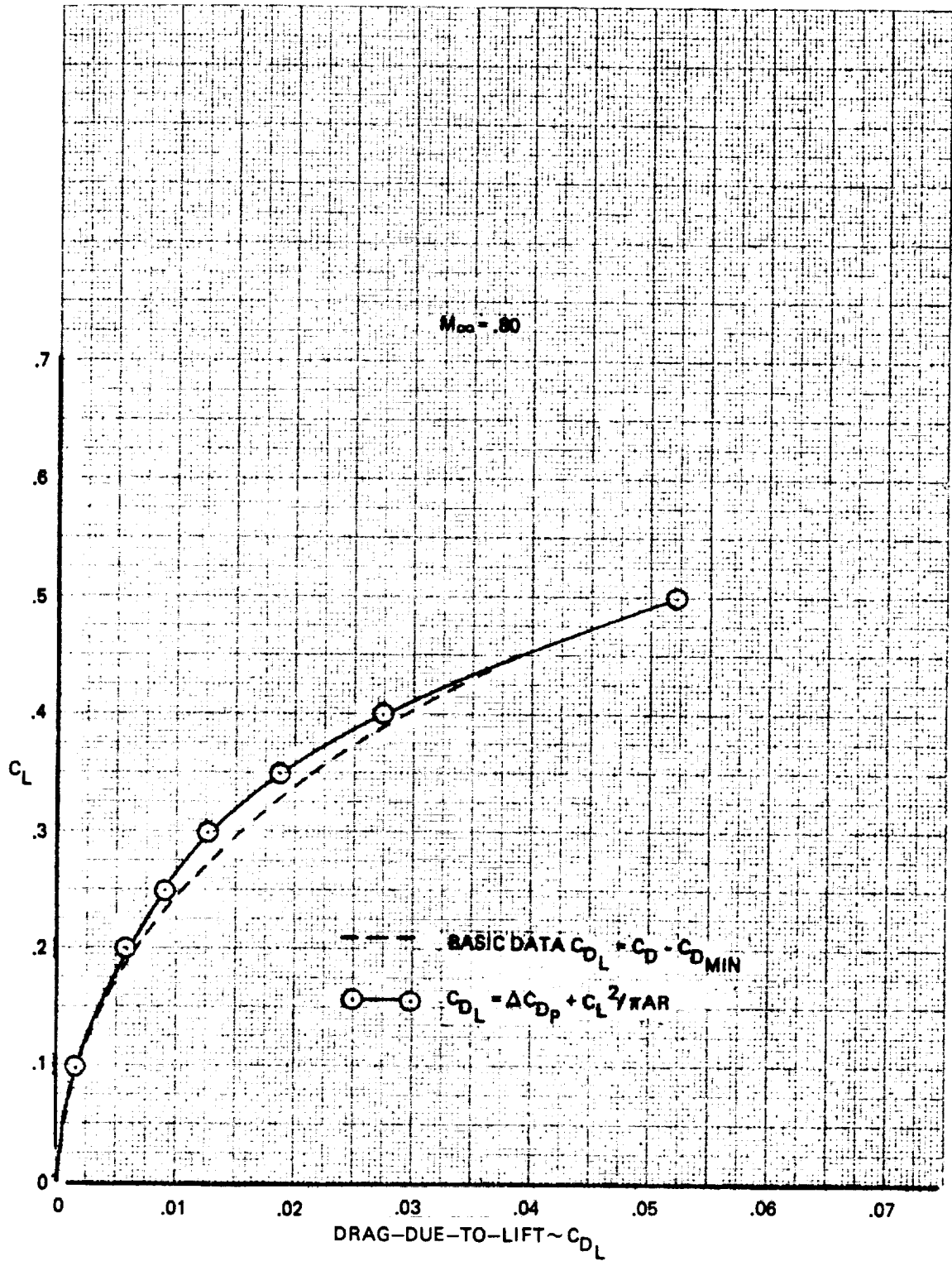
Figure 61. – Drag-due-to-lift comparison, A-4F.
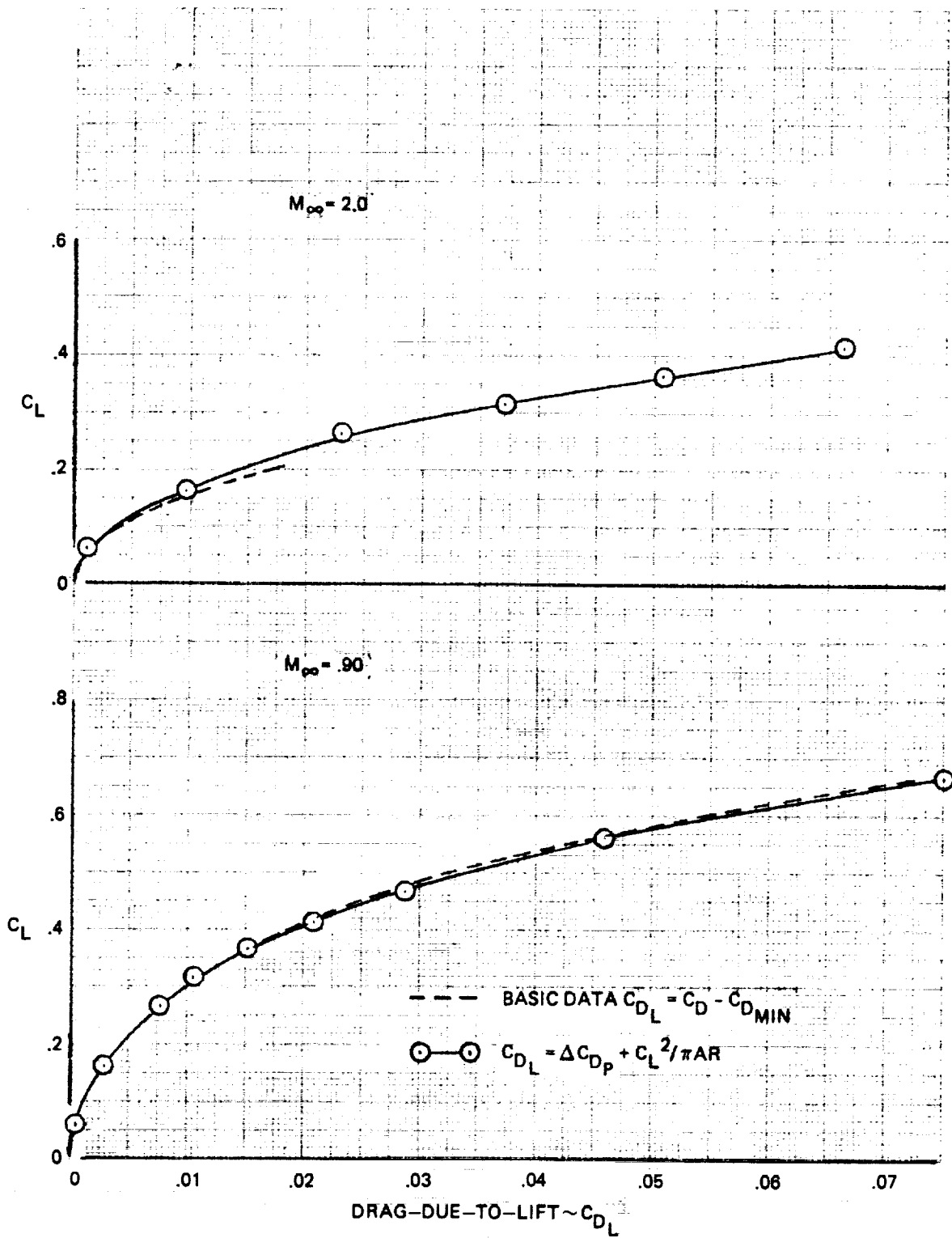
Figure 62. – Drag-due-to-lift comparison, RA-5C.
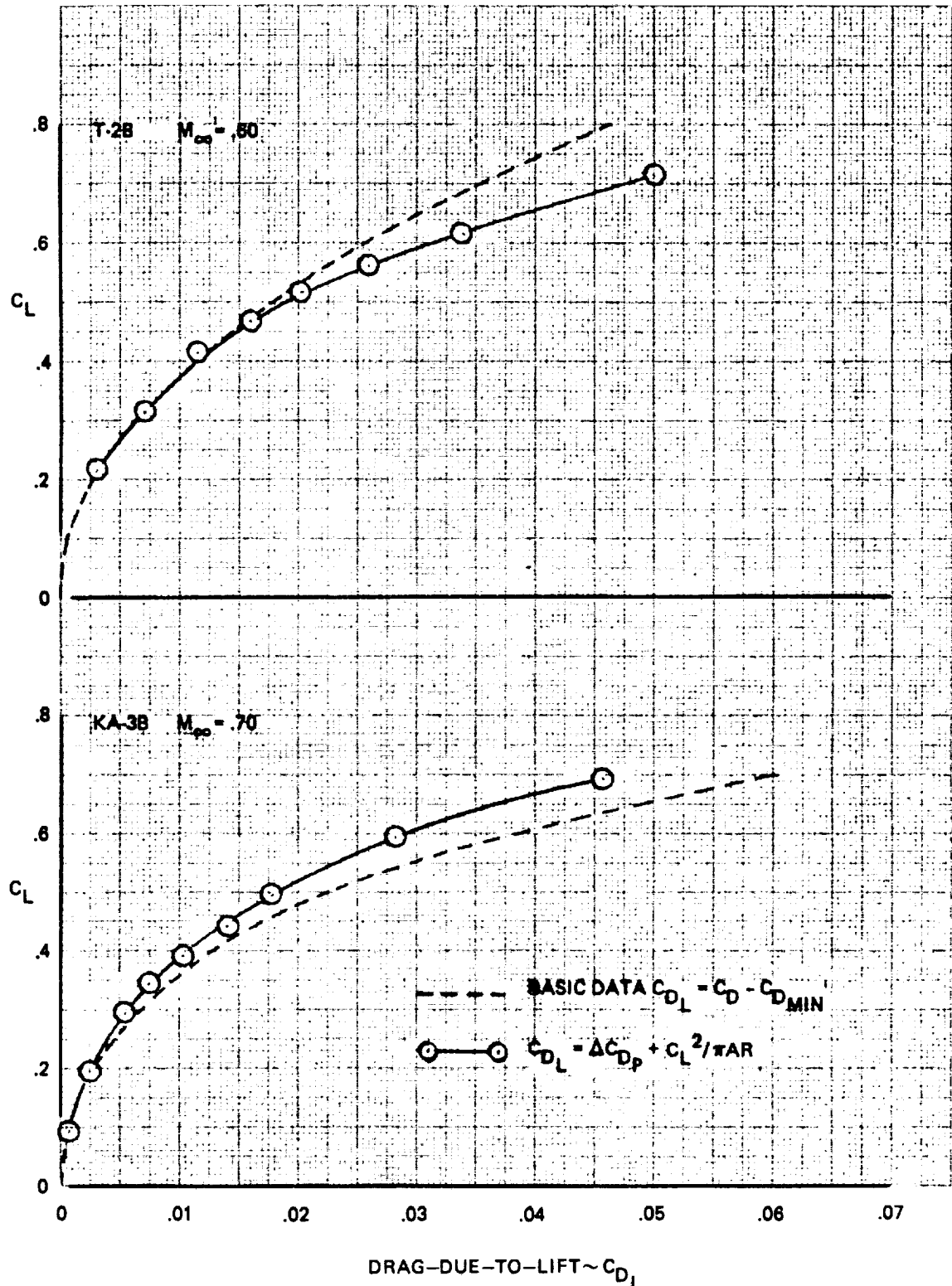
Figure 63. - Drag-due-to-lift comparison, T-2B and KA-3B.

153
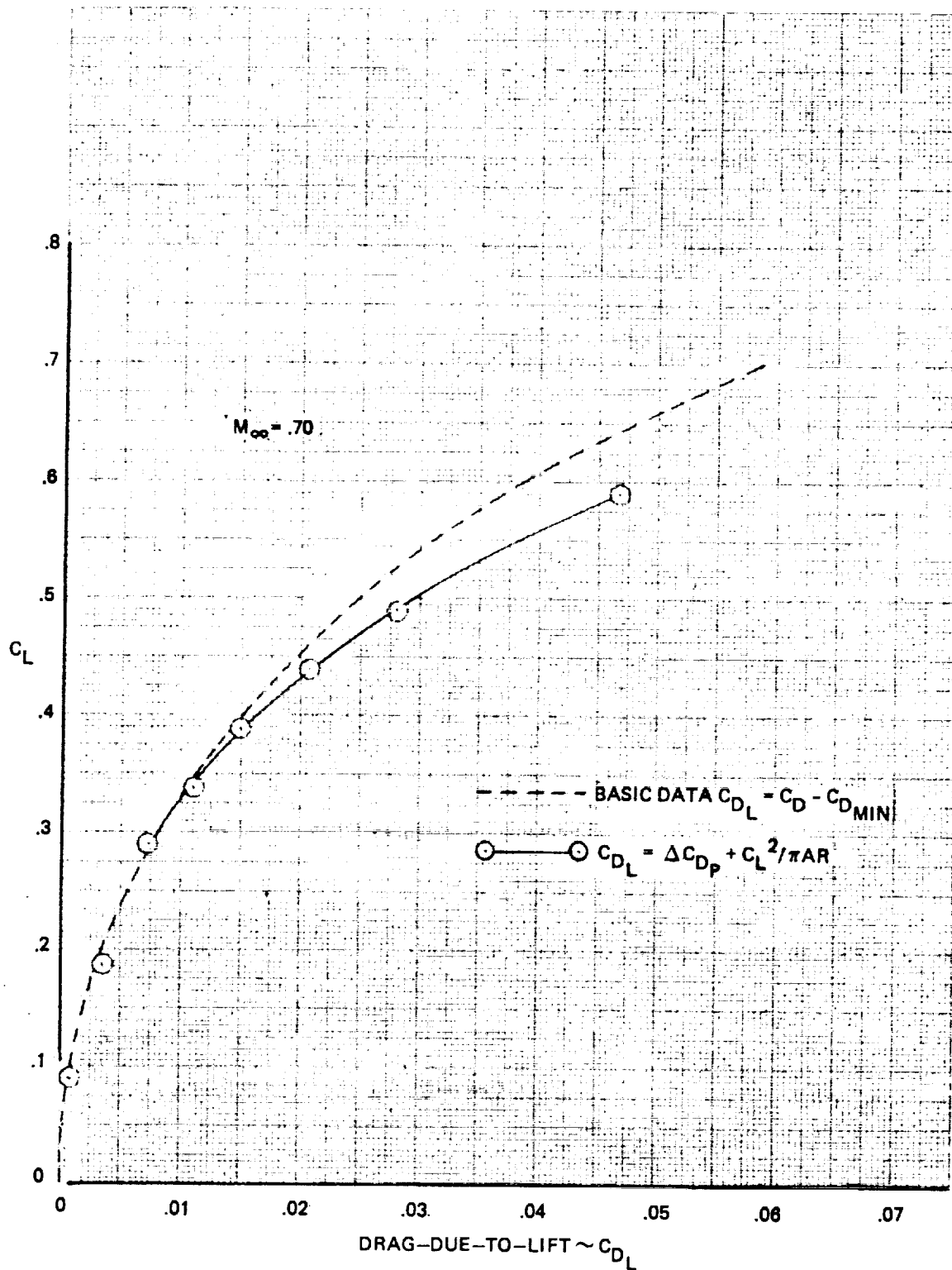
Figure 64. - Drag-due-to-lift comparison, A-7A.
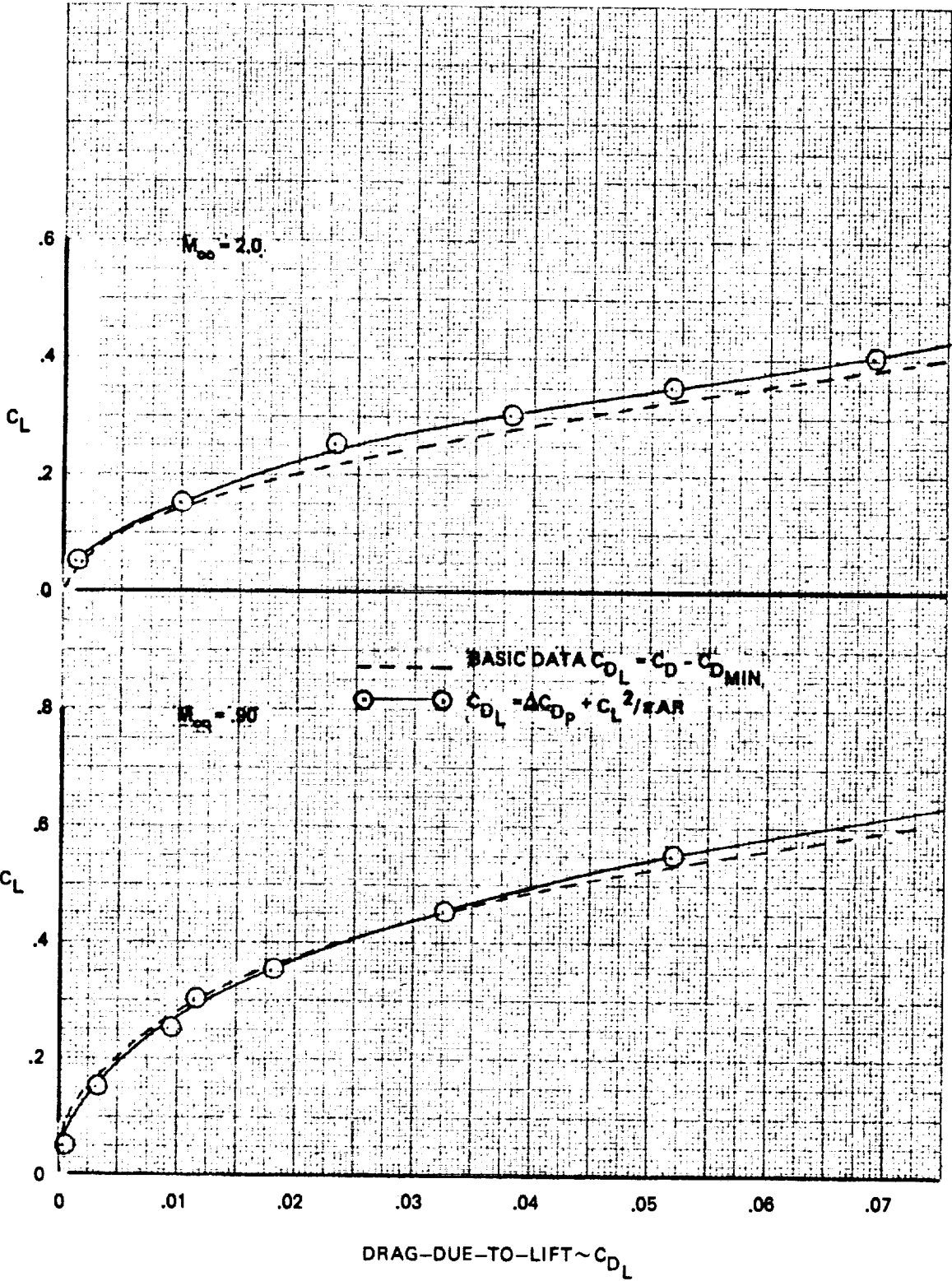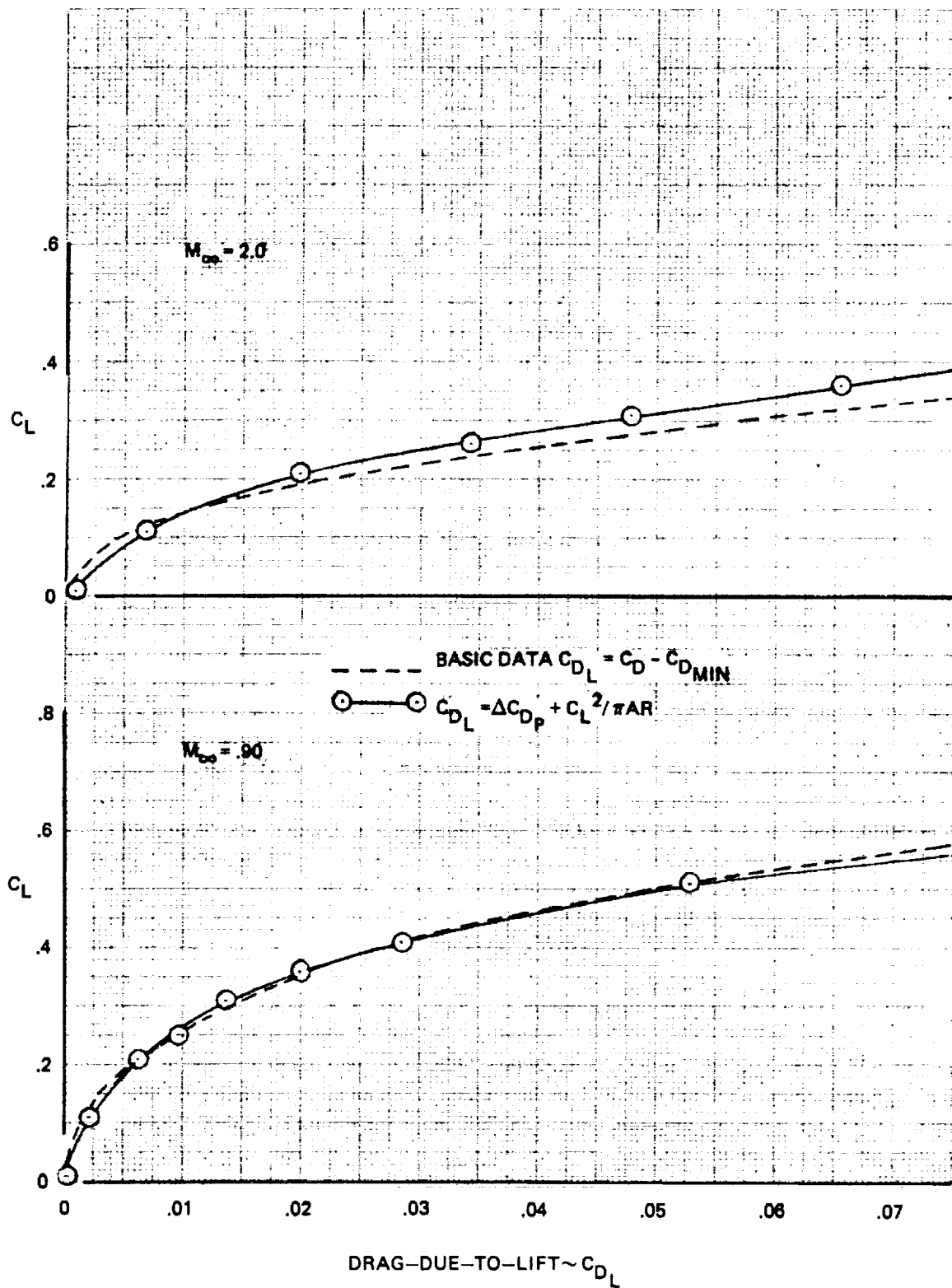
Figure 65. - Drag-due-to-lift comparison, F 5A.
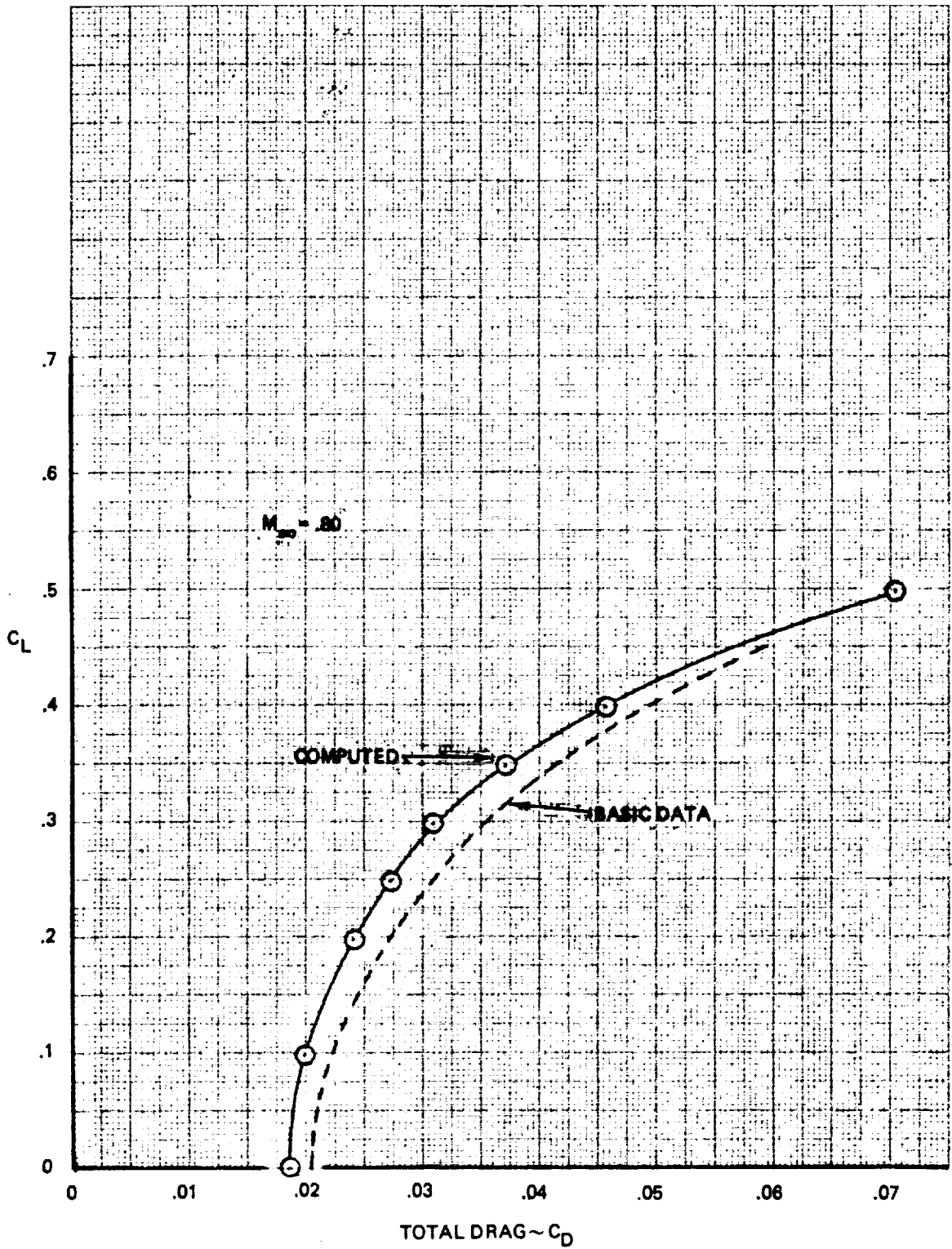
Figure 66.   Drag-due-to-lift comparison, F-4E.
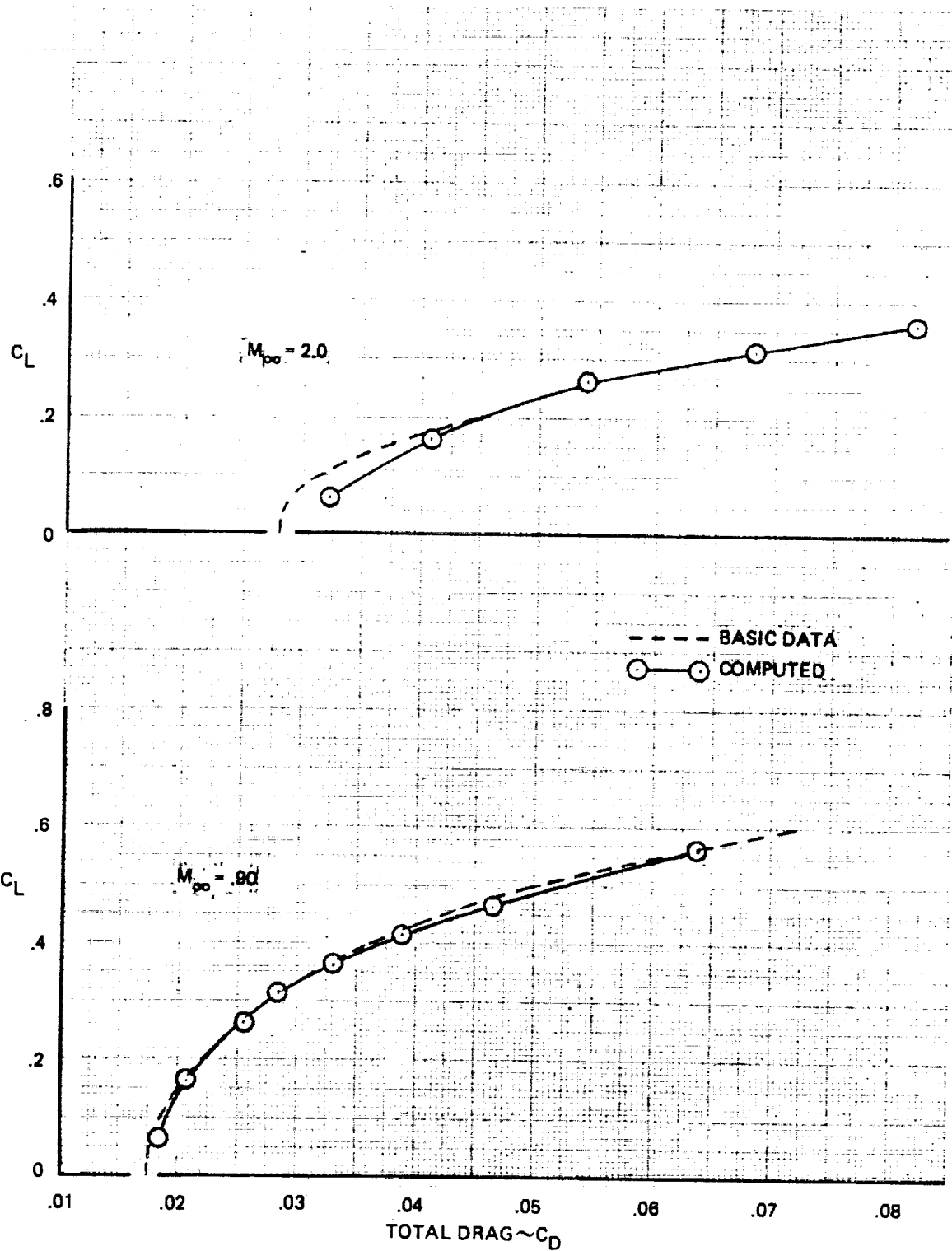
Figure 67. - Drag polar comparison, A-4F.

Figure 68. – Drag polar comparison, RA-5C.
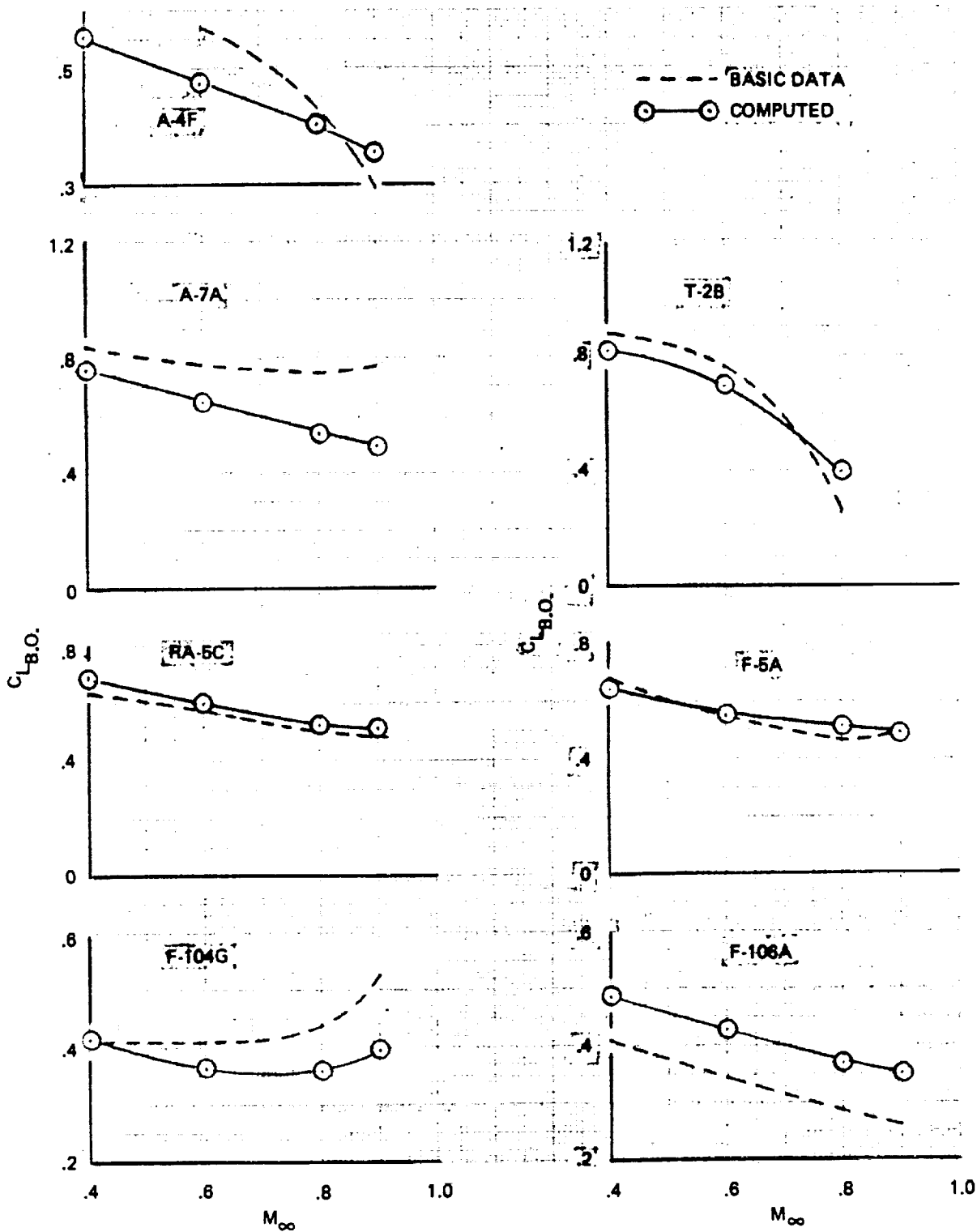
Figure 69. - Buffet onset comparison.

APPENDIX A

FORM FACTOR GENERATION

The geometry related form factor for the fuselage, as presented in
figure 6 of Section 1, was generated using results of a NASA test (Refer-
ence 39). These data, which are representative of transport bodies, were
used as the base for determining the minimum drag of a series of bodies of
varying fineness ratio. These test results are compared on figure 70 with
the estimated skin friction drag. A decided increase in pressure drag with
reduced body fineness ratio is evidenced. On figure 71 these same data are
presented as a form factor and compared with fuselages defined as an equiva-
lent length to diameter ratio. Included on this figure are the fuselage form
factors that would be predicted from other sources.

The wing form factors for advanced and conventional sections, as given
by figure 7, are based on information contained in references 34 and 40.
On figure 72, this form factor has been developed for advanced airfoil sec-
tions and data for a NACA 65 series section is also presented for reference.
The parameter $C_{D_o}/2C_F$ = FF is the 2-dimensional minimum section drag co-
efficient divided by twice the flat plate skin friction coefficient at the
test Reynolds number. The factor of 2 accounts for both upper and lower
surfaces. These data are from 2-D tests on a NACA 65, 213 a = 0.5 airfoil,
9 percent state-of-the-art airfoil, 10 percent, 11 percent, 12 percent, and
21 percent thickness advanced airfoils respectively. Flagged versus
unflagged symbols represent the same model tested in two different facilities.
On figure 73, the average fairing of $C_{D_o}/2CF$ is noted as the form factor
versus section thickness ratio. The conventional line, which was derived
from RAS Data Sheets (reference 41) assuming transition at the leading edge,
is confirmed by results from the NACA 65 series airfoil. At a thickness
ratio of 10 percent the advanced airfoil appears to carry an approximate
10 percent increased subsonic pressure drag over the conventional airfoil
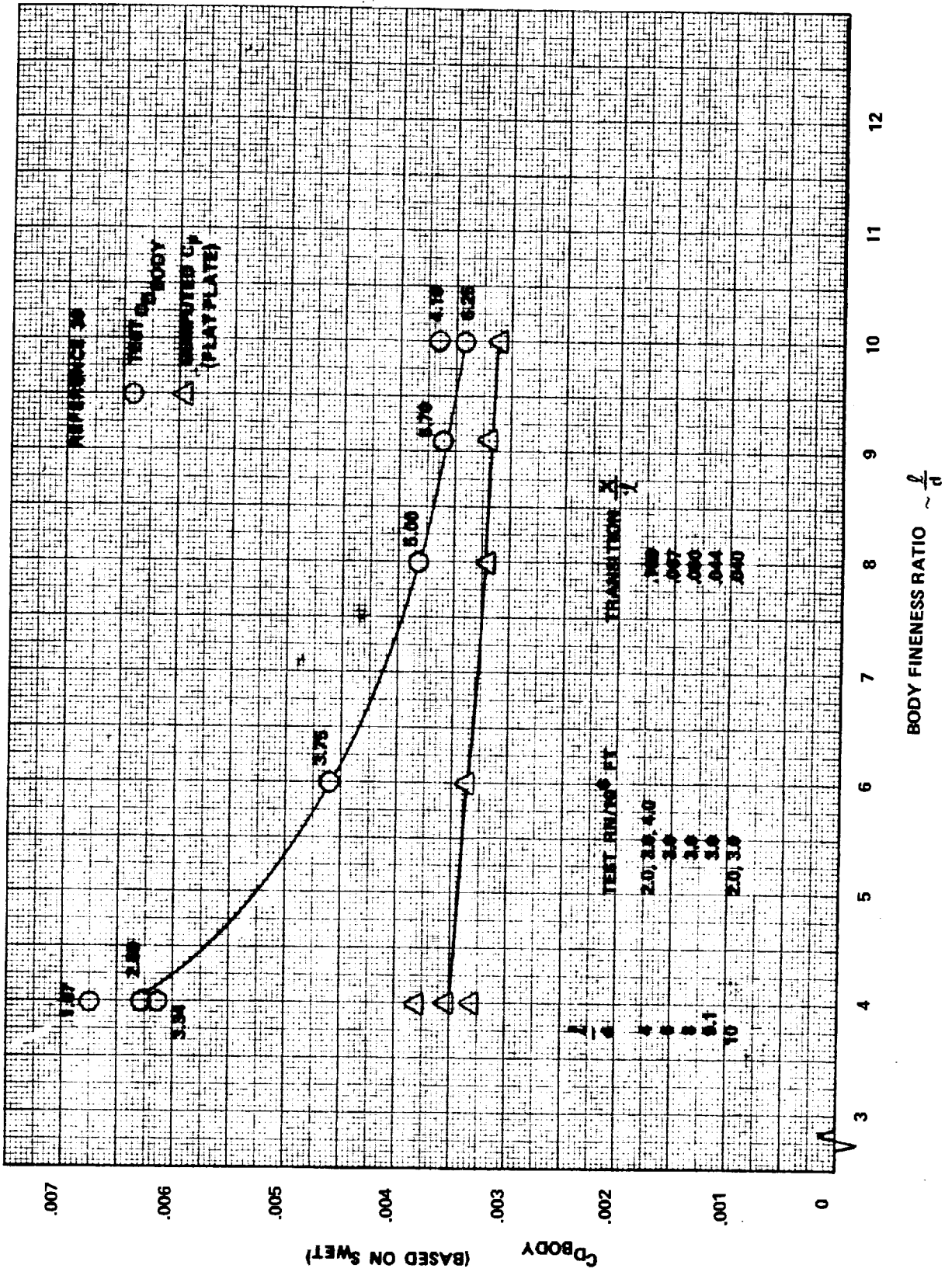sections.

160

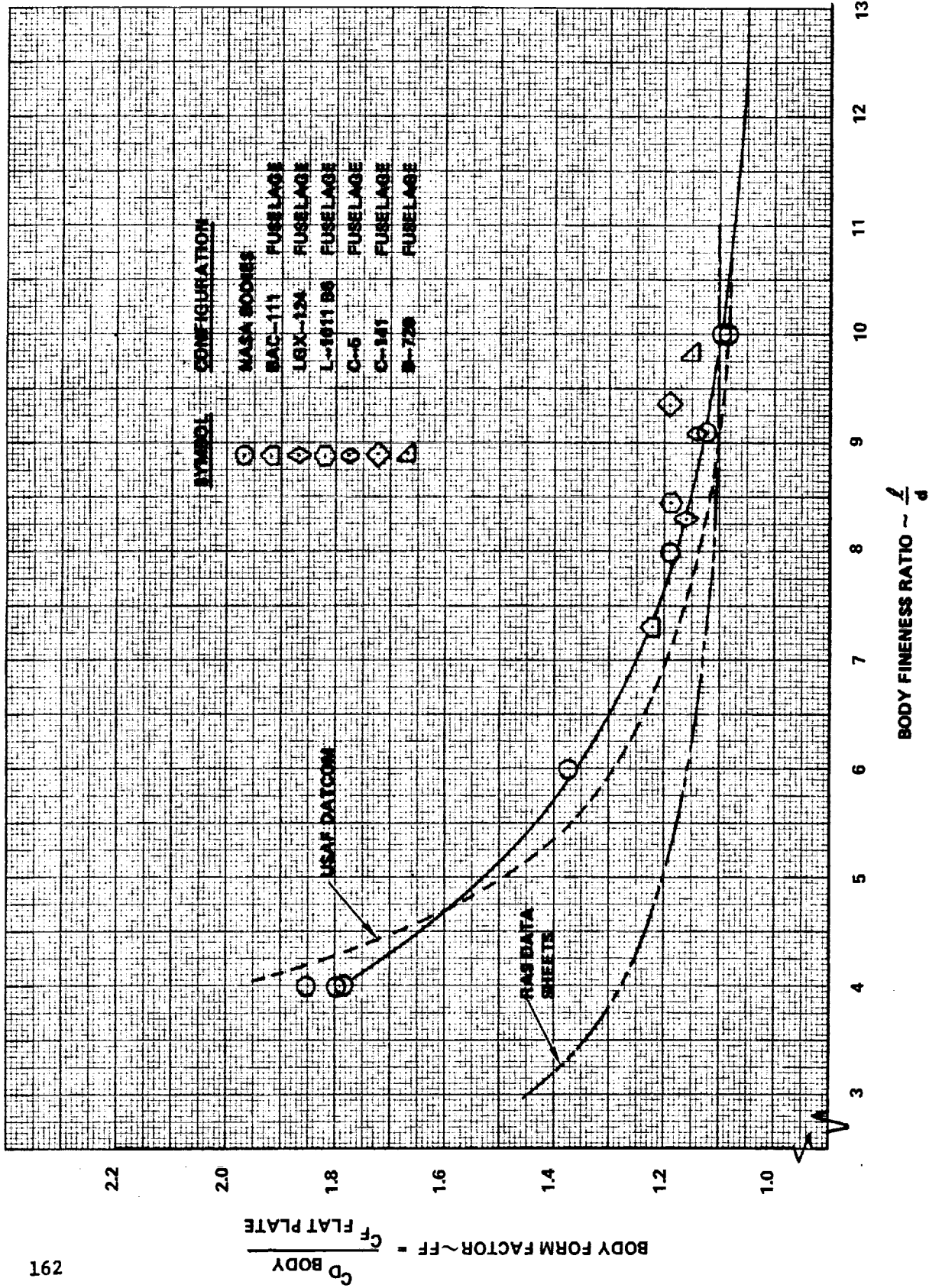Figure 70. – Variation of minimum $C_{D_{Body}}$ with body fineness ratio.

161
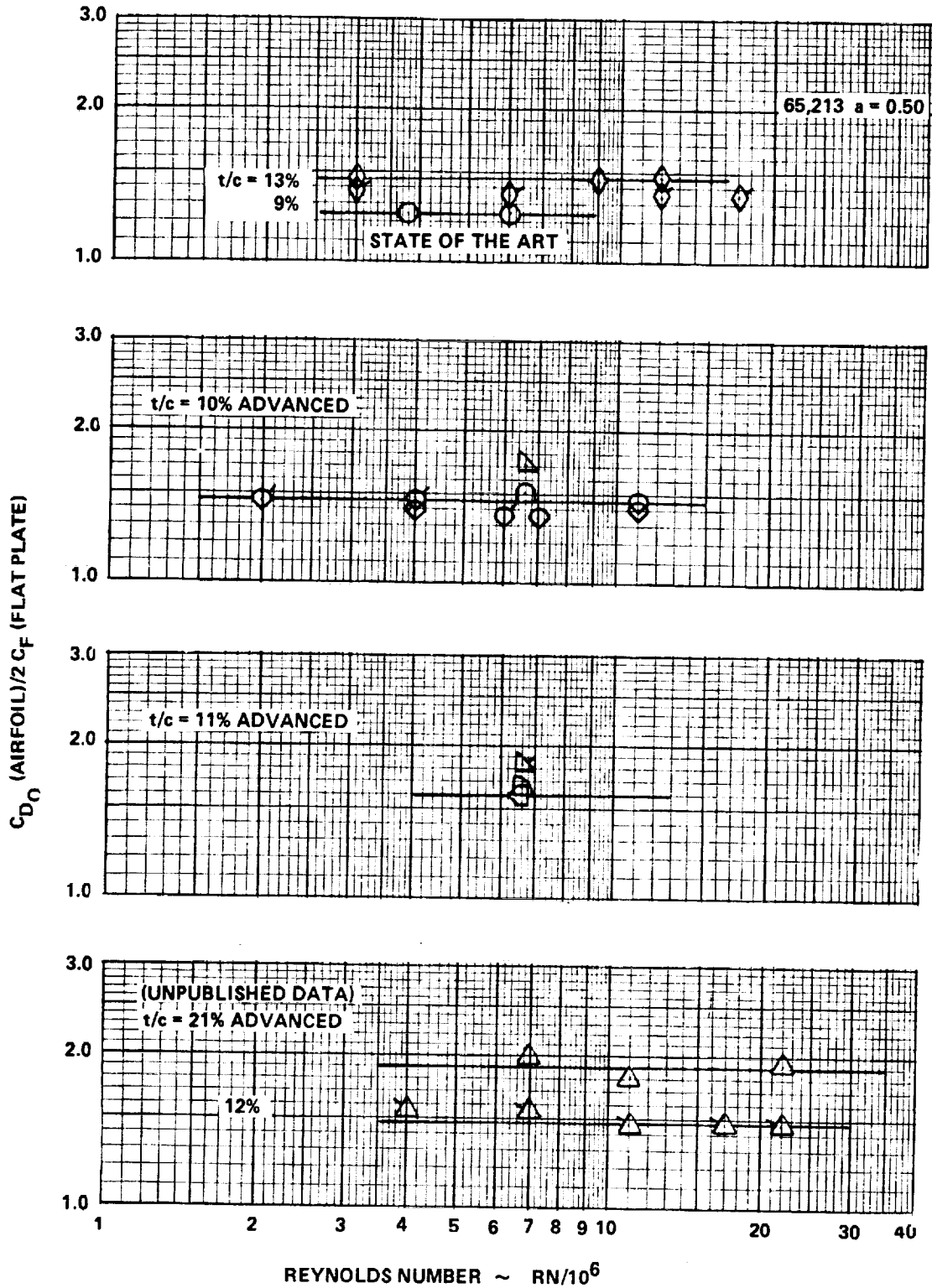
Figure 71. - Body form factor comparison.

Figure 72. - Ratio of minimum drag to theoretical skin friction drag for conventional, state of the art, and advanced airfoil sections.
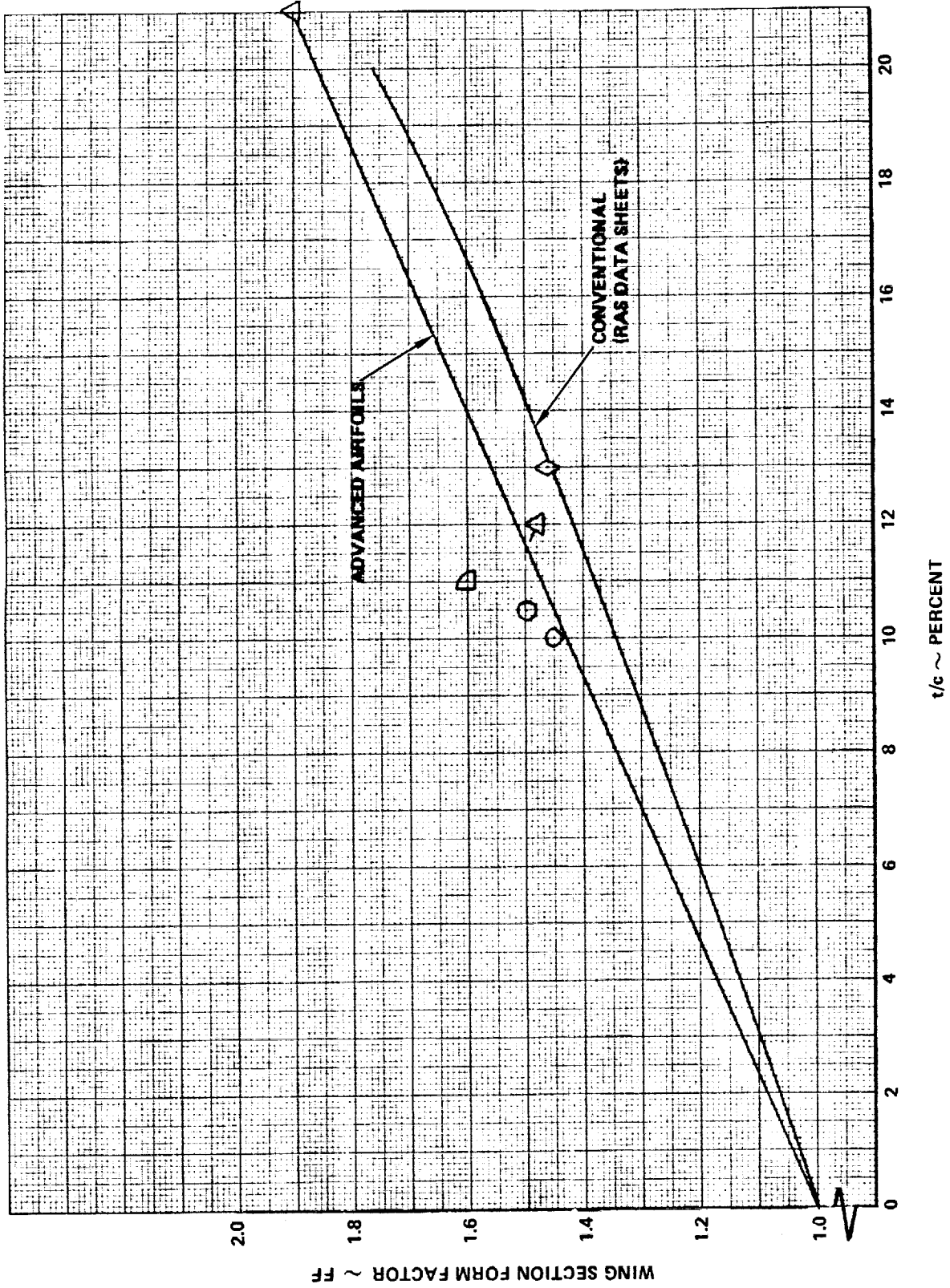
163

Figure 73. – Wing section form factor correlation.

LIST OF REFERENCES

1. Morrison, W. D. Jr.: Advanced Airfoil Design Empirically Based Transonic Aircraft-Drag Buildup Technique, NASA CR 137928. Unclassified, January 1977.

2. Elliott, R.D: Empirical Drag Estimation Technique (EDET) User's Manual, Lockheed-California Company Report, LR 28788. December 1978.

3. Elliott, D. W.: Substantiating Data Report Based on Flight Test Data for the T-2B Trainer Power with Two T60-P-6 Engines. North American Aviation, Inc. NA64H-536, 7 June 1964.

4. Wong, F. T.: Model T-37B Substantiating Data for Standard Aircraft Characteristics Charts, Based on Category II Flight Test Data. Cessna Aircraft Company, 31813-7003-120, 21 Dec. 1970.

5. Anon.: Performance Data for the Model A3D-2, 2P and 2Q, (KA-3B) Airplanes Based on Flight Test Data. Douglas Aircraft Company, Inc. 29 Apr. 1960.

6. Anon.: Performance Data for the Model A-4F Aircraft. Mc Donnell-Douglas Aircraft Compnay, MDC J 1087 23 Feb. 1971.

7. Anon.: Performance Data for the Model TA-4F (J52-P-6A Engine). Douglas Aircraft Company, Inc., DAC 33078, 27 August 1966.

8. Anon.: Performance Substantiating Data Report for the RA-5C Aircraft with J79-GE-10 Engines. North American Rockwell Corporation, 27 Feb. 1969.

9. Ohler, J. C.: A2F-1 (A6A) Basic Data Report for the Standard Aircraft Characteristics Chart of August 1959. Grumman Aircraft Engineering Corporation, XA128-105-3, August 1959.

10. Styne, H. E.: A-7B Aircraft, Basic Data for Performance Calculation. LTV Aerospace Corporation, 2-53330/8R-5345, 10 January 1968.

11. Miles, R. B.: Model F-4E Performance Data and Substantiation, McDonnel Aircraft Company, MDC A1158, 20 July 1971.

12. Ackerman, N. G.; and Warren, B. L.: F-5 Basic Aerodynamic Drag Data. Northrop Corporation, NOR-64-2, January 1965.

LIST OF REFERENCES (Continued)

13. Artificavitch, W. P.: F8U-2 (F-8C) Performance Data. Chance Vought
    Aircraft, E8R-11402, 19 May 1958.

14. Anon., Drag Basis of Gruman Design 985-11. Grumman Aircraft Engineering
    Corporation Report No. A98-A-114, December 1957.

15. Nugent, J.: Lift and Drag of A Swept-Wing Fighter Airplane at Transonic
    and Supersonic Speeds. NASA Memo 10-1-58H, Unclassified, January 1959.

16. Chewning, N.: and Vondrasek, D.: Model F-101B Flight Manual and Standard
    Aircraft Characteristics Chart Substantiation Report Based on Flight
    Test Data. McDonnell Aircraft Corporation Report No. 6907, Vol. I,
    15 June 1959, Revised 30 December 1960.

17. Chewning, N.; and Ferrante, B.: Model F-101A/C and RF-101A/C Performance
    Data Substantiation Report. McDonnell Aircraft Corporation Report No.
    5447, 15 June 1957, Revised 1 Jan. 1960.

18. Avant, N. T.: Map F-104G Performance Characteristics, Lockheed-California
    Company Report, LR 16097, 16 July 1962.

19. Smith, L.: Substantiation Report (EAR 463-Addendum I) for F-105D-
    5RE,-10RE, and -25RE. Standard Aircraft Characteristics Charts.
    Republic Aircraft Corporation Report No. 1171, March 1963.

20. Craig, R. E.: Substantiating Performance Data for the F-106A Flight
    Manual Revisions Due to the Installation of the M61A1 Gun System.
    General Dynamics, Convair Division, GDCA-DCD-72-002, 2 October 1972.

21. B-70 Aerodynamic Project Group: Estimated Performance and Drag Sub-
    stantiation Report for the B-70 Primary Air Vehicle. North
    American Aviation, Inc. Report NA-59-268-1, 15 July 1959.

22. S-3A Aero Group: S-3A Stability and Control and Flying Qualities Report,
    Vol. 3. Lockheed-California Company Report, LR 23462-3, "E" Revision,
    December 1975.

23. Miranda, L. R.: and Baker, W. M.: Progress Report on Transonic Wing
    Design Technology: 1977-1978. Lockheed-California Company Report,
    LR 28771, September 1978.

24. L. M. Evans: V/STOL High Speed Tests S-342 II. Lockheed-California
    Company, FS/75-41-02-2265, Unpublished Data.

25. Anon.: Transonic Wind Tunnel Tests of the 1/30 Scale L-1011 Airplane,
    Lockheed Tests No. N-227, N-236, N-241. Cornell Aeronautical Laboratory,
    Inc., Report No. AA-4006-W-1, March, June, July 1969.

LIST OF REFERENCES (Continued)

26. Anon.: L-1011-1 Flight Performance, RB.211-22B Engines, Lockheed-California Company Report, LR 26189, December 1973.

27. NASA/Lockheed-California Company. Contract #N00019-73-C-004, 1974. (Report to be published).

28. Blackwell, J. A., Dansby, T., Little, B. H., Jr., Ryle, D. M., Jr., Allison, H. B.: Aerodynamic Design, Test, and Analysis of the Lockheed-Georgia ATT-95 Aircraft. Lockheed-Georgia Company Report, LG 72ER 0041, 1972.

29. Ferris, James C.: Static Aerodynamic Characteristics of a Model with a 17-Percent-Thick Supercritical Wing. NASA TMX-2551, 1972.

30. Graham, Lawrence A.: Jones, Robert T.: and Boltz, Frederick W.: An Experimental Investigation of the Oblique-Wing and Body Combination at Mach Numbers Between 0.60 and 1.40. NASA TMX-62, 256, 1973.

31. Bartlett, Dennis W.: and Re, Richard J.: Wind Tunnel Investigation of Basic Aerodynamic Characteristics of a Supercritical-Wing Research Airplane Configuration. NASA TMX-2470, 1972.

32. Capone, Francis J.: Effect of Various Wing High Lift Devices on the Longitudinal Aerodynamic Characteristics of a Swept-Wing Fighter Model at Transonic Speeds. NASA TMX-3204, 1975.

33. Feagin, R.C.: Transonic Aircraft Drag Technique Applied to Military Aircraft, Vol II, Lockheed-California Company Report, LR 27975, Revised December 1978.

34. Morrison, W. D. Jr.: Empirically Based – Transonic Aircraft – Total Drag Prediction Technique – Delta Method. Lockheed-California Company Report, LR 27027, June 1976.

35. USAF Stability and Control DATCOM.

36. Harris, R. V.: An Analysis and Correlation of Aircraft Wave Drag. NASA TMX-947, March 1974.

37. McDevitt, John B.: A Correlation by Means of Transonic Similarity Rules of Experimentally Determined Characteristics of a Series of Symmetrical and Combined Wings of Rectangular Planform. NACA Report 1253.

LIST OF REFERENCES (Continued)

38. Schlichting, H.: Boundary Layer Theory, 4th Edition, McGraw-Hill, 1960.

39. Anon.: Transonic Wind Tunnel Tests of Several NASA Bodies of Revolution. CAL No. AA-4018-W-5, 1971.

40. Burdges, K. P., Blackwell, J. A., Pounds, G. A.: High Reynolds Number Test of a NASA 65, -213, a = 0.5 Airfoil at Transonic Speeds. NASA CR-2499, 1975.

41. Anon.: Profile Drag of Smooth Wings. RAS Data Sheet WINGS 02.04.02, 1957.